```
*********************************************************************************
* User name:   DGOODSON (73)                      Queue:  EL_SERVER2/LASER3
* File name:                                      Server: EL_LASER_3
* Directory:
* Description: Microsoft Word - Document1
*              February 19, 1997                          2:31pm
*********************************************************************************
*
*               DDDD   GGGG  OOO   OOO  DDDD   SSS   OOO  N   N
*               D   D G     O   O O   O D   D S   S O   O N   N
*               D   D G     O   O O   O D   D S     O   O NN  N
*               D   D G GGG O   O O   O D   D  SSS  O   O N N N
*               D   D G   G O   O O   O D   D     S O   O N  NN
*               D   D G   G O   O O   O D   D S   S O   O N   N
*               DDDD   GGGG  OOO   OOO  DDDD   SSS   OOO  N   N
*
*
*
*********************************************************************************
*
*                          L      SSS  TTTTT
*                          L     S   S   T
*                          L     S       T    ::
*                          L      SSS    T    ::
*                          L         S   T
*                          L     S   S   T    ::
*                          LLLLL  SSS    T    ::
*
*
*
*********************************************************************************
```

s(n)+d(n)

s(n) + d(n)

ŝ(n) + ŝ(n)

y(n) = s(n) + d(n)

be success had cancellation of noise

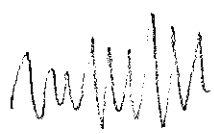

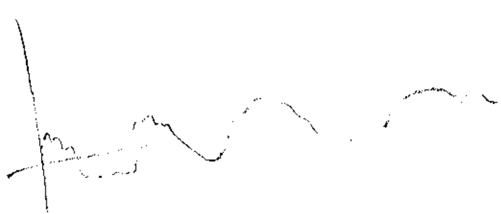

Speech production system is modelled as shown in fig. . . , This model is utilised in the synthesising of speech signal at the receiver. The vocal tract is modelled as a time-varying digital all-pole filter.

the

[ ]

A simplified block diagram of speech production system is shown in fig. In this model, the driving input, or excitation signal, is modelled as either an impulse train (for voiced speech) or random noise (for unvoiced speech). The combined ~~effect of~~ spectral contributions of the glottal flow, the vocal tract and the radiation of the lips are represented by a time-varying digital filter. ~~with the~~ is given by.

$$H(z) = \frac{S(z)}{X(z)} = \frac{G}{1 - \sum a_i z^{-i}} = \frac{G}{A(z)}$$

(Transforming Eq. equ m t)

Equation 3.1 is the well known LPC difference equation, which states that

USE OF MICROCONTROLLERS FOR DIVER MONITORING BY UNDERWATER ACOUSTIC BIOTELEMETRY IN MULTIPATH ENVIRONMENTS

by

ROBERT SH. HABIB ISTEPANIAN, BSc, MSc

A doctoral thesis submitted in partial fulfilment of the
requirements for the award of Doctor
of Philosophy of the Loughborough University of Technology

September 1994

Supervisor: Dr. Bryan Woodward, PhD, C Eng, FIEE, FRGS, MIEEE

Department of Electronic and Electrical Engineering

* To the memory of my father Shukri Habib Istepanian.

* To my dearest mother Mary for your prayers. I missed you so much.

* To my sister Rita, whose noble spirit and determination to challenge the difficult years made hard times endurable.

* To my brother Harootyun, whom without your sacrifice I couldn't have made it.

* To my beloved wife Helen, for your understanding and patience, especially in the years we were apart.

* To my daughter CAROLYN , to whom I dedicate this thesis.

Abstract

Biomedical Telemetry (Biotelemetry) is a special facet of bio-instrumentation which provides a means for transmitting physiological or biological information from one site to another. There are numerous situations in which it is desirable to monitor critical physiological reflexes and responses from freely swimming swimmers or divers.

The design and implementation of a novel multi-channel digital acoustic biotelemetry system using a single-chip microcontroller is described. It is intended for monitoring the electrocardiogram (ECG), heart rate, breathing rate and depth of a free swimming diver, but the system has a modular design that can be adapted for the transmission of digital data representing any parameter. The use of the microcontroller enables the digital data to be transmitted in a priority interrupt format from each sensor with programmable pulse width timing. A portable receiver contains an identical microcontroller and is designed to scan three crystal-controlled frequencies to provide a logical output for each detected signal. These signals are captured by a portable data logger and interfaced to a computer for further processing. This automated arrangement greatly reduces the probability of data error by increasing immunity to multipath and reverberation effects.

The advantages of such new design approach, apart from employing a high speed digital single-chip processor, is that it allows a telemetry link through its unique modular architecture. It also involves flexible hardware modules and programmable software capabilities to accommodate the current performance requirements and overcome the fundamental problems associated with realizing such systems, i.e. the trade-off between the nature of the transmitted signal, choice of transmission format, the power capability of the transmitting transducer and the sensitivity of the receiver. It also allows the design specifications to be generalized for future applications.

The system was tested successfully in a large indoor tank in the Electronic and Electrical Engineering Department to simulate the effect of a short and very shallow underwater channel with severe multipath reverberation.

The other objective of this work is to introduce new concepts of physiological analysis and monitoring, and specifically for SCUBA divers. The thesis presents a new methodology for monitoring heart rate variability during SCUBA diving using a power spectral analysis method. This method provides a physiological interpretation of the role of the autonomic nervous system in modulating the cardiovascular reflexes in response to diving activity.

The thesis also includes a pilot feasibility study on the application of Artificial Neural Networks (ANN) in the detection and likelihood classification of medical problems associated with SCUBA diving. A simple ANN-based model has been simulated to classify the likelihood of an underwater related medical disorder following certain diving profiles. It also discusses the possibility of incorporating such new analysis methods in the next generation of intelligent biotelemetry systems.

ACKNOWLEDGEMENTS

First, and above all I would like to thank the Almighty for giving me a wonderful gift and steering me in the right direction in the difficult days and in moments of despair.

I should like to express my sincere gratitude and appreciation to my supervisor Dr. Bryan Woodward for his invaluable advice, continuous support and diligent guidance throughout the years of this research. Without his moral encouragement and trust, that I will always cherish, especially in the crucial and difficult years of my study, this work could not have been possible. I also offer my appreciation to him for always being ready as my diving test subject throughout this study.

I am grateful to the committee of vice-chancellors and principals of British universities for providing an overseas research studentship (ORS) award, and to Dr. B. Vale (Assistant Registrar) and Mrs. J. Richardson, of the postgraduate office in the university, for their administrative help and support.

I should like to record my sincere thanks and appreciation to the Armenian General Benevolent Union (AGBU)-London for their financial support of my studies. I am particularly indebted to the Mr. G. Kurkjian OBE Chairman of the board of trustees, and Mr. A. Topalian, Honourary Treasurer, for their continuous support and understanding in the difficult days.

Gratitude is extended to Professor Zheng Zhaoning (visiting scholar) from Southeast University, Nanjing, China for his useful comments and interest in the research, and to Dr. Robin Hooper and Miss J. Savania from the Department of Human Sciences for providing some of the physiology and laboratory equipment.

Finally, many thanks to the technicians in the department and my friends in the Signal Processing Group, Satish, Chris, Naimmi Mohasses, Hayri, and Shahram.

TABLE OF CONTENTS

CHAPTER ONE

INTRODUCTION

1.1 GENERAL

Biomedical telemetry (Biotelemetry) is a special facet of bioinstrumentation which provides a means for transmitting physiological or biological information from one site to another for data collection. Technically, it refers to systems which require no mechanical connection. The actual or encoded parameters are usually transmitted via acoustic or radio waves, although light waves have also been used.

Biotelemetry studies in the last three decades have permitted many areas of physiological and behaviourial monitoring in diverse conditions, both for humans and animals, without the encumbrance and restriction of wires connecting the transmitter and receiver. The most widespread use of biotelemetry is the monitoring of biological information from animals and man. The importance of biotelemetry to basic biological, environmental, and medical research cannot be overstated. For example, the utility to provide real time physiological telemetry monitoring in the hospitals has become widely recognized since the early 1970's.

Biotelemetry is also used as an aid to understanding and identifying the natural causes that are linked to habitat conditions of wild animals, which in turn alter their behaviour, and how such conditions affect their mortality rates. It can also provide a means to study and predict the effects of environmental changes such as thermal and chemical pollution and other geophysical changes.

It is important that telemetry technology should be advanced to provide increased capabilities in these and other applications. One of the important areas in which biotelemetry is useful is in human underwater physiological monitoring. It is of prime importance to studies in physiology and exercise, physical stress and many other effects, and is particularly applicable to monitoring swimmers and divers.

In the case of divers, acoustic biotelemetry enables the monitoring of different evoked potentials and physiological parameters from freely moving subjects performing different underwater tasks. However, once a decision has been made to adopt acoustic telemetry, there are several considerations that have to be taken into account when designing a system. The main problem, especially in very shallow water environments such as swimming pools, is that of multipath acoustic reverberation. However, recent advances in high speed digital single-chip microcontrollers and signal processors have made it possible to overcome the various obstacles that hindered progress in the past. This thesis presents a comprehensive new design methodology for underwater acoustic biotelemetry for engineers and physiologists interested in this important research area.

1.2 SYSTEM CONSIDERATION AND AIMS OF RESEARCH

There are numerous situations in which it is desirable to monitor critical physiological reflexes and responses from swimmers or divers. Development of biotelemetry systems described here was initiated by some unusual cases observed at the Brompton Hospital in London, where cardiologists had observed sudden cardiac arrhythmia in children during swimming. The requirement was to develop a real time monitoring system to record the electrocardiogram and heart rate of a swimmer under restraint-free conditions. There are, many other useful applications for such systems; for example in a sporting context, athletes may want to monitor important physiological responses under quasi-competitive conditions.

An acoustic biotelemetry system offers a good solution, not only for swimmers in a pool but also for divers in open water. However, acoustic signal transmission can be distorted severely by multipath reverberations; this was the most challenging problem and the main disadvantage of designing a practical system. Although the system was mainly developed for use with SCUBA divers, it could be easily used for studies of marine mammals. The major aim of this thesis is to develop a state-of-the-art multi-channel programmable digital acoustic biotelemetry system, that can reliably transmit physiological data from a diver in reverberant shallow water environments. A system like this was difficult to implement in the past, but recent advances in high speed digital signal processors and single-chip technology have made such an application achievable.

A novel microcontroller-based biotelemetry system, based on a modular design approach, was developed to transmit and record the electrocardiogram (ECG) signal or heart rate, breathing rate and depth of free swimming diver.

The advantages of this new design approach, is that it provides a telemetry link through its unique modular architecture. This comprises flexible hardware modules and programmable software to accommodate the performance requirements and overcome the fundamental problems associated with realizing such systems. It also allows the design specifications to be generalised for future applications.

The system was tested successfully in a large indoor sonar tank in the Department of Electronic and Electrical Engineering to simulate the effect of a short and very shallow underwater channel with severe multipath reverberation.

The other objective of this work was to introduce new concepts of physiological analysis and monitoring, and specifically during SCUBA diving. The thesis presents a new methodology for monitoring heart rate variability during SCUBA diving using the power spectral analysis. This method provides a physiological interpretation of the role of the autonomic nervous system in modulating the cardiovascular reflexes in response to diving activity. The thesis also includes a pilot feasibility study of the application of Artificial Neural Networks (ANN) in the detection and likelihood classification of medical problems associated with SCUBA diving. A simple ANN-based model has been simulated to classify the likelihood of a medical disorder following certain diving profiles. This presents a first linkage step toward incorporating such systems in next generation of smart biotelemetry systems.

1.3 THE SCOPE AND ORGANISATION OF THE THESIS

The relevance of each chapter to the thesis is discussed below.

CHAPTER TWO introduces a historical review of underwater biotelemetry. It provides a comprehensive literature review of different biotelemetry techniques applicable for both aquatic animals and human swimmers or divers.

CHAPTER THREE discusses the major aspects of acoustic concepts related to biotelemetry in general, and underwater acoustic biotelemetry in particular. It presents a study of the main aspects and the particular considerations involved in the design of an acoustic biotelemetry system. It describes various multichannel multiplexing and data encoding techniques, and discusses their suitability for the current system. It also presents the transmission concepts and performance limitations of digital acoustic telemetry to meet such specifications, leading to the current design philosophy. The chapter outlines the physiological parameters suitable for underwater biotelemetry and the parameters considered for transmission in the present work

CHAPTER FOUR describes the design methodology of an intelligent underwater biotelemetry system, the proposed modular architecture and general system requirements. It also details the hardware and software concepts for the novel microcontroller-based transmitter, which controls the telemetry protocol of each transmission block of the four channels of data. The chapter details the transmitter design as follows:

- Description of the sensor development, interface, signal acquisition, and *in situ* calibration for each channel is presented.
- The telemetry design of a novel interrupt-based multichannel encoding method and the associated software is discussed.
- The algorithms developed for the real time QRS identification and digital pulse encoding transmission (for the continuous ECG transmission channel), together with their microcontroller-based peripheral interface and software functional concepts is presented.
- The design of the output acoustic power amplifier, programmable transmission

oscillators and the channel transmission control interface is presented. The transmitter's waterproof housing and packaging are also shown.

- The procedures for the tests carried out in the departmental tank to characterize the channel's multipath and reverberation effect, and the selection of a suitable transmission frequency and pulse width are further discussed.

CHAPTER FIVE describes the hardware and software design concepts for the microcontroller-based receiver and decoder and discusses the automated portable data logging and P.C.-based ECG monitoring systems. It also describes the experimental tests carried out in the departmental water tank and the results obtained from a freely swimming diver under such a shallow underwater environment.

CHAPTER SIX presents simulation studies and physiological analysis of the heart rate variability for a diver and discusses the results obtained from this study. It also presents a further simulation study of an artificial neural network (ANN) model for the likelihood classification of medical problems associated with SCUBA diving. A simple training Back-Propagation network structure is trained and tested on the network to verify the feasibility of using such networks in biotelemetry systems.

CHAPTER SEVEN presents a discussion and conclusion, and gives suggestions for future work.

CHAPTER TWO

REVIEW OF UNDERWATER BIOTELEMETRY

2.1 INTRODUCTION

Numerous studies have been carried out to develop systems for telemetering physiological data through air (terrestrial telemetry). Most of the biopotentials such as Electrocardiogram (ECG), Electroencephalogram (EEG), Electromyographic (EMG) signals, and other physiological variables such as temperature, respiration, blood pressure etc. have been telemetred during the last three decades from human and animals [1,2,3]. However, the emphasis in recent years has been on the development of sophisticated designs of implanted and miniaturized multichannel radio biotelemetric systems [4,5]. Such telemetry studies provide invaluable information about animals in the wild. For example it allows comparison of ecological and physiological parameters under restrained and unrestrained conditions for different species. It also provides similar information about humans under certain environmental conditions that is otherwise unavailable in experimental data [6,7].

This evolutionary approach in aerial radio frequency (RF) biotelemetry systems was not paralleled with a corresponding advance in underwater acoustic biotelemetry and certainly not for human subjects. This has been due to several constraints, emphasized in the literature, which are mainly due to the problematic nature of the underwater acoustic transmission and reception. The most serious difficulty is to extract the wanted signals from the actual received signals which is complicated by multipath interference. This problem is expounded in detail in later chapters.

Thus, the main aim of this review is to concentrate on the underwater biotelemetry systems used so far and to provide a comprehensive study on the different telemetry techniques applied both on humans and aquatic animals, because of the similarities involved in both applications.

2.2 BIOTELEMETRY SYSTEMS FOR AQUATIC ANIMALS

The first pioneering report on the electrophysiological study of free swimming fish was reported in 1938 [8]. But it was only in the early 1960's that considerable effort was expended on behaviourial and physiological radiotelemetry studies of aquatic animals, such as fish, porpoises, turtles and sharks [9,10].

Since then many electrophysiological studies using radiotelemetry techniques on free swimming fish have been reported [11,12,13,14]. The most common modulation method used was a simple (FM/FM) scheme, with the subcarrier signals modulated separately, and then combined to modulate the main carrier frequency. However, several disadvantages were discovered with these systems, such as small range, minimum battery life and the stability of VHF circuits when encapsulated. In addition, there is the very high attenuation of electromagnetic radiation in sea water. This confines such systems to very low frequencies, short ranges and fresh water telemetry applications.

Acoustic transmission offers the advantages of little transmission loss and propagation absorption for ranges up to several hundred metres. Such telemetry systems encouraged researchers to investigate the different behaviour, physiology and locomotive activities of fish species, and other marine animals in their natural habitats.

Ultrasonic biotelemetry has its beginnings in 1956 [15] and is sometimes referred to as underwater or marine biotelemetry. Ultrasonic transmitters ('Pingers') have been used in a variety of applications for studying the migration, ecology and physiology of aquatic animals such as fish, mammals, reptiles and invertebrates. Some of these studies provided a wide range of data on free ranging-animals, such as behaviourial information (e.g. habitat utilization, energy expenditures), water temperatures, depth, swimming speed and thermal preferences [16,17,18,19,20,21]. Physiological research is another aspect of marine ultrasonic biotelemetry which can provide the critical information on how animals are actually behaving and utilizing their natural habitat. Small ultrasonic tags have been used to measure heart rate activity in large vertebrates [22] and wild brown trout [23]; others have been used to measure changes in the electrical impedance between two electrodes, and transmit activity of a moving part, e.g. heart rate or scaphogathite beat [24]. Electromyograms (EMG) of fish and tail-beat frequency are other bio-electrical activity patterns that are monitored by employing ultrasonic telemetry systems [25,26]. Data obtained from these physiological parameters were correlated with other environmental and field activity factors.

However, to date few reported studies exist about the marine acoustic biotelemetry from several sensors. The behaviourial and environmental data of sharks at sea acquired from multiplexed channels measuring swimming speed, depth, compass heading, ambient light and temperature has been reported to have been acoustically telemetered [28]. The behavioral and environmental factors of salmon and codfish in the sea, and also when contained in a tank have also been monitored by standard acoustic telemetry [29,30].

There remain certain limitations on the use of both ultrasonic and radio telemetry systems in the remote sensing of aquatic animals. The advantages and disadvantages of both methods need to be weighted with respect to the study area of the animal.

Ultrasonic telemetry is well suited for studies in salt water, fresh water with high conductivity and deep water. On the other hand, ultrasonic signals are affected by the presence of macrophytes, algae, raindrops and man-made noise in natural habitats [32]. Also ultrasonic telemetred signals are attenuated by trapped air bubbles, especially in turbulent water and refracted downward by the effect of the thermocline or temperature gradients in warmer waters [33,34]. Radio telemetry, on the other hand, is suited for shallow, low conductivity fresh water, and for turbulent water environments. Provided the low frequency (100 kHz or less) receiving antennas are of small size and do not require contact with water, radiotelemetry is excellent for searching large areas to find highly mobile species (e.g.

salmon) [11,14]. Also, radio signal levels are little affected by the presence of vegetation, algae or thermocline. The disadvantages of radio biotelemetry is that it can not be used in salt water unless the subject or the animal swims or surfaces periodically, and the signal levels are attenuated by increasing depth and conductivity [34,35]. Additionally, the radio signals are deflected by metal objects and by terrain, which adds to its range and depth limitations. Furthermore, with depths greater than 5m and conductivity greater than 400 μS/m, radio telemetry will not work, especially for highly mobile aquatic species. However, in general there exist some common features for both animal biotelemetry transmitters when used in environments for which they are both suited. For example, transmitters of both types could have approximately the same battery life, housing, size, cost and encapsulation.

As a conclusion, the specific physiological, and behaviourial information from fish and other aquatic animals requires acoustic telemetry transmitters to be as miniaturized as possible, to last for as long as possible and to provide long range capability. The advanced level of integrated and hybrid technology nowadays can satisfy the requirements of micro-miniaturization and multichannel automation of marine underwater acoustic biotelemetry. This could bring this branch of biotelemetry in line with advanced aerial biotelemetry. However, there may be more differences than anticipated between fish-tracking technology and that needed for physiological monitoring of divers. The data rates are usually very low in fisheries telemetry, often only a simple 20ms ping once per second for most of the physiological or behaviourial data required. Also the multipath problem in the open sea or less reverberant habitats does not represent a real problem for such low rate transmission.

2.3 BIOTELEMETRY SYSTEMS FOR SWIMMERS AND DIVERS

The first attempts to telemeter and monitor physiological responses of human subjects in relation to their underwater activity, started in the early 1960's with the advent of the space program [1,36]. Since then various biotelemetric methods have been devised for relaying physiological parameters during swimming and diving. The three commonest telemetry methods used were the ultrasonic, electromagnetic and conductive. Considerable effort has been expended on electromagnetic telemetry using very high frequency (VHF) transmitters (up to 100 MHz) to obtain physiological data from competitive swimming subjects [37,38,39]. However, since in fresh water, the velocity and wavelength of electromagnetic radiation is reduced by about nine times, low attenuation can be easily achieved in swimming pools at frequencies up to at least 1MHz [40].

On the other hand, propagation of electromagnetic radiation in salt or chlorinated water is severely affected by the flow of conduction currents, with further reduction of velocity and a very high attenuation rate [41]. This discourages the use of VHF carrier telemetry even in swimming pool applications [42]. Several low frequency (400 kHz) RF telemetry systems with 'inductive loop' techniques were used for telemetering different physiological parameters in swimming pools [42,23,44]. However, these experiments were carried out under controlled and restricted condition dependent on circular wire loops attached to the subject and wound around the diameter of the swimming pool. Additionally, the range of the low frequency wavelength used was limited and the received signal was affected by interference caused from radio broadcasting channels. An alternative method used for underwater biotelemetry has been the conductive method with a frequency modulated current as a carrier [46]. This method, also referred to as the 'current return density' method, has been used earlier for the transmission of the gut temperature from dolphins using a 59 kHz carrier frequency [1], and for the electroencephalographic transmission from SCUBA divers [47].

This method, however, proved to be hazardous, especially when the electrode contacts necessary for the return current transmission presented electrocution paths if the return current density exceeded a certain level. Additionally, the signal could not propagate in air, i.e. when the subject was not immersed completely.

To compromise between the advantages and weaknesses of both approaches, an amphibious ECG telemetry system using a combination of electromagnetic and conductive (return) current transmission in air and water was developed [48]. This system proved viable for transmitting ECG signals from a swimmer in a swimming pool, but it involved a complicated system design in both the transmission and reception circuitry. This limited multichannel implementation using such a technique, where circuit size, weight and power supply are crucial elements in the design. In addition, the system retained the hazardous effect of high return currents into the electrodes attached to the subject, and also involved a cable connection attached to the swimmer that limited the range of transmission.

Most of the earliest studies on the physiological and metabolic responses of SCUBA (*s*elf *c*ontained *u*nderwater *b*reathing *a*pparatus) divers were done largely under controlled conditions, where the subjects where tethered to recording cables in hyperbaric chambers and special tanks [49,50.51]. These studies do not necessarily represent the same combination of environmental conditions that face freely swimming divers, and thus reflect the same physiological responses.

Other studies have been carried out with water proof magnetic tape recorders attached to the diver for recording the cardiac changes and other physiological parameters[52,53]. However, such data can only be examined after the dive, which does not allow observation of the changes in the diver's response in real time.

Although ultrasonic transmission is considered the most suitable method for underwater biotelemetry from freely swimming divers for the reasons explained earlier, especially for greater depths and longer distances. The amount of the reported research work carried out since the 1960's in this context is very limited. ?

Acoustic transmission of the ECG from SCUBA divers in the open sea using a direct FM carrier transmission at 55 kHz was reported during the SeaLab project in the United States [54,55]. Acoustic telemetry has been also used with a group of Hawaiian SCUBA divers equipped with a combination of ECG and respiration transmitters, in order to measure the physiological stress and reflexes they endured while setting fish traps at a depth of 60m [56]. In this method a frequency modulated carrier of 32.8 kHz was used to relay the electrocardiogram and respiration signals in the open ocean. On the receiver side, a manually tunable super-heterodyne system with filters was used to separate the mixed high frequency signal at 455 kHz from the carrier signal. Such receivers were largely dependent on a multipath-free underwater medium.

A similar approach was adopted to develop a simple multichannel acoustic biotelemetry system [57]. In this work each physiological channel was allocated a different transmission carrier frequency. At the receiver end, the output of the hydrophone was applied to four identical super-heterodyne systems to retrieve the carrier signals. Simple gate logic circuits were used for the sampling between the channels, and each channel was sequentially sampled at a rate of 10 times per second. However, no clear results were reported because the transmission circuitry was prone to timing errors and missing sampled data due to the simple logic design involved. In addition, the channel selectivity of the receiver was manually operated, and unsuitable for use in severe multipath environment for retrieving analogue signals such as ECG signals.

It can be seen from this review that although some attempts were carried out for the acoustic transmission in open water, no real progress has been made in recent years to build a miniaturized automated acoustic multichannel underwater acoustic biotelemetry system to overcome the main drawback in shallow underwater channels, namely multipath interference. To achieve this aim it is now possible to accommodate recent advances in microtechnology to realise a versatile programmable telemetry system.

CHAPTER THREE

UNDERWATER ACOUSTIC BIOTELEMETRY DESIGN CONCEPTS

3.1 INTRODUCTION

This chapter presents the main aspects involved in the design and implementation of a digital telemetry system with a reliable detection format and a multipath immune transmission link, particularly for severe multipath environments. It also details the additional limitations imposed for biotelemetry applications. Further, it briefly discusses the various aspects of coding and multiplexing used in radio biotelemetry and their limitations in an underwater environment. The chapter also presents the physiological parameters suitable for underwater biotelemetry and those considered for transmission in the present work.

A study of these aspects and the various trade-offs involved in such applications has led to the design philosophy and development of the present biotelemetry system.

3.2 SYSTEM DESIGN CONSIDERATIONS AND LIMITATIONS

It is essential to consider the limitations involved in the design and implementation of a particular multichannel acoustic biotelemetry system, as envisaged in the present application. First, it is useful to outline the principal aspects involved in the design of a system in a shallow reverberant environment. Secondly, it is worth considering the performance limitations involved in adopting the design principles and transmission formats of a radio biotelemetry system in such an environment. The compromise between the two main design aspects and the general requirements for underwater biotelemetry led to the final design methodology. In general, designing an underwater acoustic telemetry system, it is necessary to partition the problem into two main design aspects:

1. Reliable detection format: this includes the range, operating frequency, acoustic power and other related parameters formulated from sonar equations.

2. A multipath immune communication link: this represents the acoustic transmission format required to overcome the multipath problem in shallow underwater environments and the data encoding and modulation techniques that match the data source and allows detection of the wanted signal (direct path) from multipath reverberations.

Fig.3.1 shows a general representation of a typical underwater acoustic communication system. This consists of the main blocks for an underwater digital data telemetry architecture. In this system, the two design criteria mentioned above are interrelated where the final selection and instrument implementation has to take into consideration all the parameters involved. These will lead to a fundamental trade-off between the various design parameters involved, such as data rate, range, transmission frequency and bandwidth. However, in an underwater biotelemetry design, such limitations are not the only ones that have to be considered. There are additional performance and implementational factors that specify the problem and add further to the complexity of such systems.

The main functional requirements for an underwater multichannel biotelemetry system are:

(i) The design and organization should be flexible enough to accommodate any combination of biopotentials and/or electrically transduced physiological parameters with a minimum of re-engineering effort.

(ii) The ability to acquire as many independent channels as possible.

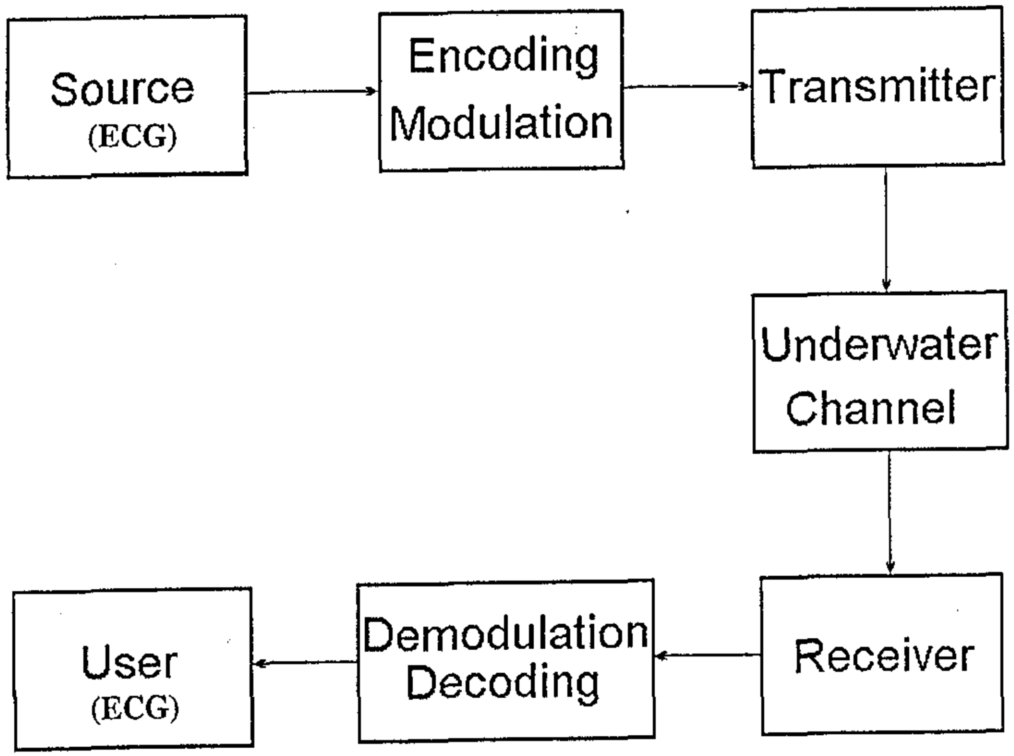

Fig.3.1 Generalised underwater acoustic communication system

(iii) Detection of the appropriately timed, activated physiological events.

(iv) Sufficient electronic sophistication and miniaturization.

(v) Batteries with a life commensurate with the power requirements of the transmitter circuitry.

This section presents a study of all these considerations, together with the different limitations and the other factors which have led to the present modular design philosophy.

3.2.1 Detection and sonar equations

In order to establish the design of the system to satisfy the first criterion it is necessary to examine the different requirements and constraints involved and to group them according to the overall effects of the environment and the performance of acoustic telemetry.
To do this, calculations can be made using standard sonar equations [34,58,59]:

$$SL + DI_T = NL - DI_R + TL + DT \tag{3.1}$$

where

SL is the source level,
DI_T is the transmitter directivity index for a directional source,
TL is the transmission loss between the transmitter and receiver,
NL is the isotropic noise level,
DI_R is the receiver directivity index
DT is the detection threshold (Recognition Differential).

passive

Although the sonar equation (3.1) is derived for an active sonar, many of the parameters are applicable to passive applications and it can be expressed in telemetry applications to represent the present system where the signal travels in one direction and the effects of the ambient noise (rain,ocean surface,shipping) for short ranges is not predominant and can be neglected. Therefore Eq.(3.1) can be modified to represent the present application as:

$$SL = RL + TL \tag{3.2}$$

where RL is the received signal level.

In the following the parameters involved in the sonar equation are briefly explained. The source level is a measure, in dB referenced to 1 μPa, of the power flux (W/m^2) delivered into the water by a source and is always referred to a standard range ($1m$) from the acoustic centre of the source. The source level is related to the acoustic power P_a by:

$$SL = 170.8 + 10logP_a + DI_T \ dB \tag{3.3}$$

For the omnidirectional transducers used here (D1/170, Universal Sonar Ltd., U.K.), the directivity index is zero for both transmission and reception.

A maximum operational range of 100m is assumed for the current system.

The acoustic output power is the product of the electrical Power P_e and the transduction efficiency i.e ($\eta = P_a/P_e$), therefore source level can be written in terms of the electrical power as:

$$SL = 170.8 + 10log(P_e.\eta) \quad dB \ re \ 1 \ \mu Pa \ at \ 1m \tag{3.4}$$

where:

$$P_e = V^2_t \,/\, R_{eq} \tag{3.5}$$

V_t is the rms voltage applied to the transmitting transducer (projector),

R_{eq} is the equivalent resistance of the hydrophone.

This power, conventionally reckoned at 1m from the 'acoustic centre' of the source, is reduced progressively between the projector and the hydrophone by geometrical spreading and frequency dependent absorption. This is described collectively as transmission loss (TL). For short ranges, the power is reduced by spherical spreading as the reciprocal of the square of the range r, i.e $P_a \propto 1/r^2$. This can be represented by:

$$TL = 20logr + \alpha r \qquad (3.6)$$

where α is the absorption coefficient, which is frequency dependent.

Given an absorption coefficient of α = 0.022 dB m^{-1} (22 dB km^{-1}), corresponding to a frequency of 70 kHz used here, the transmission loss is thus given by:

$$TL = 20logr + 0.022r \qquad (3.7)$$

The principal approach in this design criterion is a study of the trade-off between the various requirements and constraints calculated from the above equations leading the best choice.

3.2.1.1 Acoustic propagation in shallow water

In order to justify the use of ultrasonic biotelemetry it is important to identify briefly the propagation and attenuation mechanisms of the acoustic signals and the relevant environmental characteristics associated with the current application.

In general, ultrasonic propagation is well suited for studies in both salt water and fresh water. However, the propagation of ultrasonic signals through water is adversely affected by several variables [34,59-61]:

(i) The decrease in sound intensity due to geometrical spreading.

(ii) The effect of thermal stratification on the range of the acoustic signal. This is because sound travels faster in warm water than in cold water which results in signals being refracted downwards from the warmer water [59].

(iii) The loss due to absorption and the conversion of acoustic energy to heat. Nevertheless, the amount of loss depends upon the frequency of the acoustic signal. This loss is relatively small at low frequencies but rises rapidly with increasing frequency. Over the range of frequencies usually employed in underwater data telemetry applications (20-250 kHz), the loss is expressed as dB/m or dB/km and is approximately proportional to the square of the frequency. For example at 50 kHz the loss due to absorption is of the order of 12 $dBkm^{-1}$, relative to 1 μPa at 1m, whereas the loss is 58 $dBkm^{-1}$ at 500 kHz [60,62]. In practice, it was found that for short to medium ranges up to several hundred metres, any frequency below 200 kHz is suitable. However, if a range of several kilometres is required the frequency must be usually less than 30 kHz.

3.2.1.2 Choice of transmission frequency

The choice of an optimum frequency of propagation in a shallow water environment and in particular for a specific biotelemetry application is difficult. This it because the choice depends crucially on the propagation and attenuation mechanisms and noise characteristics of the water [62]. Thus, the acoustic energy, and hence battery energy, required to achieve a particular range is frequency dependent mainly as a result of absorption.

For the ocean, where absorption and noise are well characterised, the choice is no problem for a given range requirement and a set of receiver characteristics. In fresh shallow water, however, predictions of range can only be approximated and the assumption that the low frequency noise conditions in lakes and rivers are identical to that in ocean is not correct. This is because of lack of comprehensive data on either absorption or noise. In particular, absorption will vary considerably from one body of water to another because of the varying amounts of varying amount of suspended matter which seem to exist even in very clean water [31,32]. Nevertheless, in the present system the transmission frequencies were selected close to the resonant frequency of the available acoustictransducersi.e. 70 kHz; these have a Q of about 4.1. This dictated the available bandwidth at the receiver and the design of a bandlimited receiver. This choice is a suitable compromise between a smaller transducer but larger acoustic output required at high frequencies and the larger transducer but smaller acoustic output at low frequencies.

3.2.1.3 Signal level and range calculations

To select the signalling for an acoustic telemetry system appropriate for a reverberant shallow channel, it is important to calculate the expected receiver level to determine the level of noise masking the detected signal. This will also allow the design of the receiver pre-amplifiers and filters. Also, the limitation of a maximum range of operation is essential if reliable telemetry is required. Once the maximum range is determined, the acoustic source level to achieve it may be calculated from values for receiver sensitivity, the required signal-to-noise ratio and transmission loss.

The expected receiver level is determined by considering the required acoustic output power and the specified range of operation at a given frequency. The design began with the determination of the required transmitter power to achieve a satisfactory signal-to-noise ratio at the receiver for an assumed range of 100m.

For the specified range and the absorption coefficient given at 70 kHz, Eq. (3.7) yields a transmission loss of :

$$TL = 20\ \log(100) + 0.022(100) = 42.2\ \text{dB}$$

A typical response curve from an *in situ* calibration carried out for the used hydrophones used here is shown in Appendix A. It can be seen that each hydrophone has a sensitivity R_s at 70 kHz of -201 dB re 1V μPa^{-1}.

The appropriate electrical parameters here are: an electrical power of 0.4 W, an equivalent hydrophone resistance R_{eq} of 276Ω and an assumed transduction efficiency of 80% i.e. $\eta = P_{ac} / P_e = 0.8$.

Substituting these values in Eqs.(3.5) and (3.4), the expected level of the received signal can be calculated as:

$SL = 170.8 + 10 \log(V^2/R_{eq})$ dB re $1\mu Pa$

hence

$20 \log (Vr/R_s) = 20 \log(Vt) + 104.2$

Substituting for receiver sensitivity (in dB) yields:

$20 \log(Vr/V_t) = -96.8$ dB

From these figures it can be seen that for a transmitter voltage of approximately 30 $V_{p\text{-}p}$ voltage, Vr should be 0.45 $mV_{p\text{-}p}$ at 100m maximum range. Similarly, the expected received voltage at the hydrophone is approximately 60 $mV_{p\text{-}p}$ at a range of 4.5m in the tank.

These calculations show that after a preamplification stage with suitable gain, the predicted signal level at the hydrophone should be easily detectable at the farthest range of the system. However, less gain adjustment is required in the latter case for shorter ranges. This concludes that the restrictive parameters assumed at this stage fulfils the design criteria within the operational requirements.

3.2.2 Acoustic communication channel and biotelemetry transmission format

The effects of the multipath in short-range shallow channels result in a taxing problem that precludes direct application of classical communication techniques. Over the years several telemetry and communication systems have been proposed to overcome the problem of different underwater channel characteristics [63,64]. However, such methods utilise complex configurations and require powerful computational and instrumental capabilities that may not be compatible with biotelemetry requirements.

However, burst transmission reduces the problem and allows a reliable underwater communication link especially in a shallow reverberant channel. The short pulse (burst) transmission is advantageous in cases where it is possible to correctly extract information from the signal simply utilising a transmission pulse interval that is always greater than the reverberation decay time.

The depth/range effect in the severe multipath test environment is illustrated in Fig.3.2 for a typical underwater geometry of the water tank. This shows that an estimate of the time delay between the direct path and a surface reflected signal may be obtained from the geometry of the test location. By assuming that the multipath reflects half way between the transmitter and receiver and that geometrical spreading from the point source is spherical, the time delay τ_d between the direct path and the multipath is given as:

$$\tau_d = \frac{[2\sqrt{\frac{L^2}{4}+h^2}]-L}{c} \qquad (3.8)$$

where

c is the speed of propagation of sound in water (typically 1500 m s^{-1}),

L is the transmitted distance,

h is the depth of the transducers beneath the water surface.

For the test location in the water tank (9m long x 5m wide x 2m deep), if the depth of the transducers below the water surface h was approximately 1m, and the average distance from the transmitter r was 4.5m, then τ_d= 282 μs.

From this analysis it can be seen that the first multipath occurs approximately 280 μs after the direct path. This represents approximately a burst of three bits at a data rate of 10 kbit/s. From the experimental test, it was concluded that the multipath interference in the test tank, was very severe, and nearly of the same magnitude as the direct path signals especially if the water surface is smooth as was the case here. The measured reverberation decay time was in the order of 20 ms for a one-bit burst transmission length of 100 μs. Thus, a high burst

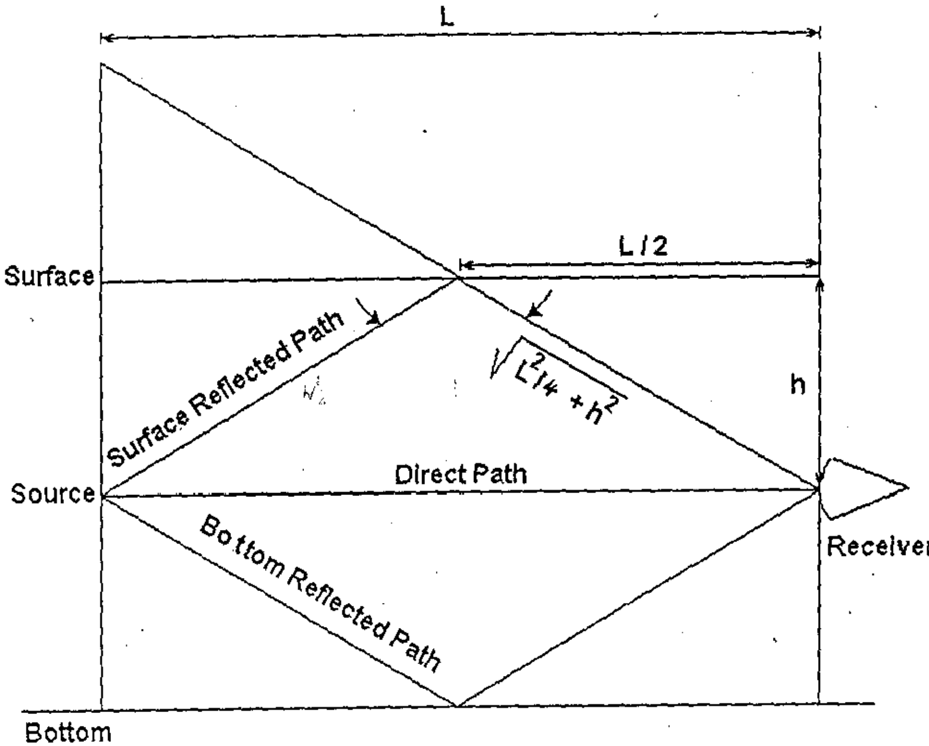

Fig.3.2 Underwater acoustic parasitic path representation

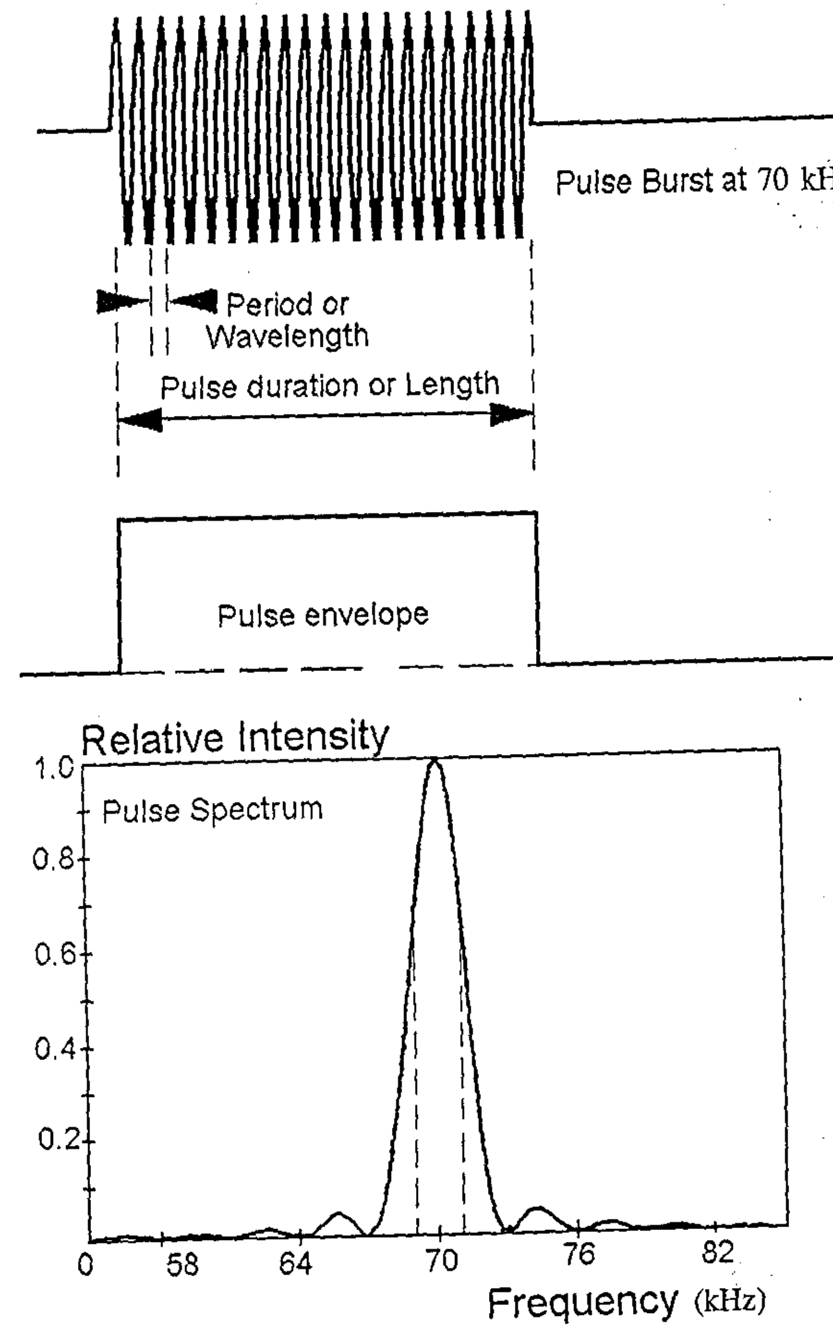

Fig.3.3 illustration of acoustic burst transmission

transmission rate with such small depth-to-range ratio (≤ 0.2) will not make it practical in the receiver to detect and separate the successive main reflections from the multipath reverberations, because of the overlapping of the direct and multipath reflections.

To overcome this problem, the present system utilized a much slower but narrower burst transmission format, with a digitally modulated carrier frequency, that always allows the transmitted pulse interval between the successive bursts to be greater than the reverberation decay time and to allow the reverberations to die away before the next data bit is transmitted.

However, it is also important to mention that the choice of the minimum pulse width also depends on the Q-factor of the transducers used and on the transmission frequency, since the pulsed sonar transmits a short burst consisting of several cycles at the sonar operating frequency.

Fig.3.3 shows a typical illustration of a transmitted pulse with the associated number of pulses. The transmitted pulse width τ is given as [61]:

$$\tau = (N/f_0) \tag{3.9}$$

where N is the number of the cycles at the operating frequency, and f_0 is the operating frequency of the transducer. It can be seen that for a specified pulse width to satisfy this equation the Q-factor of the transducer should be $\leq N$ in order to allow for the built up of the acoustic envelope in the transducer.

From the measured and calculated data in Appendices A and B, N=10, f_0= 68.9 kHz, and Q=4.1. Thus, from Eq.(3.9), τ= 0.145ms. However, the bandwidth of the transmitted pulse must be smaller than the bandwidth of the transmitting transducer to attain maximum power peak transmission and is given as:

$$BW_T = f_0/Q = 69.8/4.1 = 17 \text{ kHz}$$

Hence, $\tau \geq 1/17x10^3 \geq 0.06$ ms.

Considering these limitations, and from the practical tests carried to characterise the multipath problem in the tank, it was shown that the best compromise for burst transmission was as follows: A pulse width of 100 μs with a one bit burst transmission at a maximum rate of approximately 50 bit/s. This was suitable for the current application, and satisfied the measured Q of 4.1 and the transmission frequency of around 70 kHz.

Additionally, a biotelemetry system requires only a slow transmission rate because of the slow rate of change of the physiological signals. For example, the maximum possible heart rate of a healthy person could reach 210 beat/min., the maximum breathing rate is only 15 breath/min.[65], and the maximum calibrated depth pulse rate in the present work is 20 bit/s. Thus, these pulse interval and bit rate characteristics are compatible with the functional requirements of the pulse modulation formats adopted for both the telemetry of parameters such as heart rate and breathing rate and the ECG transmission in the present system.

3.2.3 Data Encoding, Modulation/Demodulation and Decoding

The previous section presented the main acoustic design concepts for digital acoustic biotelemetry over short ranges in a shallow underwater channel. This section outlines the other functional aspects of the system. From the generalized architecture for the system shown in Fig.3.1, the source encoding operation matches the data source bit stream to the modulation and improves the system's reliability by means of coding. The modulation operation on the other hand matches the encoder output to the characteristic of the transmitter and the acoustic underwater channel. The decoding at the receiver inverts the linear operations of the coding to retrieve the transmitted data.

This process can impose severe computational demands, especially for complex encoding methods such as sequential decoding or maximum likelihood Viterbi decoding methods [66,67]. Thus, the use of such computationally demanding methods in this application is not justified. This is essentially on account of the complexity involved in the encoding/coding, which is not compatible with the small size and low power requirements of the transmitter.

Encoding methods have been studied extensively in the digital communication and information theory literature, and a large number of methods and algorithms are available [68-70]. In this thesis, the emphasis will be on data encoding and modulation techniques suitable for acoustic and radio telemetry in general and for underwater acoustic biotelemetry systems in particular.

In conventional radio biotelemetry systems there are many methods of encoding biological data into a RF carrier, both for analogue and digital transmission. In the digital case there is a variety of schemes for source encoding. The most commonly used methods, known as *pulse modulation,* are [2-7]:

(i) Pulse Width Modulation (PWM),
(ii) Pulse Position Modulation (PPM) or Pulse Interval Modulation (PIM),
(iii) Pulse Code Modulation (PCM).

Fig.3.4a shows the binary pulse trains of these three digital encoding techniques. For PWM, the time between the leading edges of the pulses is constant while the width of the pulses varies with the analogue data. For PPM signals, it consists of serial pulses of fixed duration where the sample amplitudes proportionally displace the pulses from a selected time reference. For PCM encoding, it converts each data sample from the periodic analogue-to-digital conversion of the data into a number of pulses (a word) and these pulses represent a digital value to each sample.

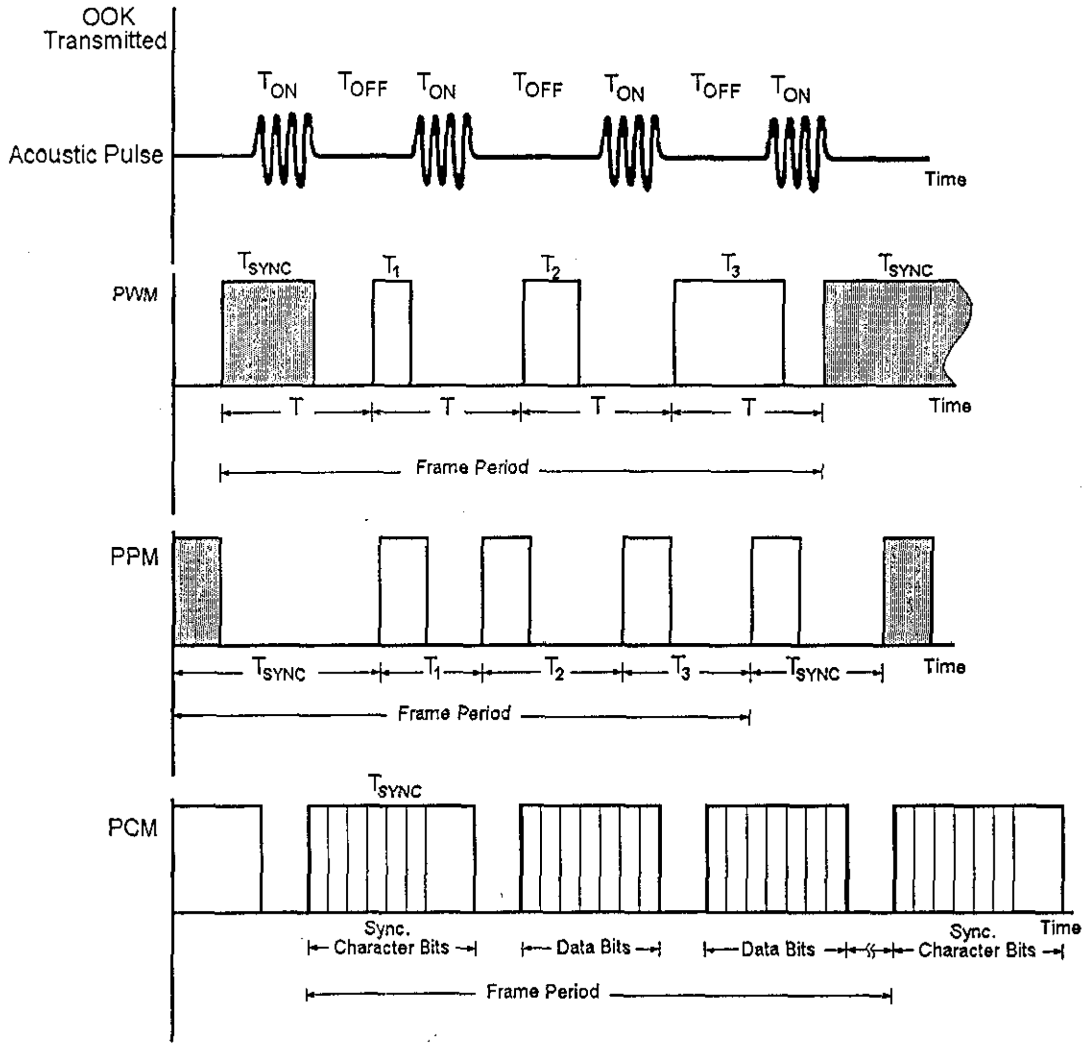

Fig.3.4a Timing diagram of PWM, PPM, and PCM

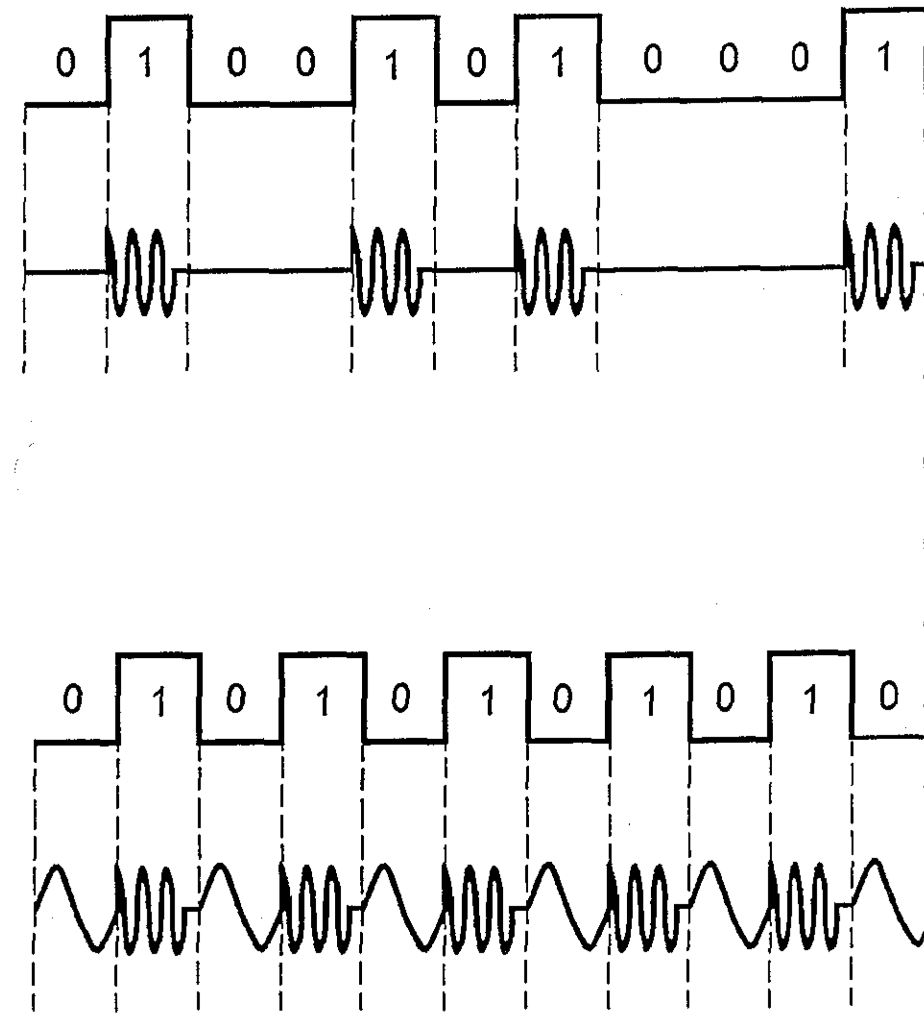

Fig.3.4b Transmission format of OOK and BFSK

Each method has its specific advantages and disadvantages in biotelemetry applications. With the PWM approach, errors can result from transmitted pulse length distortions caused by multipath interference at the receiver; the result is that a sequence of transmitted symbols may be incorrectly detected. Furthermore, more power is required during the (ON) duty-cycle length within the transmitter circuit, i.e. it is less energy efficient.

Although comparatively immune to multipath transmission, PPM is simpler to implement with relatively high accuracy and is energy efficient compared to other formats. But it is susceptible to Doppler effects and is therefore best suited to fixed installation telemetry links. Additionally, a resolution limit can be imposed by errors in the measurement of time intervals between a pair of received pulses and the synchronization gap. This is due to the increased number of coded pulses that cannot be transmitted at intervals less than the time required for the last significant multipath echo to arrive. However, PCM is the most efficient method of encoding data compared with the PWM and PPM. The performance of the PCM is superior to the other techniques as it offers the greatest signal-to-noise ratio of all modulation formats. It is also highly immune to transmission impairment and noise and requires minimum bandwidth [71,72]. But the increase in circuit complexity as compared to the other methods, has limited its application as compared to the PWM and PPM [3,71,72].

In radio biotelemetry, there are two basic methods of modulating the RF carrier with a digital data stream:

(i) Amplitude Modulation (AM);

(ii) Frequency Modulation (FM).

Amplitude modulation is obtained by varying the amplitude of the RF carrier with a modulating signal, in this case a binary pulse train, while keeping the frequency constant. The most common way of doing this is to turn the RF carrier on with the 'ones' of the data stream and off with zeros. This represent 100% amplitude modulation and is known as ON/OFF keying (OOK), as shown in Fig.3.4b. Frequency modulation is obtained by varying the frequency of the RF or acoustic carrier, in this case again a binary pulse train, while keeping the amplitude constant. This is commonly known as the Binary Frequency Shift Keying (BFSK), as shown in Fig.3.4b.

In underwater acoustic telemetry, modulation methods have principally been amplitude shift keying (ASK) and frequency shift keying (FSK), although there has been some recent work on phase and quadrature phase modulation (QPSK) [73]. However, phase modulation of a carrier is impractical in biotelemetry applications for the following reasons:

(i) Signal-to-noise ratios better than 20dB are rarely achieved in such an environment, so there would be very limited dynamic range.

(ii) The fluctuation of non-linear multipath propagation of the acoustic signal produces a combination of signals with randomly varying phase distortions and fluctuations at the hydrophone, largely because of the phase-tracking problem [74]. To overcome this requires a very complex hardware set-up utilizing adaptive tracking and estimation methods.

The FSK approach is a relatively simple, low-performance form of digital modulation and is useful for telemetry transmission of low-rate digital data for up to 1500 bits/s in open water [75,76]. However, this method is still prone to reverberation problems because the constructive and destructive interference of the overlapping signals affect the identification of the binary bits. Also there is a requirement for two carrier frequencies, hence the power required to transmit a data word is high, since every bit requires a separate pulse transmission. This is not compatible with the efficient and limited energy requirements of a biotelemetry system. Demodulation of the FSK signals is also complicated by problems of maintaining time synchronization, as this requires self-synchronization to extract the transmitted codes.

The operation of a binary shift keying (BFSK) modulator in a shallow water environment does not match with the slower bit rate transmission and the minimum bandwidth considerations of BFSK in the receiver. Since binary FSK is a form of frequency modulation, the formula for *modulation index (MI)* used in FM is also valid for BFSK and is given as [70]:

$$MI=\frac{|f_m-f_s|}{f_b} \longrightarrow BR. \tag{3.10}$$

where f_m is the mark frequency of the transmission;

f_s is the space frequency of transmission;

f_b is the input bit rate. (BR)

Now let us consider the present severe multipath channel and the requirements of the system. The mark/space frequencies are 70kHz and 68kHz, dictated by the bandwidth characteristics of the projector and hydrophone, to prevent mutual interleaving in the receiver. Additionally, the minimum bandwidth for BFSK is dependent on the modulation index. Consequently, in BFSK the modulation index is generally kept below 1.0 (between 0.5 and 1.0), so either two or three sets of significant side frequencies are generated.

Thus, for MI = 0.5, Eq.(3.10) yields f_b = 2000 / 0.5 = 4000 bits/s

This bit rate, although considered adequate in open water digital data acoustic telemetry applications, is too high for the bit rate requirements and receiver considerations in a multipath environment.

The difficulties with underwater data transmission using ASK and particularly OOK in reverberant environments have been previously recognized and studied [77,78]. ASK systems are considered simpler to implement and require less hardware for the bit transmission and detection synchronization compared to the other approaches. They also provide several unique interrogation codes depending on the frequency bands and the number of channels. ASK is also more power efficient as it requires a single carrier transmission, making it more suitable for biotelemetry applications. However, the approach is still susceptible to multipath reverberations. Nevertheless, the system performance and reliability can be considerably improved by proper detection design in the receiver and greater transmitter power.

3.2.4 Multiplexing systems

For multichannel biotelemetry applications, there exists two main multiplexing systems [2-7]:

(i) Frequency-division multiplexing:

In frequency-division multiplexing (FDM) each data channel modulates a sinusoidal sub-carrier with a different frequency. To accomplish this, an oscillator with a different frequency band is provided for each sensor as shown in Fig.3.5a. Each of the input signals is sub-modulated by a sub-carrier frequency before modulating the main RF carrier. There are different combinational configurations within this category, such as FM/AM, FM/PM and FM/FM. The most widely used in radio biotelemetry is the FM/FM method. However, this multiplexing format is not practical in an underwater environment because of the FM non-linearities, the unreliability of identifying the data from different channels in the receiver, and the different behaviour of the RF channel from the acoustic channel because of the multipath problem. The amplitude, phase and frequency scintillation, the transmitted signal and the S/N considerations of the sub-carriers caused by multipath interference, make the use of conventional tracking and demodulation methods used in radio systems impractical to detect and to discriminate the complex frequency sub-carrier parameters involved [79].

(ii) Time-division multiplexing:

In time division multiplexing (TDM) several channels of data can be transmitted in a pulse modulation format. It is also the usual method for digital signal multiplexing, whether alone or in conjunction with previous analogue signal multiplexing, as shown in Fig.3.5b. Each of the different signals is sampled at a different time, and then one of the pulse modulation techniques, usually PCM, PPM or PWM, is applied. In TDM multichannel telemetry systems it is important to identify reliably the data from different input channels as it is received. To accomplish that, it is possible to use asynchronous transmission and label each channel with an identifiable *label*, or add synchronization pulses preceding each individual block of

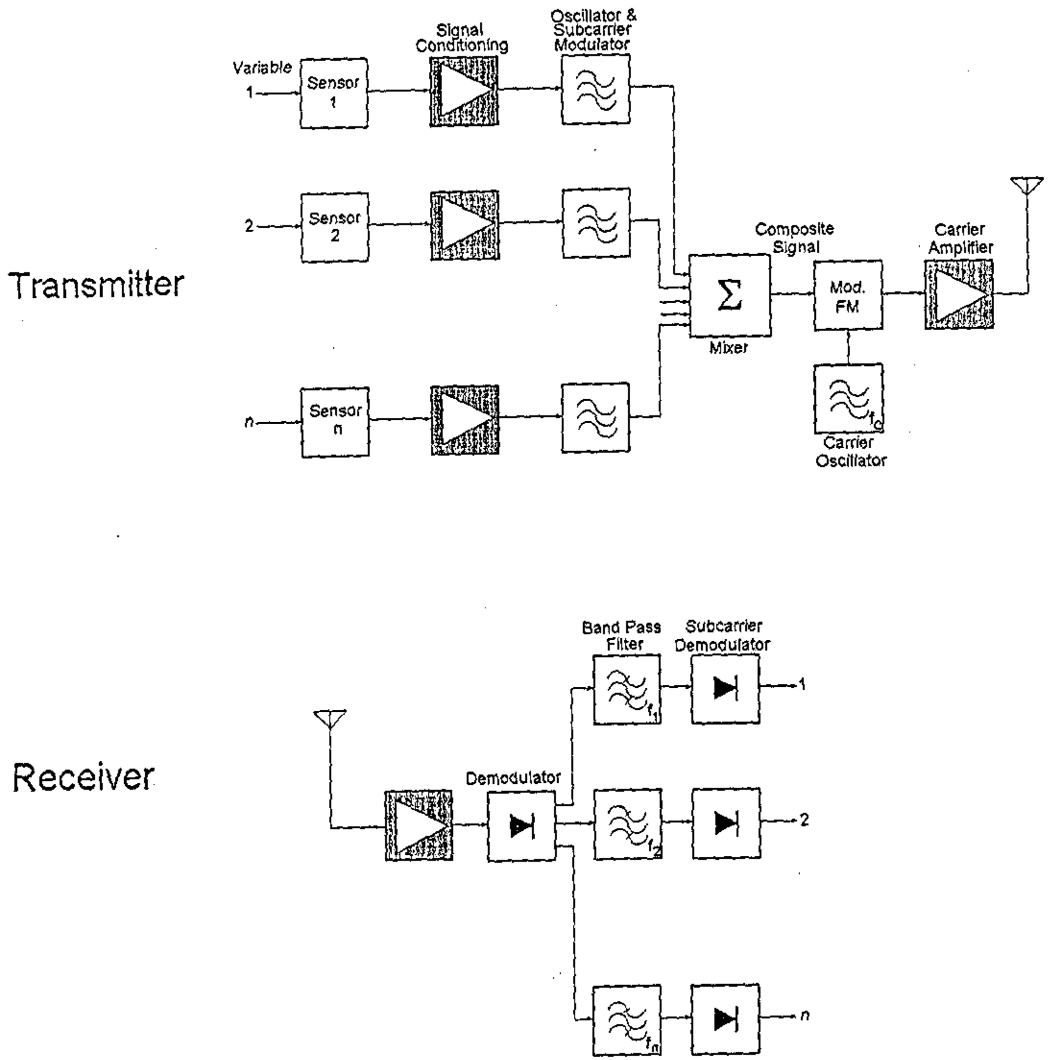

Fig.3.5a Block diagram of frequency-division telemetering system

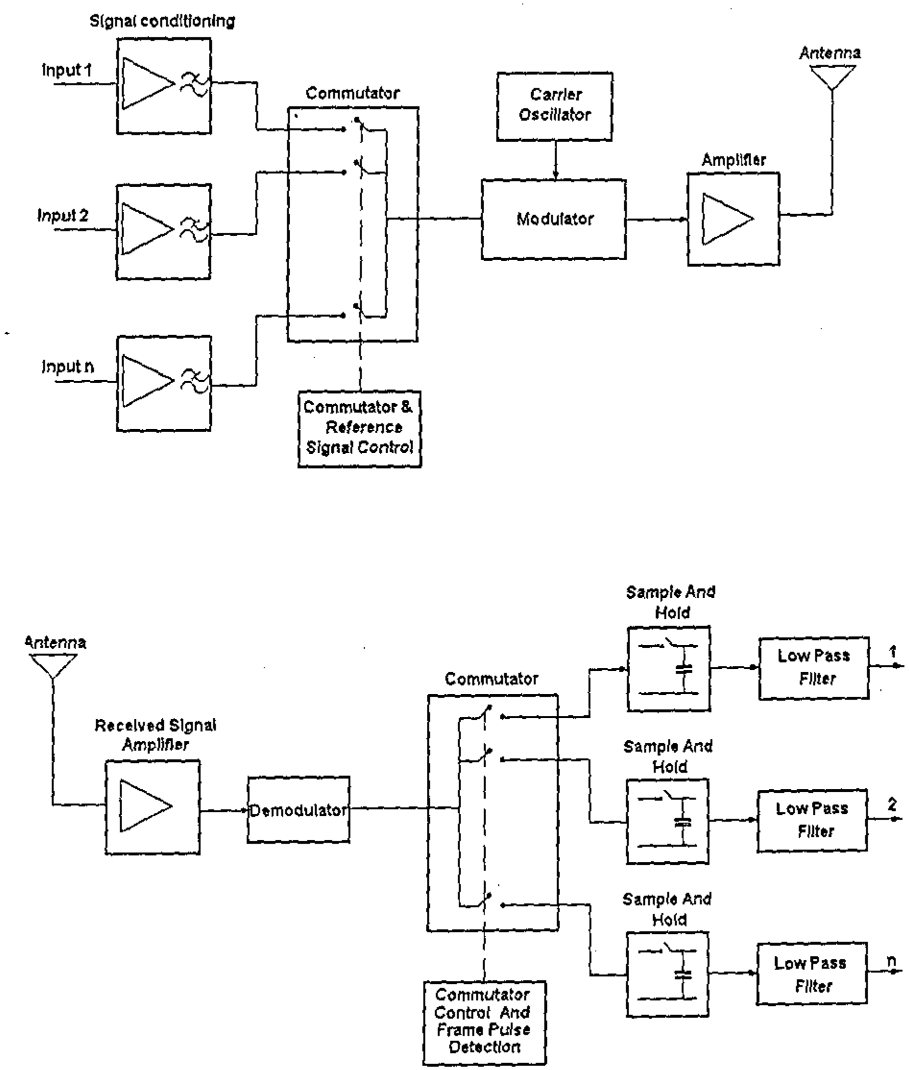

Fig.3.5b Block diagram of time-division telemetering system

transmitted data signals. The hardware in the receiving unit detects the presence of this synchronization pulses and then identifies the different channels with respect to this *label.*

3.3 Physiological parameters adaptable to underwater biotelemetry

Physiological signals suitable for underwater biotelemetry are divided into two types [80-83]:

(i) bioelectrical variables, e.g. electrocardiogram (ECG), electroencephalogram (EEG);

(ii) physiological variables, such as blood pressure, respiration rate and skin temperature.

In addition, certain physiological parameters are of interest, notably depth and water temperature, because these are interrelated with the bioelectrical and physical variables. In (i) the signals are obtained directly in electrical form, whereas in (ii) (with the exception of respiration rate) they are measured as variations of resistance, inductance or capacitance.

Since the early work on underwater biotelemetry, the ECG and heart rate have been considered the most appropriate parameters for underwater transmission. This is mainly due to the clinical importance and the relative simplicity of the transducers and sense electrodes involved. In this thesis, the combination of heart rate, respiration rate and depth were selected because it enables a suitable correlation to be made between the human physiological condition and underwater activity. However, for the detailed classification of sensors and the physiology of bioelectrical events can be found in several biomedical instrumentation references [80-83].

3.4 Concluding remarks

In summary, for the design of a general purpose underwater acoustic biotelemetry system there is no clear-cut way to employ either of the data encoding and/or the modulation and multiplexing techniques discussed in this chapter. This is because, as with many other systems, compromises must be made between the functionality of the design and the reliability, size and power consumption requirements. The flexibility desired can be achieved by software control or simple hardware changes. The new biotelemetry design methodology described in detail in the next chapter conforms to such requirements and adapts a flexible architecture to allow such compromises under different underwater environmental operations.

CHAPTER FOUR

BIOTELEMETRY TRANSMITTER DESIGN METHODOLOGY

4.1 General description and overall biotelemetry system organization

This chapter details the design methodology of a transmitter for an underwater biotelemetry system based on a modular design approach for a set of hardware modules for the transmitted physiological parameters.

Fig.4.1 shows a block diagram of the underwater biotelemetry system architecture;this comprises transmitter and receiver subsystems. These consist of a central microcontroller-based chip in the transmitter and receiver with modular electronic blocks (subsystems) for the different sensor interfaces to the central processor to define the transmitter-receiver protocol under synchronized software control. This configuration meet the acoustic biotelemetry design criteria discussed in Chapter Three and provides a low-cost general purpose platform for fast prototyping. In this work a novel 8-bit single-chip microcontroller serves as the central function and processing unit for the multi-sensor interface and the individual signal conditioning circuits. It multiplexes the outputs and/or encodes the physiological data as appropriate to the user's requirements, and to a format compatible with different underwater environmental considerations. The appropriate communication capabilities and the biotelemetry protocols were determined by examining biopotential data and physiological signals selected for the current application.

The telemetry of pulse rate and depth data is accomplished with a novel inverse data rate interrupt multiplexing hierarchy in which the processor forms a real time interrogator with each biopotential module linked to it. An identically synchronized software and interrupt priority control structure is implemented in the receiver for maximum timing accuracy and minimum transmission error.

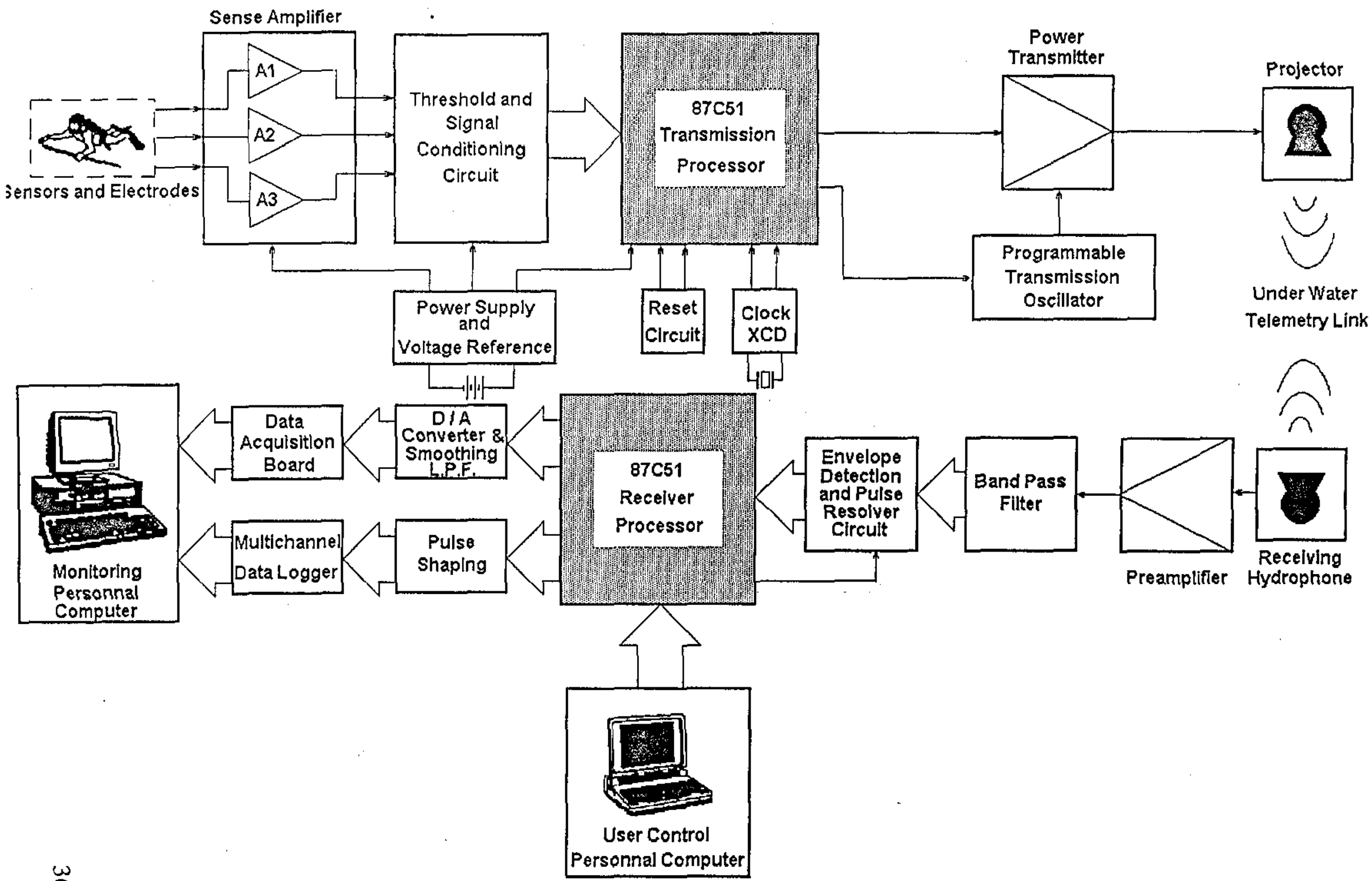

Fig.4.1 Functional block diagram of the underwater biotelemetry system

The telemetry of the analogue ECG signal is achieved by microcontroller-based QRS identification, DPCM/OOK data encoding and transmission algorithms. The same sequence of inverse sample decoding of the received pulses with the appropriate digital-to-analog conversion (DAC) and filtering is implemented in the receiver to retrieve the original transmitted signal.

This flexible interaction of hardware and software with synchronized central microprocessing units in the transmitter and receiver is the novel feature of the intelligent prototype architecture presented in this chapter.

The main emphasis in this chapter is on the detailed hardware design and implementation, together with the software development and testing of the programmable transmitter. This involves the following:

(i) detailed electronics and development of the bioelectrical signals with the pressure (depth) sensing, acquisition and associated signal conditioning circuitry;

(ii) design procedures and development of an efficient power amplifier for a transmitting transducer compatible with the power circuitry;

(iii) details of the multiplexing and interrupt-based hierarchy developed for multichannel transmission;

(iv) for the ECG transmission channel, the hardware and the software for the QRS feature extraction algorithm, the DPCM data encoding and on/off keying (OOK) transmission;

(v) description of the waterproof housing and attachment of the transmitter to the diver;

(vi) description of the underwater pulse transmission and testing procedures in the tank to characterize the required transmission format and pulse width in such a severe shallow multipath environment.

4.2 Transmitter hardware design and realization

The detailed transmitter hardware design philosophy is presented here as applied to the complete programmable automated underwater biotelemetry system.

4.2.1 Bioelectrical and pressure acquisition sensors and signal interface modules

4.2.1.1 Heart Rate and ECG module

4.2.1.1.1 ECG signal characteristics

The *electrocardiogram* (ECG or EKG) is a graphical recording or display of the time-variant voltages produced by the myocardium during the cardiac cycle. Fig.4.2 shows the basic waveform of the normal electrocardiogram with typical durations of the important ECG parameters [80,81,83]. The normal heart rate value considered by cardiologist in his usual diagnosis lies in the range of 60 to 100 beats per minute. A slower rate than this is called *bradycardia* (slow rate) and a higher rate, *tachycardia* (fast rate). The first pulse, called the 'P' wave, is generated by the pacemaker node in the heart. The next pulse, called the 'QRS' complex, represents the electrical signal generated by the ventricles contracting. The 'T' wave which follows the QRS complex is generated by the muscles of the ventricles as they relax, or repolarize. A detailed discussion of the biology of the cardiac cycle, its constituent patterns and the pathological conditions associated with the excitation in the heart is beyond the scope of this thesis and can be found in several medical and physiology texts [83,84]. The signal processing problem and bandwidth considerations for the ECG signal detection depends mainly on the different electrocardiography applications. These can be categorized into three main applications [80,81,83]:

1. The direct clinical recording used for the standard 12-lead ECG, and Holter tape analysis where the bandwidth required is 0.05-100 Hz.

2. In ambulatory and pathological patient monitoring applications such as in intensive care units, the bandwidth is restricted to 0.5-50 Hz. In these environments, rhythm

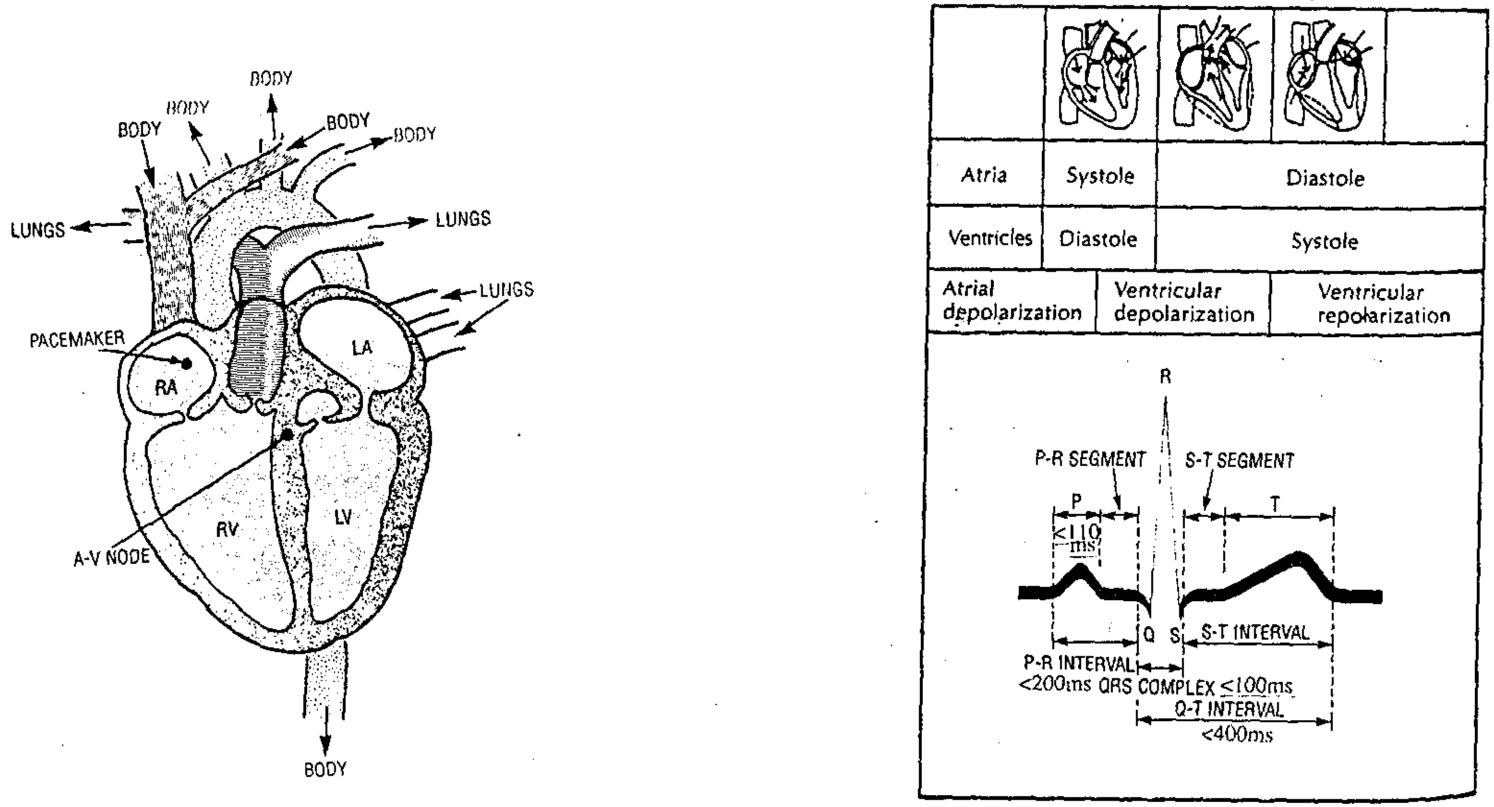

Fig4.2 Typical electrocardiogram with associated timing of the cardiac events

disturbances (arrhythmias) are principally of interest rather than subtle morphological changes in the signal.

3. In many non-pathological studies of circulatory physiology and telemetry applications, it is necessary to convert the electrocardiograms into a number of event processes, i.e. detecting the P-waves and the QRS complexes in particular as a measure of the heart rate variability (HRV). Some departure from the clinically recommended diagnostic quality in respect of the frequency response is customary, when monitoring active subjects or operating under severe environmental conditions such as underwater.

The bandwidth here maximizes the signal-to-noise ratio for detecting the QRS complex within the normal bandwidth of 0.5-50 Hz. Such a restricted bandwidth attenuates the higher frequency noise caused by muscle contractions and the lower frequency noise caused by motion of the electrodes (baseline changes) due to subject movement. In this application the detection accuracy is high but to some extent depends on the appearance of the filtered signal.

Fig.4.3 shows the typical power spectra of the ECG, QRS signals and the other noise sources [85]. From this it can be seen that the QRS power is centred in region the 2-20 Hz band with a maximum at about 10-12 Hz. This provides useful information about the QRS complex and the design of the effective optimal filters. However, the ECG spectrum may vary as a function of the morphology of the signal. The muscle noise is non-uniformly distributed and subject to a large degree of variability depending on the level of the contraction force and on location of the electrodes. It has been observed experimentally that an increasing contraction level produces significant frequency shifts in the characteristic low-frequency peaks (2-10 Hz range). The presence of muscle fatigue also induce changes in the spectral distribution.

However, for practical situations and exercise regimes such as the current application, it is important to design a filter that permits an accurate estimate of the QRS-complexes and their occurrence times and satisfies the practical limitations associated with the recordings under such circumstances.

The peak amplitude of an ECG signal is usually about 1mV. Thus, an ECG amplifier with

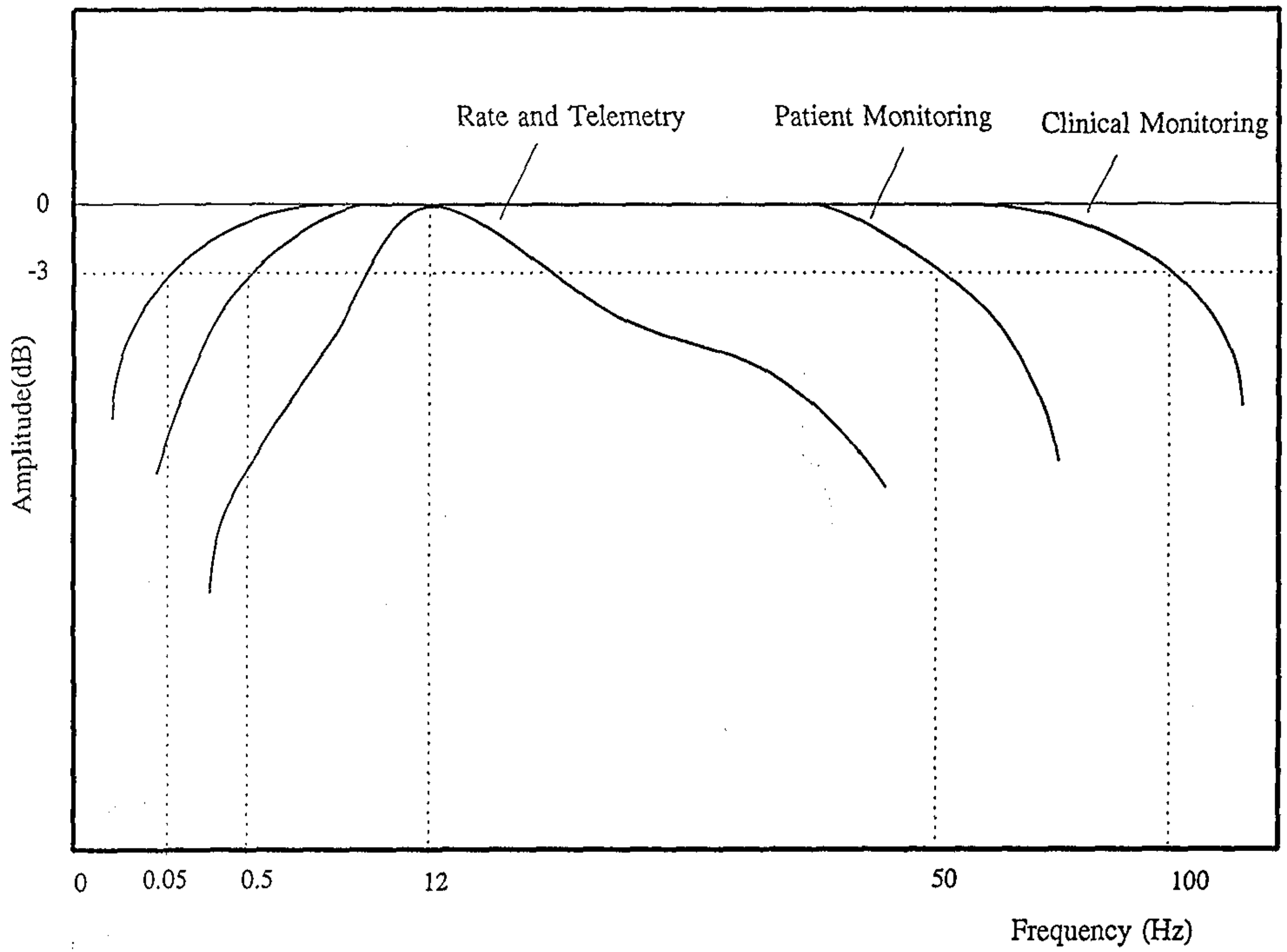

Fig.4.3 Typical bandwidths used in electrocardiography

high gain (about 1000), with typical 0.05-100 Hz frequency response, high input impedance, and low output impedance is required to bring the peak signal into a range of about 1 V for further processing.

4.2.1.1.2 Artifacts and practical considerations concerning exercise ECG telemetry

In clinical applications and under normal conditions, several standard electrode sites are usually used for the ECG recording [80,81,83]. However, in ambulatory recording and in biotelemetry applications it is desirable to have as few electrodes as possible in order to reduce noise and minimize the number of attachments. A typical monitoring configuration uses two active electrodes as differential inputs to the amplifier and a third common or ground electrode [86]. This technique is almost universally used because differential amplifiers can be designed with a high common-mode rejection ratio (CMRR) and high input impedance to provide high level of noise immunity and thereby maintain satisfactory ECG monitoring.

Electrocardiographic (ECG) signals, as for any ambulatory electrical signal, may be corrupted and are prone to various kinds of noise sources. Several practical difficulties are encountered in ECG detection and electrode positioning since the ECG amplitude can vary when the electrodes on the sternum are moved as little as 2-3 cm [80,81]. Additionally, the telemetry of the ECG and heart rate signals applied for further remote examination and clinical interpretations depends strongly on a clear, noise-free ECG recording in the absence of interference associated with the heart contraction. Proper skin and electrode preparations are necessary to prevent ingress of water to the electrodes that could attenuate the signal by the shunting effect of the water leakage path. However, for a diver wearing a dry suit, isolating the electrodes by water-proof surgical tape allows optimum skin contact. This preparation allows a satisfactory recording and diagnostically interpretable ECG during exercise.

The various types of the noise sources, and how these should be rejected or minimized, are important factors to be considered in the ECG transmitter design. In general, there are three major sources of noise in a typical ECG signal which may be summarized as:

(i) *Electrical interference*

Electrical (power) line interference induced on ECG signals has two forms: electrostatic and electromagnetically induced pick-up [87]. The 50/60 Hz and RF interference are the predominant forms of mains supplied electrical interference. The 50/60 Hz interference is eliminated in our design by using a battery as the DC power supply source. The other form of electrical interference can be eliminated by proper ECG amplifier design, such as using micropower high common mode rejection ratio (CMRR) amplifiers in order to reduce the interference noise due to the common mode voltage usually inherent in the ECG amplification circuitry [88].

(ii) *Mechanical interference*

Such interference is mainly caused by two noise sources:

A. *Electrode contact noise*: This is the major mechanically induced artifact, and is due to the contact between the electrode and the skin. It effectively disconnects the measurement system from the subject. The loss can be permanent or intermittent, and is mainly caused by a loose electrode and the movements of the subject. This switching action can result in large artifacts, since the ECG signal is capacitively coupled to the transmitter system.

B. *Motion artifacts*: These transient (but not step) baseline changes are caused by changes in the electrode-skin impedance with electrode motion, and are assumed to be due to the vibration and movement of the subject. Mechanical interference is very significant in biotelemetry applications, especially in underwater systems, but can be reduced by proper electrode attachment and skin preparation [89].

In summary the mechanical artifacts can be particularly minimized by the following steps:

(1) protecting the transmitter by enclosing it in a special water-proof housing.

(2) careful insulation of the electrodes and the connecting cables and maintaining a low resistance path between the chassis and the electrodes, i.e. making the cable connections as short as possible.

(iii) *Physiological interference*

Noise interference, which is physiological in origin, manifests itself in two forms:

muscle contractions and respiration-induced baseline drift.

A. *Muscle contractions (EMG)*: Muscle tremor noise and contractions cause artificial level potentials to be generated. The baseline electromyogram is usually in the microvolt range and therefore is usually insignificant.

B. *Respiration-induced baseline drift*: Such drift can be represented as a sinusoidal component at the frequency of respiration added to the ECG signal.

For all these artifacts, the high frequency (0-1 kHz) muscle tremor noise and low frequency (0.15-0.3 Hz) baseline wander can be minimized by proper electrode positioning and skin preparation and by proper filter design [81,89].

4.2.1.1.3 Instrumentation design of high resolution QRS and R-R wave detector

In order to fulfil the ECG and heart rate telemetry requirements, compatibility with the different transmission formats (digital or analogue) is necessary. A high resolution and versatile QRS and R-R detection processor was designed to meet these requirements. The general arrangement of the circuit used to extract the QRS complex and the R-R triggering intervals is shown Fig.4.4. The major design considerations are:

(i) Use of an efficient low-noise ECG amplifier with sufficient gain of the input stage to reduce the noise contribution of succeeding stages to a negligible level;

(ii) Effective analogue band pass filtering with a bandwidth narrow enough to isolate the predominant QRS complex centred at about 10-12 Hz and attenuate the low and high frequencies of the baseline drift, electromyographic noise and other interference noise sources.

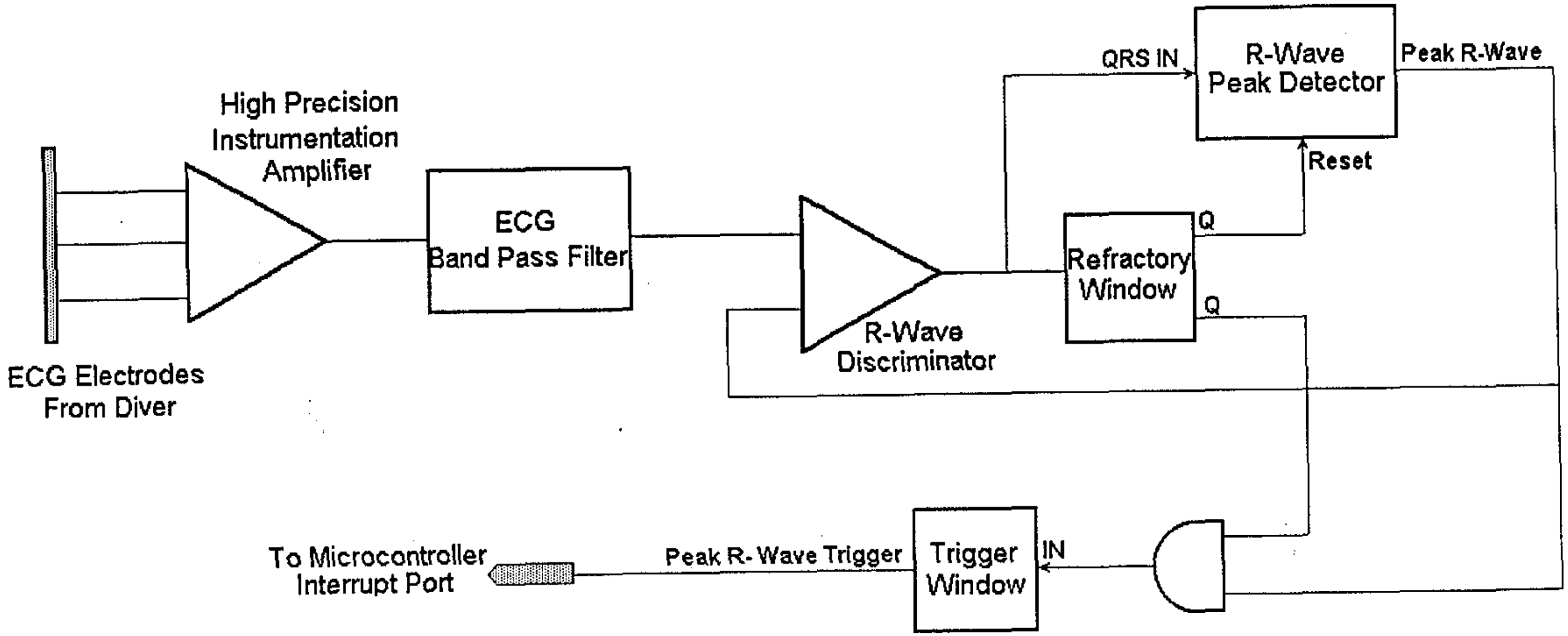

Fig.4.4 Block diagram of the ECG amplifier and R-wave high resolution preprocessor

(iii) Large range of gain adjustments for subsequent processing steps;

(iv) High resolution determination or the peak R-R intervals based on peak detection, threshold detection and time windowing circuits.

4.2.1.1.4 ECG amplifier and QRS filtering stages

The main requirements of the ECG amplifier are the gain and frequency response. It must provide a high gain (1000 or more) and it must be an AC amplifier. The reason for this requirement is that metallic electrodes used in this work (such as Ag-AgCl) are applied to the electrolytic skin and produce a DC potential. This potential tends to be of the order of 1 to 2 V, so it is more than 1000 times higher than the signal voltage. By making the amplifier respond only to AC, we eliminate the artifact caused by the DC potential. Thus, the basic configuration of the amplifier must be an AC-coupled instrumentation amplifier with high input impedance, DC suppression and high CMRR with excellent noise performance.

The frequency selected for the -3dB point of the ECG amplifier must be very low, close to DC, because the standard ECG signal waveform contains very low frequency components as shown in Fig.4.3. ECG amplifiers normally use 0.05-40 Hz to eliminate muscle artifact and lurching effects due to movements and possibly the effect of the electrode water leakage. However, wearing a dry suit and keeping the electrodes away from water eliminate this effect.

Several analogue designs have been reported on the ECG amplification for ambulatory and patient monitoring [86,90]. These are not suitable for the current application due to the complexity, multi-chip operation, inherent circuit noise and power consumption. However, recently developed integrated circuit instrumentation amplifiers allow an approach to ideal operation.

The present design uses the (INA-101, Burr-Brown) high precision instrumentation amplifier. This monolithic one-chip amplifier combines all the required stages of integrated circuitry with low noise (13nV/Hz at f_0 =1 kHz), high CMRR (106 dB min. at 60 Hz) and input impedance of $10^{10}\Omega$ with very low power consumption suitable for battery operated circuits.

Fig.4.5 shows the circuit diagram of the ECG instrumentation amplifier and the QRS filtering stages, together with the three chest electrodes (V1,V2, and V0). A potentiometer is used to null the DC offset voltages common in ECG appearing at the output at a time when it should be zero (i.e., when V1 = V2, so that V1-V2=0). The gain of the circuit is set to approximately 1000 by:

$$A_{vd} = (40\ k\Omega/R_g) + 1 \qquad (4.1)$$

where R_g is the external gain potentiometer, and the 40 kΩ represents the internally set gain resistances of 20 kΩ each that determines the gain of the amplifier according to Eq.4.1.

This stage is followed by a multi-stage analogue band pass filter comprising four alternately cascaded second-order Butterworth low-pass and high-pass filters with different rolloff characteristics, as shown in Fig.4.5. The -3 dB bandwidth of each low-pass and high-pass filter was adjusted to produce the required narrow band pass with a centre frequency at about 12 Hz and a nominal bandwidth of about ± 8 Hz. The filters were implemented using a quad micropower, low noise op-amp (type LM324) suitable for battery operated applications. Experimental tests on the circuit have shown that such cascaded band pass filtering is required to suppress base line drift due to the changing electrode impedance and respiration noise (about 0.2 Hz) and muscle tremor noise (up to 1 kHz). The Q value of the band pass filter determines how well the signal of interest is passed without being sharply attenuated. The Q the filter is given as:

$$Q_{fil} = f_c / B.W. \qquad (4.2)$$

where f_c is the centre frequency and $B.W.$ is the signal bandwidth.

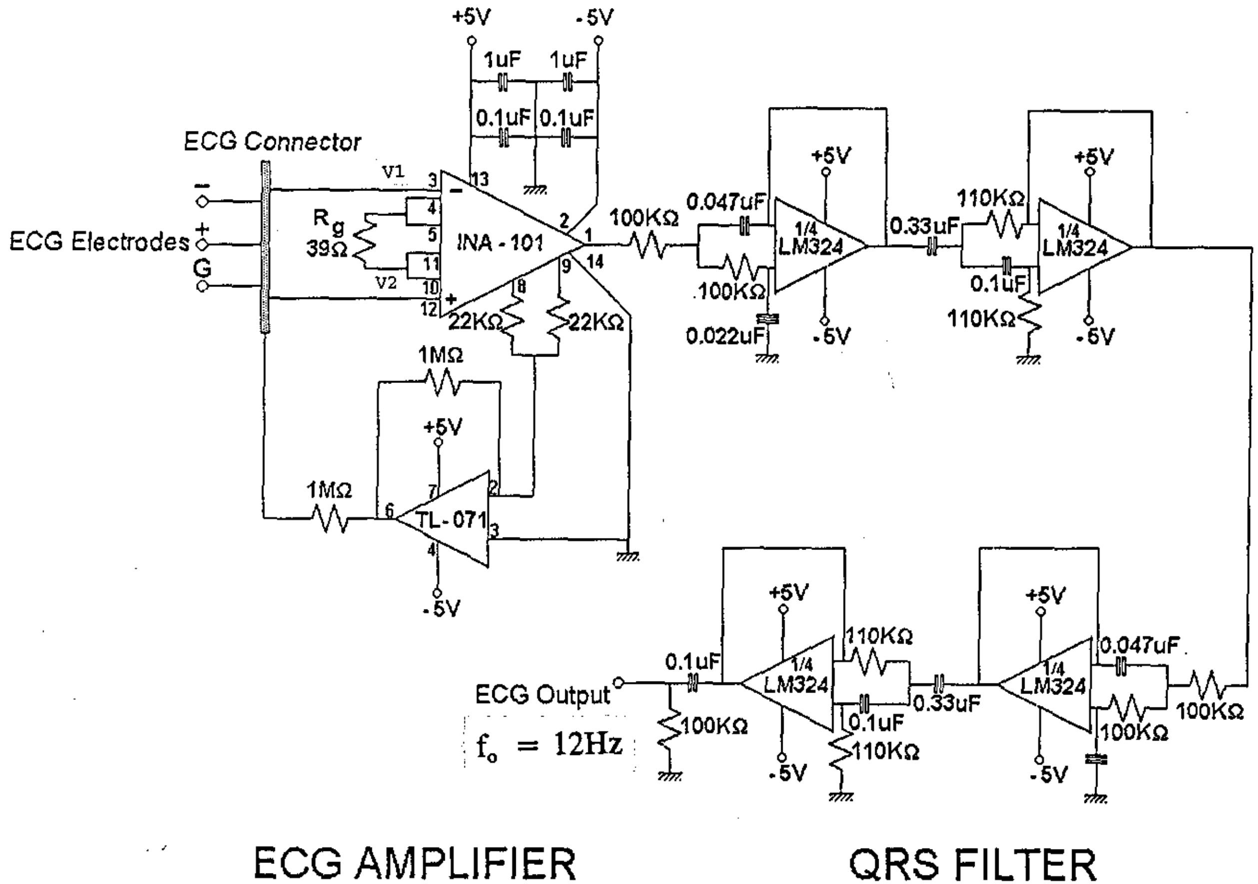

Fig.4.5 Schematic diagram of the ECG amplifier and QRS filtering stages

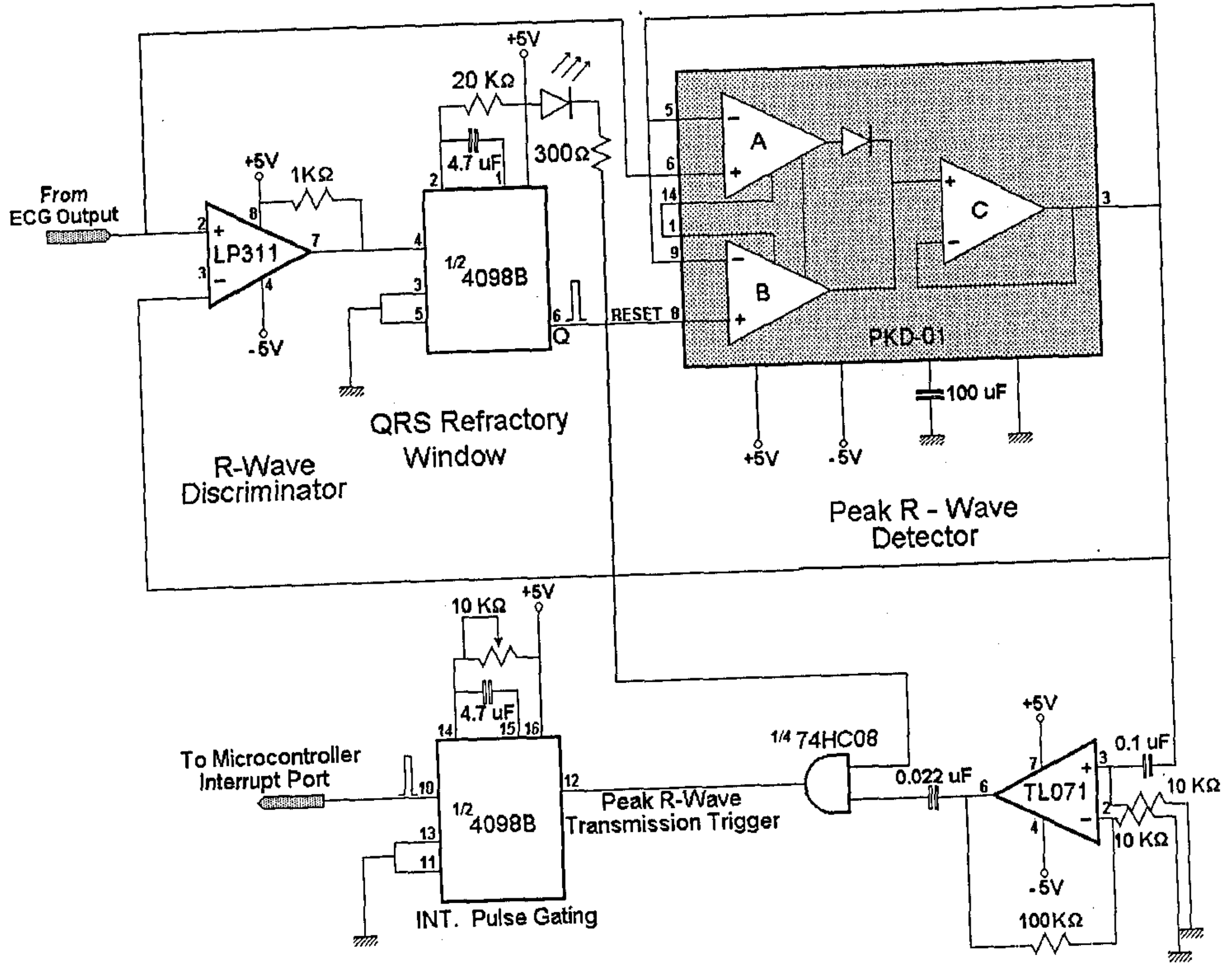

Fig.4.6 Schematic diagram of the peak R-wave high resolution preprocessor

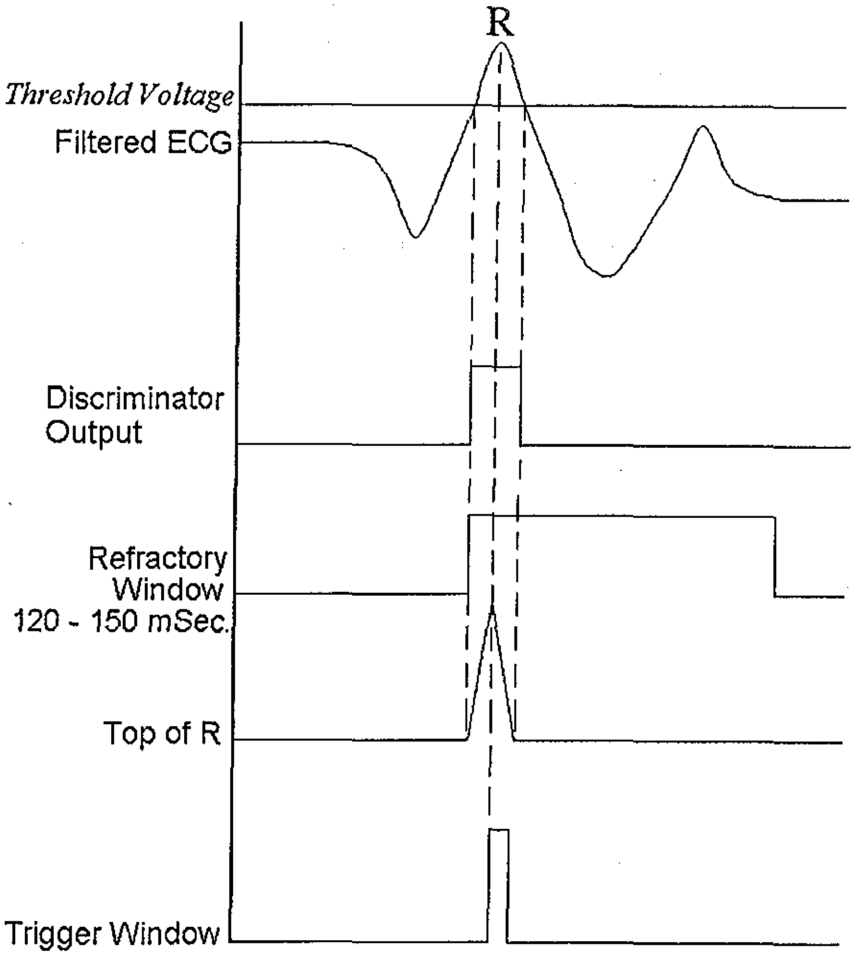

Fig.4.7 Timing diagram of the peak R-wave preprocessor

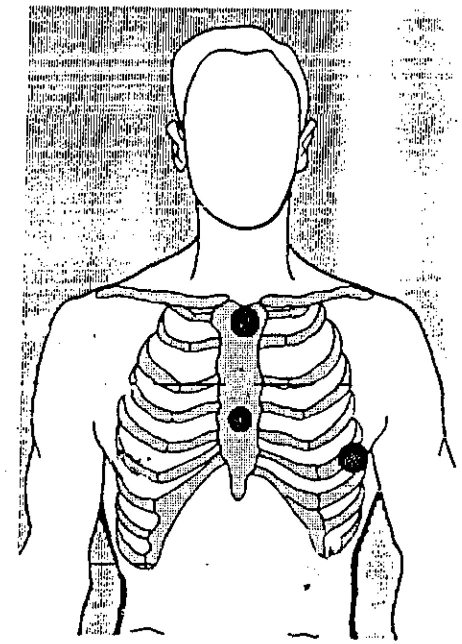

Fig.4.8 Typical ECG electrode positioning on the chest on a diver

However, a high value of Q_{fil} results in a very transient oscillatory response with a centre frequency of 12 Hz, the Q_{fil} value of 1.5 was found experimentally to maximize the signal-to-noise ratio for the QRS complex.

4.2.1.1.5 High resolution R-wave peak detection circuit

The ECG signal from the QRS filter is passed to a high resolution R-R wave pre-processor, shown in Fig.4.6, whose operation is described with reference to the timing diagram Fig.4.7.

First, the filtered ECG signal is detected by a comparator circuit (LP311). The proportional baseline threshold for the discriminator is set by two potentiometers. As the discriminator is based on a proportionality principle relative to the R-wave, a wide range of amplitudes of the QRS can be detected, ranging from 200mV to 1.2V. The leading edge of the high output of the discriminator triggers a monostable (CD4098) to produce a 120-150 ms QRS pulse representing a refractory period containing the R-wave peak. The width of this window may be adjusted to eliminate the possibility of false detection such as multiple triggering on the same QRS complex. Simultaneously, the leading edge of this window also triggers a monolithic high precision peak detector (PKD01), which is fed directly from the filtered ECG signal. This ensures that only the R-wave peak of the QRS complex is detected during the refractory period, and only if the last peak detected is the highest peak. The gated output peak triggers a monostable (CD4098) and provides a peak pulse (100-300 μs) required for triggering the specified interrupt port of the microcontroller chip connected to this output.

The accuracy of the circuit was tested initially on a simulated signal representing an ECG signal consisting of truncated triangular waves of 30 ms with different periods from 200 ms to 1s durations. The maximum period error observed never exceeded 0.1 ms. The circuit was also tested in the laboratory on a subject doing continuous exercise to study the circuit's response with the artifacts caused by electrode motion and respiration.

The heart activity is detected by commercially available silver-silver chloride electrodes (type 2239-3M) stuck on to the chest; three electrodes were used, connected to the circuit by special

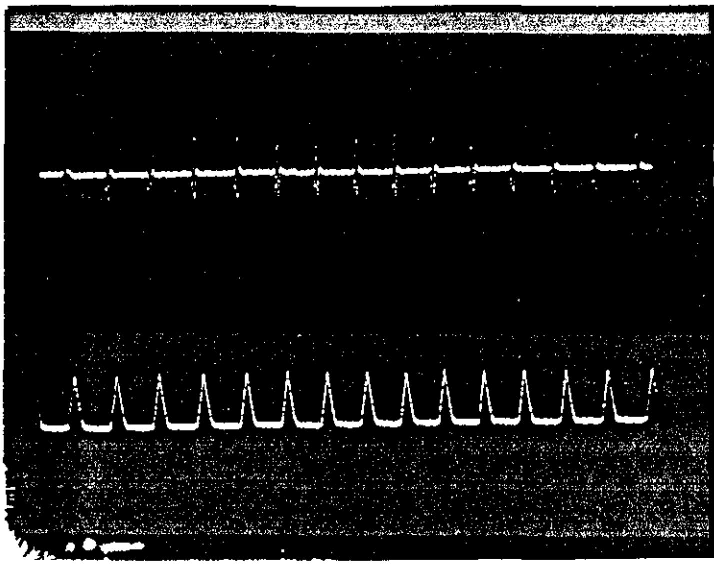

Fig.4.9 Oscillogram of the filtered ECG signal and the corresponding R-R waves

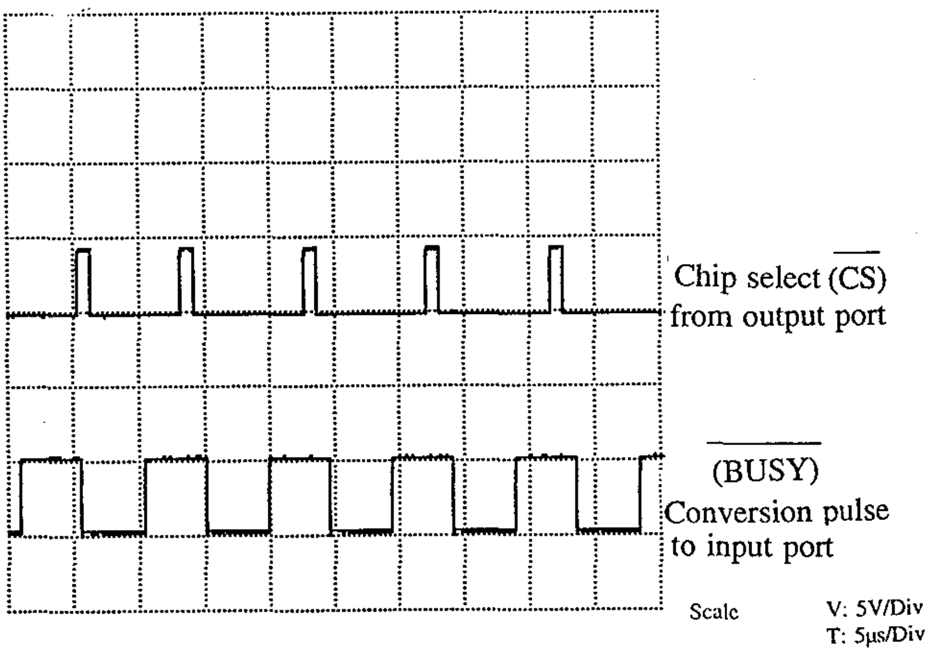

Fig.4.11 ECG A/D conversion and timing interface pulses

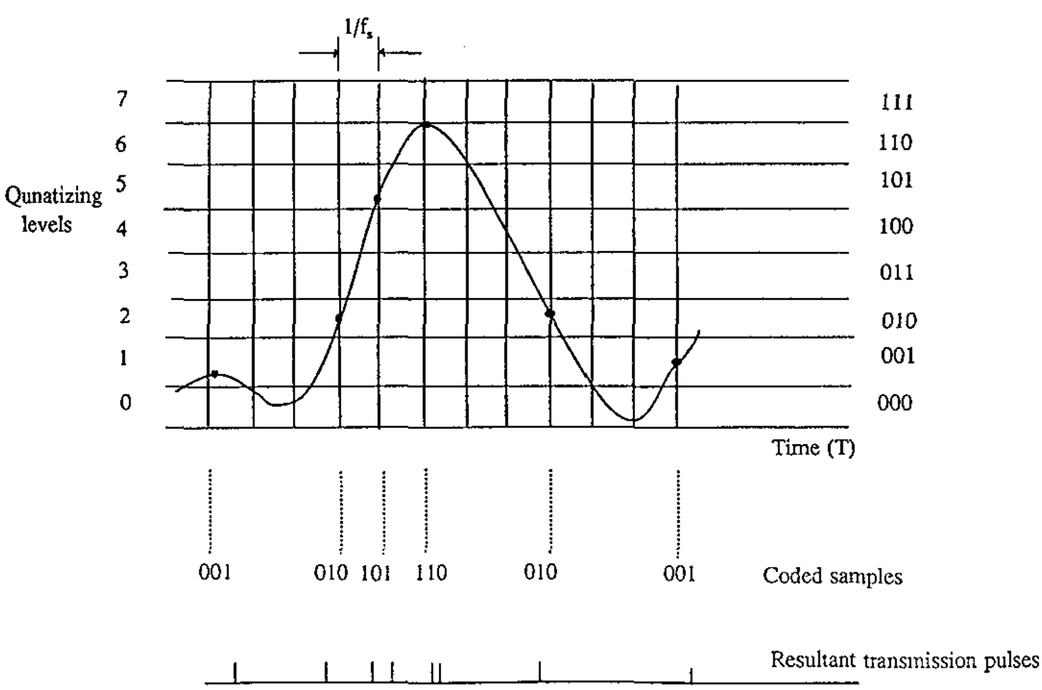

Fig4.12 ECG sampling and Quantizing effects

connectors (3M) mounted through a cylindrical underwater pressure proof cavity cover that will be explained later in the chapter.

The diver's dry suit protects the electrodes from water and surgical tape provides additional protection from body sweating. The most suitable electrode positions for producing a strong QRS complex were found to be as follows: near the top of sternum, i.e. an inch or so below the point at which the chin touches the chest; about four inches below the subject's left arm-pit (on the third rib); near the bottom of the sternum. The first two electrodes are the sensing points and the third is the ground (common electrode), to create a neutral ground and stabilize the signal. These positions are illustrated in Fig.4.8. The placements have allowed successful R-R wave peak detection. Fig.4.9 shows an oscillogram of the filtered ECG signal acquired from a test subject and the corresponding R-R peak waves from the pre-processor circuit. This circuit provides both an accurate determination of the R-R interval required for the precise triggering of the heart rate telemetry transmission, and the direct ECG output transmission.

4.2.1.1.6 ECG sampling and input interface concepts

The raw ECG signal from the skin electrodes is amplified and band-pass filtered using the same preprocessing hardware used for heart rate transmission. The module was designed to retain the quality of the resultant signal and to retain adequate accuracy for ECG telemetry.

(i) *Sampling rate and bit level consideration:*

The sampling rate and quantizing accuracy for the analogue-to digital conversion (A/D) of the ECG signal are very important aspects in the digital processing and the telemetry of the sampled data. The required sampling rate for the elimination of aliasing is dependent on the quantization level, ECG information bandwidth and the filtering used. It can be shown that the minimum required ECG sampling rate (f_s) to avoid spectral overfold must be [91,92,93]:

$f_s \geq 2.2 f_{LP}$

$$f_s \geq 2 f_F \left[\log^{-1} \left[(6n - K_{ECG} \log(f_F/f_{ECG}) / K_{ECG} + K_F \right] \right] \tag{4.3}$$

where

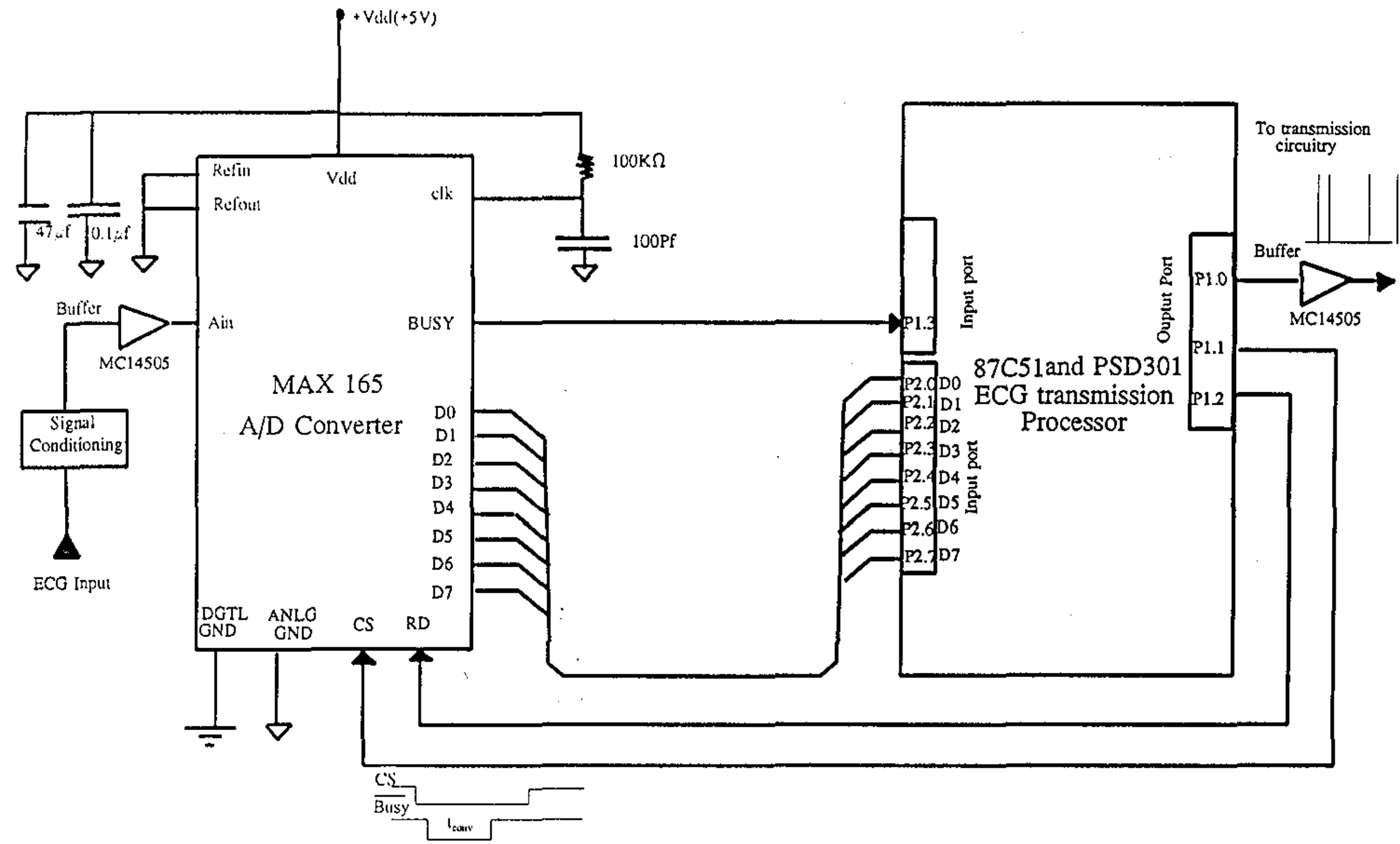

Fig.4.10 Schematic diagram of the ECG sampling and the microcontroller interface circuitry

f_F = The 3dB filter's high cut-off frequency (20Hz),

f_{ECG} = The break frequency of the final slope of the ECG spectrum (usually approximated at 60 Hz),

K_{ECG} = The high frequency roll-off (dB/decade) of the f_{ECG} spectrum beyond 60 Hz (usually estimated as 20 dB/decade)

K_F = The slope value applied to the ECG filter in dB/decade (6 dB/decade for the Butterworth filter used),

n = number of bits

Substituting the filter design and estimated values from [92,93] in equation 4.3 yields a minimum sampling rate of $f_s \geq 116$ Hz. A sampling rate of 200 samples per second, with a resolution of eight bits, because this rate is generally considered most appropriate for a wide range of clinical electrocardiogram data processing applications [91]. It also is sufficient for all the QRS information to be accurately reproduced considering the filter's centre frequency of 12 Hz, the nominal bandwidth ± 8 Hz and the memory capacity of the processor.

It is also known that increasing the number of bits used to represent an amplitude (12 or 16-bit) increases the amount of binary information that must be stored [91]. If an excessively high sampling rate is used, an enormous amount of data will be collected that must be stored in the limited RAM area of the processor. This in turn will require large memory expansion which will not be practical in this case in terms of size and power consumption. Fig.4.10 shows a schematic diagram of the A/D conversion interface circuitry used for the real-time ECG sampling and QRS detection. It uses an 8-bit A/D converter (MAX165) interfaced with the 8-bit microcontroller's I/O ports and control lines as shown. This converter was chosen because of its high speed (5μs) microprocessor-compatibility and its track and hold (T/H) capability. This T/H function allows full scale signals up to 50 kHz to be digitized accurately. In addition to its minimum power consumption, these facilities allow it to be easily interfaced to the current microcontroller and make it ideal for the current application. The A/D conversion and sample input is achieved under the relevant conversion software control. Fig.4.11 shows the associated sample conversion and timing interface pulses. The figure shows the conversion time $\overline{\text{BUSY}}$ of 5μ after the $\overline{\text{RD}}$ command is taken low by the processor.

(ii) *Quantizing accuracy:*

Several factors set the required quantization level for the ECG including the selected step size that preserves the sensitivity, the required dynamic range to avoid clipping and the resolution required for adequate ECG analogue-to-digital conversion. Figure 4.12 illustrates a practical example of eight-level quantization which correspond to 3-bit binary code accuracy chosen to simplify the process in which the ECG is sampled and quantized in this application. If, for example, the amplitude of each ECG sample in Figure 4.10 were represented by a series of 7-bits as is the case in our application, the conversion would have an accuracy of 1 part in 128 because $2^7 = 128$.

For clarity of the discussion and the calculations involved, it is necessary to outline some of the standard definitions involved when specifying the number of bits selected to accurately represent the ECG signal amplitude in such a practical situation.

The required number of bits (*n*) for the ECG to achieve the necessary sensitivity is given by [91,92,93]:

$$n \geq [\ 20 \log (V_{FS} / |V_{ECG}|) + 20 \log (\ |V_{ECG}| / V_{SEN})] / 6\ dB/bit \qquad (4.4)$$

where V_{FS} is the peak-to-peak input to the A/D converter,

V_{ECG} is the ECG's QRS magnitude, classically assumed to be 1mV_{pp},

V_{SEN} is the desired signal step level.

Substituting for V_{FS} of 700 mV_{pp} and V_{SEN} of 2.73mV then from equation 4.4 $n \geq 8$. This agrees with the initial assumption of a quantization level of eight levels chosen in this application.

The span or the (linear dynamic range) represent the total analogue value of the signal from maximum to minimum points of the amplified ECG signal [91]. Thus:

Dynamic range = Maximum analogue value - minimum analogue value (4.5) also,

$$\text{Step size} = \text{Dynamic range} / 2^{n+1} \qquad 2^{n} - 1 \qquad (4.6)$$

where $n+1$ is the total number of bits in the corresponding digital code (n = bit position of the MSB). Amplitude resolution is the same as step size. It is the smallest analogue change resulting from changing one bit in the digital number.Thus,

$$\% \text{ Resolution} = \text{step size} / \text{dynamic range} \times 100\% = 1/2^{n+1} \times 100\% \qquad (4.7)$$

Using equations 4.5 to 4.7 it is possible to calculate the number of bits required and the quantization error that permits sufficient conversion accuracy of the sampled ECG signal to transmit and accurately reconstruct the wave from the samples without excessive loss of the clinically significant information of the original ECG signal.

The exercise ECG signal acquired from the skin electrodes, and after passing through the amplifier with an approximate gain of 1000 and the band-pass filter stages shown Fig.4.5, has a dynamic range of approximately -0.3 to +0.4 V, i.e. 0.7 V_{p-p}. Since we used an 8-bit A/D conversion (n=7), then referring to Fig.4.12, and considering the 8-bit (255 levels) representation instead of the 3-bit illustration, equation 4.5 yields a dynamic range of 0.7V. If this range is represented by 255 levels, then from equation 4.6 each level represents a step size of $0.7/2^{8}$ = 2.73 mV. Hence, the number of levels required to yield a 2.73 mV resolution with a dynamic range of 700 mV_{p-p} is 700 mV/ 2.73mV = 256.4

Therefore, 8-bit quantization is adequate to sample the signal faithfully for the desired resolution where good performance is obtained in this application. Also, from equation 4.6 this level provides a percentage resolution of 1/256 x 100% = 0.391%. Thus, such resolution is adequate for the accuracy of the conversion used for the ECG signal, as the standard percentage should be at least 1% and preferably between 0.1-0.5% with reference to the dynamic range of the signal channel. However, even a 7-bit resolution (128 level of quantization) of the ECG signal will keep the error of any approximation under one percent (0.78%) of the dynamic range, and that is within the practical accuracy limits required for acceptable and interpretable ECG exercise recording and without excessive loss of the information [91,92,93]. The scaling of the ECG samples is achieved by adding a threshold level to each bipolar sample and then dropping the 8-th (sign) bit. This threshold magnitude is calibrated experimentally and selected to avoid signal saturation so that the maximum ECG level does not exceed half the full-scale conversion level of the A/D converter used.

This scaling ensures that the whole 7-bit dynamic range is utilized efficiently and represents the original signal without loss of significant sample information accuracy and prevents spurious detection by excessive quantization. Practically, in this application it modifies the original samples in a format compatible with increased coded bit frame transmission rate from a ratio of 1 for 8-bit samples/frame to 8/7 for 7-bit samples/frame essentially required for the reverberant underwater transmission.

In summary, we have offered an analytical base for selecting the sampling frequency and quantization level for the ECG prior to the detection and transmission process. The only objective of the such criteria would only be to preserve the essential ECG signal information while allowing efficient underwater data transmission.

4.2.1.2 Breathing rate module

4.2.1.2.1 Breath-Breath thermal contact sensing technique

The assessment of respiratory performance while diving requires a suitable non-invasive method of determining the breath-to-breath period which is not susceptible to muscle artifacts or sensitive to continuous movement. This appears to rule out the use of the transthoracic impedance method that was adopted for some aerial telemetry applications [2,3,4,5]. Such methods depend on the simultaneous measurement of the ECG signal and the extraction of the basal impedance changes accompanying the respiratory activity induced by the changes in the current density distribution between the voltage sensing electrodes resulted from the effect of respired air on lung resistivity. This combinational measurement is obviously not applicable in the current application due to the sensitivity of the respiratory signal on the electrode placement and body movement and the counter effect of the respiratory-induced

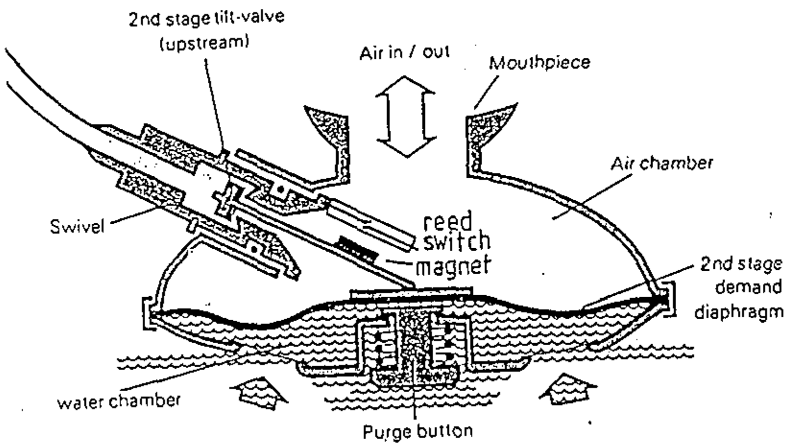

Fig.4.13-a Mounting of a miniaturized mechanical magnet switch in the demand valve

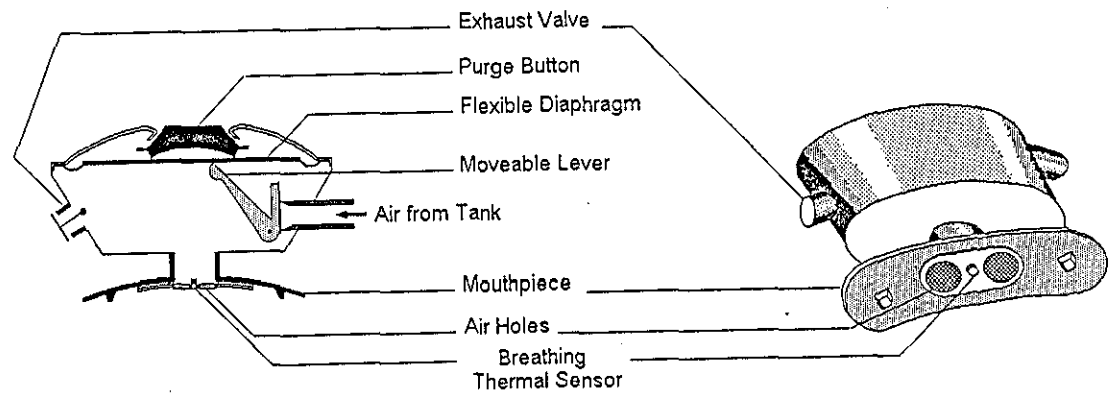

Fig.4.13-b Mounting and positioning of the thermal Breath-to-Breath sensor in the aqualung

heart movements and noise artifacts on the quality of the ECG signal recorded. Under clinical and physiological situations other devices are used in which the body movement is either controlled or is insignificant such as spirometer and pneumotachometers. The obvious disadvantages of these methods is that they require insertion of the devices into the airway, which is some application such as the current one may be neither practical nor desirable.

The simplicity, compatibility, safety and potential for accurate and continuous monitoring were the reasons to designing a new and alternative sensing device compatible with the underwater breathing apparatus. The simplest type of such sensor is an on-off switch activated by the diver's breathing. This can be a magnetic reed switch mounted inside the second stage of a conventional two stage aqualung demand valve as shown in Fig.4.13-a. However, such a mechanical configuration proved inaccurate, due to the missing pulses caused by shallow breathing.

An alternative new device was designed which is based on the principle of the thermal respiratory difference between breathing in and breathing out. To detect this respiratory variation a solid state thermistor sensor was soldered to the centre of a copper disc mounted in the demand valve. The sensor was soldered to the internal side of the copper disk to increase the thermal contact area, and surrounded by epoxy resin to insulate and waterproof the junction. The disk was mounted on the air in/out opening of the mouth piece in the second stage of a two-stage aqualung, as shown in Fig.4.13-b. This non-invasive technique provides a respiration rate in terms of the temperature variations of the diver's breath during inhalation and expiration.

This method has proved more practical and accurate in determining the exact breath-to-breath period during the dive. It was also shown not to be prone to artefact and noise sources and spikes associated with slow-varying physiological parameters. A special signal processing circuit has therefore been designed for this purpose.

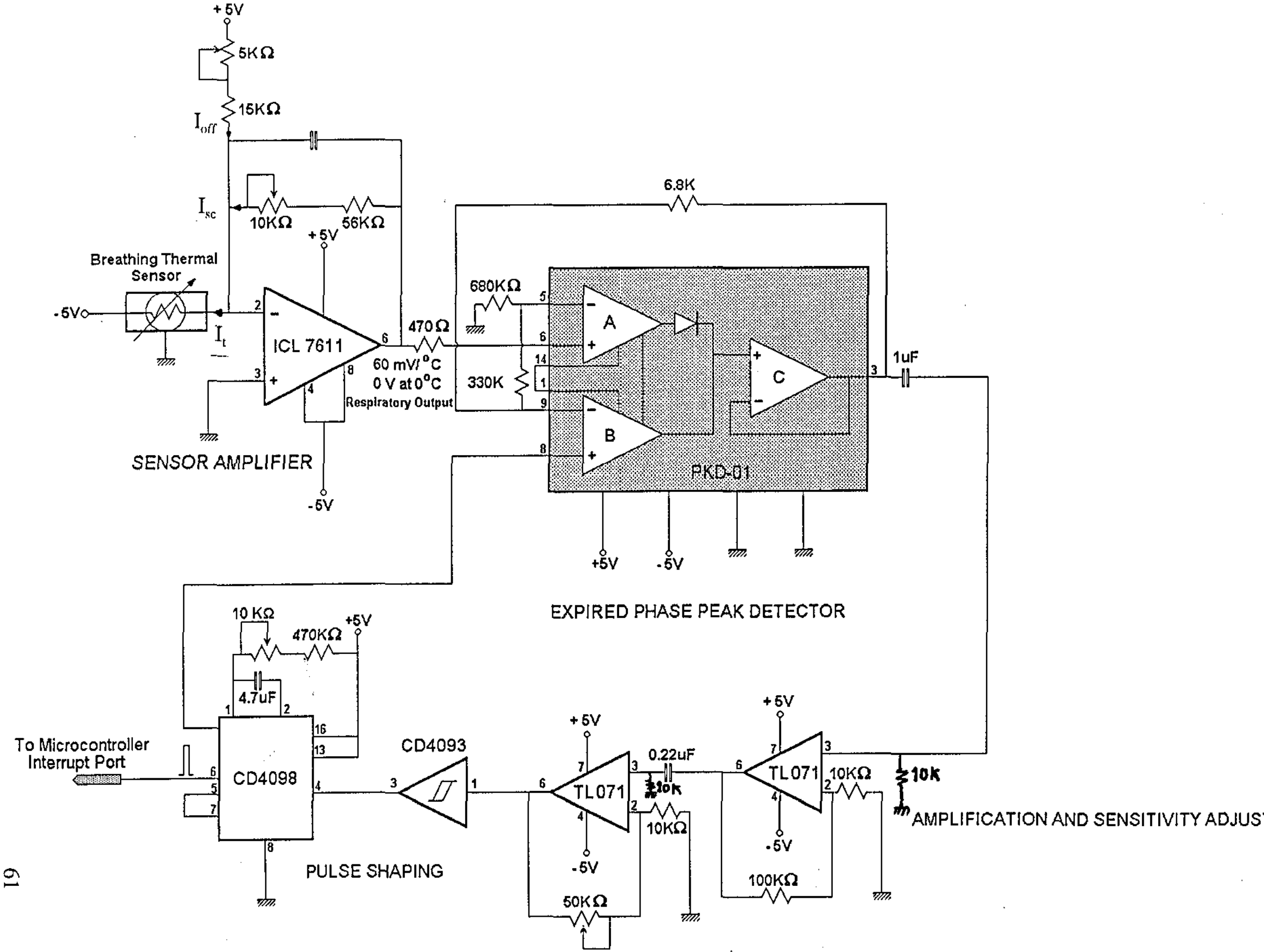

Fig.4.14 Schematic diagram of the breathing rate circuit

4.2.1.2.2 Breathing rate circuit design

The novel signal processing circuit, designed for measuring breathing rate, is shown in Fig.4.14. The system comprises two principal sub-circuits: the thermal sense circuit and the breathing rate detector. The circuits were designed to provide an accurate output of the low rate signals during diving and minimise breath-to-breath errors.

(i) *Thermal sense circuit*

The thermal sensor used is a two-terminal IC (AD590KH) that outputs a current of 1μK sensitivity, i.e. it gives a current output scaled to 1μA per degree absolute (Kelvin). Thus a current of 273 μA indicates 0°C. It needs no linearization circuitry, voltage reference or bridge compensation and can be used over a temperature range (-50 °C to 150°C). Its high-impedance current output makes it invulnerable to voltage drops and noisy lines, and non-linearity is quaranteed less than ± 0.1% over the hole range. These specifications makes such a sensor suitable for the current application. However, given that the sensor provides such an output, it is obvious that analogue processing is necessary to give the required reference voltage level for the breath-to-breath peak detection and to convert it to a digital output to the microcontroller interrupt port. The offset and scaling functions are performed by the sensor amplifier circuit shown in Fig.4.14. The scaling was set by assuming a constant offset current I_o. It is clear that any change in sensor current ΔI_t will be reflected through the scaling (feedback) resistance R_{sc}. Thus:

$$\Delta I_t = \Delta I_{sc} \qquad (4.8a)$$

Hence, assuming the summing end of R_{sc} is at zero potential, this change in current gives a corresponding change in the output voltage of the amplifier,i.e :

$$\Delta V_t = \Delta I_{sc} R_{sc} = \Delta I_t R_{sc} \qquad (4.8b)$$

For the current application, a scaling output of 60 mV/°C or 1μA/°C was found necessary for the next processing phase. Thus from equations 4.8a and 4.8b:

$$R_{sc} = \Delta V_t/\Delta I_t = 60\text{x}10^{-3}/\ 1\text{x}10^{-6} = 60\ \text{k}\Omega$$

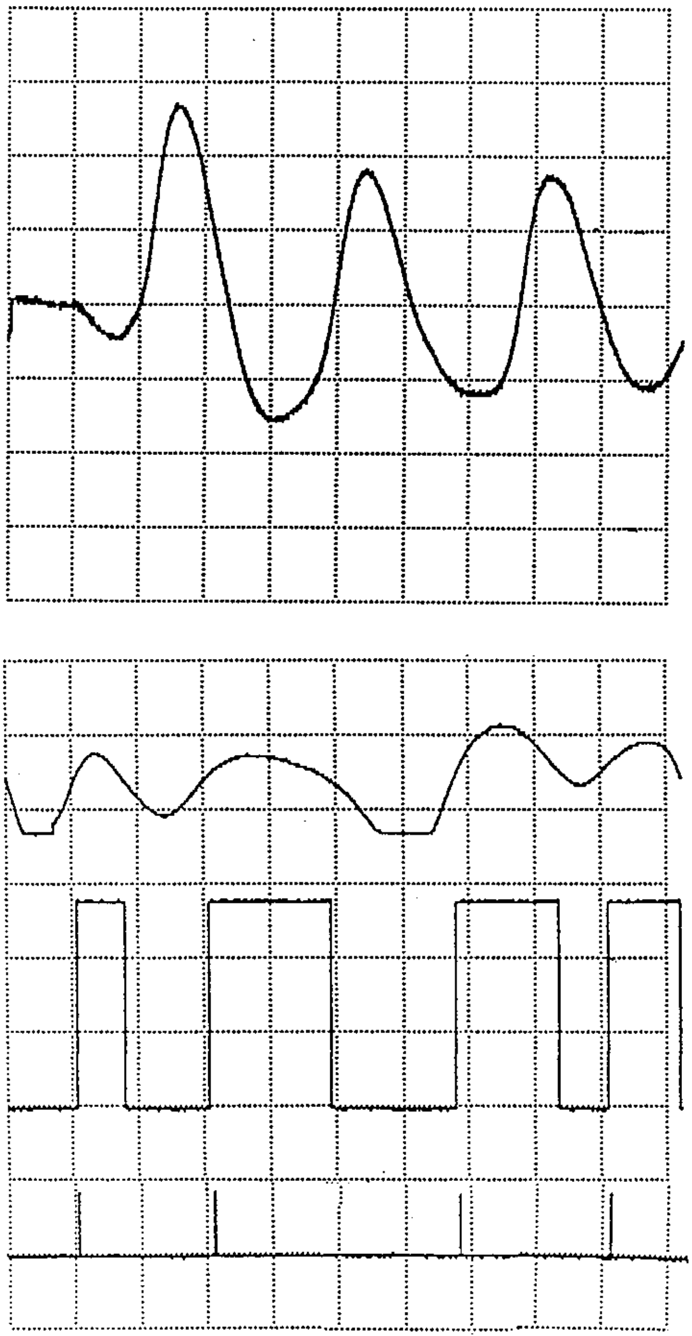

Fig.4.15 Breath-to-Breath thermal-respiratory response and the corresponding rate pulses

This was implemented as shown in Fig.4.13, by choosing R_{sc} as a combination of fixed resistor with a 10kΩ multi-turn trimming potentiometer to give sufficient adjustment to trim out the sensor error and resistor tolerances.

For the offset circuitry, the sensor will usually be sinking approximately 273μA at 0°C from the summing junction. Hence, the offset resistor must supply the same current to the node in order to balance this out. The offset scaling was selected at the appropriate temperature, typically in the range 5-10°C for British waters, to null the sensor output. With the 5V reference source voltage used here, the offset resistance can be given by:

$$R_{off} = 5/273\text{x}10^{-6} = 18.315 \text{ k}\Omega$$

This was also implemented as a combination of a fixed resistance in series with a 5kΩ multi-turn potentiometer for exact adjustment as shown in Fig.4.14.

(ii) *Breathing rate detector*

The respiratory signal output from the sense amplifier is fed to a monolithic peak detector integrated circuit (PKD01). This detects the expiry phase peak of the respiratory signal. This is followed by two amplifiers (TL071) used to adjust the resultant signal to a predetermined amplitude. This adjusts the gain sensitivity of the device to a level suitable for observing clear thermal-respiratory variations and to prevent amplifier saturation. It also determines the trigger level of the monosatble circuit (CD4098) triggered through a Schmitt trigger (CD4093) at the detected positive signal amplitudes of the near maximum expiry peaks in the breathing signal. Fig. 4.15 shows a typical breath-to-breath thermal-respiratory flow signal and the corresponding rate pulses measured from the aqualung mouth-piece.

4.2.1.3 Depth (Pressure-sensing) measurement module

A versatile circuit is designed which converts changes in the physical parameter representing the diving depth (hydrostatic pressure) into a digital signal of proportional frequency coded by a pulse repetition (PRR) used to provide the digital inputs to the allocated microcontroller port. This pressure-to-frequency conversion has the potential benefit that the digital telemetry output signal is less subject to the reverberant interference, especially in a severe multipath

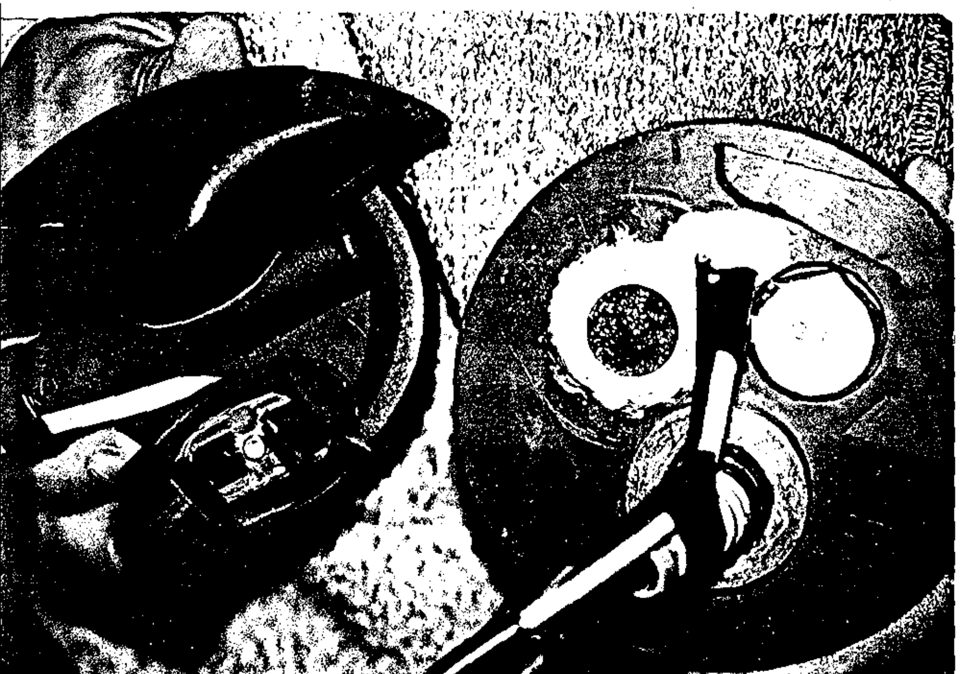

Fig.4.16 Depth/pressure and breathing sensor mounting on the transmitter

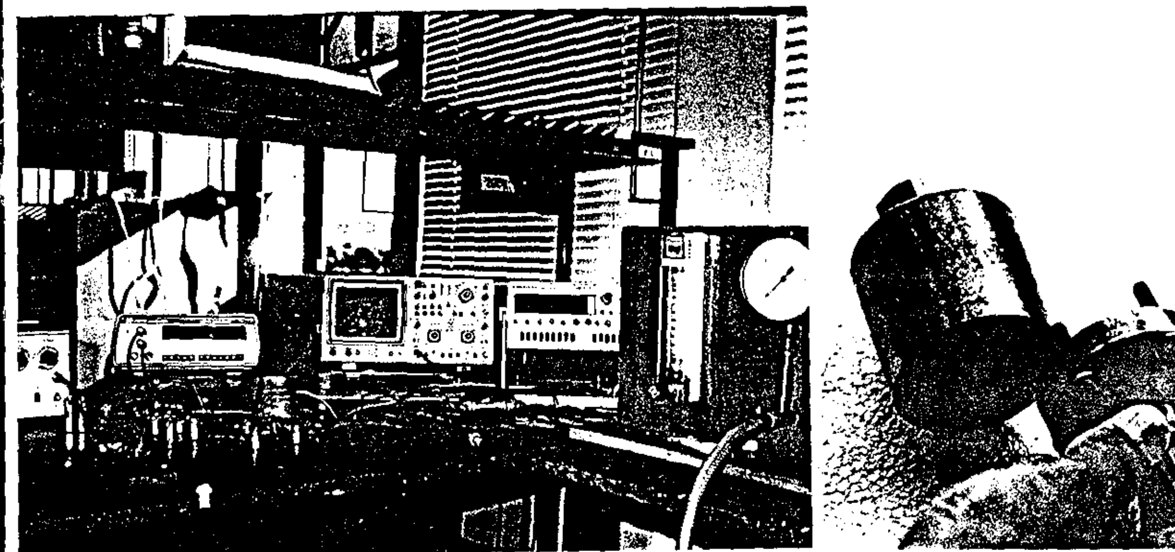

Fig.4.18 Experimental depth/pressure sensor housing and calibration set-up

environment. Additionally, the sensor combined with the telemeter depth conversion circuits must be reliable, accurate, interchangeable, rugged and miniaturised into the complete acoustic transmitter system. Another benefit is that the input signal fed to the microcontroller is already in serial digital form, thus analogue-to-digital converters are not needed for the microcontroller interface.

(i) *Pressure sensor*

The pressure sensor selected (SensorTechnics SCC100A- Rugby,Warwicks.,England) is a miniature semiconductor device typically suitable for different oceanographic equipment such as sonobouys and depth gauges. It is rated for pressures of 0-100 psia and is therefore suitable for depths down to 60 m. Typical specifications include internal temperature compensation, ensuring precise operation between 0°C to +50°C and having linearity within ± 0.5% and temperature error of 0.25%/°C. It is a differential piezoresistive pressure sensor that consists of a four-arm strain gauge bridge diffused onto a silicon pressure sensitive diaphragm with a sealed reference air space. The piezoresistive sensor chip is housed in a compact package and isolated from measured media by a resilient polymer membrane. Its overall diameter is 19mm. The sensor was mounted on an the sealed flange of a cylindrical pressure housing so that it was in direct contact with the water, as illustrated in Fig.4.16. The external contact surface of the sensor was covered with a thin waterproofing silicon compound (MS4) material for additional protection.

(ii) *Pressure-to-frequency converter and signal coupling to the microcontroller*

The basic functions performed by the pressure telemetry circuit shown in Fig.4.17-a are: (1) the sensor bridge circuit, (2) the differential amplifier, (3) voltage-to-frequency (pulse repetition rate-PRR) converter and (4) DC-supply conditioner. Fig.4.16-a shows the schematic details of each circuit.

The zener diode and the op-amp amplifier (LM308) provide the constant current source through the sensor bridge. When the pressure sensor is at the surface with atmospheric pressure at 14.69 psia (0 m depth), the reference pressure, the bridge is assumed to be balanced. During diving, any stress on the silicon diaphragm will cause a change in the

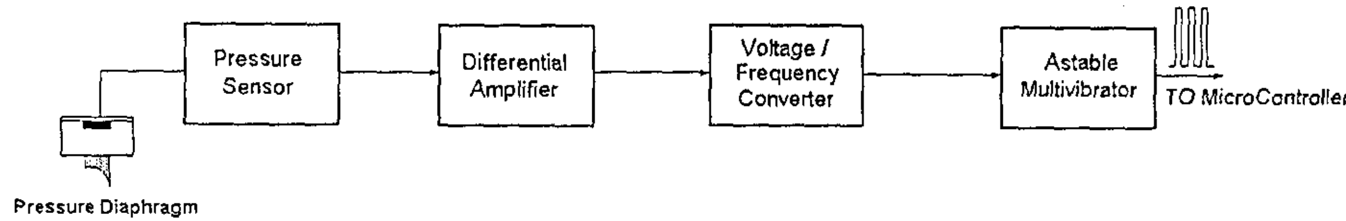

Fig.4.17-a Block diagram of the pressure-to-PRR converter

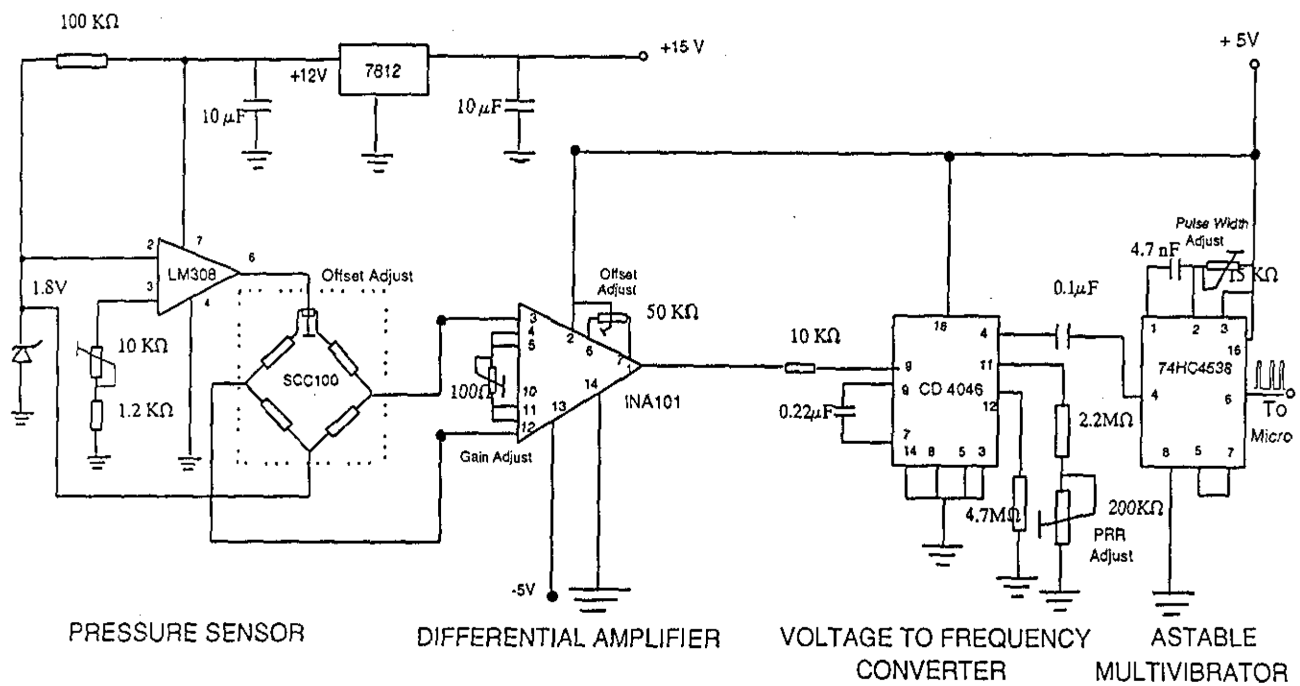

Fig.4.17-b Schematic diagram of the pressure-to-PRR converter

balanced values of the sensor's bridge resistances, i.e. two resistors increase in value and two decrease. This causes the bridge to unbalance, producing an output voltage which is proportional to the pressure difference. This voltage, which is in the millivolt range, is amplified and used to provide the drive signal for the conversion circuit. A low-power, high precision instrumentation amplifier (INA-101) is used to differentially amplify the sensor signal. The appropriate zero offset voltage of the sensor when no pressure is present, and gain output calibrations are set by the multi-turn precision potentiometers shown in the Fig.4.17-b. The output voltage is fed to the voltage-to-frequency converter that consists of two circuits. A voltage controlled oscillator (74HCT4046) produces a square wave output with a frequency proportional to its input voltage, and an astable multivibrator (74HC4538) provides the narrow tone-coded serial pulses that are fed to the microcontroller input port for transmission. In order to preserve the accuracy of the pressure measurement with respect to battery terminal voltage, the sensor circuit is powered from a +15V step-up switching dc/dc converter board (MAX743), with a fixed 12V regulator (78L12) to maintain a constant power source which feeds the sensor bridge.

(iii) *Sensor performance and calibration*

The sensor was tested over a wide pressure range, mounted in a stainless steel cylindrical pressure chamber that can withstand pressures up to 150 psia. Fig.4.18 shows the experimental chamber and calibration set-up. The sensor was exposed to different pressure variations, and the full scale output of the differential amplifier stage was calibrated to a maximum 3V at 55 psia. Fig.4.19 shows output square wave frequency variations of the V/F convertor and the resultant pulse repetition rate pulses.

A full scale rate variation was selected according to the calibration procedures of the depth transmitter taking into the consideration the maximum rate of PRR transmission limited by the underwater multipath environment and the reverberation decay time to the maximum diving pressure of 60 psia. A linear relationship is obtained between the circuit output and the applied pressure. Fig.14.20 is a typical calibration plot, showing the relative variation of the coded pulse repetition rate (PRR) as a function of input pressure. The limits are 600 pulses per minute (ppm) for +14.69 psia (0m depth) and 1250 ppm at 55 psia for a 3V full

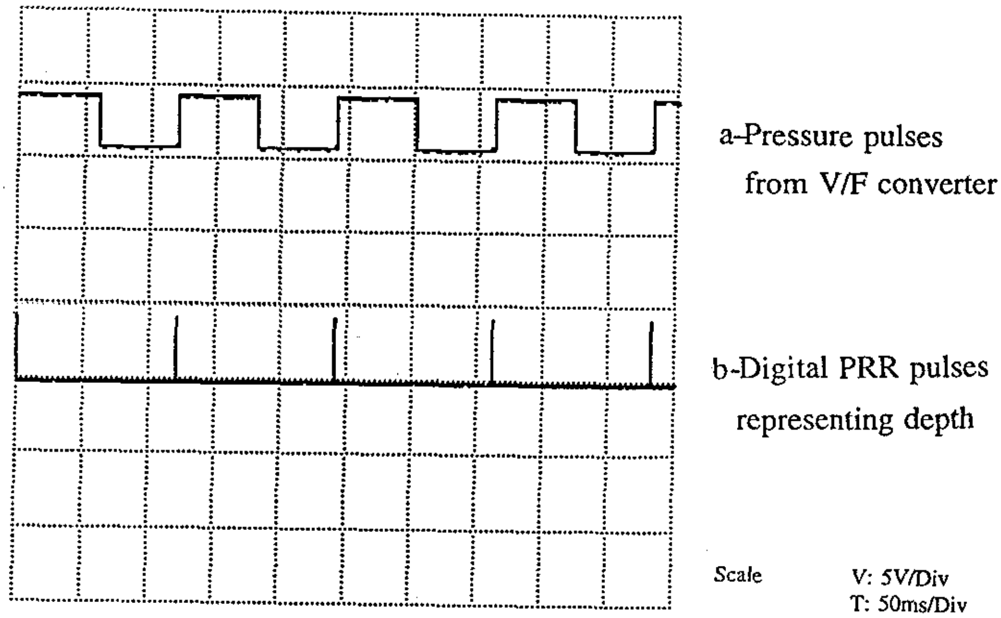

Fig.4.19 Pressure frequency variations from V/F and the PRR converter pulses

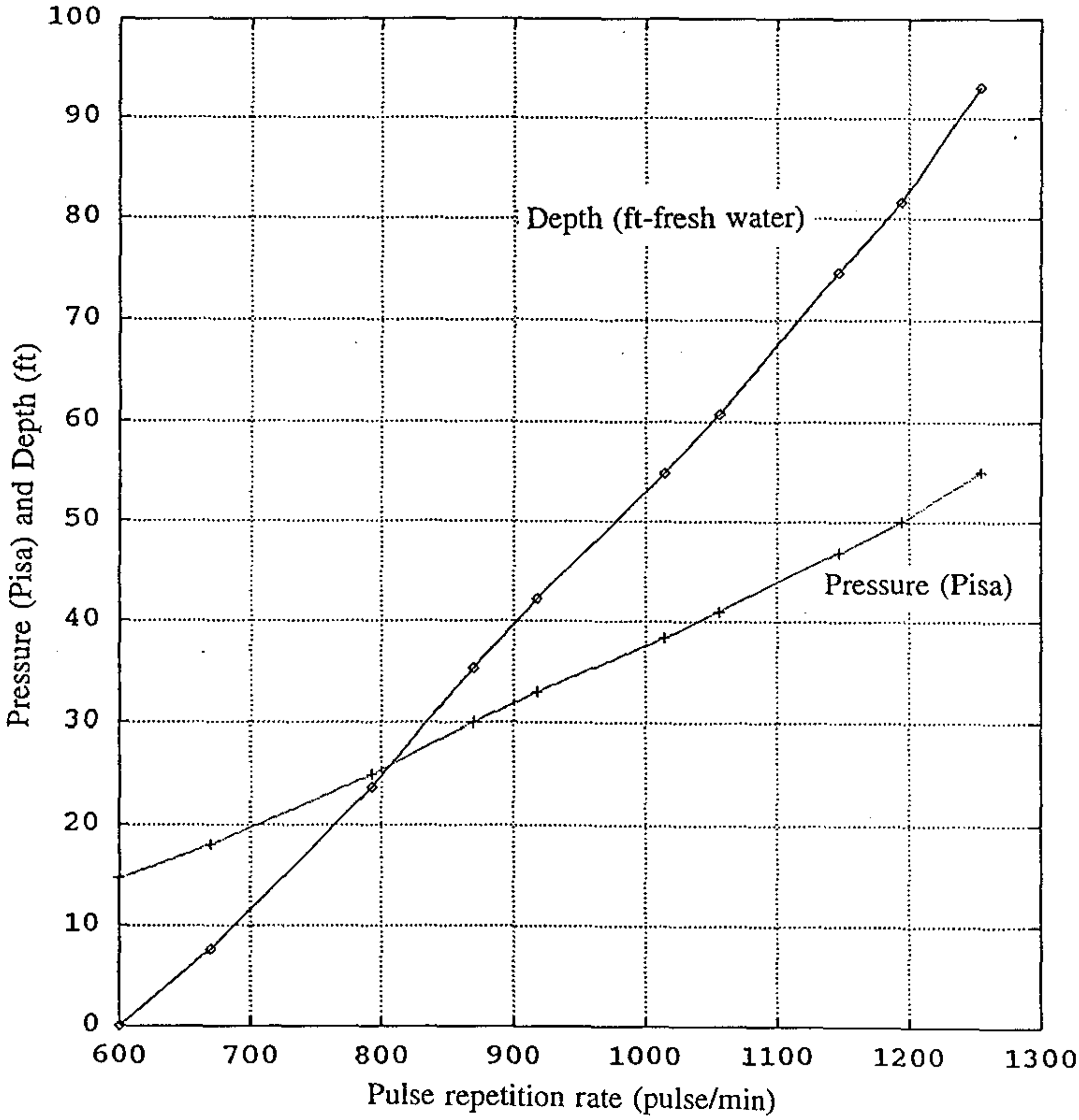

Fig.4.20 Typical calibration graphs of the depth/pressure sensor

scale output at 93 feet (28m) depth. This range of transmitted pulse rates satisfies a compromise between both the underwater multipath slow data transmission rate requirement, and a good resolution for ascent or descent, assuming an average PRR change of 10 pulses/min/ft. However, such resolution can be easily increased if required, by adjusting the frequency range of the V/F convertor provided that the underwater environment is more multipath free. The small non-linearity (<±1%) for the full scale in the curves could be attributed to the variations in the DC supply voltage, or the change in the exposed ambient temperature on the sensor circuitry. However, the sensor's temperature compensation feature was not employed because its inclusion decreases pressure sensitivity by half and further loads the battery supply. Since the water temperatures are unlikely to change by more than about 3-5°C during a dive, it was decided that additional pressure sensitivity was more important than the small advantage of temperature stabilisation.

4.2.2 Efficient power amplifier design and transmitter power sources

Chapter Three described the procedures of characterizing the acoustic power requirements to achieve the desired range. The power amplifier's role is to deliver the calculated power to the radiation resistance to enable the adequate signal detection at the specified range. In acoustic telemetry, the design of the power amplifier is often a dominant factor in determining transmitter size and life time. High efficiency design gives long life with small batteries.

This section describes the different power amplifier topologies appropriate for acoustic biotelemetry and identifies the most suitable design criteria. The detailed design of the suitable class is discussed with regard the supply voltage and the chosen power source, power output and circuit complexity.

4.2.2.1 Power amplifier classifications for acoustic telemetry

In this section a brief background of the power amplifier classifications is presented and indication of which efficient classes of interest is surveyed.

Generally power amplifiers are identified by a letter designation referring to the class of operation such as classes A,B,C,... etc. Classes A, B and C are well described in the literature [94,95]. Classes A and B are linear power amplifiers and as such are used when the envelope of the output must be proportional to the input signal such as in SSB and suppressed carrier or normal AM amplification. For a class C amplifier, efficiency is directly related to the conduction angle and a trade-off of the power gain versus efficiency exists, since the amplitude of the input current pulse must increase as the conduction angle decreases to maintain the same output power. In these designs the practical amplifiers have efficiencies between 35% and 60 % [94]. In addition, providing the correct drive and bias is difficult and optimum performance usually requires a certain amount of adjustment. However, a class B amplifier has been successfully used for an acoustic transmitter [96]. While such amplifiers can simplify circuitry, they have the disadvantages of low efficiency and poor frequency stability due to the output transducer reactance variation and the requirement for transformers.

When evaluating amplifiers for use in an acoustic transmitter the driving waveform is an important factor to be considered, since the best way to generate frequencies is by low power digital oscillator circuitry. The driving signals are thus square wave voltages and switched-mode power amplifiers are the logical choice for high efficiency. The design of such amplifiers can be simple and efficiencies of 80-90% are practically possible without tuning or adjustment.

The two types of switched-mode amplifiers which are suitable for acoustic telemetry are classes D and E. Although class D could provide a high efficiency amplifier, typically 90%, one of its major limitations is that the driving waveform must have an amplitude of at least the V_{cc} of the circuit to achieve maximum efficiency, so special drivers are required to eliminate the power loss in the input circuit. Another inherent power loss is due to the capacitance of the power transistor which must be charged twice each cycle. The class E amplifier is a relatively new type of amplifier [97], and employs a single transistor as a switch as shown in its basic circuit topology in Fig.4.21-a and the associated switching waveforms in Fig.14.21-b.

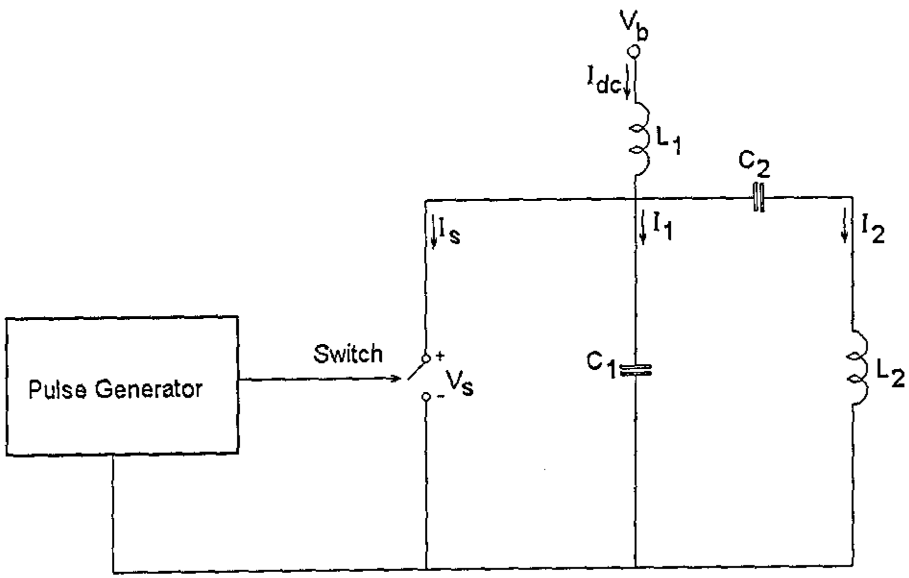

Fig.4.21-a Class-E power amplifier circuit topology

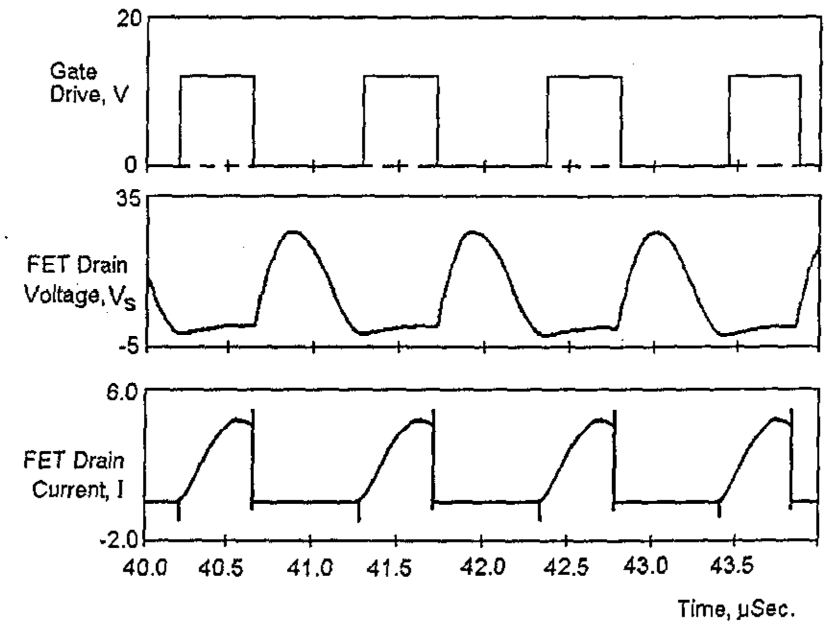

Fig.4.21-b Voltage-current representation of the class-E amplifier

The improved operational characteristics such as the use of a single switching device and efficiencies typically of 90% with no additional power circuitry and the elimination of power losses compared to the class-D makes this class the best suited switching amplifier to miniaturized acoustic transmitters.

A detailed analysis of the Class E amplifier is given in [97,98] and the effects of circuit variations are examined in [99]. A brief circuit operation can be described as follows:
The current in the L_2-C_2 branch is nearly sinusoidal with a frequency equal to that of the switch drive. This is a consequence of the high Q of the branch. While the switch is closed, L_2 and C_2 supply current back to the switch (i.e. I_2 is negative), no current flows through C_1, and the voltage across the switch is zero. When the switch opens, L_2 and C_2 continue supplying current (i.e.I_2 is still negative);however, this current now flows through C_1, resulting in a positive voltage across the switch. When the current in the L_2-C_2 branch reverses(i.e I_2 becomes positive), the charge on C_1 supplies the current, reducing the voltage across the switch. When the voltage across the switch becomes zero the switch is closed and the cycle is repeated. The inductor L_1 in series with the power supply, acts as a current source, with a constant DC component, supplying the energy dissipated during each cycle. At a specific operating frequency, i.e. class point the voltage and current are close to 90^0 out of phase and the voltage across the switch i.e. (active device) V_s has a value of zero with zero slope, just as the switch closes. This ensures there will be no large peak current in the switch and minimises the switching losses of the driver, which is considered a major obstacle in other switched-mode power amplifiers.

However, *a priori* determination of the exact class E point, i.e. minimum-loss operation, is difficult as it requires prior knowledge of the operating frequency and the dependency of the critical quality factor (Q) of the load network (minimum loss point) on the frequency and load variations. Such design problems can be tackled by using low on-resistance high switching speed devices such as VMOS devices and specifying the drive coupling design procedures with the acoustic hydrophone characteristics and equivalent circuit coefficients to obtain the optimum amplifier operating mode.

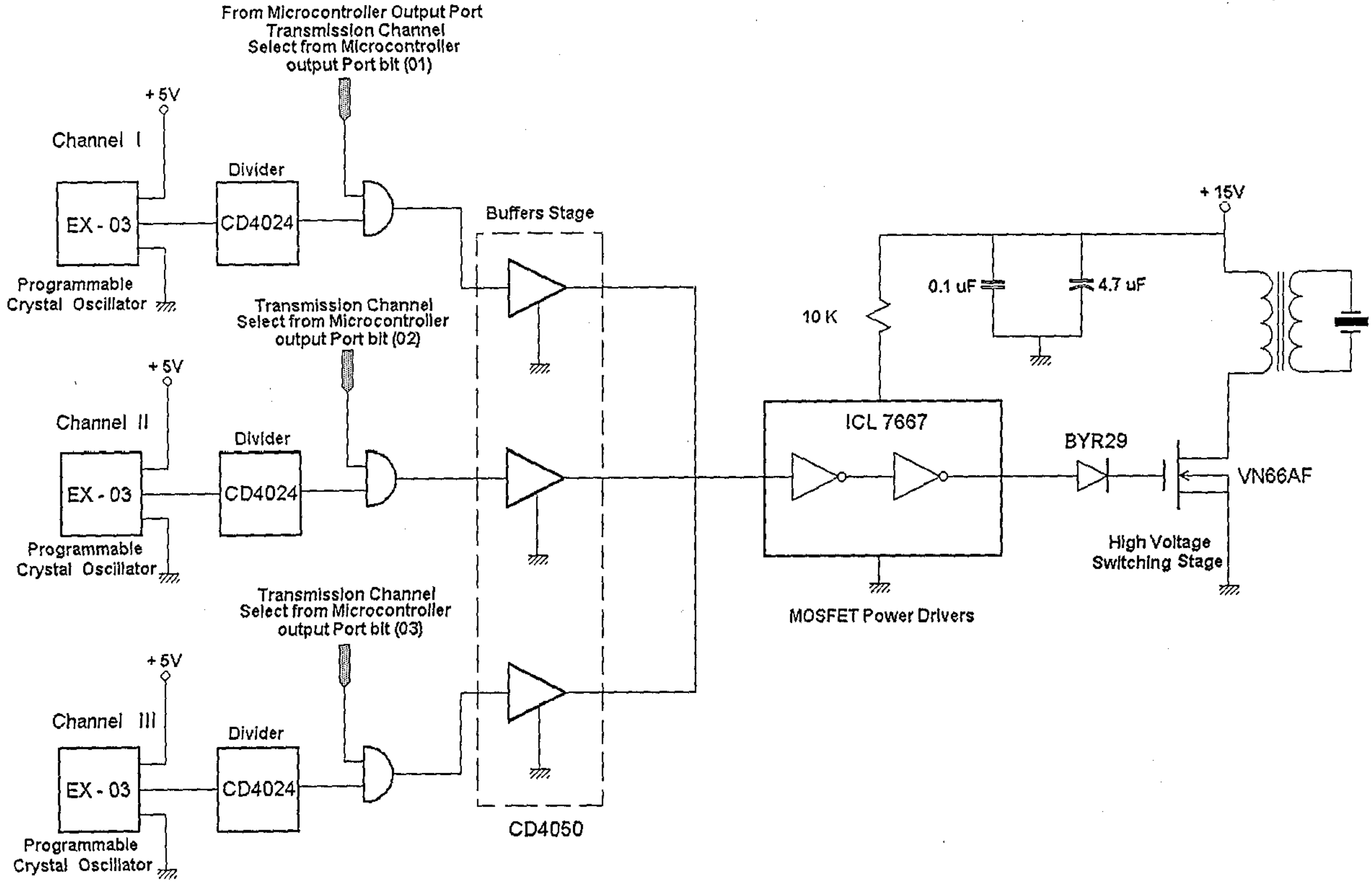

Fig.4.22 Schematic diagram of the microcontroller-based gateable power amplifier

4.2.2.2 Class E power driver design and acoustic output transducer characterization

The design of the practical class E power amplifier suitable for acoustic telemetery requires a preliminary choice of the operating frequency and the maximum power that can be transmitted efficiently to the projector. The compromise choice between the transmission frequency and the power were discussed in Chapter Three. However, a prior knowledge of capacitive and inductive parameters of the acoustic hydrophones is important to determine the proper matching with the projector and operating conditions of the amplifier.

The amplifier was designed a 25mm diameter omnidirectional ball projector (type D-170, Universal Sonar Ltd.,U.K.). This has a resonant frequency close to 70 kHz, and a Q-factor of about 4.1. The admittance locus and the detailed inductive and capacitive components of the projector's equivalent circuit were measured using a HP-4192A Hewlett-Packard impedance analyzer. The specifications and the plots are shown in Appendix A. From the measured specifications and the calculated output requirements outlined above, a class E power amplifier was designed as shown in Fig.4.22.

The detailed design procedures are given in Appendix B. The amplifier was constructed using a VMOS power FET (VN66AF), which is capable of switching a current of up to 3A in 4ns. Like all FET devices it requires a voltage to switch it on, and its drain-source resistance goes from 1MΩ with no gate-source voltage to about 3Ω with applied voltage. In this design the projector is connected to the drain through the matching tuned step-up transformer, and the source is grounded.

The FET gate drive is accomplished using a monolithic high-speed dual MOSFET driver (ICL7667) to convert the TTL gating level signals into high current outputs required to drive the amplifier from the switching CMOS buffered (CD4050) microcontroller selection I/O port gated with the programmable oscillators specified for the channel transmission as shown in Fig.4.22. Polystyrene capacitances with very short leads were used for the FET connections to the board to minimize ringing effects at switch shut-off due to lead inductance.

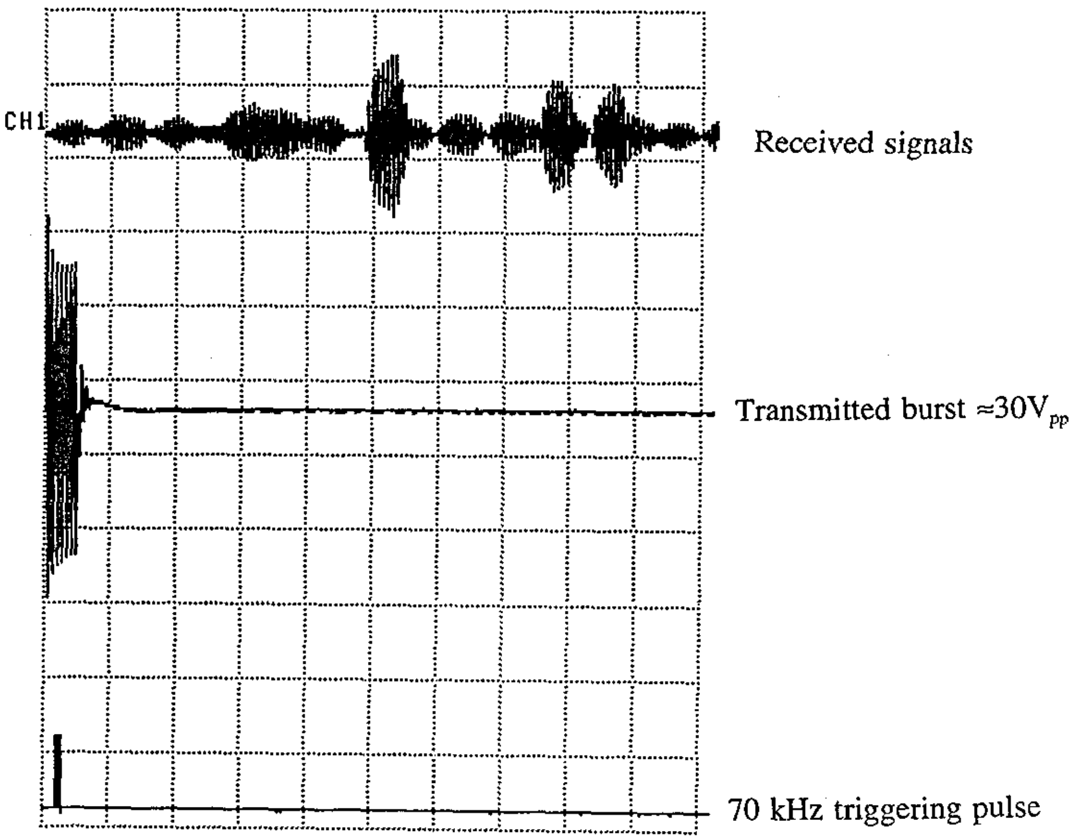

Fig.4.23 Microcontroller triggering pulse and the transmitted burst across the projector

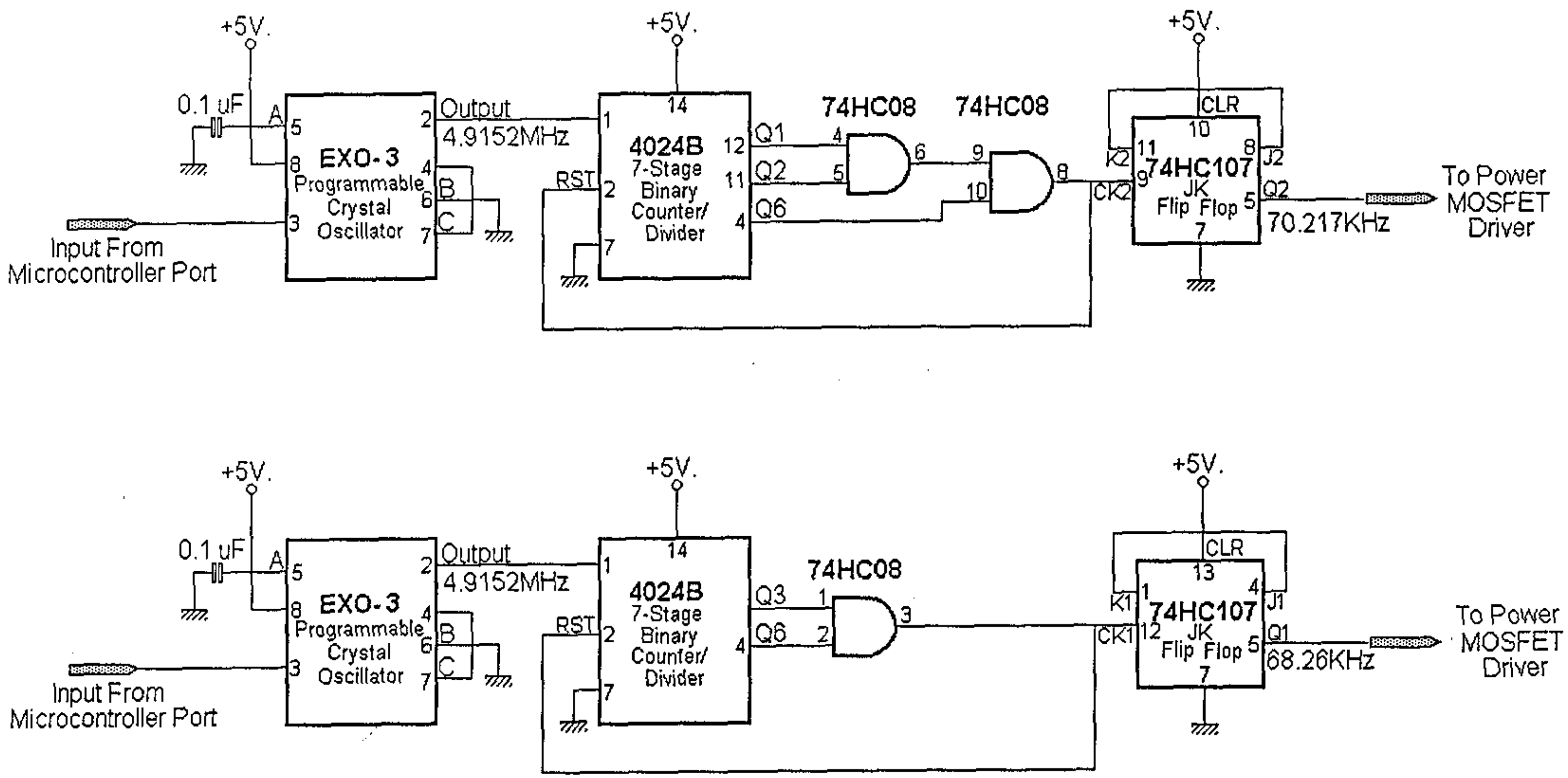

Fig.4.24 Schematic diagram of the programmable transmission oscillators

The excitation DC power supply voltage applied to the projector is derived from a CMOS step-up dc-dc converter (type MAX743) which can generate up to 100mA load current. A voltage of +9V powered from a single alkaline battery is stepped up by this switching regulator to an output of +15V which in turn produces approximately 30 V_{pp} across the water-loaded projector for 100 μs transmission burst. This output voltage across the projector is sufficient for achieving a detection level at the receiver at the maximum specified range discussed in Chapter Three. The amplifier circuit was tested successfully and it performed according to the design specifications under the microcontroller triggering control. Fig.4.23 shows the 70 kHz trigger pulse and the transmitted output burst across the projector. The performance of the amplifier is calculated with a transmission pulse width of about 100 μs and an average transmitter switching duty cycle of about 0.2, which results in a power supply current of approximately 38mA. Accordingly, the calculations of efficiency leads to efficiency of (0.4 W delivered to load /15V DC x 0.038) = 0.701 or approximately 70%.

This can be considered an improved efficiency compared to classes A and B designs of power amplifier classes mentioned earlier in this section, and relatively close to the assumed theoretical transduction efficiency. The theoretical efficiency of the class E driver is 100%; however, this is not achievable in practice because losses in the passive and active components cannot be eliminated and some redesigning with different
coil winding could increase the power supply-to-load efficiency to 75 or 80 percent.

4.2.2.3 Transmission frequency oscillators

The design of the basic reference oscillator in the transmitter circuitry is based on a miniature CMOS crystal-controlled oscillator chip (EXO-3) equipped with a programmable frequency divider. The small size, low power consumption CMOS IC (20 μA at 5V typ.) and highly stable operation with wide range operating power supply voltages of +3V to +6V makes this circuit suitable for medium size acoustic transmitters. Divisions from 1/2 to $1/2^8$ of the standard internal crystal frequency (19.6608 MHz) are achieved simultaneously using the on-chip frequency and frequency select circuits. The exact transmission frequencies for the three operating channels, breathing rate (68.26 kHz), heart rate and ECG (70.217 kHz), and depth

(72.28 kHz), are selected by divide-by-N CMOS divider circuits following the reference oscillator and implemented using CD4024B, 74HCT08 and 74HCT107, as shown in Fig.4.24. This identical synthesizer configuration for each channel can thus produce 2 kHz spaced frequencies within the bandwidth dictated by the resonance frequency and Q-factor of the projector.

4.2.2.4 Power supply source for the transmitter

The merits and suitability of power sources for telemetry have been well established and discussed by several references [100,101]. However, it is not practical to use some of the power sources for this project such as biological batteries, RF coupled and magnetic induction sources or Galvanic cells. The main emphasis will be on the best sources suitable for the current application that will be summarized here. The most widely used power sources in telemetry applications are 'primary batteries' that derive their power from some irreversible chemical process. The major consideration in selecting the convenient battery type are size, weight, cost, efficiency and availability. The most favoured types of batteries with useful characteristics suitable for underwater biotelemetry are lithium, mercury oxide, silver oxide and alkaline batteries. From the discharge characteristics for these batteries [100,101], lithium cells have the most advantages of higher energy density, higher cell voltage; thus they represent the best choice. However, their cost is relatively high and they are more suitable for smaller and miniaturized marine telemetry applications. Silver oxide has an advantage over mercury in that more than two cells will permit reliable operation of CMOS circuitry, while alkaline batteries have a lower discharge time characteristic than lithium, mercury or silver oxide. This type remains preferable although not the best choice for some applications, especially for medium size, high-power transmitters (i.e. acoustic output of 0.5 W or more), where alkaline batteries are capable of delivering the high current required to drive the acoustic transducer during transmission, in addition to their low cost, reliability and availability. However, the problem associated with the voltage drop in alkaline batteries can nowadays be solved by incorporating dc/dc linear switching regulators and using their output to power voltage-critical circuitry. The different hardware modules of the transmitter require a number of different supply voltages:± 5V,+12V and +15V. To avoid a multitude of batteries, a common power supply has been provided for the ± 5V. It uses a dc/dc converter with an on-off switch and is powered by two Duracell #MN1500 AA size alkaline batteries. This is a miniaturized supply board (70mm x 40mm) with one integrated circuit (MAX655 CMOS step-up switching regulator, Maxim Integrated Products, Inc., Sunnyvale, CA, USA). A 3V input voltage is stepped up by this circuit to +5V. The -5V is obtained by connecting the +5V output of the circuit to a voltage inverter (CMOS ICL7661, Harris Semiconductors). This circuit is capable of supplying ± 5V at 60 mA with input voltages ranging from 2.2V to 3.1V. This was found sufficient to power the physiological sense circuits for 2-3 hours. Also, for our application, we have found that using the MAX743 single integrated switch-mode regulator powered from a single 9V alkaline battery (Duracell # MN1604) efficient enough to drive the +15V supply of the power amplifier circuit for approximately 2 hours. The microcontroller board is powered by a separate miniaturized supply board (40mm x 20mm) step-down dc/dc regulator (LM2574, National Semiconductors), powered from a separate 9V alkaline battery for separate efficient and prolonged operation of the processor and memory chips. The 12V regulated power for the pressure sensor circuitry is provided by a low power linear regulator 78L12 powered from the +15V output of the MAX743. This multi-module supply configuration allowed a continuous and efficient experimental telemetry transmission of approximately 2 hours. However, the battery life for either a given DC drain or equivalent pulse transmission mode can be calculated in a straightforward manner [100,101]:

$$T_{days} = V_b \times mAh \,/\, (P_e \times \tau_{bit} \times 24) \qquad (4.9)$$

where T_{days} the ideal duration of the battery life time in days

V_b the nominal battery voltage

mAh the rated capacity of the battery in mAh

P_e the electrical power for the transmitter in mW

τ_{bit} the duration of the transmitted pulse in ms

Representative data given from the manufacturer of the Duracell #MN1604 with nominal voltage and nominal capacity of 9V and 550 mAh respectively, and substituting for τ_{bit} and P_e of 0.1ms and 500 mW for the transmitter, equation 4.9 yields a theoretical battery life of approximately four days. However, there are several reasons why a practical transmitter will not fulfil this expectancy. These could be mainly caused by longer pulses and higher current demands, temperature fluctuations, moisture invading the encapsulation or variations in the nominal capacity and voltage values due to long storage. It must also be noted that there are two types of battery incorporated in the present transmitter design that would attribute to the operational time of the transmitter.

4.2.3 Single-chip Microcontroller

The unique requirements imposed by underwater biotelemetry suggested the use of a microcontroller-based transmitter that maintains complete control of the telemetry units and performs all external communication tasks as illustrated in the system architecture shown in Fig.4.1. In the prototype system the transmitter is implemented using a general 8-bit single-chip Intel-87C51 microcontroller based on the 8051 internal architectural, as shown in Fig.4.25. This processor can provide the flexibility necessary to satisfy a variety of application requirements. In addition to the system configuration it provides a solution to design a general purpose transmitter which can be re-built and re-programmed as an intermediate module and interfaced via appropriate software to the other transmitter modules.

The 87C51 chip features the key design requirements of small size, re-programmable capability and +5V battery low-power supply. The other "on-chip" features are two programmable 16-bit timer/event counters that can be programmed to perform a wide variety of tasks. These include the generation of accurately timed high-speed pulse sequences; and synthesis of PCM digital pulses with different pulse characteristics such as duty cycle and pulse width. Further on-chip facilities include a 4kbyte EPROM memory, 8 x 128 bytes RAM, four 8-bit I/O ports with a multi-source, two-level prioritized interrupt structure. The on-chip EPROM can be re-programmed using standard 5-V Quick-Pulse programming equipment, and both RAM and EPROM can be expanded off-chip to a maximum of 64 kbytes. In the current work, an off-chip expansion RAM and EPROM memory was required for the telemetry software. The direct off-chip memory interface is done using the WSI-PSD301 programmable microcontroller peripheral with memory, as shown in Fig.4.26.

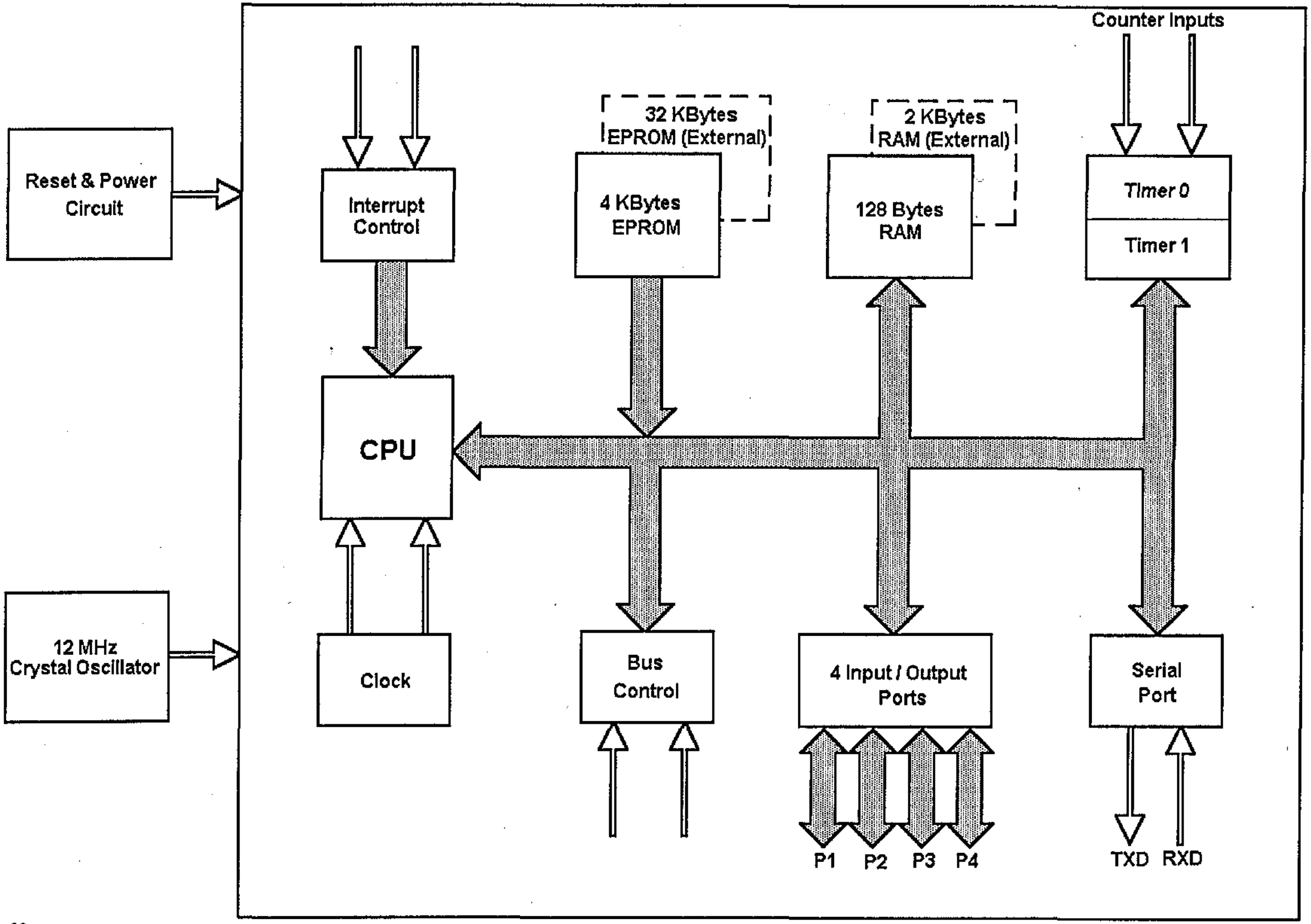

Fig.4.25 Block diagram of the 8051 microcontroller architecture

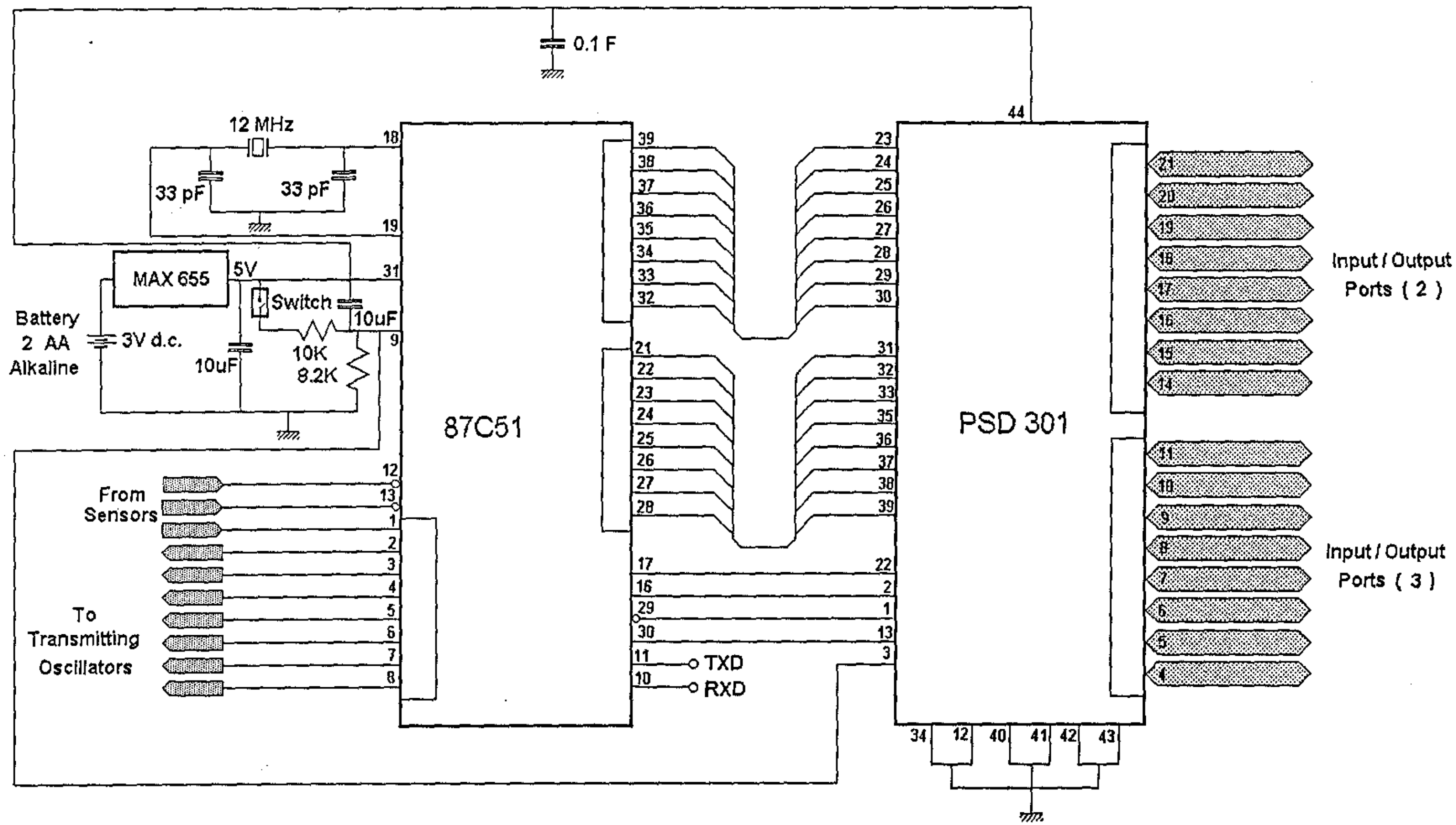

Fig.4.26 Schematic diagram of the 87C51H microcontroller interface with PSD-301 RAM/EPROM memory peripheral

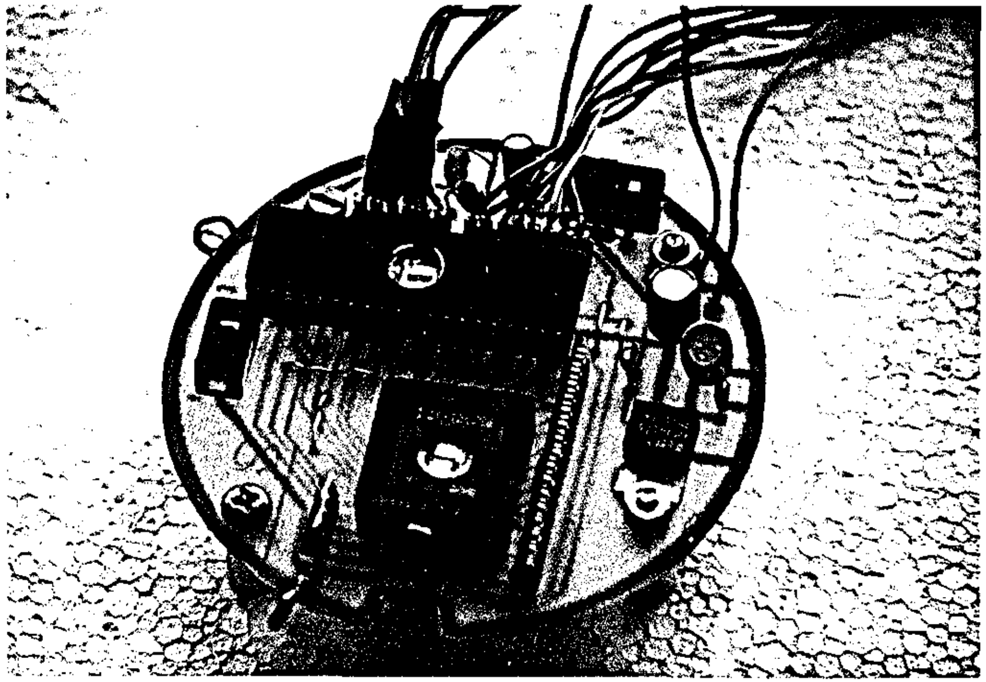

Fig.4.27 Photograph of the microcontroller board in the transmitter circuit assembly

This chip provides a single-chip solution with simplified compatible system integration by combining RAM, EPROM, programmable decoding and configurable I/O ports that expand the microcontroller when the on-chip memory resources are not sufficient. The mappable memory architecture of the chip allows the configuration of the additional EPROM and RAM into different blocks with a resolution of 4 kbytes or 2 kbytes. In the present system, the chip was programmed to provide additional EPROM configured as 32 kbytes, and partitioned into eight equal mappable blocks with a resolution of 4 kbytes each for future channel expansion. The additional RAM was configured as a 2k byte memory block. The chip's memory configuration and programming was done using system development tools from WaferScale Integration, U.S.A. [102]. This includes IBM PC/XT/AT or compatible software development, plug-in programmer board and remote socket adapter to program the chip.

This memory expansion allows the system to perform all the required real-time signal identification and transmission algorithms, and proved adequate for the transmitter performance. Fig.4.27 shows the single-chip microcontroller and the memory peripheral circuit board in the transmitter construction. The microcontroller development test system consists of an IBM-486 compatible P.C. and the Intel 87C51 emulation module (ICE-51FX/PC). The assembly source programmes are written on the P.C. and cross-assembled into an ASCII-coded machine program. Then the programs are down-loaded to the evaluation module via an RS-232 serial communication interface. The in-circuit emulation has the capability of allowing testing and debugging i.e erasing, reprogramming and verifying the EPROM contents on the 87C51 chip using the same I/O environment as the target device [103].

Once the programs are correctly validated and tested the final version is converted in the HEX format and programmed on the target processor placed on the transmitter board using a Stag ZM-2500 universal programmer. On the target prototype board a 12 MHz crystal oscillator is used to increase the execution speed and allows a 'cycle time' of 1μs for each machine cycle of 12 clock pulses. This provides an increased execution speed and calculation accuracy required for the exact timing subroutines in the system's software.

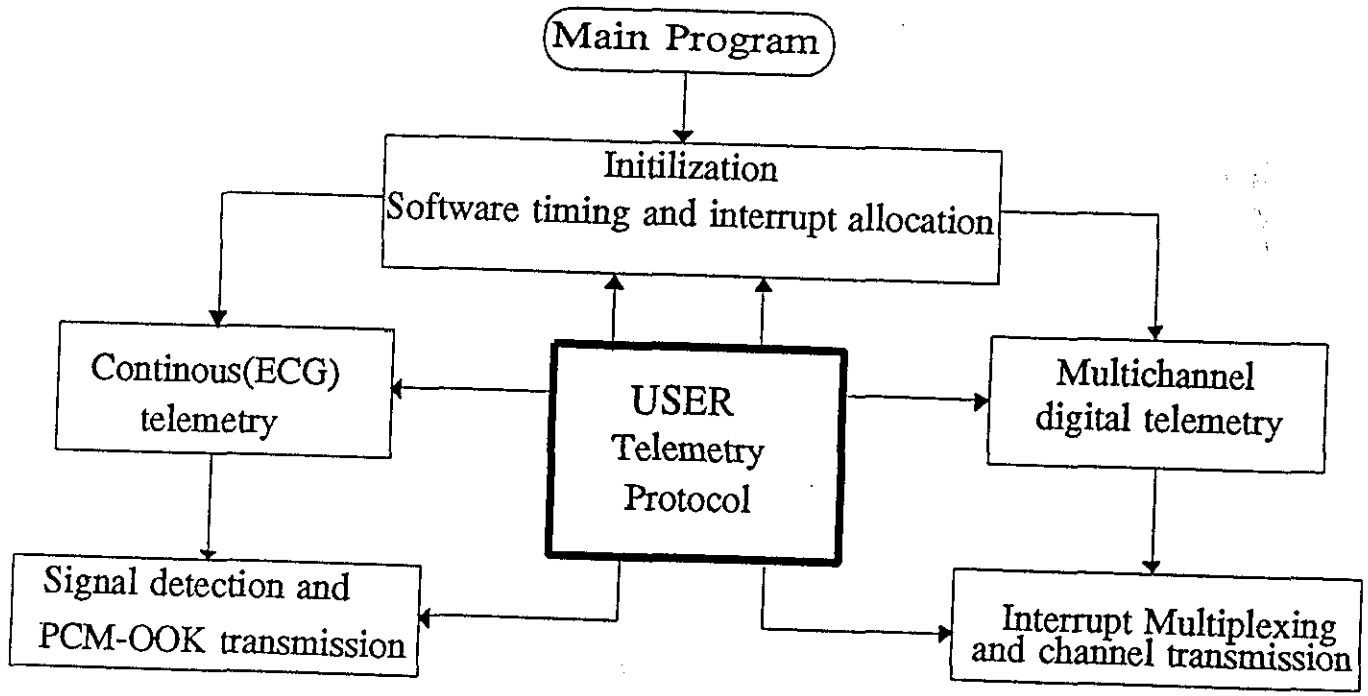

Fig.4.28 Software overview of the telemetry transmitter

4.3 Transmitter software features and algorithm terminologies

The modular design of the transmitter features a microcontroller as the central processor for the complete control of the biotelemetry units as illustrated in Fig.4.1. Its software has been chosen to perform the separate tasks of physiological data acquisition, processing and transmission. The two major tasks assigned to the software in this work are:

(i) Multichannel transmission of digital data, i.e. heart rate, breathing rate and depth.
(ii) Telemetry of continuous ECG signal transmission.

However, the software and modular hardware are flexible and allow interchange between any of the above transmission formats (intermittent or continuous physiological channel) and according to the monitoring requirements. It should be noted that minimal software and hardware changes are required for additional sensors or different coding schemes. The development of such an embedded control system requires a very specific software design. The overall control, computational tasks and algorithmic calculations that instigate the two transmission formats are accomplished by the relevant 'assembly software programming' written for the central 87C51 processor dedicated for each task. The assembly programming approach is ideal for such bit level work, offering the advantages of high execution speed and determination of the exact timing involved in the software development, in addition to the availability of the emulation facilities in the department.

This centralized single-chip functional control offers a highly flexible and versatile configuration due to the compatibility of the hardware with the other transmitter modules, and allows a choice of transmission mode without any hardware alterations in the signal acquisition and transmission modules.

The block diagram of the transmitter software overview is shown in Fig.4.28. The software structure consists of two main programming environments defining the telemetry trans-receiver protocols. The main program consists of the software and hardware initialization of the I/O peripherals and control tasks of the 87C51. The control tasks include the vectored interrupt allocations, timer settings for the transmission and pulse width control. After the initialization is complete the processor enters the required mode of transmission. Thus, the programmable flexibility of the system allows adaptation to continuous (analogue) or digital transmission.

These two basic processor software modes and the associated digital encoding algorithms designed for the transmitter's operation are now explained in detail.

4.3.1 Multichannel transmission of digital data

4.3.1.1 Interrupt based coding and multiplexing concept

In this mode the microcontroller acts as a multiplexing system for recognizing and transmitting three channels of information (heart rate, breathing rate and depth). A novel 'inverse' interrupt priority multiplexing hierarchy is established to achieve maximum timing accuracy and minimize errors on the most critical channel measurements.

The main disadvantages of the usual digital scanning and data sampling from different channels is that of transmission in a multipath environment. This means that the number of pulses encoded for transmission must be transmitted at intervals less than the time required for the last significant multipath echo to reach the receiver. This will lead to a slower transmission rate from each channel and increase the error in the rate or interval measurement. This concept is explained with reference to Fig.4.22 and the timing diagram in Fig.4.29.

The microcontroller is programmed as an interrogator with the output of the three digital channel circuits described earlier in sections 4.2.1.1.5, 4.2.1.2.2 and 4.2.1.3. This is implemented by linking the digital output from each channel to a specified interrupt and input port of the microcontroller's external interrupt (INT0, INT1), and input ports (port 0) connections, and assigning a single output bit port for each channel from a configured output port (1) for output transmission as shown in Fig.4.22.

The interrupt interrogation procedure is based on an inverse priority level assignment with each channel's pulse rate. This means that under program control the lowest pulse rate (from

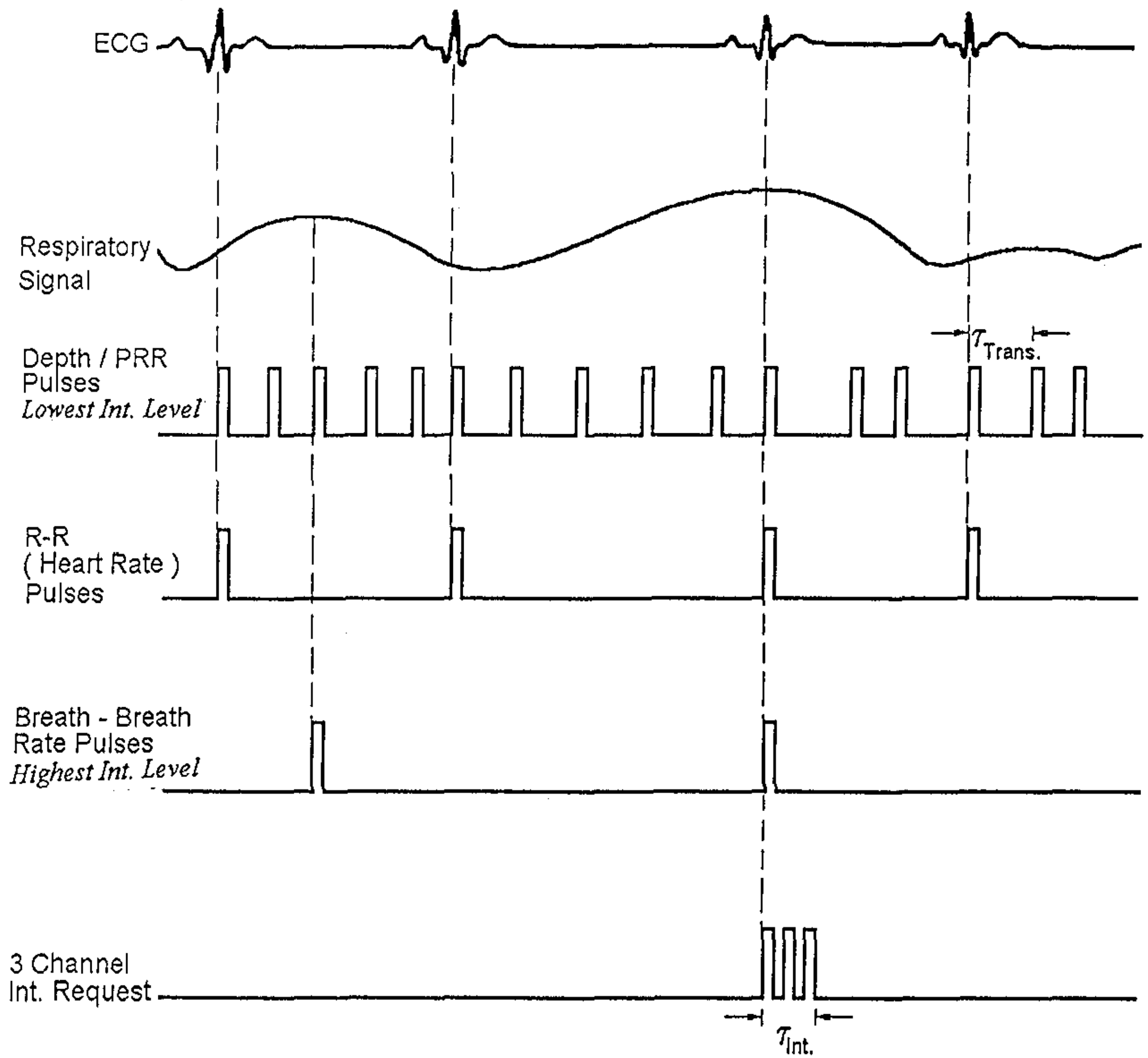

Fig.4.29 Timing diagram of the interrupt-based multichannel coding and transmission

the breathing sensor) is allocated the highest priority interrupt (INT0) by a special interrupt priority register, and the highest pulse rate (from the depth sensor) is allocated the lowest priority, while the heart rate (R-R measurement) is allocated the medium priority (INT1). The maximum accuracy is thus assured using this multiple-interrupt multiplexing hierarchy. This is based on the fact that the two highest priorities are well separated on the time axis, for example due to the large difference in between the heart rate or R-R pulse interval that spans approximately between 1200 ms (50 beat/min.) and 300 ms (200 beat/min.) and the much slower breathing rate (2-15 ppm). This allows the handling of interrupt routines to end always before the next interrupt is received and allows the lowest priority (highest rate) to be serviced without frequent interruptions as shown in Fig.4.29. Hence, the channel/interrupt assignment is given as:

$$p = n \quad (n = 1,2,3.....N\ ,\ p=1,2,3...P) \qquad (4.10)$$

where n represent the total number of channels classified as n=1 representing the slowest rate channel, and n=2 as the next highest rate ....N, representing the highest rate channel.
p represent the total interrupt priorities assigned for p=1 representing the highest priority channel and p=2 the next level..... P, representing the lowest priority channel.

Given one short pulse is sent per channel in order to reduce the power consumption of the system. The real-time sampling frequency of the multi-interrupt ON/OFF triggering sequence f_{sm} is given by:

$$f_{sm} = 1 / N_{ch}\, t_{ch} \qquad (4.11)$$

where N_{ch} is the number of the multiplexed channels

t_{ch} is the transmitted pulse period of each channel

In the case of the current three channel telemetry, N_{ch}=3 and t_{ch}=0.1ms, the sampling frequency for each channel is 3.3kHz. This is more than adequate for most diver monitoring applications and the biological channels involved considering the slow rate data involved.

The only limitation in this method is the possibility of pulses of all three channels instantaneously coinciding for triggering the transmission of more than one level, as shown in Fig.4.29. The probability of such an event is very low, but in this case the higher priority interrupt must persist followed by the two lower priorities waiting interrupts. This means that

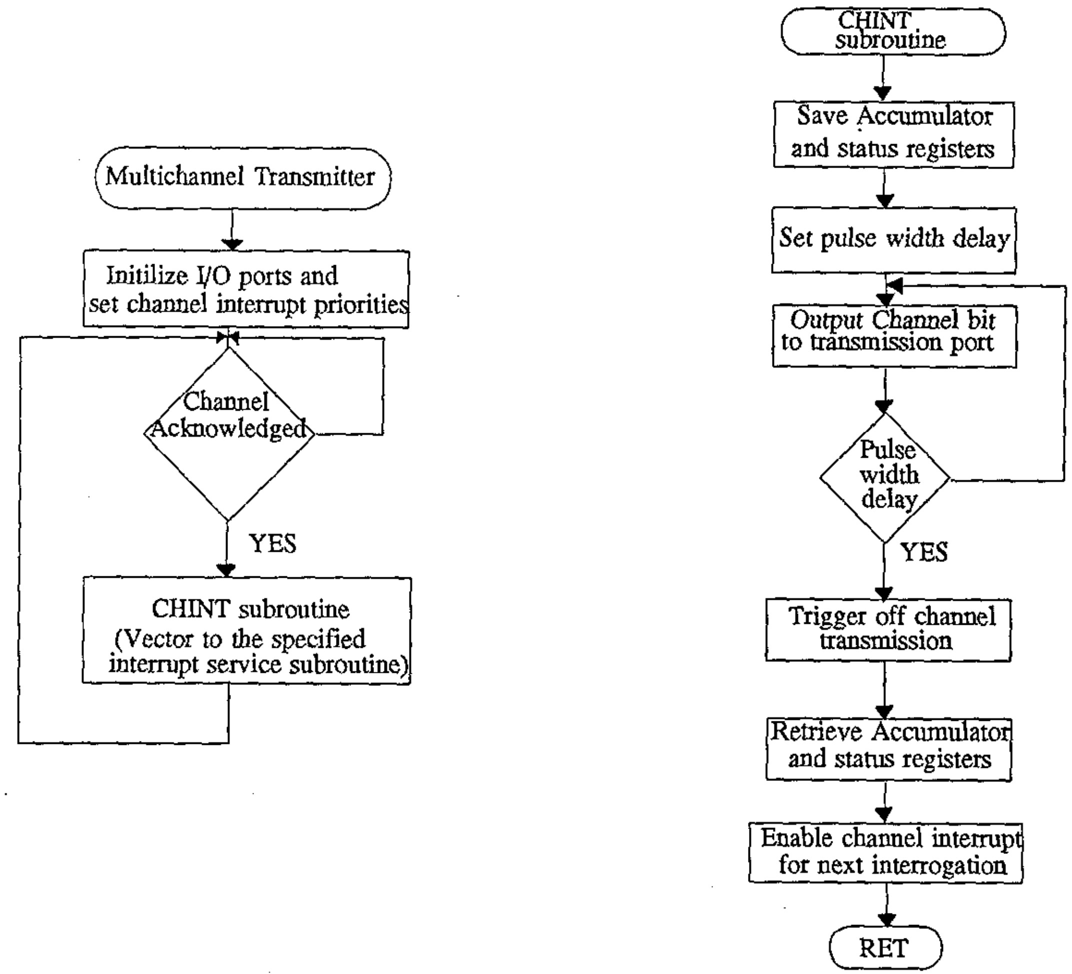

Fig.4.30 Flow chart of the multichannel transmission control software

the lowest level (depth) is missed if the total time required for the interrupt service routines of the three channels τ_{int} exceeds the transmission delay of the highest bit rate between successive transmitted bits, τ_{Trans}) i.e. $\tau_{int} \geq \tau_{Trans}$, which depends on the degree of multipath reverberation decay time and the geometry of the underwater environment, as explained in section 3.2.1.3. However, the minimum calibrated time delay, τ_{Trans} for the highest priority channel in the current system is about 20ms for depths exceeding 93 feet (28m), while the maximum interrupt service timing for triggering the next transmission pulse is less than 1 ms. Hence, this channel-timing arrangement minimizes the error possibility. Such accuracy can be limited if the reverberation decay time is much smaller or the maximum transmission bit rate is increased, which depends on the underwater environment.

This versatile approach allows the user to define the hierarchy services according to the physiological signals involved and the format of the transmission required, in addition to maximum accuracy and synchronized transmission of data with minimum error. Additionally, this multiplexing structure obviates the need for a synchronized pulse or interval for the multichannel synchronization frame. This is because of the allocation of transmission frequencies, each channel having a separate crystal controlled oscillator to an identical processor allocation in the receiver that scans and discriminates the same individual channels, as will be explained in the next chapter.

4.3.1.2 Multichannel transmitter control software

The sequencing of the three-channel multiplexing logic is shown in Fig.4.30. The flow charts are self-explanatory. The main sequence of the program starts with initializing the I/O ports, enabling the interrupt channels and setting the internal timers. It must be noted that since the 87C51 has only two external interrupt levels, the lowest priority, assigned to the depth sensor, is a single input bit that the processor scans continuously. If the bit is 'active' then the processor moves to the channel's transmission subroutine. If it is interrupted by any of the other high priority channels then it stops the interrogation process and serves the specified interrupt subroutine, then returns to the main program. The channel interrupt subroutines initially saves the status and other used registers where each channel is allocated a separate bit in the output port (port 1) programmed to trigger the specified transmission crystal

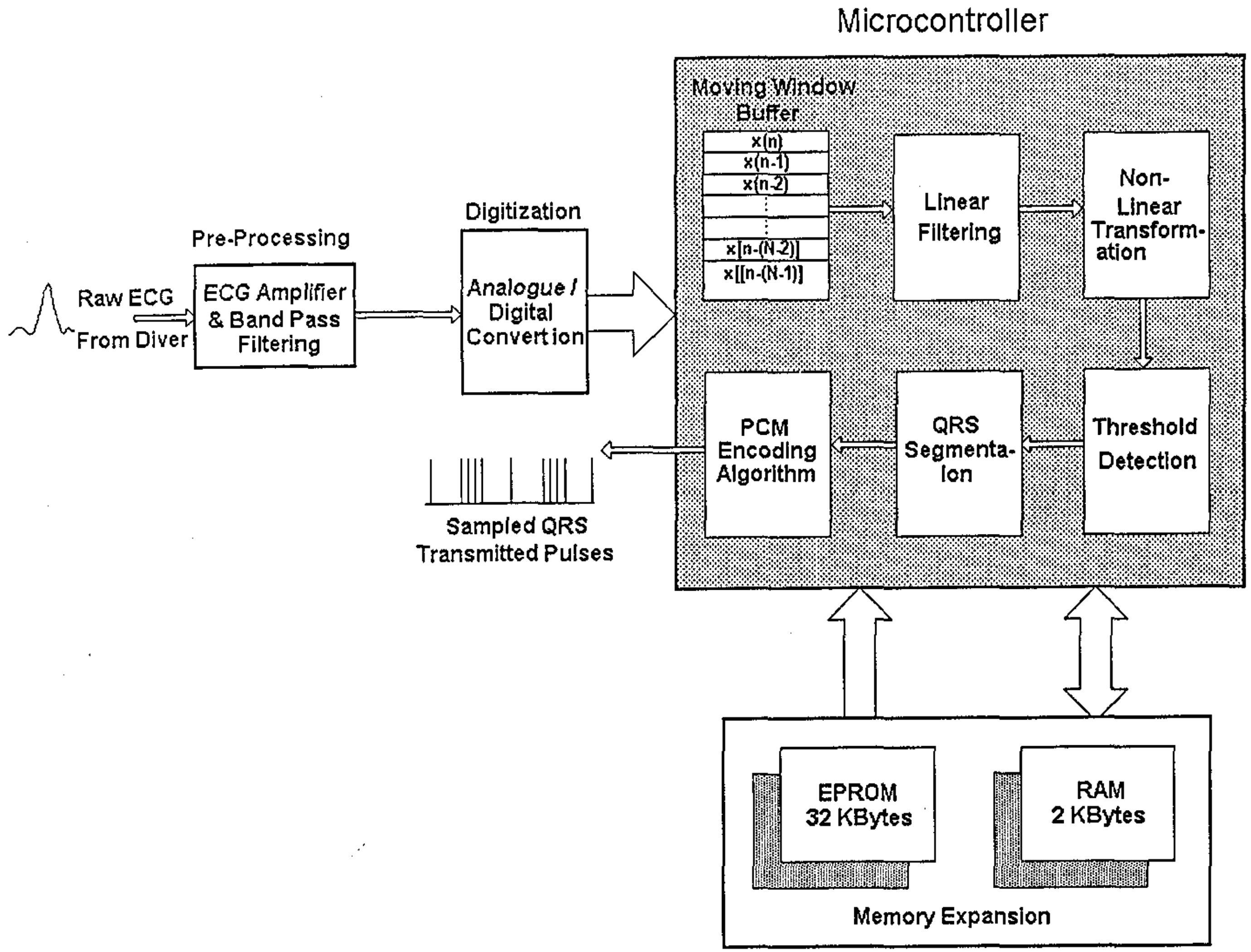

Fig.4.31 Block diagram of the QRS detection an DPCM/OOK transmission algorithms

oscillator channel. The required width of the transmitted acoustic burst to switch the class-E power amplifier can be programmed according to the depth/range calculations, receiver bandwidth and degree of multipath reverberations present in the underwater environment, as explained in section 3.2.1.3. This is achieved by setting the contents of an internal 16-bit timer/counter to generate a fixed delay by the required pulse width. This can be further controlled and adjusted externally by triggering optional monostable circuits connected to these ports.

4.3.2 Telemetry of continuous ECG signal transmission

The other transmission format assigned to the transmitter software in the current system is for continuous ECG telemetry. The problem of the ECG transmission is divided into two main successive processing algorithms. Fig.4.31 shows a block diagram of algorithmic concepts involved in this telemetry task. The resulting digital signal passes successively through a sequence of processing steps that are implemented entirely under software control.

This software processing is based on the following algorithms:

(i) QRS detection and feature extraction.

(ii) Digital pulse code modulation and On-Off Keying (PCM/OOK) transmission.

4.3.2.1 QRS detection and feature extraction

The QRS detection is the first and most critical stage in the telemetry process due to the complexity of the ECG signal. Although several QRS detection algorithms have been designed and implemented for real-time clinical patient monitoring in recent years [104], the most common and successful approach used in clinical practices is based on *template matching* (average magnitude cross-difference) method [105]. In this method a model template is generated from the raw ECG signal, then the incoming ECG data are compared with the QRS template and threshold comparison is applied to detect the QRS complex. However, such a method is only suitable for P.C.-based stationary patient monitoring and requires a large memory for saving the templates. Significant computational power is needed for the calculations of a complex template matching algorithm. This makes such a method unsuitable for telemetry applications, especially its realization using a battery-powered microcontroller with limited memory size and fixed point computational capabilities.

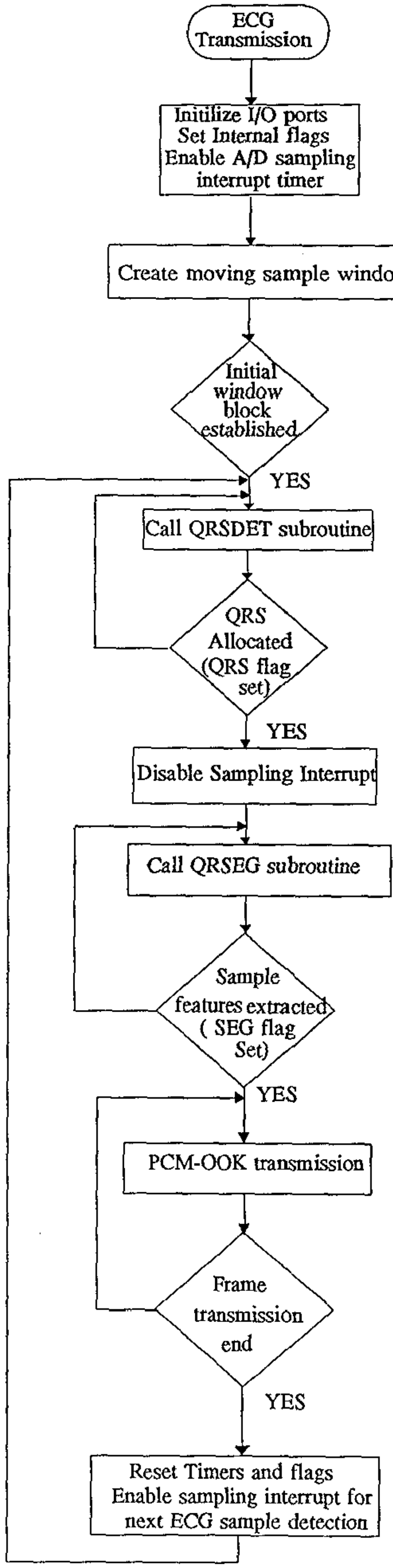

Fig.4.32 Flow chart of the real-time microcontroller-based ECG transmission

In general, such algorithms although suitable for patient monitoring are not applicable for a real-time underwater biotelemetry due to the limitation imposed by the complexity of the algorithm, speed of execution, suitability for underwater transmission, power and size requirements, and the various noise and signal degradation factors.

The basic criteria behind the detection algorithm chosen and modified in this work as a compromise solution for the above limitations is the higher correlation that exists between the adjacent samples constituting the QRS complex than the random noise inhibited within the raw ECG signal. Fig.4.31 shows the processing blocks involved in the QRS detection and feature extraction algorithm. It is mainly based on a succession of three stages of QRS detection transforms [104,106], followed by a sample segmentation and QRS feature extraction stage adaptable for the subsequent PCM/OOK transmission algorithm. These algorithmic stages are:(i) linear filtering, (ii) nonlinear transformation, (iii) refractory blanking and detection threshold and (iv) QRS sample segmentation and main feature extraction. This algorithm provides simple yet adaptively effective and implementable procedures compatible with the current hardware and software architectures.

The program is initiated by reading a new sample after a single interrupt-driven sampling period delay (5ms) generated periodically by the 16-bit internal timer facility. The 8-bit ECG data samples are fed into a moving window buffer in the RAM area of the microcontroller. Since the interval of the QRS complex in healthy subjects is typically <120 ms, as shown in Fig.4.2., a moving window width of 100 sample block (500 ms) in the RAM is chosen to cover the whole PQRS at the selected sampling rate. For every new sample of data (byte 1) fed into the memory block, the oldest data point (byte 100) is continuously removed and the new sample is passed through the detection process, i.e. the window advances by one sample interval. This process is repeated until the exact QRS feature is extracted within the time frame of the window. Then the program moves to the next (PCM/OOK) transmission phase. The main ECG transmission program and the associated subroutines are explained in the following sections with reference to Fig.4.32(a-c) that shows the detailed flow chart of the successive detection algorithmic and assembly processing steps.

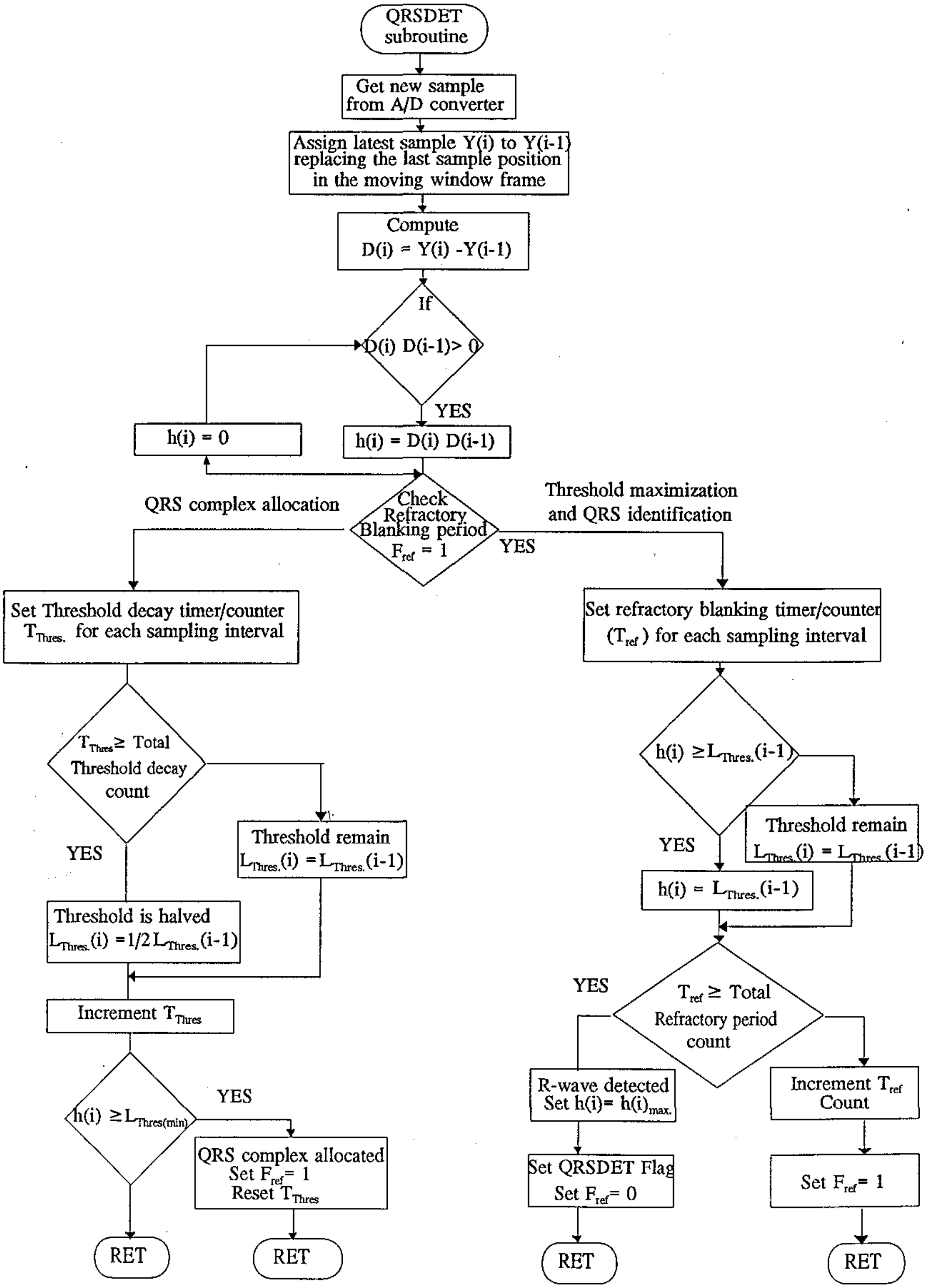

Fig.4.32a Flow chart of the QRS detection algorithm

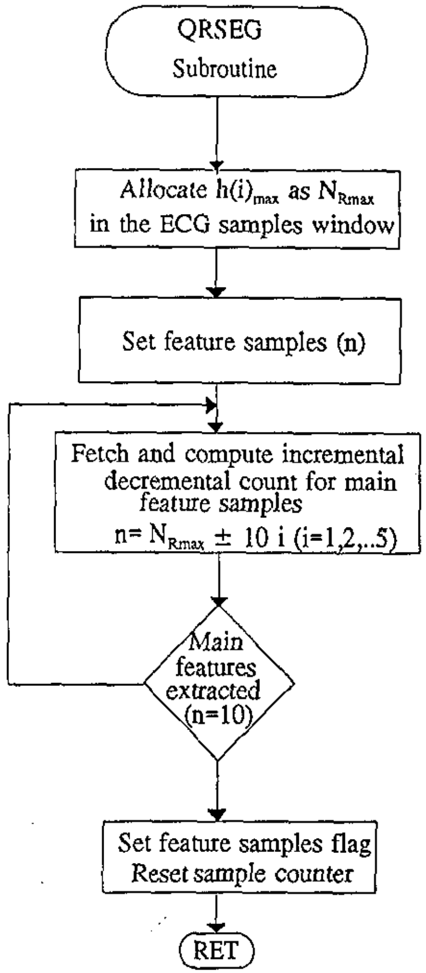

Fig.4.32b Flow chart of the sample segmentation and feature extraction

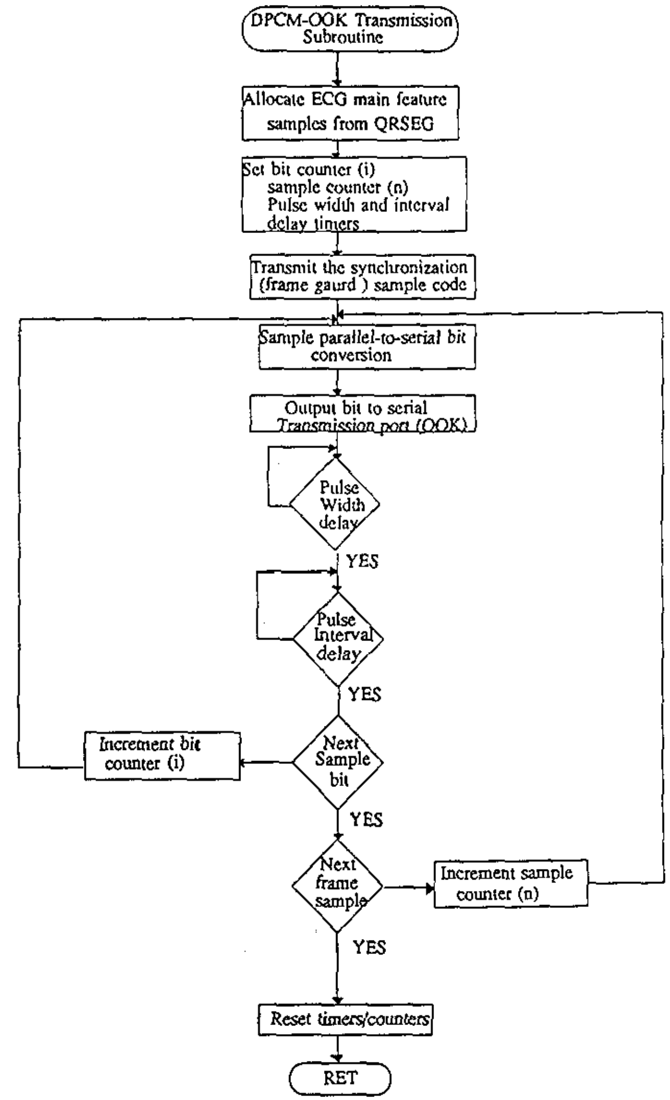

Fig.4.32c flow chart of the DPCM/OOK transmission

(i) *Linear Filtering*

The first step is the application of backward difference filtering, a standard technique for digital linear filtering, and to provide the basis for the next processing stage. Let $Y(i)$ where i=1, 2, ... n, denote the present ECG sample and n is the total number of the samples in the buffer window. Then the ECG signal is approximated by computing the first-order backward difference, $D(i)$ as follows:

$$D(i) = Y(i) - Y(i-1) \qquad (4.12)$$

where $Y(i)$ is the present sample

(ii) *Non-Linear Transformation*

Next is the non-linear transformation that consists of point-by-point multiplication of the signal samples. This transformation serves to make all the data positive prior to the subsequent adaptive threshold stage, and also accentuates the higher frequencies in the signal obtained from the differentiation process. These higher frequencies are normally the representative characteristic of the QRS complex. The output of the non-linear transform is given by:

$$h(i) = \begin{cases} D(i)D(i-1) & \text{if } D(i)D(i-1) > 0 \\ 0 & \text{otherwise} \end{cases} \qquad (4.13)$$

where $h(i)$ is the nonlinear transform output.

(iii) *Refractory Blanking and Detection threshold*

In this procedure the squared waveform is passed to an adaptive threshold detector that continuously examines a pre-specified refractory blanking period of 120 ms set experimentally immediately after the R-wave sample allocation to prevent multiple QRS false detection and blanks the detection process before the next pulse. As shown in Fig.4.32a the processor first checks the status of an internal refractory flag F_{ref}. If the flag bit is not set then it branches to the *QRS complex allocation* subroutine. In this subroutine the program sets a fixed internal threshold decay time. Once this delay has elapsed, the current threshold value is halved and compared with the latest *h(i)* value from equation 4.13, then the last threshold level $L_{Thres.}$ is maintained and the next sampling process is repeated.

Fig. 4.33 shows a typical ECG signal obtained from an exercising subject connected to the transmitter system for measuring the noise level in the system. The maximum noise level during the test procedures was measured as $\pm$ 200 $mV_{p\text{-}p}$. This maximum floating noise level was selected experimentally to determine the lower bound allowed for the minimum threshold level to decay in the detection process. The other main loop of the decision process is the *threshold maximization* subroutine. This loop is activated by a special counter/timer incremented each time if the resultant refractory flag is set. A comparison process is followed between the current *h(i)* and last $L_{Thres.}$ value. If the result is positive i.e $h(i) \geq L_{Thres.}$, then the current *h(i)* value is allocated to the current $L_{Thres.}$, if not the last $L_{Thres.}$ is maintained. The process is continued until the maximum *h(i)* value, $h(i)_{max}$ is detected, representing the current peak R-wave sample. Consequently the program checks if the refractory delay has elapsed, then the refractory flag and the relevant counter/ timer are reset and the subroutine returns to the main program, otherwise the refractory flag remains at the set status until its time elapses. However, immediately following this stage where the R-wave and QRS complex samples have been detected within the current moving window frame, the program passes to the next processing stage, while setting $L_{Thres.}$ at the last maximum value of $h(i)_{max}$ for detecting the next QRS complex.

(iv) *QRS sample segmentation and main feature extraction*

In this part of the detection algorithm the program freezes the current window and segments the main block to 10 samples representing the main QRS features from the contents of the 100 samples RAM memory block for subsequent coding and transmission. The segmentation and feature extraction process is essential as it is not possible to digitally code and transmit all the samples of the memory block within the time frame between two successive QRS pulses. This takes into consideration the reverberation decay time for the transmission of each coded data sample. This process minimizes the required transmission time by a ratio of 1/10th of the original time between two successive pulses, and consequently reduces the transmission sampling frequency by the same factor, i.e. scales the transmission sampling frequency f_{sc} to 20 Hz from the original 200 Hz. This enables the slow rate transmission required in the multipath environment. Furthermore, this frequency is still much higher than the required Nyquist sampling rate of the original sampled signal in the time-window block f_{sw} of 2Hz (1/500ms), i.e. $f_{sc} >> 2f_{sw}$ required for the ECG sample data transmission.

The RAM memory address of the detected sample $h(i)_{max}$ representing the peak R-wave sample in the detection program starts the segmentation process from the contents of the original data samples. This is done by successive incremental counting every 10th. sample then decremental counting in the RAM memory block with reference to the identified position of the $h(i)_{max}$ sample. The segmentation process is explained with reference to Fig 4.32b and Fig.4.34. Assuming the position of $h(i)_{max}$ is N_{Rmax} then the subroutine counts the new samples up as $N_{Rmax+10i}$ and decrements down as $N_{Rmax-10i}$ where i=1,2,..5 (i=1,2,..4 for decrement count) is the original sample's position count. The forward-backward segmentation process within the detected window block allows the program to extract other features in the ECG signal such as the P-wave. The resultant 10 samples representing the main features of the PQRS signal are thus extracted for the coding and transmission. Fig.4.35 shows a real-time sampled QRS segment obtained by the sampling process, exhibiting the main features to be coded.

4.3.2.2 Digital pulse code modulation and On-Off Keying (PCM/OOK) transmission

The next phase of the software processing is the sample pulse coding and On-Off transmission control. This algorithm is explained with reference the general block diagram in Fig.4.31, Fig.4.32C and the PCM timing sequence shown in Fig.3.4a. The stored digital samples obtained from the detection algorithm are coded into 7-bits on a sample-by-sample basis: a block of 11 time slots of binary coded digits is mapped per transmission frame in accordance with the encoding format, including the code slot to provide word frame synchronization for the data block.

Clearly, the more sample time slots allocated per frame, the higher the information rate achievable for a given frame rate. On the other hand, as we increase the number of time

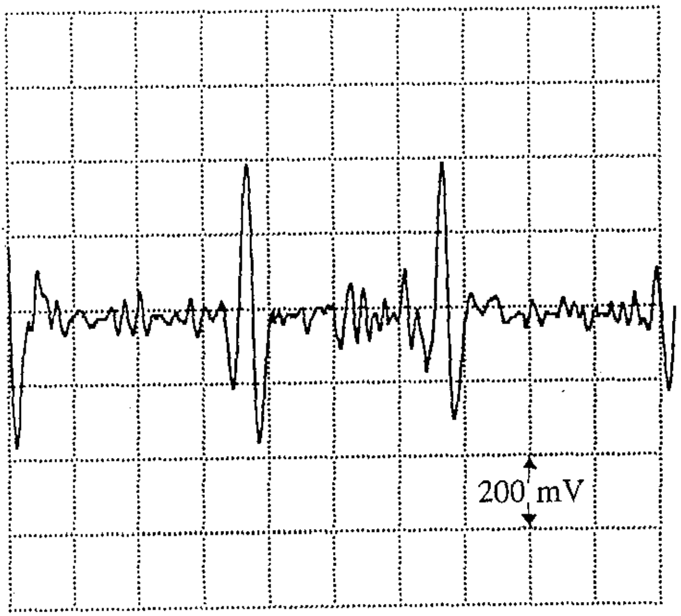

Fig.4.33 Noise level in an exercise ECG signal

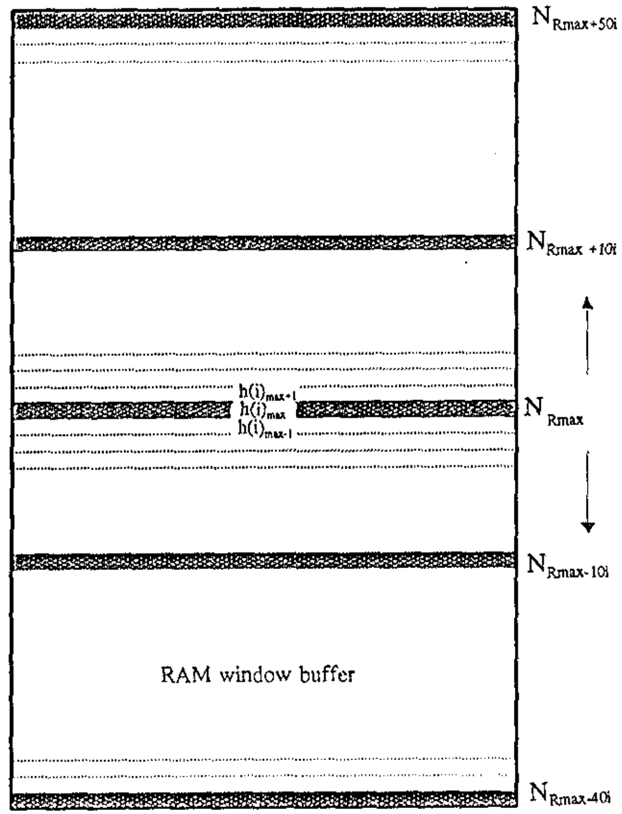

Fig.4.34 Memory block segmentation of sampled ECG signal

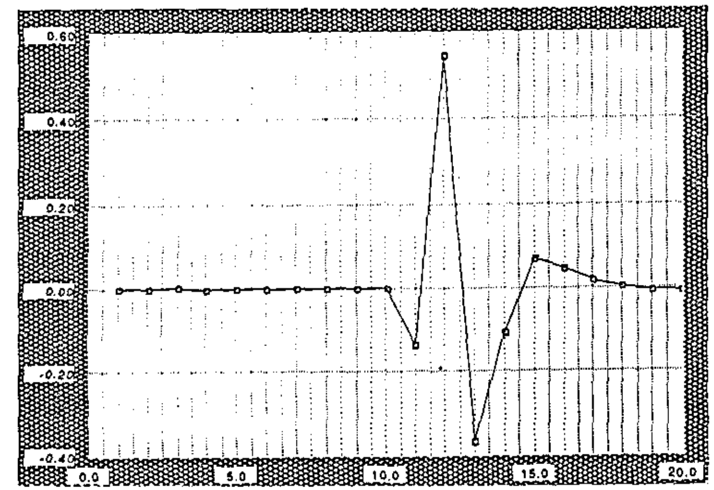

Fig.4.35 Sampled QRS segment with main feature data points

slots, synchronization becomes more difficult: for correct decoding of the data from the incoming signal, timing information relating to the frame boundaries and time-slot locations become difficult to detect in the receiver. The characteristics of the ECG transmission in a multipath reverberant environment limits the potential information of the input frame of digital data. The main limitations are time interval restricted by the adjacent QRS complexes of the incoming ECG signal that could be shortened or prolonged depending on the exercise and workload, and the degree of reverberation decay time. Since pulses cannot be transmitted at intervals less than the time required for the last significant multipath echo to reach the receiver this imposes limitations on the digital frame transmission rate. However, the coding/transmission scheme used here represents a compromise between maintaining long intervals between transmission and data rate compatible with the degree of reverberation. Furthermore, the scheme's digital timing structure can be reprogrammed in the transmitter software to adapt flexibly to different multipath requirements. In the current testing environment, assuming the time interval between the successive QRS signals is τ_{QRS} and if $0.9\tau_{QRS}$ is used for the frame transmission to allow an additional coding security gap between each transmitted ECG frame. The transmitted contents in the 10 digital ECG samples and the synchronization slot are each represented by 7-bits, allowing 10 intermittent bit spaces between each transmitted slot. Thus, for the current frame structure, the transmission bit rate f_{bit} in this case is given by:

$$f_{bit} = 1/\tau_{bit} = 1 \;/\; [(0.9\ \tau_{QRS} \;/\; (10+1)x7 + 10)] = 96.66 \;/\; \tau_{QRS} \qquad (4.14)$$

where τ_{bit} is the time interval for one-bit pulse transmission in the frame.

This means that the maximum transmission bit rate in this case is dependent on the instantaneous heart rate or the R-R interval that varies according to the degree of the exercise and the reverberation decay time of the multipath present. This can be reprogrammed according to the requirements and the nature of the environment. However, the variation in the bit rate shown equation 4.14 does not affect the system's heart rate accuracy readings while the ECG signal is being monitored as this is done by separate hardware processing from the direct R-R interrupt measurements based on a coding method from the ECG module discussed in the section 4.3.1.1.

The pulse coded parallel-to-serial conversion program starts with the initial transmission of the 7-bit synchronization (frame guard) code (111 1111) to signal the receiver processor that the next 10 slots represent new ECG data. This is followed by serial transmission of the scaled 7-bit coded data samples, as explained in section (4.2.1.1.6). The program first fetches the ECG samples from the RAM area in the lookup table allocated from the detection algorithm. Then it transmits successively the 7 serial bit-by-bit format and outputs the 1 or 0 bit within the frame to the specified output port bit connected to the channel's output On-Off keying transmission circuit. The width of the transmitted bit pulse of 100μs is programmed together with the appropriate pulse interval τ_{bit} maintained at 20 ms and found suitable for the tank experiments. The QRS detection and PCM algorithms occupied 1084 bytes in the microcontroller's EPROM, and the execution time of the QRS detection algorithm was on average less than 1.3 ms.

4.3.3 Transmitter housing

The complete transmitter was constructed using printed circuit board techniques for each module. These were implemented on separate single sided boards, each 0.75mm thick and 95mm in diameter. Fig.4.36 shows the final transmitter housing and mounting details. The judicious partitioning of the circuitry reduces the overall size and allows the boards to be placed back-to-back in the housing using special fastening bolts prepared for the boards. The completed and tested transmitter boards were placed in underwater cylindrical buoy as shown in Fig.4.37. The underwater housing is constructed from tubular and solid PVC. It is 115mm in diameter and 350mm in total length with one end completely sealed with a transparent PVC cover while the other end is a removable cover carrying the depth sensor, connecting cables and the ceramic projector. It was machined and made depth proof by an O-ring seal. The buoy comprises a battery compartment and an electronics compartment. The lower battery compartment carries the alkaline batteries and the dc-dc converter and regulator circuits with special for connections with transmitter electronics. The upper compartment contains the transmitter sensors, signal processing and drive electronics and the microcontroller boards connected through water-proof plugs to the projector. The piezoelectric depth sensor is mounted on the outside surface of the cylinder's cover, which is machined with a fitting having an O-ring seal to provide a water proof connection. The surface of the sensor is also

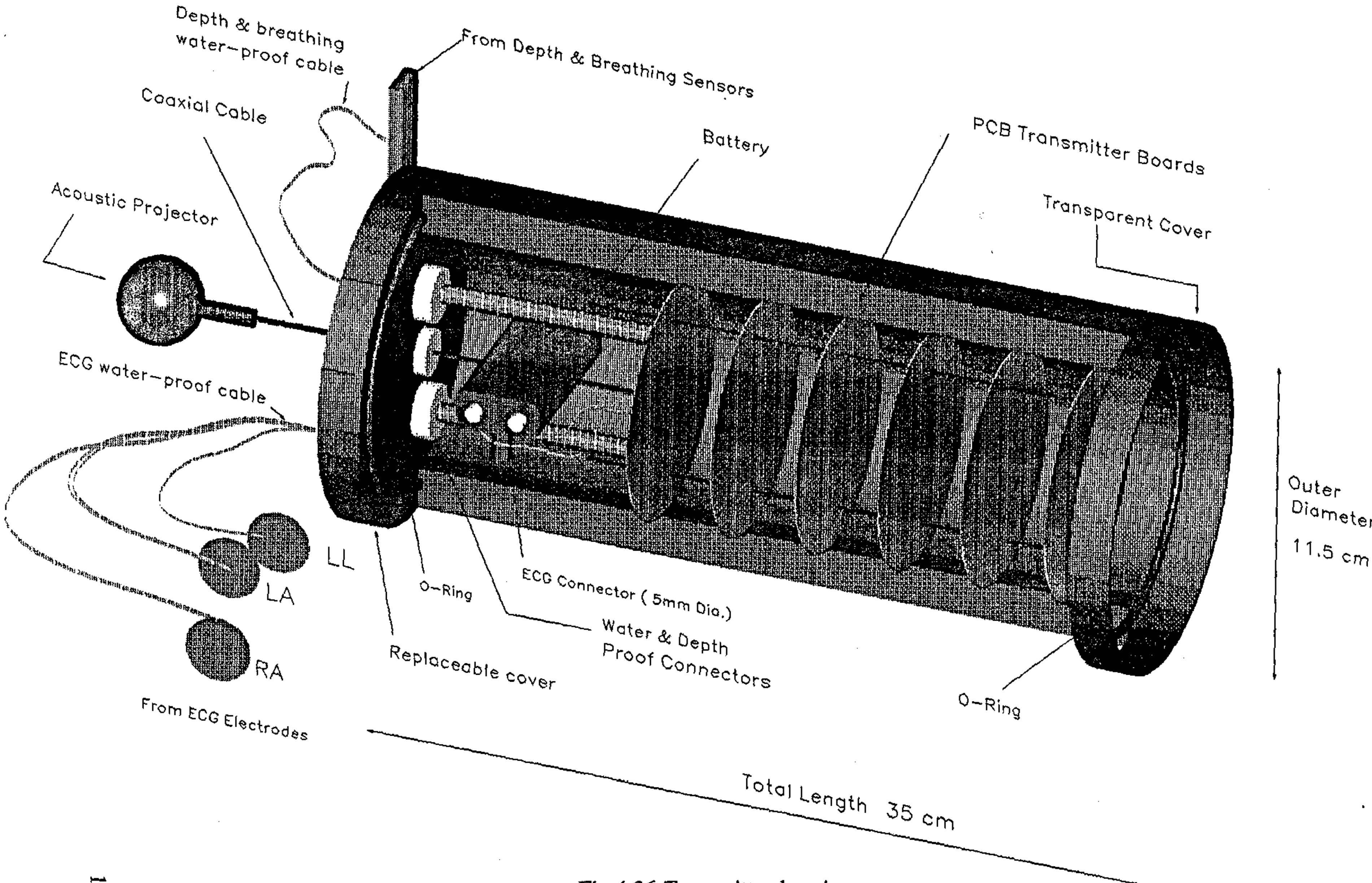

Fig.4.36 Transmitter housing

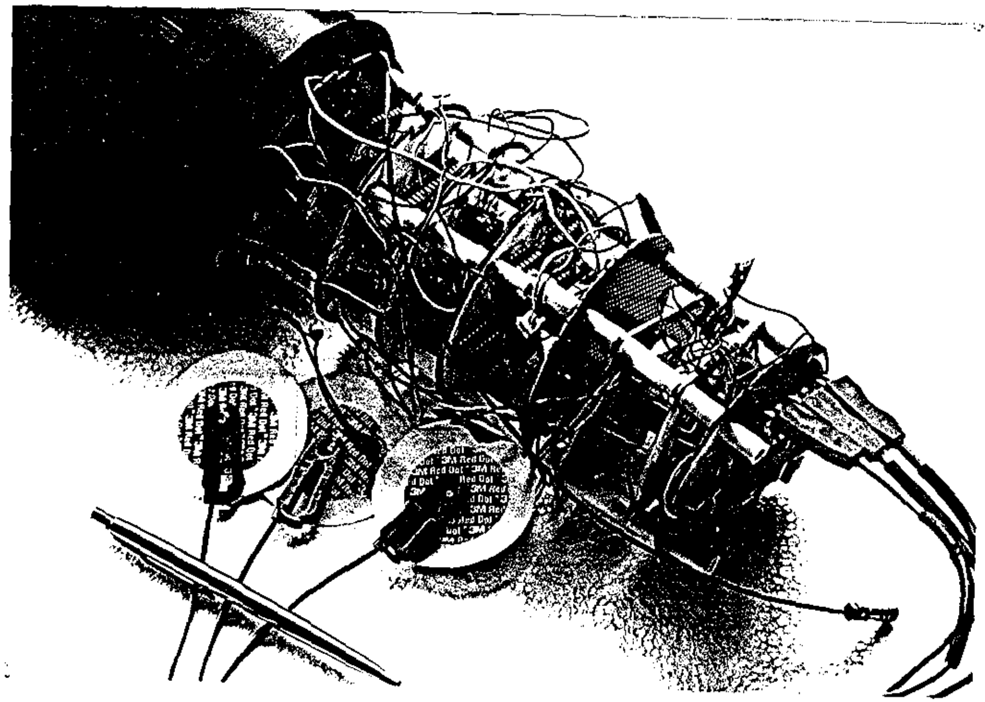

Fig.4.37 Photograph of the complete transmitter realization

Fig.4.38b Transmitter mounting on a diver's tank

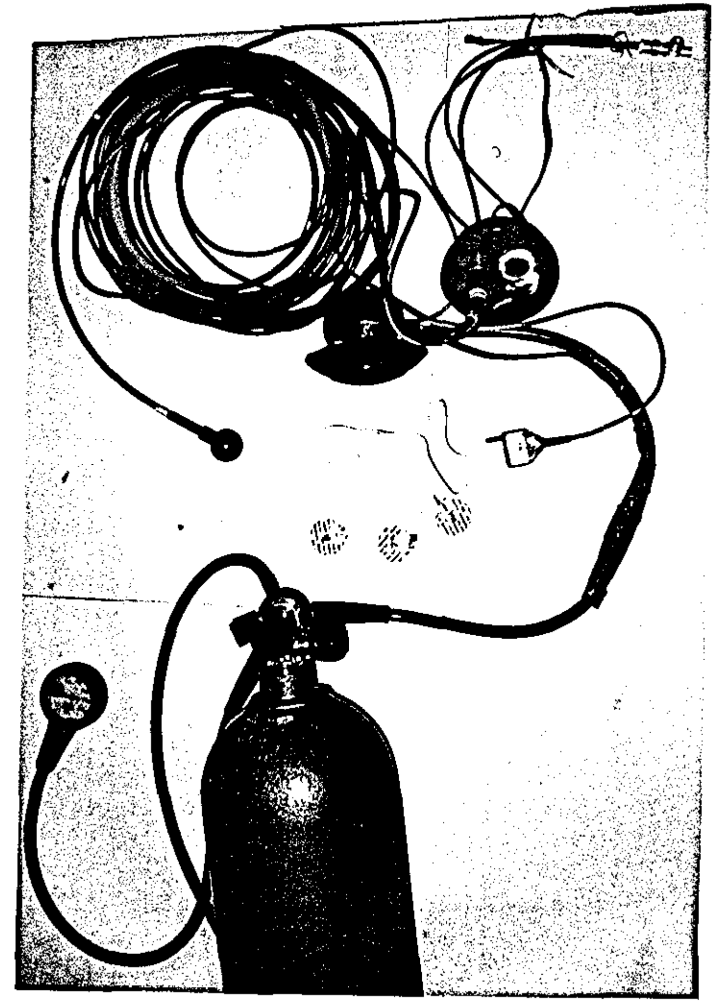

Fig.4.38a Photograph of the telemetry sensors with SCUBA kit

covered with 2mm of MS4 silicon compound. Similar water-tight machined connections were made for the acoustic projector and the ECG electrode leads. Fig.4.38 shows the transmitter and how it is attached to typical diving equipment and its mounting on the SCUBA diver. The housing is fitted to the diver's air tank by a special belt tailored and the ECG leads are connected from the chest to the transmitter through the neck seal of the dry suit by water proof plug-in connectors.

4.3.4 Experimental tests for underwater transmission in the departmental tank

In order to validate the performance of the acoustic telemetry link under varying operating conditions, the effects of the multipath in a very shallow reverberant underwater environment were investigated. The effects resulting from the movement of the transmitter in a confined shallow environment such as a swimming pool were also studied. The aim here was to study the limitations imposed on the performance of the communication link coded for such conditions. To study these constraints and the influence of the multipath reverberations on the performance of the system an experimental set-up was implemented in a large departmental water tank for simulating shallow communication channel.

(i) Water tank and gantry system

The water tank is made of concrete, with a thin plaster and a gloss paint layer but with no acoustic lining. Its inner dimensions are 9m long, 5m wide and 2m deep. It is equipped with a movable gantry used to move the hydrophones with three degree of freedom on steel rails. Tap water was used in the experiment. Under experimental conditions, the temperature was 16.0^{0}C, and the salinity was assumed to be zero. The temperature in the tank during the experiments was quite constant (within 1 ^{0}C) and as a result the sound speed in water was assumed to be constant at 1500ms^{-1}.

(ii) Experimental set-up and test results

The complete underwater communication test system is shown in Fig.4.39. The transmitting and receiving instrumentation set-up consists of on-off keyed pulsed signal derived from a programmable pulse generator (Hamek HM8130) to control the pulse widths, sequence codes

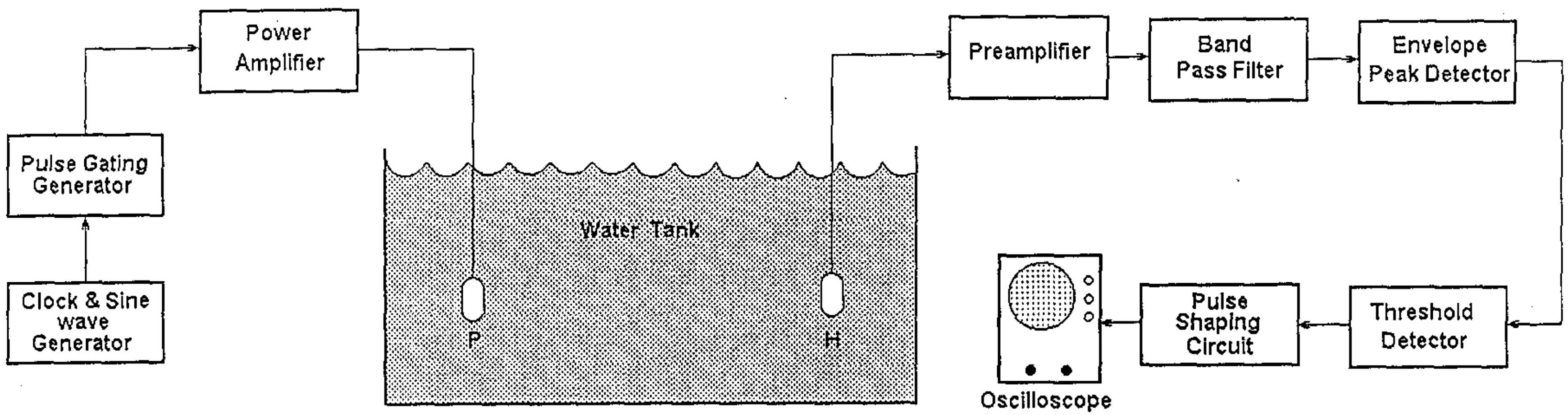

Fig.4.39 Block diagram of the experimental underwater communication test system

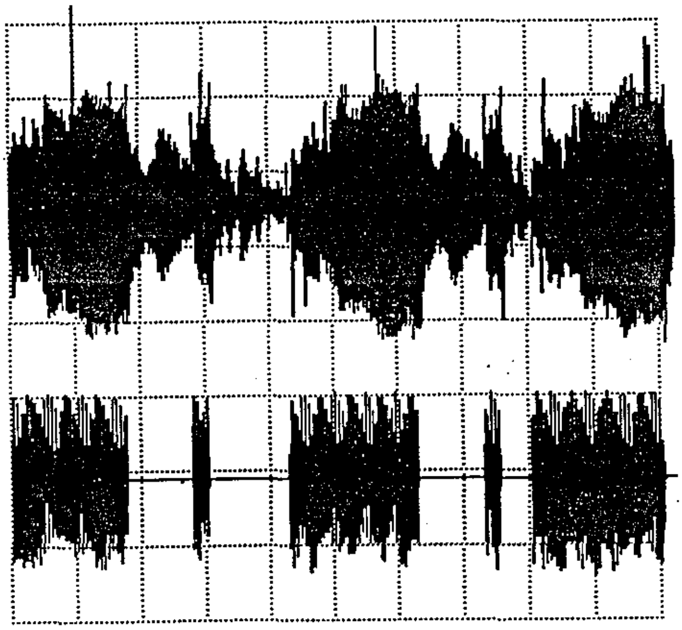

Fig.4.40a Multipath propagation in the tank for transmission rate of 100 Hz and pulse-width of 4ms

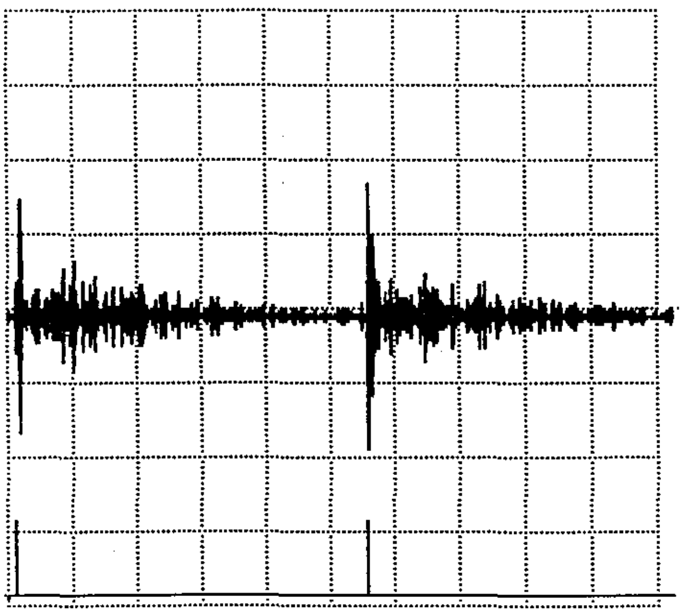

Fig.4.40b Multipath effect for transmission rate of 20 Hz and pulse-width of 0.1ms

and carrier signal, generated by a function generator (Farnell LFM3) fed to a low noise power amplifier whose output is connected to the projector. The receiving hydrophone was lowered to depths from 0.5m to 1.5m in 0.5m steps and fixed at the middle of the tank, i.e. 4.5m from each end. The projector was located at different depths and ranges from the hydrophone and acoustic burst transmissions were generated to assess the multipath effect in terms of transmission rate and pulse width. Fig.4.40a shows sample response of burst transmission with different binary coded sequences and the corresponding impulse responses at the receiver. The range was 2m and both the projector and hydrophone were at 1m depth. The transmission bit rate was set at 100 Hz and the pulse width adjusted to 4ms. It can been seen that the effect of successive multipath overlapping on the receiver signal at higher transmission rates and long pulses in such that it is not possible to discriminate individual direct path because of the destructive multipath between successive transmissions. Fig.4.40b shows another sample response from a similar range but the projector lowered 0.25m deeper than the hydrophone depth and at slower transmission bit rate 20Hz corresponding to pulse width of and 0.1ms. It is obvious from the above responses that in such a shallow environment, narrowing the pulse width and lowering the transmission rate and thus allowing for the reverberation time decay over greater time durations, it is possible to discriminate the direct path from the multipath at the receiver. Furthermore, it was found that due to the geometry of the tank and the measured responses, the best position of the receiving hydrophone was in the middle of the tank at a depth of 1m. This was noticed especially from the bottom and surface where severe multipath occurred even with low transmission rates and narrow pulses. Such serious overlapping was noticed when lowering or elevating the projector by at least 0.2m from the bottom or the surface of the tank. Similar severe multipath reverberations were noticed as the projector was located within 0.1-0.2m any each side of the tank. These increased in proportion to the transmission pulse width increase. This could be attributed to the no-movement boundary areas enclosed by the six surfaces identifying the near surface and sides areas where it is not possible to discriminate the direct path from the multipath. This is due to the close reflection boundaries created by the symmetry of the tank and consequently this restricts the diver's movement to within these boundaries. The mathematical derivations and equations relevant to this topic is beyond the scope of this thesis but can be referred in several underwater acoustic processing references [63,64,75].

CHAPTER FIVE

BIOTELEMETRY RECEIVER DESIGN AND EXPERIMENTAL RESULTS

5.1 RECEIVER HARDWARE DESIGN AND REALIZATION

The design of the acoustic telemetry receiver is divided into three functional subsystems as shown in Fig.5.1. These are (i) hydrophone and receiver preamplifier circuitry, (ii) band-pass filtering with pulse discriminator and detection modules, (iii) receiver command and data logging module.

The main function of the receiver is to scan the crystal-controlled transmitting frequencies and provide the logical output pulses for a detected input signal which in turn is relayed through the single-chip microcontroller-based command unit. The command processor provides the timing control and pulse decoding functions for each channel; this is synchronized with the telemetry protocols described in Chapter Four. It also serves as an interface for data collection between each acoustic channel and the data logger and acquisition units. The detailed hardware design and the function of each unit is discussed below.

5.1.1 The hydrophone and preamplifier circuitry

The input to the receiver consists of an omnidirectional hydrophone (type D-170) identical to the projector and is linked to the receiver by a coaxial cable. The two-stage low noise hydrophone preamplifier is shown in Fig.5.2. The input section is based on a BiFET op-amp circuit (AD743, Analog Devices), whose ultra-low noise performance (2.9 nV/√Hz at 10 kHz), high dynamic bandwidth (up to 4.5 MHz) and constant low offset voltage makes it a good choice for this application. The circuit is designed with the following -6dB bandwidth filter characteristics:

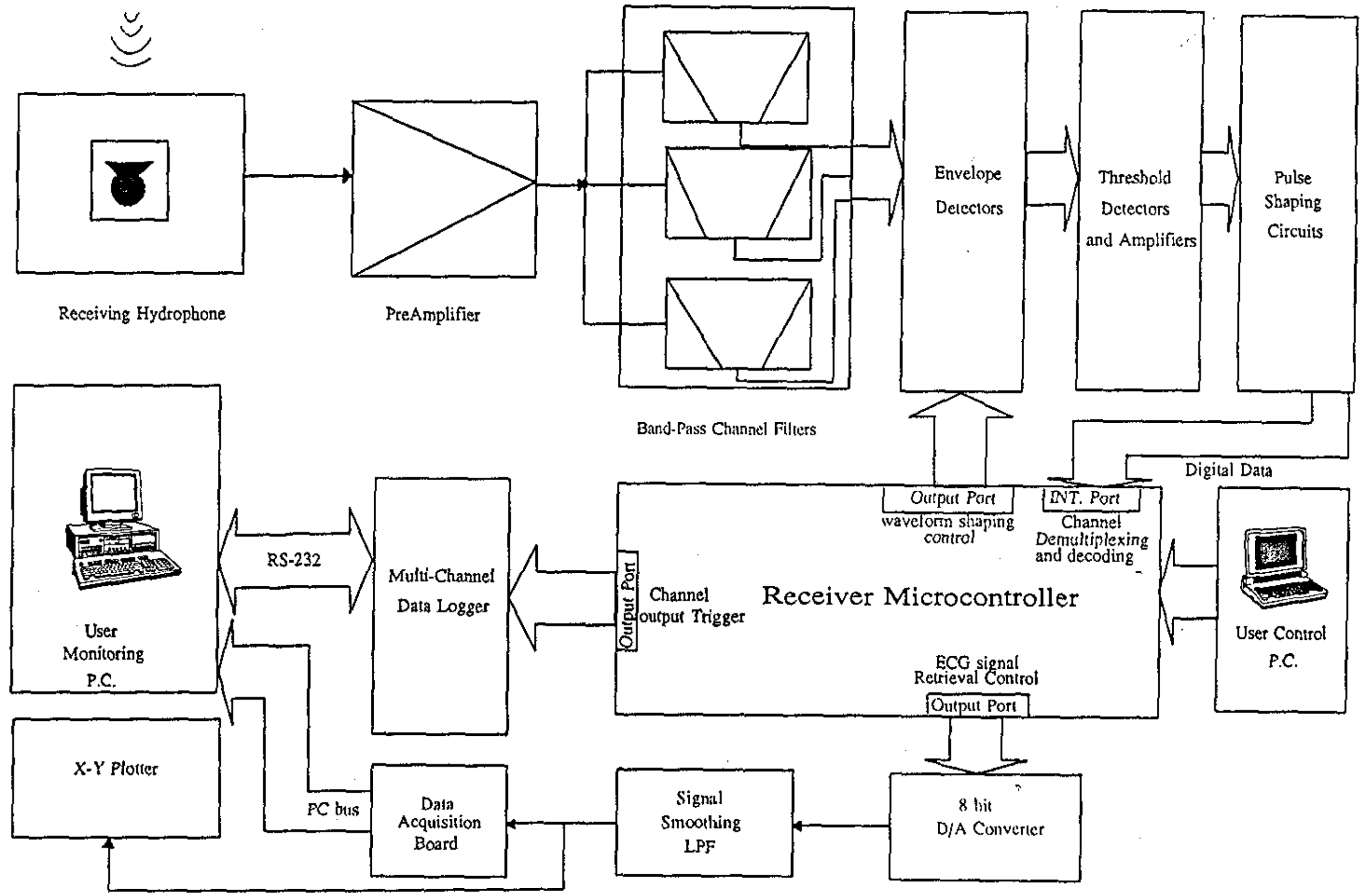

Fig.5.1 Functional blocks of the receiver hardware system

-Low cutoff frequency = 23 kHz,

-High cutoff frequency = 100 kHz,

-Nominal passband gain = 40 dB.

The required low and high frequency cutoffs with 20 dB/decade attenuation and nominal gain values are determined by adjusting the RC time constant relation of C_1, R_1, C_n, and R_2 as shown in the circuit. The gain of the amplifier can be further adjusted by a second stage low noise amplifier (OP-37GN) which amplifies the signals by a further 10 dB or more if required. The circuit was powered by a regulated ± 5V supply from a single 9V alkaline battery to eliminate pickup noise and signal distortion. The circuit was shielded and the input was connected to the hydrophone output by a coaxial socket.

5.1.2 Band-pass filters and digital pulse discrimination modules

The functional block of the receiver as shown in the schematic diagram of Fig.5.3 comprises three identical modules; consisting of narrow tuned band pass filters and digital pulse discrimination circuits. The front-end band pass filters are used for separating the received signals into the group of transmitted frequencies centred at 68.26 kHz,70.21 kHz, and 72.28 kHz respectively.

The main requirement of the filter is to provide accurate filtering of the three channels that lie within the -3dB frequencies of the transducing element, i.e. between 61.3 kHz and 78.3 kHz needed for the ASK tone detection. These channels should have a suitably wide 'passband' so as to allow for slight variation in the filters centre frequencies that may arise from inaccuracies in the component values. However, the centre frequencies for the various channels are ultimately determined by those that were generated digitally in the transmitter.

The filters used here were 8th-order active filters (MAX274). This one-chip IC consists of four independent cascadable 2nd-order sections, permitting 8th-order filters to be realized for centre frequencies up to 150 kHz, and having a centre frequency accurate to within ± 1% over the full operating range.

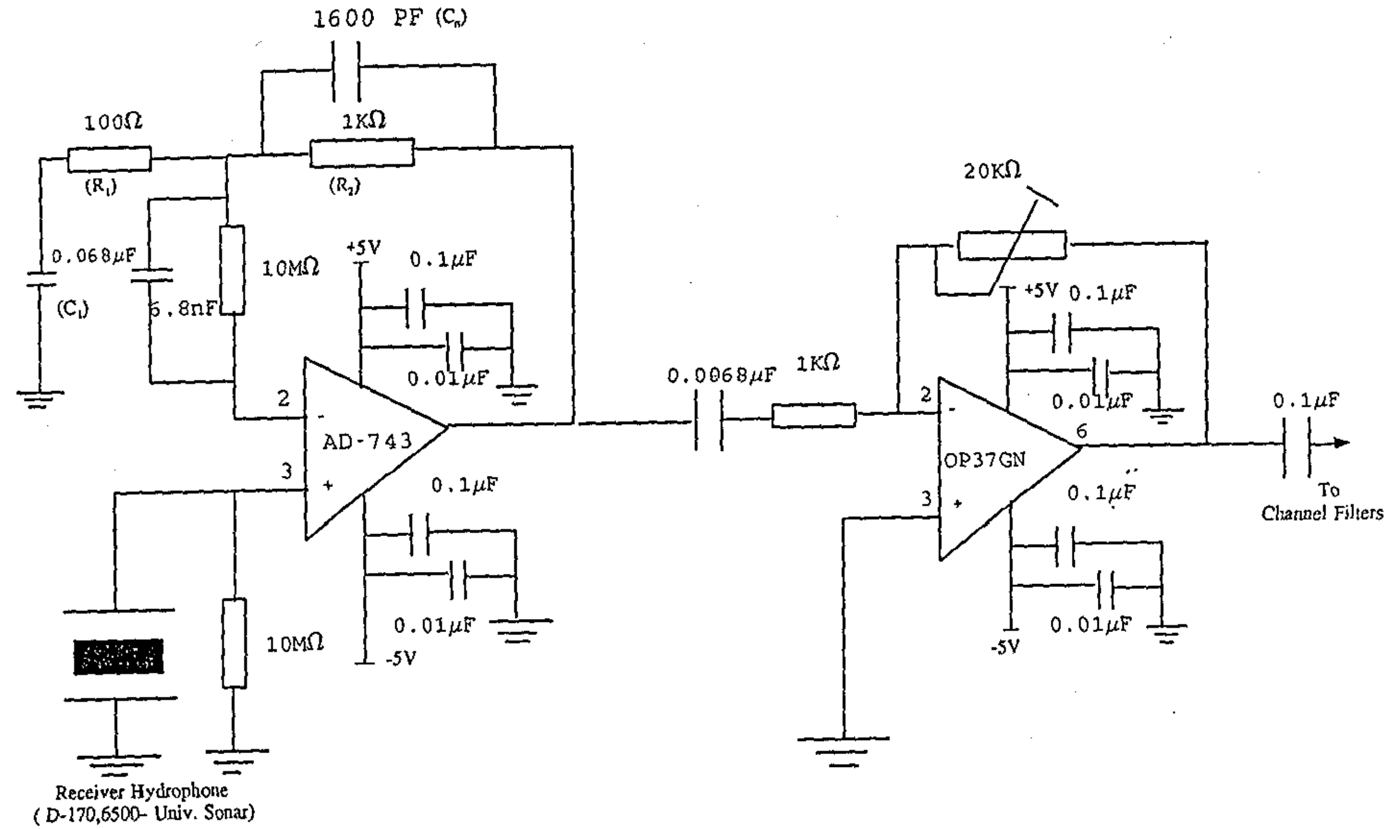

Fig.5.2 Schematic diagram of the preamplifier circuit

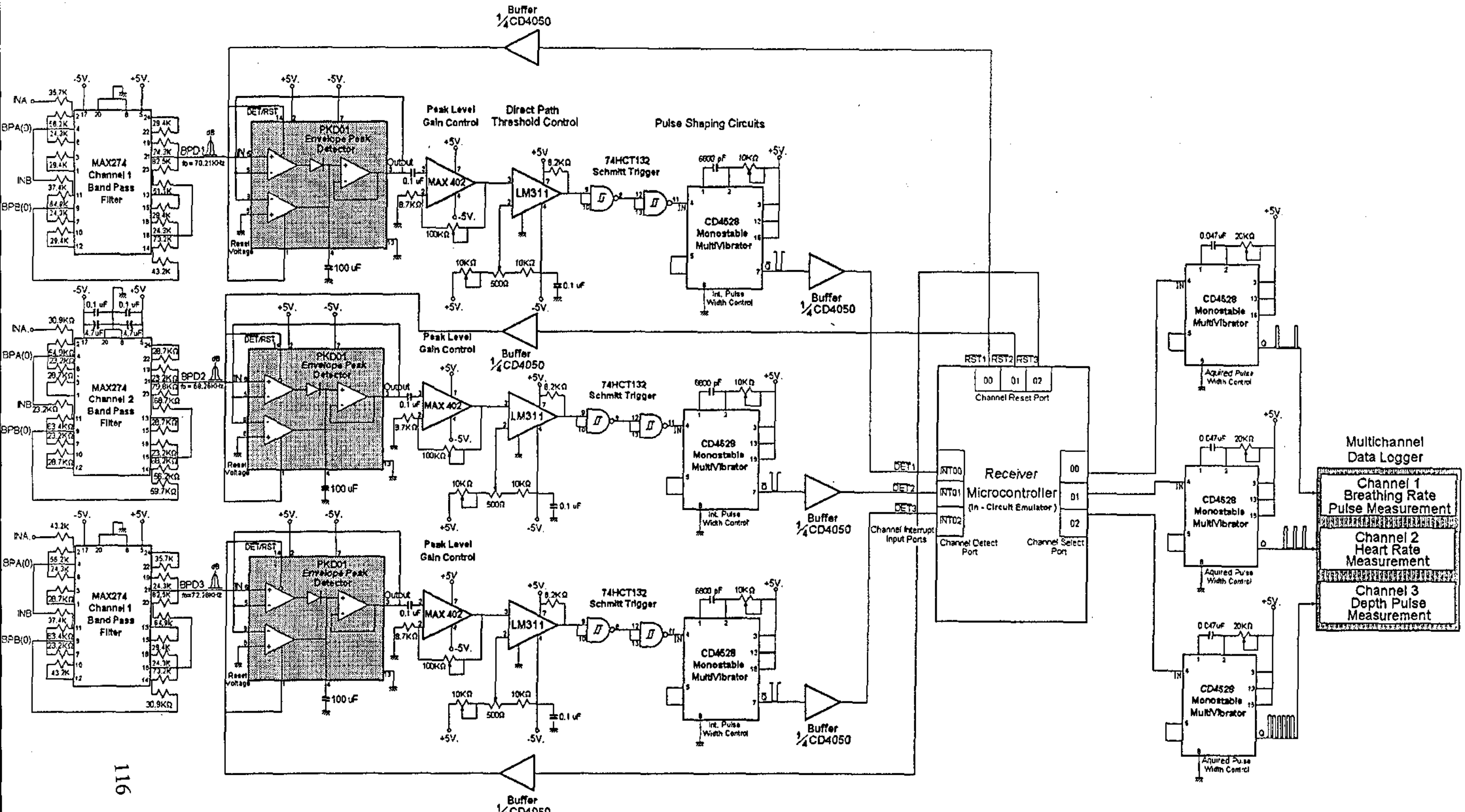

Fig.5.3 Schematic diagram of the multichannel receiver system

The 8th-order Butterworth filters were designed using a special active filter design and simulation software provided by the manufacturer (Maxim Integrated Products. Inc., Sunnyvale, CA.) for this chip. The design process depends on the number of cascaded sections, the required centre frequency, bandwidth and the overall filter gain.

The filters were designed using a strict stop band specifications to allow for maximum channel separation and received signal distingishability with characteristics as follows:

- Passband = Fc +/- 0.5 kHz
- 46 dB stopband = Fc +/- 1.5 kHz
- overall gain ≈ 20 dB (adjustable) → see figure 5.4 (attenuation)!!

The filter values calculated by the simulation results were implemented using ± 0.1% value resistances for maximum accuracy. The realization of the 8th-order filters produced highly desirable characteristics and separation responses. Fig.5.4 shows the results of a simulated response of a typical BPF design centred at 68.26 kHz and the corresponding spectral response of the filter. The filtered waveform signals are coupled to time-controlled envelope peak detectors by the receiver processor where the output is compared with adjustable threshold level circuits and passed to pulse shaping circuits that convert the detected signal output into digital format compatible with I/O processor interface. These discriminate the detected peaks from the reverberant effects of the transmitted signal and are driven in parallel by the signal output from each individual channel and each received pulse is discriminated in a similar manner. The detection method provides signal indication of the presence or absence of predetermined frequencies in each incident acoustic wave.

This programmable logic arrangement of "Frequency Diversity Exclusion-FDE" decodes only those signals showing a presence of pre-selected frequency transmissions and the absence of other frequencies.

The multiplex timing control arrangement of the detection process as shown in Fig.5.3 is again based on multi-interrupt triggering interrogated by the receiver command processor. The

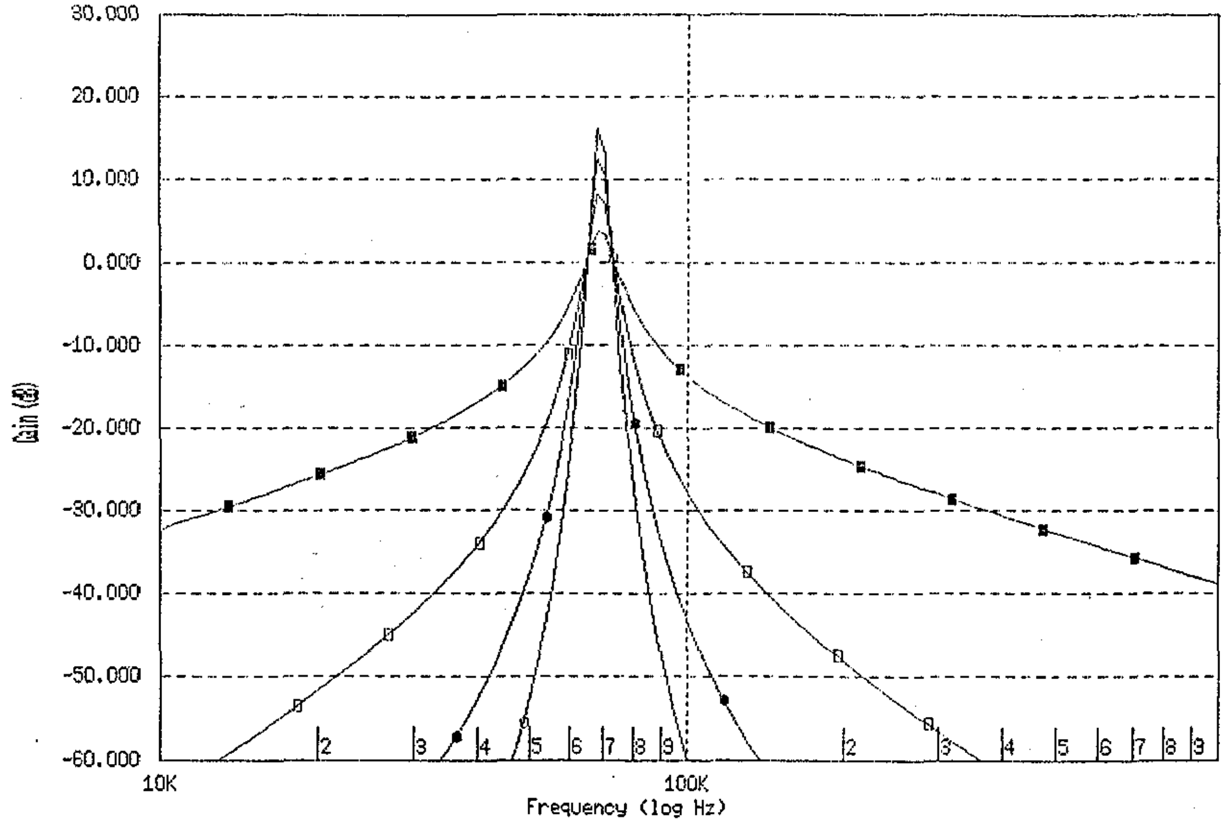

(a) simulated response

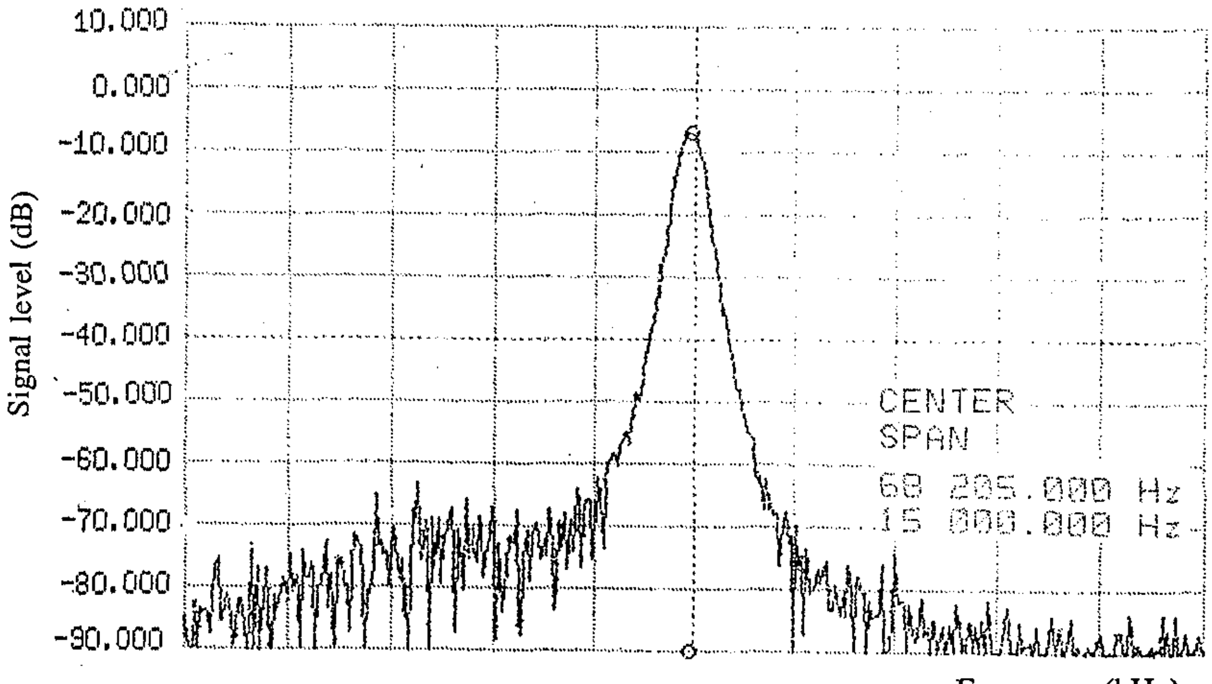

(b) measured response

Fig.5.4 Simulated and measured responses of the band-pass filter channel priority hierarchy is allocated identically as in the transmitter.

Once the appropriate channel is acknowledged, the microcontroller performs two operations. First it disables the detection process of the corresponding channel by resetting the function of the channel's envelope detection circuit. Then it triggers the appropriate output port pulse to the data logger. The channel is inhibited for approximately 20 ms, an interval determined experimentally, after which it alternatively starts enabling and inhibiting the detection circuit in 0.5ms window pooling intervals ready for the next received signal interrupt acknowledgment. This 'memorized' interrupt/timing control arrangement ensures that each channel is only open for reception at the time at which a corresponding transmission is expected and the trailing reverberation effect of the previous burst transmission has ceased. Fig.5.5 shows the timing diagram of the multichannel receiver operation illustrating the detection and logging of the heart rate signals.

5.1.3 Receiver microcontroller and data logging interface

The telemetry receiver processor acts as the main channel demultiplexing, decoding and time synchronizer unit. The chip can be programmed according to the required mode of operation synchronized with the transmission modes, as explained in sections 4.3.1.1 and 4.3.2.2. The two principal modes are the multichannel digital demultiplexing mode and the digital pulse decoding, frame synchronization and digital-to-analogue conversion control of the digitally pulse coded ECG signal transmission.

In this first mode it basically scans the three frequency synthesised transmission channels through an identical interrupt hierarchy, to which it is asynchronously linked to the transmitter. This telemetry link is achieved by the memorized gate timing control of each receiver channel. The trigger pulses from the corresponding microcontroller output port are captured by a multi-channel data logger (Grant/Eltek, Model 1200, Cambridge,England), as shown in Fig.5.3.

This portable logger consists of four channels equipped with programable pulse count and recording interval selection options for measurement of instanteous heart rate, breathing rate and depth data.

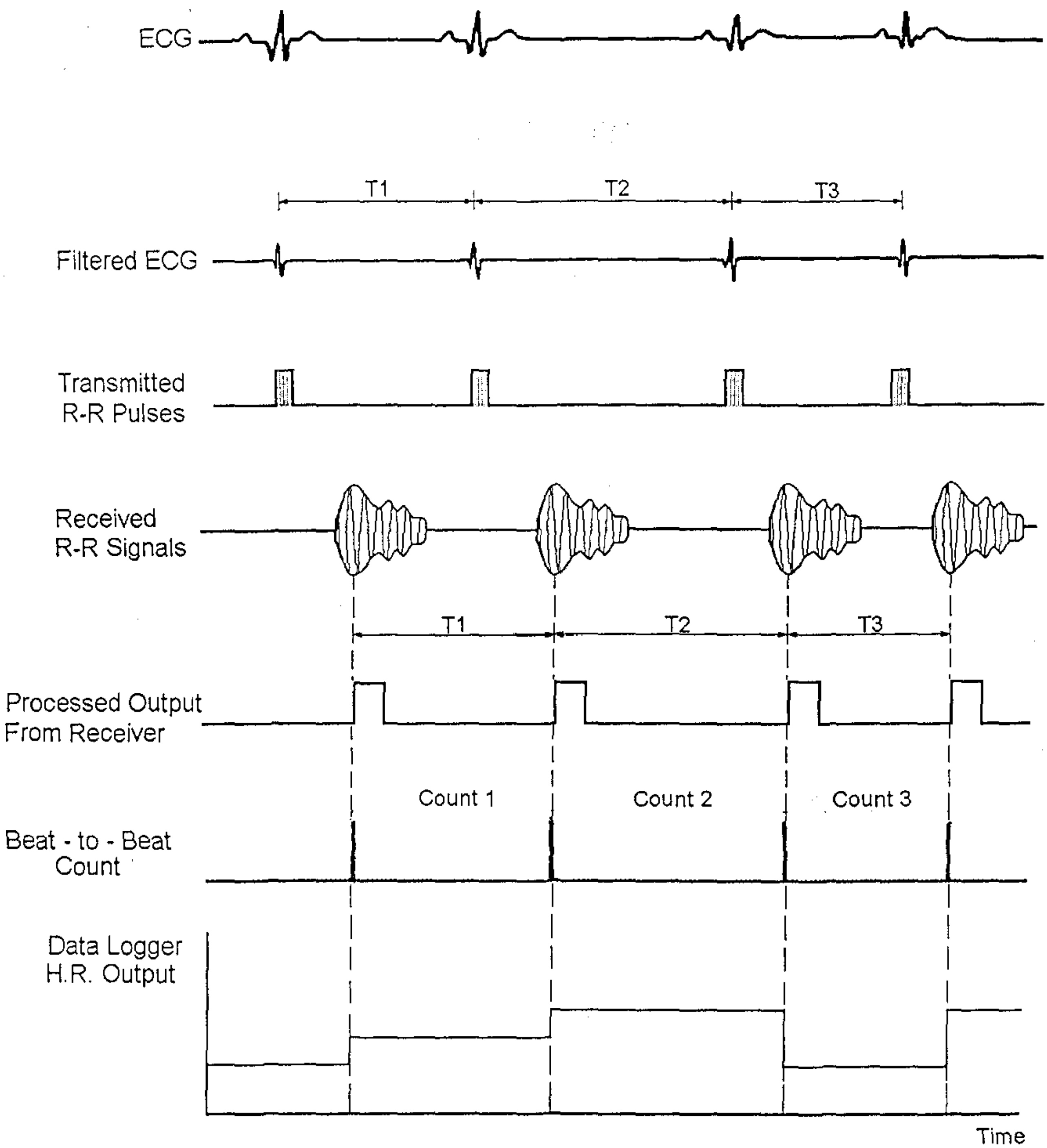

Fig.5.5 Timing diagram of the receiver operation illustrating the heart rate logging channel

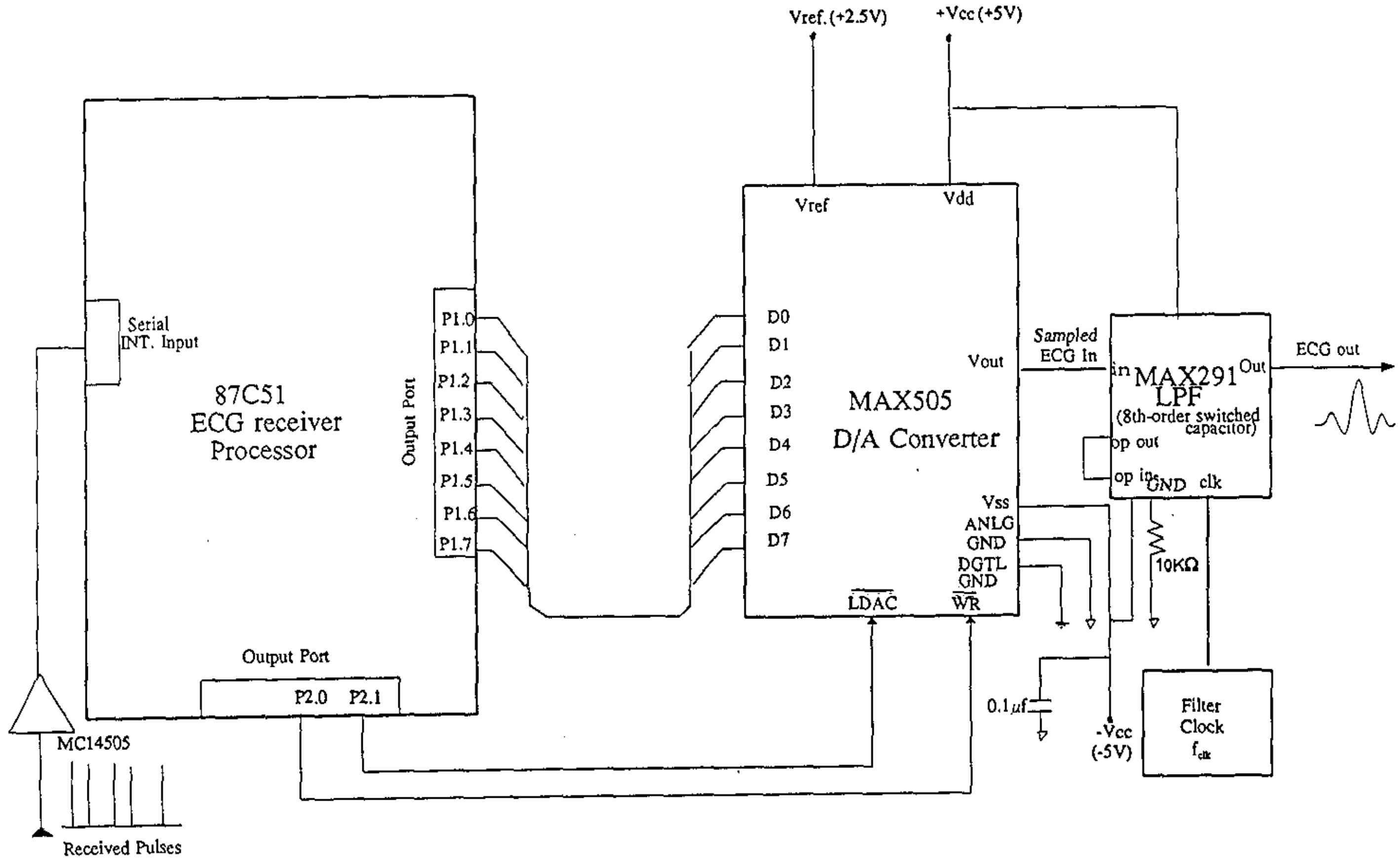

Fig.5.6 Schematic diagram of the ECG receiver and signal retrieval interface

The logger is designed with an in-built display to review the recorded data and is equipped with an RS-232 serial interface to down load the data to a portable IBM-compatible computer for supervisory data monitoring and further analysis. The instanteous heart rate readings are calculated using the formula:

$$H.R. = (n\text{-}1) \times 60 \,/\, m \quad \text{beat/min} \tag{5.1}$$

where n is the number of received (R-R) pulses within a fixed time interval and m is the time interval between the first and last beat pulses measured to the nearest 0.1s.

The time intervals for the average heart rate measurement are set at 5s for accuracy and timing correlation with the heart reading intervals obtained from the Polar system.
The other channels (depth and breathing rate) were measured by recording the received pulses by the logger programmed to count the pulses over the same time interval i.e. 5s. averaged for recording intervals of 1min.

In the second mode the chip is programmed to decode the received pulse coded ECG samples and synchronize the reception of each transmitted ECG frame. Then it reconstitutes the original analogue ECG signal from the decoded sample words stored in the on-chip RAM using an 8-bit D/A converter (MAX505).

This is interfaced to the appropriate output ports and the output is consequently passed to a switched capacitor 8th-order low-pass filter (MAX291). This smoothing filter is tuned to the received samples by an external clock operating with 100:1 clock-to-signal frequency ratio for smoothing out the sampled ECG signal as shown in Fig.5.6. The reconstructed ECG signals can either be interfaced to a PC-based data acquisition board such as (Amplicon DASH-27, Brighton, England) or to an X-Y plotter for strip-chart viewing and further analysis.

5.2. RECEIVER SOFTWARE

The microcontroller at the receiver is operated on PC-based Intel-87C51 emulation module (ICE-51FX/PC) that can provide a fast and flexible environment to run the receiver command programs into the Intel ASCII machine code by simply loading the specified program to the computer and activating the processor in-circuit emulation board connected to the receiver.

The software design of the receiver processor is based on the inverse functional operation and execution of the trans-receiver telemetry protocols explained in the Chapter Four. Fig.5.7 shows a block diagram of the software organization and operation in the multichannel interface mode. The program initializes the I/O, vectored interrupt priority ports for each channel and resets the internal timers. The processor then waits for the received channel pulse and the interrupt activation. The program then resets the channels envelope detector to disable the channel and starts the internal timer to count for the reverberation decay time. It also triggers the corresponding output port bit to the logger via the output monostables that control the data logger trigger pulse widths. Once the reverberation decay time has elapsed the receiver is re-enabled again over 0.5ms set/reset pooling intervals for the next pulse acknowledgement.

In the second (ECG) mode of operation the processor acts as a digital pulse coded decoder and its function is divided into two main successive subroutines. It first receives and identifies the serial code pulses assigned in each transmitted ECG frame. This is obtained from a input high speed interrupt-timer based bit used for scanning the incoming pulses obtained from one of the receiver channels as described in the first mode of operation.
The program first identifies the synchronization (frame guard) code, then performs the serial-to-parallel conversion and queues the memory samples into the ten original transmitted bytes. Finally, it controls the transfer of each allocated sample block successively to the D/A circuitry and then for further display and/or monitoring and analysis. The D/A circuitry is scaled similarly to the A/D conversion in the transmitter for the bit matching in the receiver, i.e. for the maximum retrieved ECG level not to exceed half the same full-scale reference bit level of the D/A used. Fig.5.8 shows the flow chart of the ECG sample decoding and signal retrieval program.

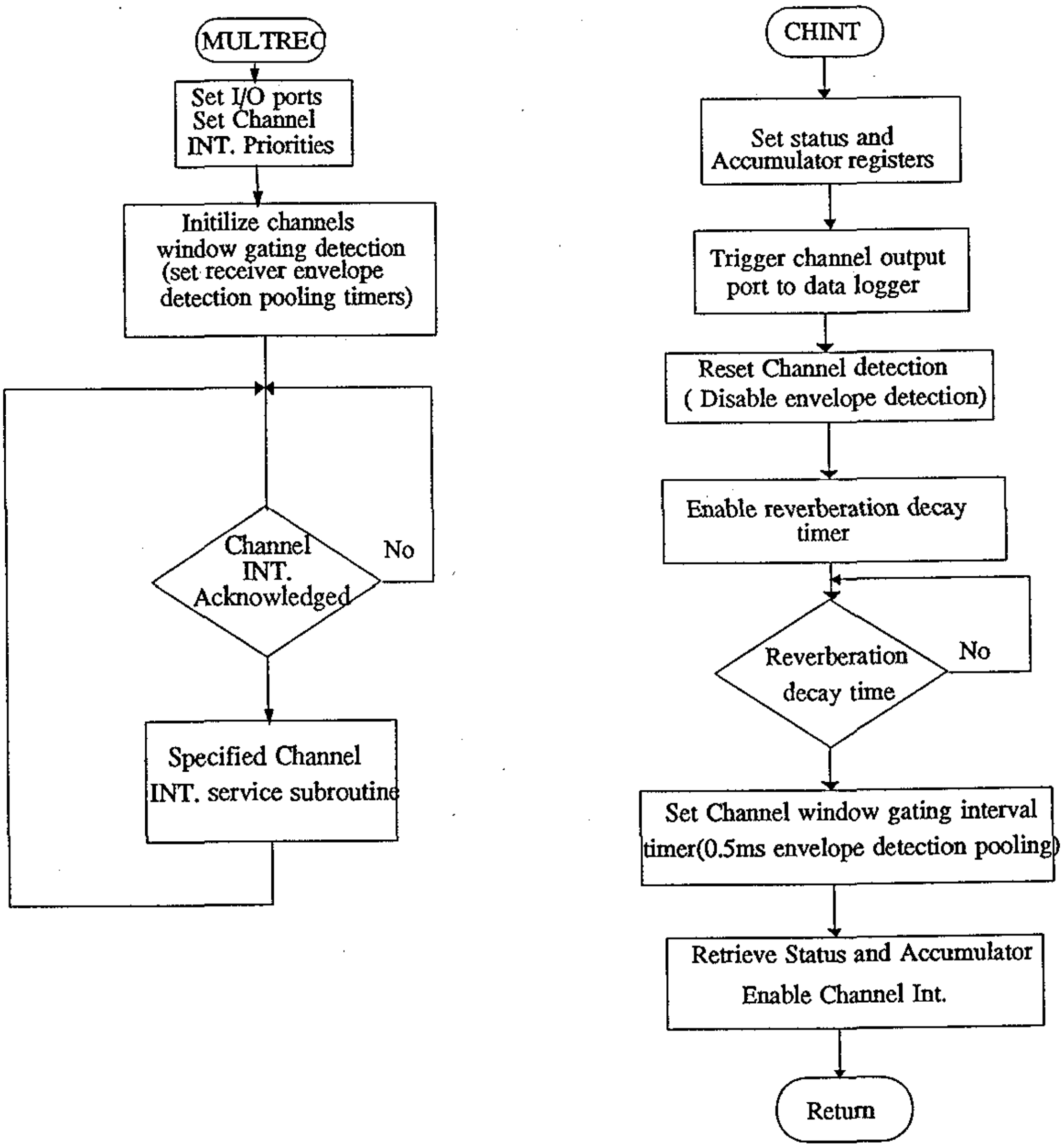

Fig.5.7 Flow chart of the multichannel receiver program

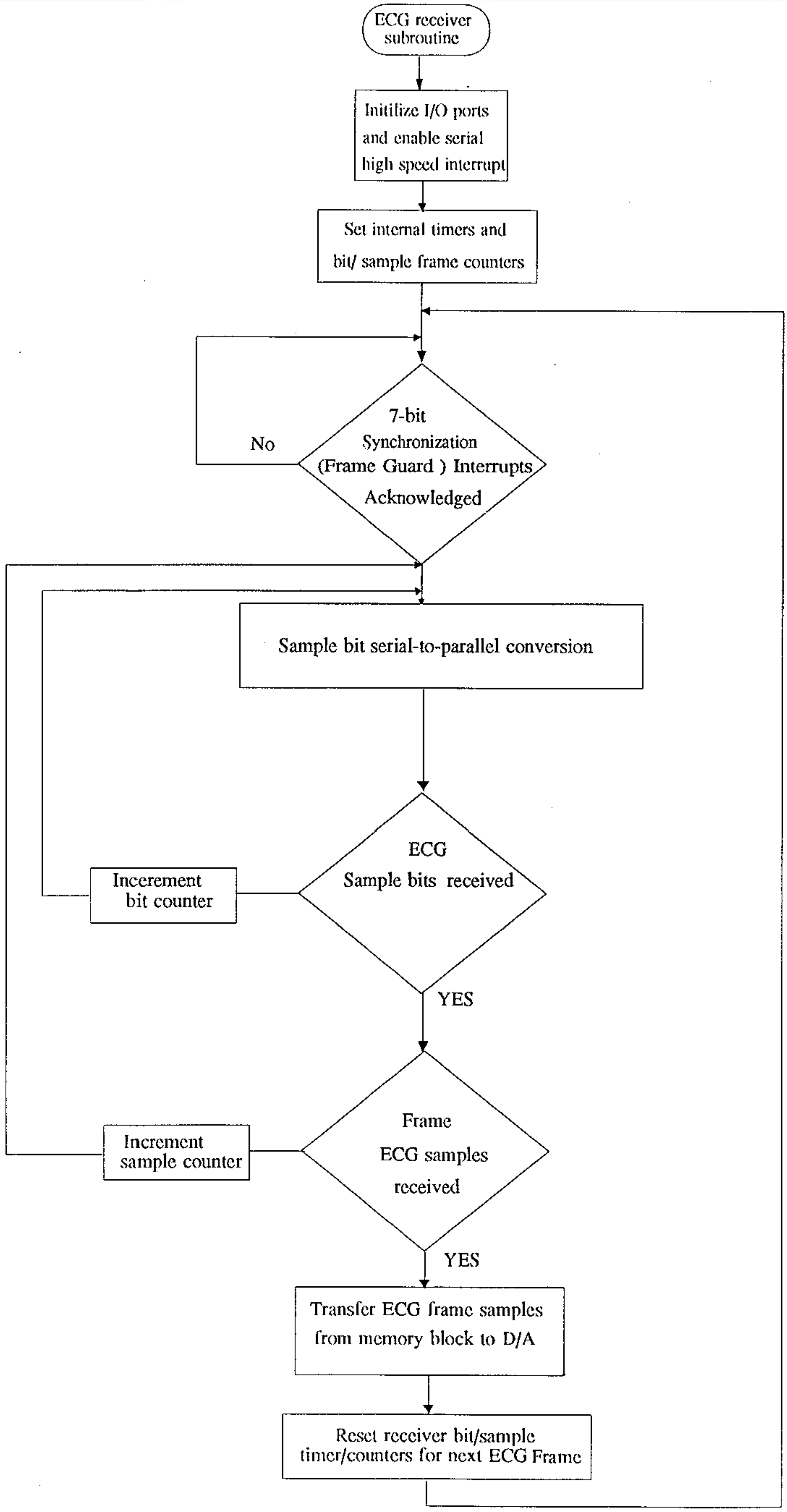

Fig.5.8 Flow chart of the ECG receiver program

5.3 SYSTEM PERFORMANCE TESTING AND EXPERIMENTAL RESULTS

In order to evaluate the performance of the system, experimental tests were carried in a large indoor tank described in section (4.3.3) to test the complete system's capability and validate its performance and functioning in a shallow underwater environment. Fig.5.9 shows the receiver and data logging hardware set-up.

The pre-dive preparations included ensuring proper electrode positioning and good connections of the sensors and their housing attachments to the SCUBA kit as described in section 4.3.3. The external signal adjustments and calibrations in the transmitter included correct acoustic generation and reception of the combined data by the projector and hydrophone. The diver also wore a short range heart monitoring system (Polar Electro Sport Tester-Finland) equipped with chest strap and wristwatch-type receiver [138,139]. This was used for simultaneous correlation and comparison between the telemetred heart rate and the measurement obtained by this system. Fig.5.10 shows a view of the diver's ECG electrode positions and also the heart rate monitoring strap.

The instrumented SCUBA diver was asked to swim in the tank performing various manoeuvres. These included three diving protocols each of four minute duration. The phases were as follows: (a) lying motionless in the bottom of the tank, (b) hard swimming, (c) lying down again. Fig.5.11 shows the general arrangement of the biotelemetry system for monitoring a diver in the tank.

Three channels of data were successfully observed and distinct ECG signals were received during the exercise phases of the trials. Fig.5.12(a) illustrates a transmitted ECG signals and the corresponding R-R tone triggers from the gated microcontroller output port and the channel oscillator, while Fig. 5.12(b) illustrates the transmitted R-R tone bursts from the output of the power amplifier. Fig.5.12(c) shows a sample of transmitted ECG signals and the received bursts corresponding the R-R peaks used for the heart rate telemetry measurements. Fig.5.13 shows the received DPCM with the frame synchronization pulses and the reconstructed ECG samples before and after the low-pass filtering. Stable and clear heart rate

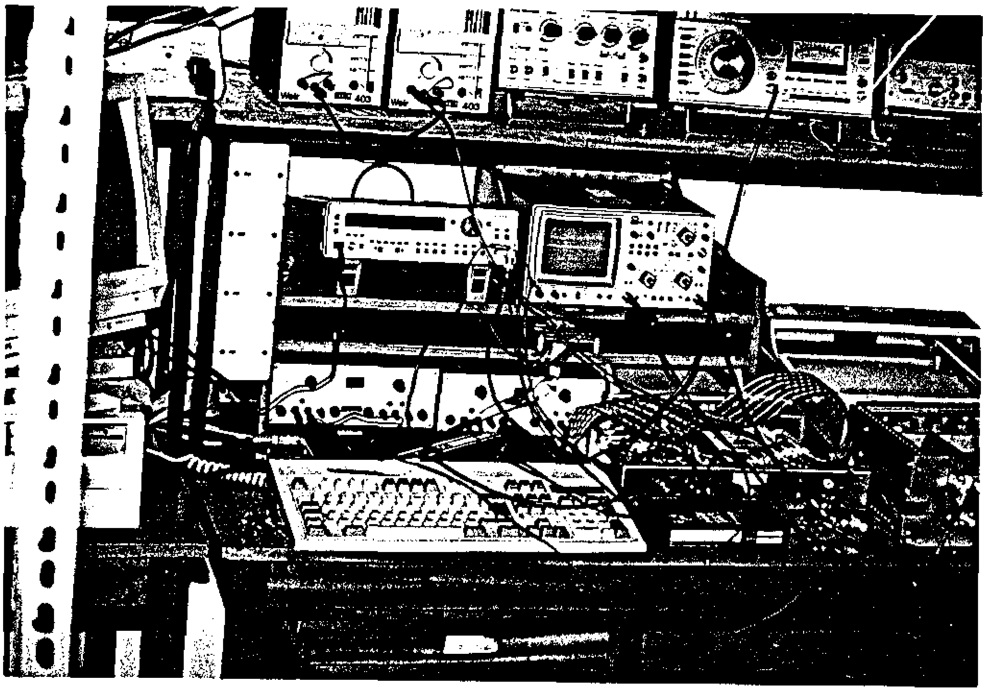

Fig.5.9 Telemetry receiver set up

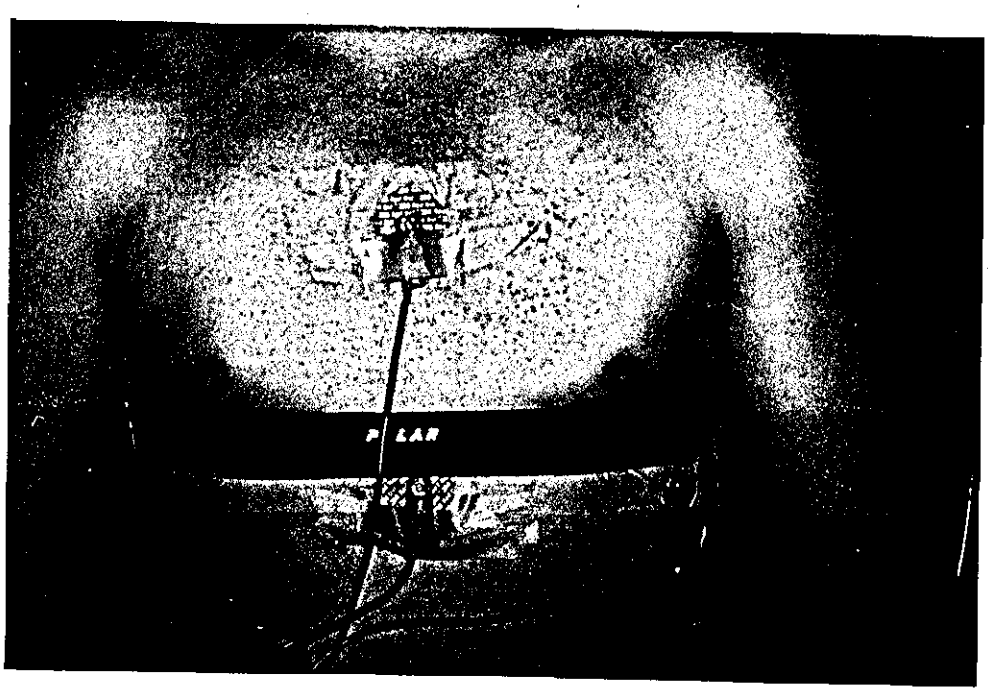

Fig.5.10 ECG electrodes and heart rate monitor positions on a diver

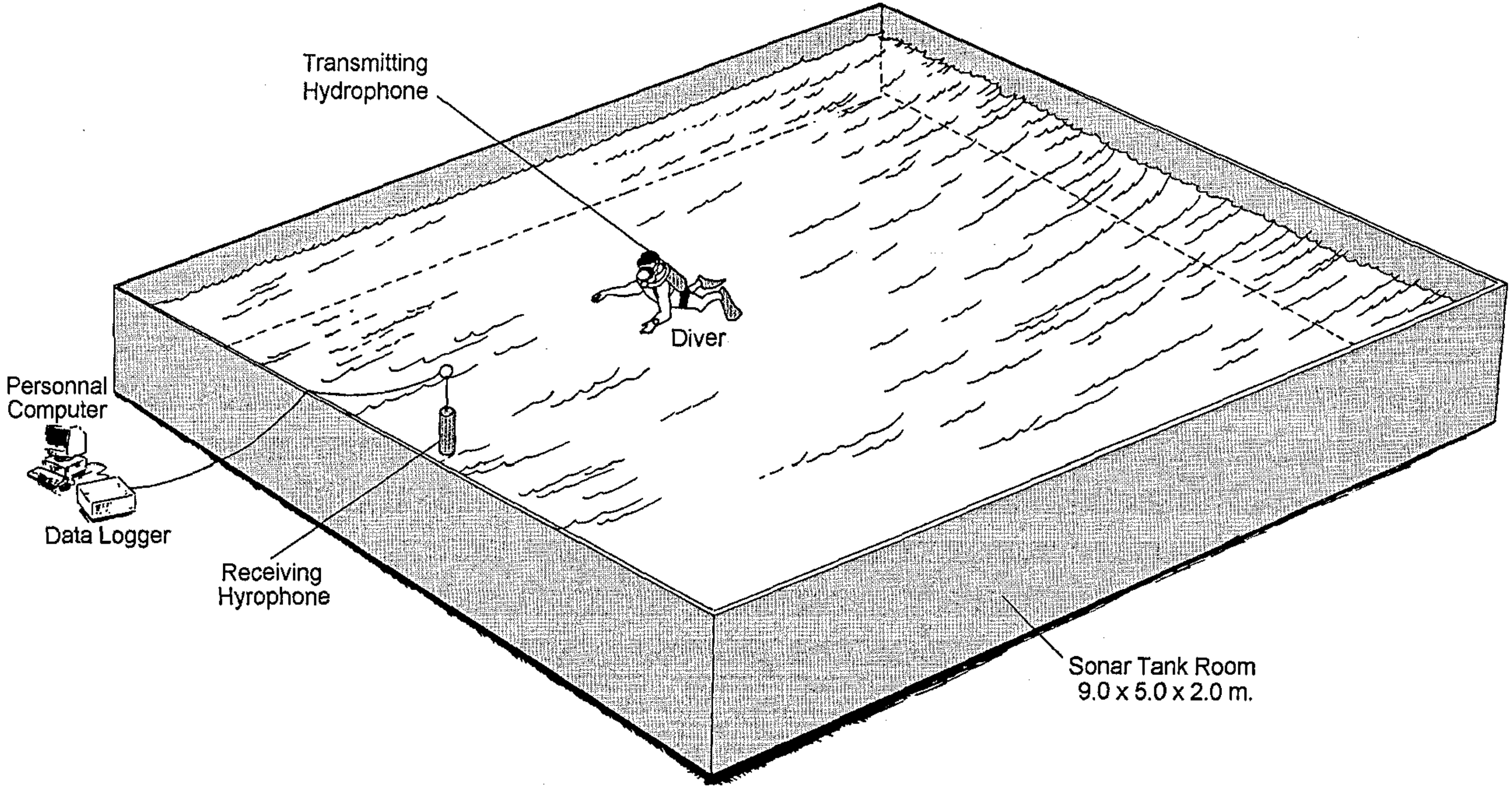

Fig. 5.11 Biotelemetry system for monitoring a diver in the tank

and breathing rate signals were obtained by the system prior and after the dive. Fig.5.14 shows a typical ECG and breathing signal chart recordings obtained simultaneously from the two channels before the dive.

For the ECG telemetry trial, the quality of the recording was sustained for the first 10 minutes of the dive. Fig. 5.15 shows a section of the underwater telemetered ECG recordings obtained from the diver in the bottom of the tank. The clear QRS complexes observable during the diving implies the successful QRS detection and transmission with no discontinuity before and after the submersion. The quality of recording was sustained during the first phase of the diving exercise, before some signal loss was noticed during swimming, probably due to the change in the diver's position or electrode contact with the skin. However, increased signal degradation followed, and there was a signal loss at the end of swimming phase. This was attributed to water leakage into the electrodes from the neck seal of the diver's suit. It could be also associated to the heart rate increasing more than the maximum limit allowed for bit transmission programmed according to Eq.4.14 set at 90 beats/min for the current test environment.

For the multichannel recordings, time-multiplexed heart rate, breathing rate and depth measurements and data logging correlation were obtained during a 12 minute dive.
Fig.5.16 shows the acoustically telemetered heart rate and breathing rate data logged by the system and the simultaneous heart rate measurements recorded by the Polar heart rate monitor during the dive for comparison. The absolute percentage error correlation between the telemetered heart rate data and the data measured by the heart rate monitor is shown in Fig.5.17. The depth variation is not shown as the average depth was constant at approximately 4ft(1.2m) logged by the pressure/depth channel at 635 ppm and due to the shallowness in the tank.

Fig. 5.18 shows the performance of the depth/ pressure channel from separate tests conducted in the tank. The telemetred depth data were measured by lowering the depth sensor mounted on the transmitter at different depths to a maximum of 5ft(1.5m) restricted by the depth of the tank. The water temperature variations were considered constant. As indicated in Fig.5.18,

Fig.(5.12) Transmitted ECG signals illustrating R-R tone transmission

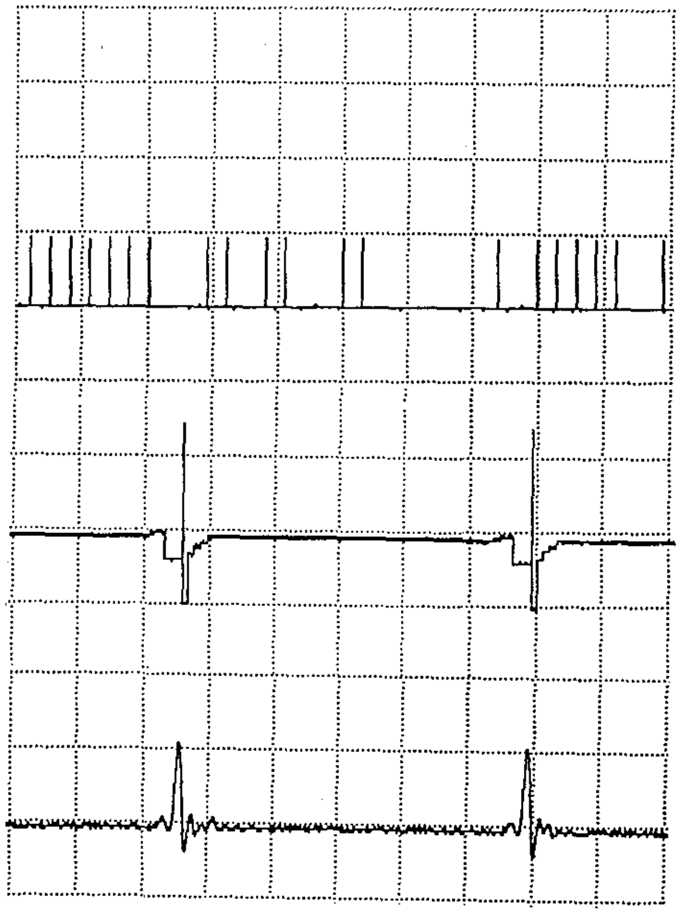

(a) Received PCM frame pulses,
showing the 7-bit synchronization word
V: 5V/Div
T: 100ms/Div

(b) Reconstructed ECG samples,
before filtering

(c) Reconstructed ECG signal,
after filtering

V: 0.5V/Div
T: 200ms/Div

Fig.5.13 Received PCM pulse and reconstituted ECG samples at the receiver

Ch1

Ch2

V: Ch1-0.2V/Div
Ch2-0.5V/Div
T: 10s/Div

Fig.5.14 Simultaneous channel recordings of the ECG and breathing signals prior to submersion a linear relationship was obtained between the performance and calibrated data of the sensor. The maximum percentage error referred to the calibrated data was <1% at the maximum test depth. This error could be attributed to the logging process, or slight variations in the sensor's component circuitry and ambient temperature variations and owing to the fact that the sensor is an integral part of the signal converter circuitry since it converts resistance variations into frequency variations.

Dive regimes	Avearge Heart Rate (beat/min ± S.D.)	
	Measured	Telemetered
Lying motionless	74 ± 2	76 ± 3
Circular swimming	106 ± 8	109 ± 7
Follow-up lying	89 ± 10	91 ± 11

Table 5.1 Comparative results between telemetered and measured heart rate data

The important measure established by the system's test is the comparative evaluation between the telemetred and measured heart rate data. Table 5.1 shows the comparative results between the telemetered and measured heart rate data during the diving regimes. The maximum heart and breathing rates logged by the system were 122 beat/min and 15 breaths/min respectively telemetred during the swimming phase while the minimum heart and breathing rates were 68 beat/min and 3 breaths/min telemetered during the first phase. The average percentage error between the telemetered and measured data during the dive was ± 3.3%.

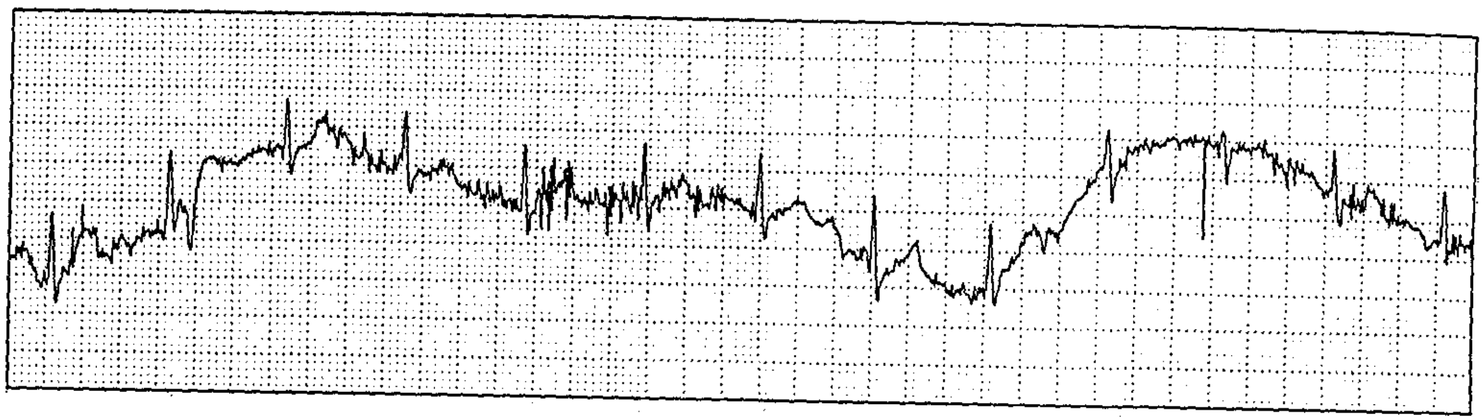

V: 0.5V/Div
T: 1s/Div

Fig. 5.15 Telemetered ECG recording from a diver in the tank

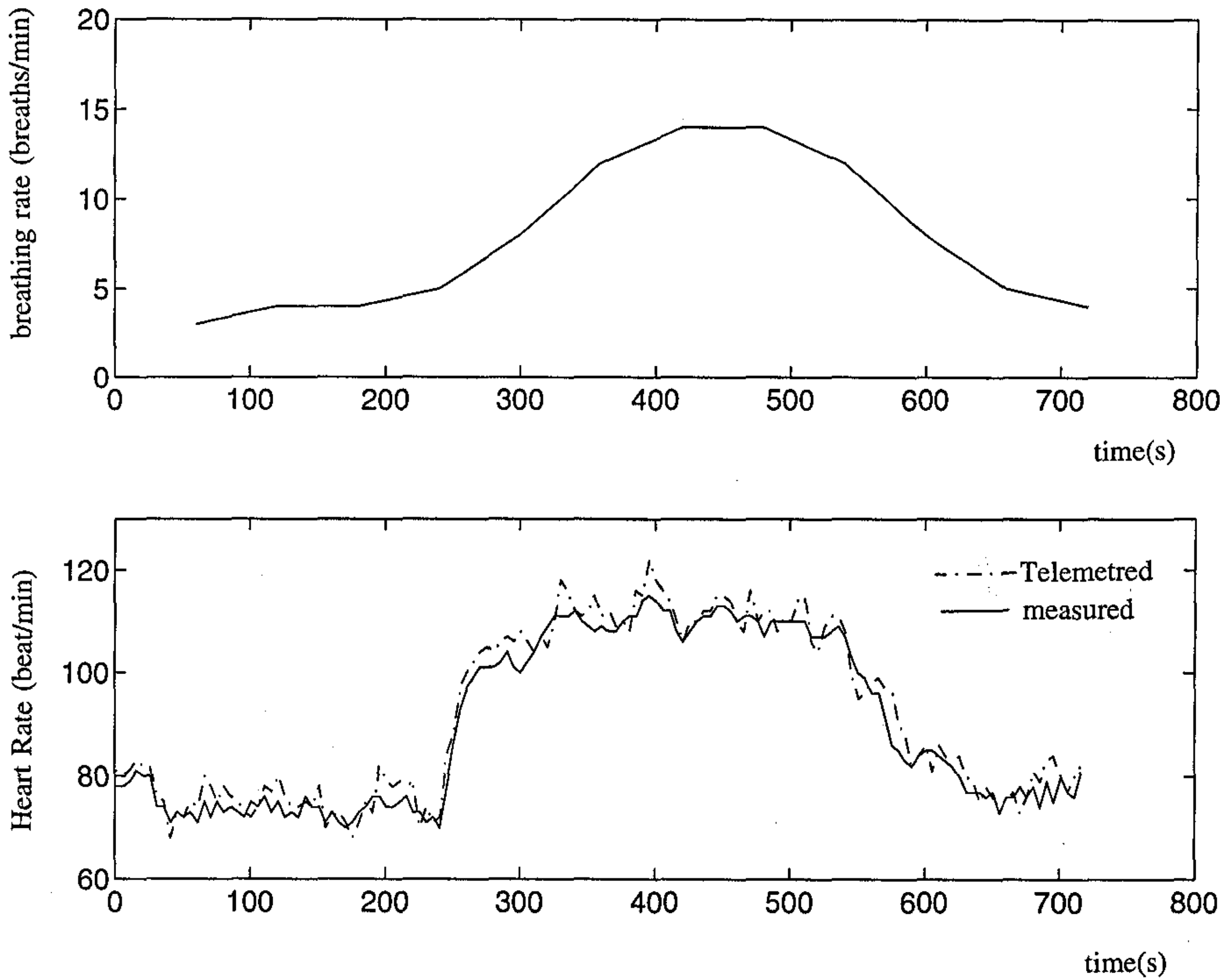

Fig.5.16 Dive time versus telemetered heart rate and breathing rate data in the tank

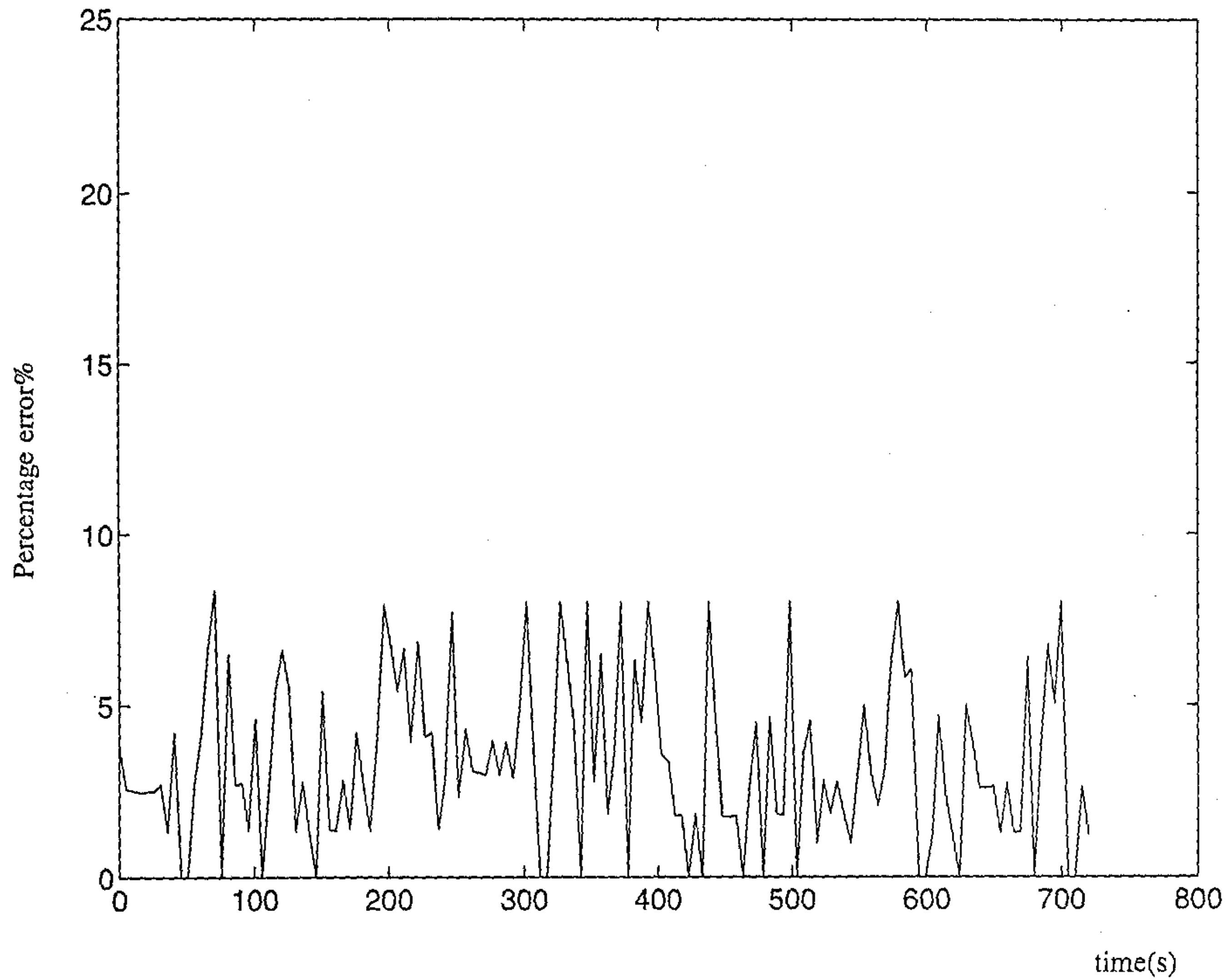

Fig.5.17 Error correlation between the telemetred and recorded heart rate by the monitor

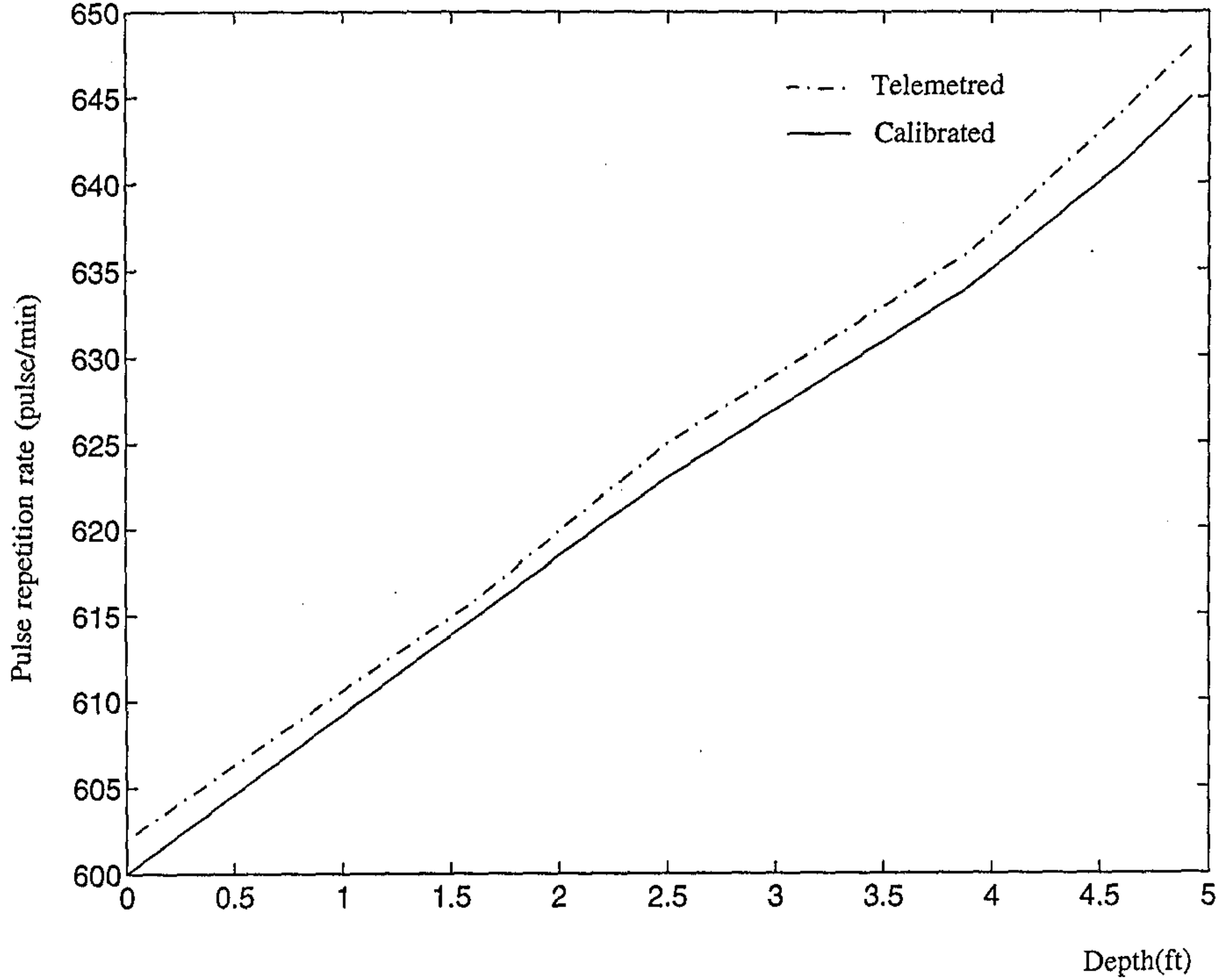

Fig.5.18 Performance of the depth/pressure telemetry in the tank

However, such percentage is acceptable as most commercially available heart rate monitors have a loss in accuracy between 1% and 3% at higher heart rates (> 150 beat/min). This average error can be attributed to several factors:

(i) The accuracy of the R-R detection in the transmitter and the pulse interval measurement by the transmitter. These can be attributed to the error in the R-R detection in the heart rate channel in the transmitter due to the subject or electrode movements.

(ii) Error caused by the receiver detection and decoding of the channel samples that are equivalent to the coded OOK transmission tone bursts. These can be attributed to missed or false detections due to the movement of the diver closer to the walls or the bottom of the tank that corrupt acoustically the received signal in a confined shallow channel, as discussed in Chapter Three.

(iii) Precision error in the calculations of the heart rate values from the received pulse by the data logger given by Equation *5.1* set by the manufacturer at $\pm 1\%$.

Initial interpretation of the results shows that the heart rate and breathing rate results exhibit bradycardia following submersion then a steady rise of the heart rate associated with corresponding increase in the breathing rate as the swimming exercise progresses. However, there was steadily decrease of the heart rate and the breathing rate following the swimming exercise. Some heart rate oscillatory variations were noticed by the end of the third phase. These oscillations seem to be controlled by the autonomic system that operates the heart rate mechanisms. However, these preliminary findings depend on the state of diver's fitness, the time taken to reach the plateau. The significant the heart rate variations could be attributed to combined physiological reflexes associated with several stimulation factors, such as the cold water immersion, or the release of catecholamine into the general circulation [140-144].

However, the pressure effects by increased depth on the heart rate and breathing rate were not considered here due to the shallow test environment.

Further physiological interpretations of the heart rate variability responses to increased pressure and diving manouvers are introduced in the next chapter.

These results have demonstrated the successful testing of the system for real-time data monitoring of freely swimming diver and demonstrated the simultaneous physiological monitoring of the diver's status in such a shallow underwater environment.

CHAPTER SIX

PHYSIOLOGICAL ANALYSIS AND SIMULATION STUDIES

6.1 Introduction

This chapter presents two different feasibility studies and introduces new concepts that can be incorporated into future biotelemetry systems for medical diagnosis and physiological analysis.

The first section presents a frequency domain analysis method to interpret the physiological mechanisms associated with heart rate variability during SCUBA diving. The second part of the chapter presents a hypothetical predictor based on the use of Artificial Neural Networks (ANN) for the likelihood classification of medical problems associated with SCUBA diving.

The emphasis here is for small scale studies and limited to the preliminary results obtained. These studies offer a physiological contribution relevant to future biotelemetry research.

6.2 A FREQUENCY DOMAIN ANALYSIS OF HEART RATE VARIABILITY DURING SCUBA DIVING

6.2.1 Introduction to heart rate variability analysis

Power spectral analysis of heart rate variability (HRV) is generally accepted as an important signal processing technique for medical research and for the assessment of both physiological and clinical conditions. It has been shown that the HRV power spectrum provides a non-invasive tool to monitor the autonomic control of the heart both in normal and pathological subjects [110-114]. In fact, the HRV reflects the modulation of the sinus-atrial node generated by the sympatho-vagal balance, i.e. the heart rate is controlled by the balance between the parasympathetic (PNS) and the sympathetic nervous system (SNS) activity of the sinoatrial node. The actions of the SNS and PNS to an organ have opposite effects. For instance, when the blood pressure becomes too high the PNS inputs are activated to decrease the heart rate, and when the blood pressure is too low the SNS increases the heart rate. However, a detailed description of the autonomic system is beyond the scope of this thesis and can be found in several human physiology texts [107,108].

Since the first work reported in this area of research [109], several studies have been carried out to quantify the balance of the activities of the two systems in terms of their relative spectral powers. This has been shown to provide a useful means of assessing the status of the autonomic nervous system in different pathologies such as hypertension, myocardial infarction and diabetic neuropathy [110-112].

Although in the time domain the oscillatory nature of the heart rate shows apparently random variations it does not convey how well the heart is regulated as a blood pump. It is this oscillatory nature that conveys information concerning the cardiac neuroregulatory mechanisms, which can be seen and explained in the frequency domain. The power spectral density (PSD) analysis of the HRV is typically divided into three distinct spectral bands [112,113]:

1. A very low frequency (VLF) fluctuation portion (0.0-0.04 Hz) which has contributions from the PNS, SNS and the renin-angiotension system (RAS) and other thermoregulatory mechanisms. These spectral peaks are difficult to identify in different human subjects, and are still under further research and investigation.

2. A low frequency (LF) portion (0.04-0.16 Hz) which is generally associated with the SNS.

3. A high frequency (HF) portion (0.16-0.4 Hz) which is associated primarily with the PNS.

However, much of the research in this area has been focused on the two prominent superimposed peaks embedded in the LF and HF portions of the spectral distribution which are of particular interest in the present investigation. These peaks are now recognised as the physiological rhythms correlated to the neurocardiac control system.

Agreement exists that one peak, centred around approximately 0.25-0.3 Hz, gives a quantitative estimation of the respiratory sinus arrhythmia (RSA), and the amplitude of this peak indicates the vagal activity [113,114]. The second peak, at a frequency of approximately 0.06-0.1 Hz, and has been related to the arterial pressure control mechanisms [113] and is called the Mayer rhythm. An increase in power in this band is considered to be an index of increased sympathetic activity.

For many years, studies have been carried out on heart rate variations during swimming [115-117], forced head submersion [118,119], and skin diving [120-123], but these HRV patterns did not clearly characterize the exact contribution of the autonomic nervous system as has been shown for other pathological conditions. So far as is known, no study has been attempted on the characterisation of the heart rate variability during SCUBA diving. The influence of such underwater exercise on HRV has been studied here to allow a direct correlation between the HRV rhythms with specific diving activity. In turn, this may lead to a hypothesis to explain the HRV characteristics and may contribute to the still unexplained deaths that have been reported for diving [124,125].

6.2.2. Signal Processing and Power Spectral Analysis

The power spectral analysis of HRV data sequences was carried out using two methods:

1. Fast Fourier transformation (FFT);
2. Autoregressive (AR) spectral estimation.

(i) The FFT power spectrum method:

In this method the spectral content of the HR data was analyzed using the classical FFT power spectrum method, represented as the sum of the squares of the real and imaginary parts of the Fourier transform of the data [126]. The relevant computational equations are omitted here, due to the detailed explanation of the standard FFT method as discussed in several references on digital signal processing [126,127].

In general, the estimate of the power spectrum P(k), is the squared magnitude of the results of an FFT carried out directly on time series data, defined as:

$$P(k) = |X(k)|^2$$

or

$$P(k) = \frac{1}{N\delta t} \left| \delta t \sum_{n=0}^{N-1} x_n \exp(-j*2\pi f n \delta t) \right|^2 \qquad (6.1)$$

with sampling interval $-0.5\delta t \leq f \leq 0.5\delta t$ and X(k) is the complex entity representing the Fast Fourier Transformation. It is well known that the spectrum calculated using the FFT method causes a spurious contribution in the spectrum and produces pseudo-peaks (caused by the finite data length and probable influence of noise), especially in short data segments and time series [128,129]. In addition, the frequency resolution of the FFT is poor and window functions are needed which might attenuate or eliminate signals of interest. The AR method provides far superior and provide greater resolution and shows better capability for modelling the short-term segments than the FFT method, as will be shown later.

An FFT analysis was performed for a 256-point data array representing instantaneous heart rate tachogram segments, each of 4 min intervals. Before calculating the spectrum, the mean heart rate was subtracted from the actual time series and weighted with a Hamming window function for improved analysis.

(ii) The Autoregressive (AR) spectral estimation method:

The AR model is the most popular signal processing method because its parameter estimates can be calculated by solving a set of linear equations [130]. Unlike the classical FFT-based analysis methods, the AR resolution is not dependent on data block length or the number of of samples, but rather on the model order and the possibility of avoiding windowing procedures. It also produces a more consistent and smoother spectral estimation [129,130].

The AR method is also called *all pole* method [129]. Each sample of a signal can be expressed as a linear combination of previous samples and an error signal *e(n)*. The error signal can be assumed to be independent of the previous sample [135]. The Maximum-Entropy Method (MEM) [131,132] is based upon an extrapolation of the known values of the autocorrelation function (or estimate) using the autoregressive model as the basis for the extrapolation. The analytical calculation by this approach leads to a relatively simple algorithm for computation of the spectral estimation.

The MEM spectrum of the data samples can be estimated by the set of the AR-parameters *a(p,n)*:

$$P(f)=\frac{\sigma(p)^2\delta}{\left|\sum_{n=0}^{p} a(p,n)\exp(-j2\pi * f * n * \delta)\right|^2} \tag{6.2}$$

with:

$P(f)$ is the output power spectral density,

$\sigma(p)^2$ is the power of white noise or prediction error,

f is the frequency

δ is the sampling interval, $-0.5\ \delta \leq f \leq 0.5\ \delta$

p is the order of the process, $n{:}n=1,\ldots,p$.

$a(p,n)$ are the AR-parameters or weights of the p-long prediction-error filter, with $a(p,0)=1$

The MEM spectrum is strongly dependent on the order of the prediction-error filter used for spectrum estimation. Low orders result in a smoothed spectrum whereas high orders might introduce spurious details to the spectrum [134]. The order of the model chosen is typically the one which minimizes Akaike's final prediction error FPE(p) figure of merit [135-137] and as shown in Appendix C. This is determined objectively, based on the experimental data under test and the validity checks carried out to determine the optimal order from the assumed model. In this study the validity of the model was checked by testing the whiteness of the prediction error, and the choice of the optimal AR model was performed by applying the Akiaki Information criterion explained in Appendix C. A 17th- order model was found to give the best spectral estimate for the data under test.

The fundamental concepts are presented here. The relevant time series parameter estimation and model order estimation equations are presented in Appendix C. More detailed reviews of the Burg algorithm can be found in modern spectral estimation references [129,130,137].

6.2.3. Measurements and experimental procedures

(i) Measurements

The ECG signals were obtained from a diver with a special microprocessor-based short range radio telemetry heart rate monitoring system, Model-4000 manufactured by Polar Electro, Kemple, Finland. It has two parts: (1) a battery-powered ECG sensor with contact electrodes and a transmitter worn on a chest strap, and (2) a wristwatch-type receiver. The sensor is activated by attaching it to the in-built ECG electrodes on the transmitter strap. The materials, surface design, configuration and placement of the self-contained contact ECG electrodes have been upgraded several times to minimize the electrical noise artifact created by motion and muscle contraction under operating conditions.The signals are transmitted at a frequency of 5MHz over a maximum distance of about 1m.

During diving, the receiver was conveniently placed in an inside pocket of the diver's dry - suit to protect it from water ingress, to minimize extraneous signals created by the diver's motion and to ensure radio communication with the transmitter.

The instantaneous heart rate is calculated from the R-R intervals between successive ECG signals, which are digitally averaged prior to display using a recursive method. This is done by an in-built single-chip CMOS 4-bit microprocessor in the receiver. The microprocessor program also employs an error pulse detection algorithm that serves to reject occasional missing signals or artifactual signalling, thus improving the reliability of the data. The algorithm is based on calculating the first reading according to the first four pulses. Thereafter every other result is taken into account by averaging, and the averaging time is dependent on the heart rate. The averaged data representing the instantaneous heart rate appears on the LCD display on the receiver. The averaged data are stored in binary form using one of the three storage-recall routines. The stored data and their exact timing can be recalled from the receiver's memory using an RS-232 serial interface connected to an IBM-compatible PC so that a permanent graphic record of the heart rate over time can be obtained.

The HR monitoring system used here has been validated during different exercise protocols in the laboratory against direct chart electrocardiogram recordings. The correlation coefficients ranged from 0.97-0.99, and the average error never exceeded -0.8 to +3 bpm, with the long term stability of better than 3bpm/year. The system is considered the best HR monitor from the standpoint of validity, stability and functionality [138,139].

The instantaneous heart rate data tachogram obtained from the system was applied to a cubic spline interpolation method to generate an equidistantly arrayed HRV series at 0.5 s intervals. A record length of 480 sample points (i.e. 4 minutes of data) for each successive diving phase were analyzed.

(ii) Experimental Procedure

Electrocardiogram signals have been obtained from a professional diver, aged 51, with a wide range of SCUBA diving experience at nationally qualified instructor level with more than 1000 dives. For the purpose of analysis and comparative study, the diving experiments were carried out in two different underwater environments. The first trials were carried out in open water dives at the national diving centre at Stoney Cove, Leicestershire, U.K. The trials were carried out when the temperature in the lake was an average of 9°C. The second trials were conducted in the tank room of the department of Electronic and Electrical Engineering, Loughborough University of Technology (the details of the tank are given in 4.3.4) and the temperature was 16°C. In both experimental protocols the diver wore a neoprene dry suit and carried SCUBA for breathing compressed air. In the open water trials the heart rate data were obtained during several dives to 20ft (6m) depth, which is the shallowest depth at which decompression stops are normally made by sport divers in the United Kingdom. The trials were carried out with identical dive profiles divided into seven 4-minute intervals. The seven phases of the dive were as follows: (a) Entering the water and submersion, (b) changed posture and slow finning, (c) further slow swimming, (d) fast finning, (e) lying motionless in a horizontal attitude, (f) kneeling, (g) ascent in a vertical attitude.

In the tank diving, a similar experiment was carried out was with the same diver, but with less manoeuvrability due to the limited underwater area and depth of only 2m. The dive was divided into three 4-minute of exercise phases as follows: (a) Entering the water and slow swimming around the tank, (b) fast swimming around the tank, (c) lying prone and ascending.

6.2.4. Results and Discussion

To analyze the HRV power spectrum obtained during the different SCUBA diving phases, a comparative off-line analysis of the data was performed on a SUN IPXS-Sparc computer work station and the results were plotted using a HP Laser Jet 3 printer. Fig. 6.1 illustrates a typical heart rate variability tachogram obtained during the open water trials. The three phases of the dive under analysis here, shown in Fig.6.2, are: submersion and descent to 20ft (phase-a); changed posture and slow finning (phase-b), and the fast finning (phase-d).

Fig.6.3 shows the power spectrum plots of the HRV during the same three phases obtained using the FFT-based and the AR model-based methods as a comparison. Although both methods show LF and HF peak variations during the different phases, it is clear that the latter method produces a smoother spectrum with fewer spurious peaks. It also provides greater resolution and shows better potential for modelling the short-time data samples than the classical FFT.

In the first phase the fall in the heart rate is seen immediately after body and face immersion. This is reflected by an apparent LF and augmented HF component as shown in Fig.6.3(b). The consistent LF component and increased HF oscillations during submersion and descent is associated with both the occurrence of bradycardia (slowing of the heart rate) during submersion which is a well understood physiological response in diving animals and humans [140]. This bradycardia results from the immersion of the body, and especially the face, in cold water [141]. This is initiated by the stimulation of various receptors and affected by

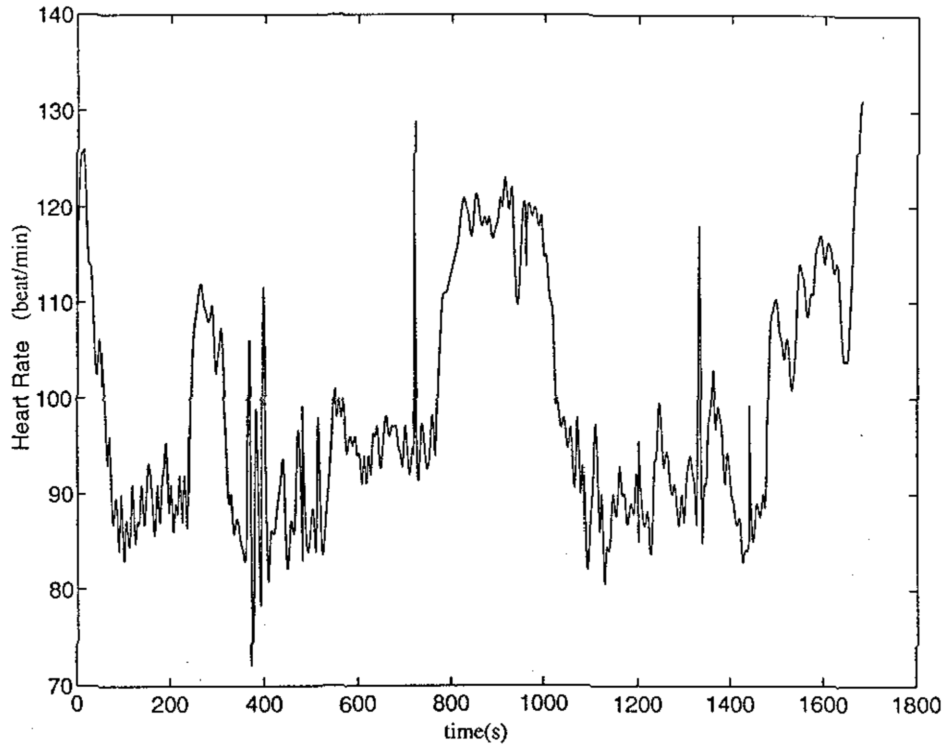

Fig.6.1 Instantaneous heart rate variability tachogram during an open water dive

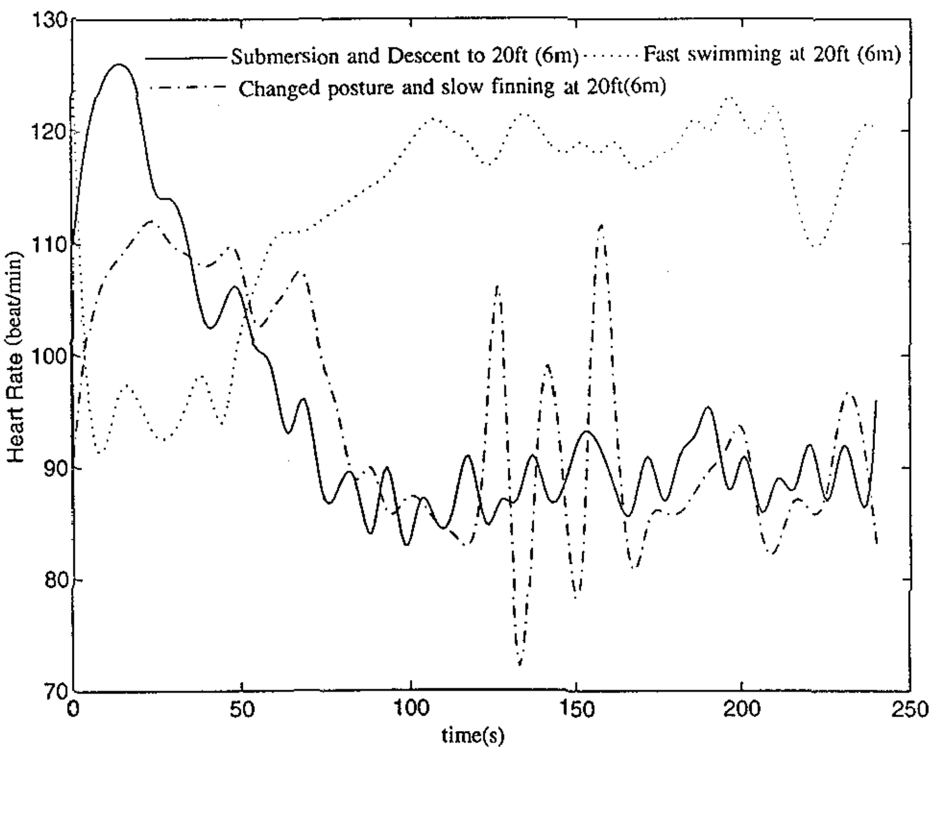

Fig.6.2 The heart rate variability during open water dive (a) submersion and descent, (b) slow finning and (c) fast swimming

increased activity of the vagal intervention of the heart, and vasoconstriction in peripheral vascular beds, i.e. enhanced HF component [142]. In addition to this, the thermal comfort zone of a diver immersed in water is between 33℃ to 35℃, and vasoconstriction in peripheral tissues associated with lower HR occurs normally with water temperatures below 29℃ [143]. However, the consistent (LF) oscillations might be caused by the transient tachycardia (increased heart rate) resulting from the descending exercise, that must be due to the muscle contraction accompanied by the rise in the sympathetic tone.

In the next phase a diminished (LF) oscillation is noticeable and the withdrawal of the (HF) peak, attributed to the postural change and the slow finning exercise. This result agrees with important early studies, which showed that there is an inverse effect between the postural changes from supine to upright positions and the LF oscillations [113], and also substantive findings that assume the increase in heart rate at low to moderate intensities of exercise, is primarily mediated by PNS withdrawal [144].

However, the fast finning phase shows increased LF and HF peaks. This reflects the fact that this exercise consisted of heavy muscular movements that might cause an increase in transmural thoracic pressure, which is reported to induce tachycardia [145]. Considering the vagus effects over the entire range of the HR fluctuation in the two latter phases (b and d), these results reflect the reduction in vagal activity occurring during steady exercise and the restoration of the vagal tone occurring at the end of the intense exercise [112,113,144]. The pattern of increase in the LF peak during higher exercise intensities, supports the concept of increased SNS activity to the sinoatrial node at higher heart rate of approximately 100 beats/min [146].

Fig. 6.4 shows the 3-D plots of the power spectra for the whole open water dive (averaging seven segments of 4 minutes) computed using the both methods. Again, comparison between the two spectra demonstrates the superiority of the AR spectral estimation over the spurious FFT for short record lengths. It can been seen that there are enhanced HF oscillations, especially for the submersion and underwater finning phases. This indicates that the diving response consists of bradycardia and hypertension, and that endurance-trained divers are

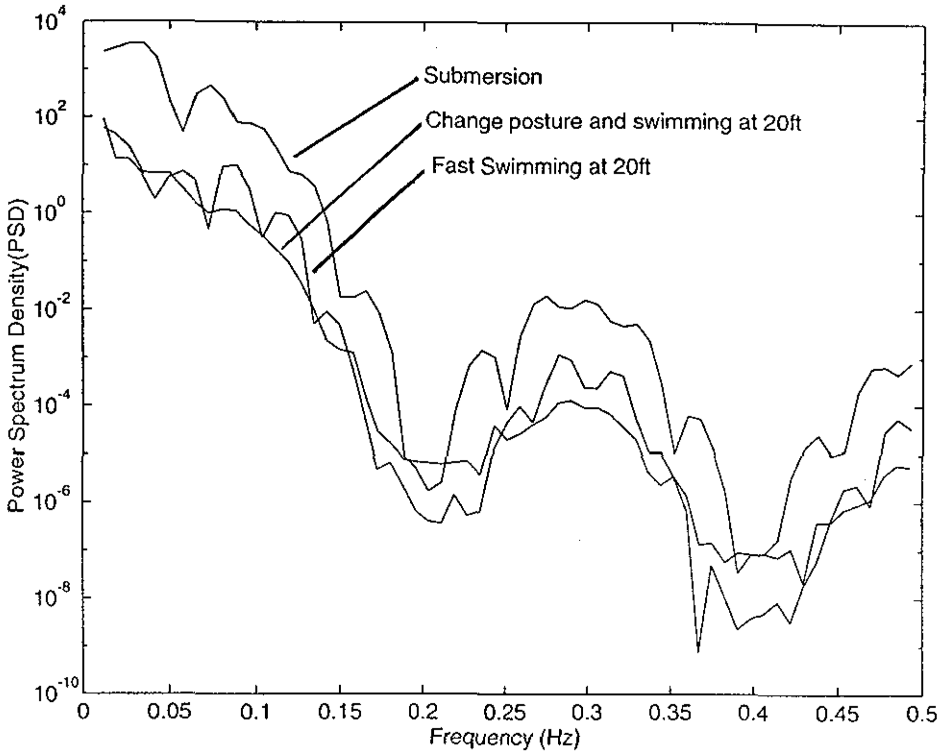

(a) FFT method.

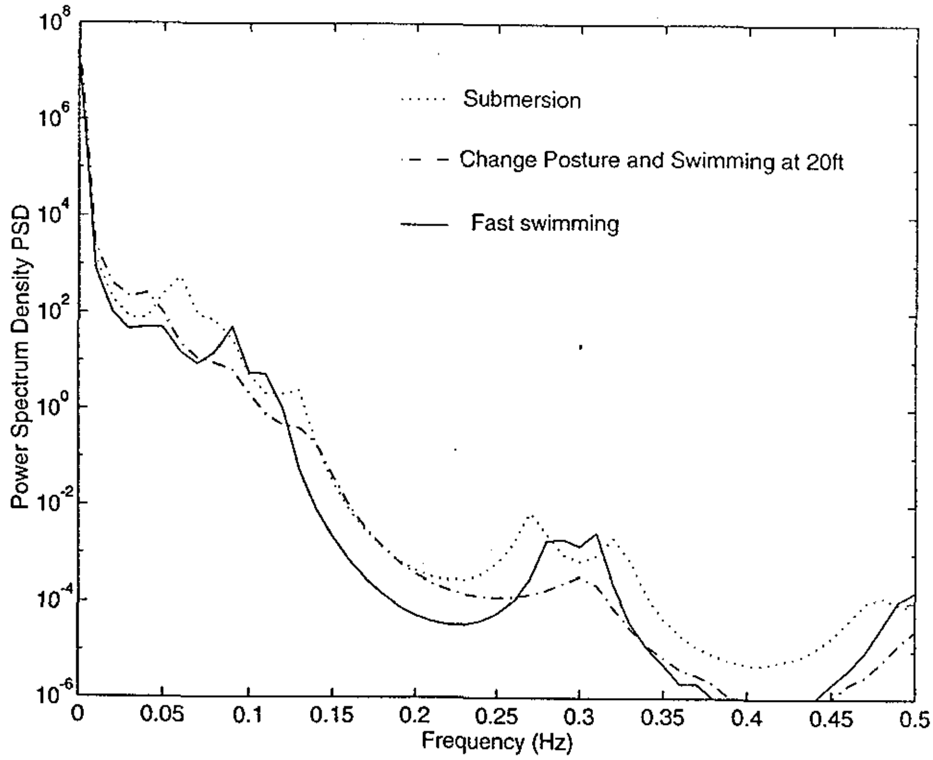

(b) the AR method.

Fig.6.3 The power spectral density of the HRV during three phases of exercise (a) using the FFT method and (b) using the AR method

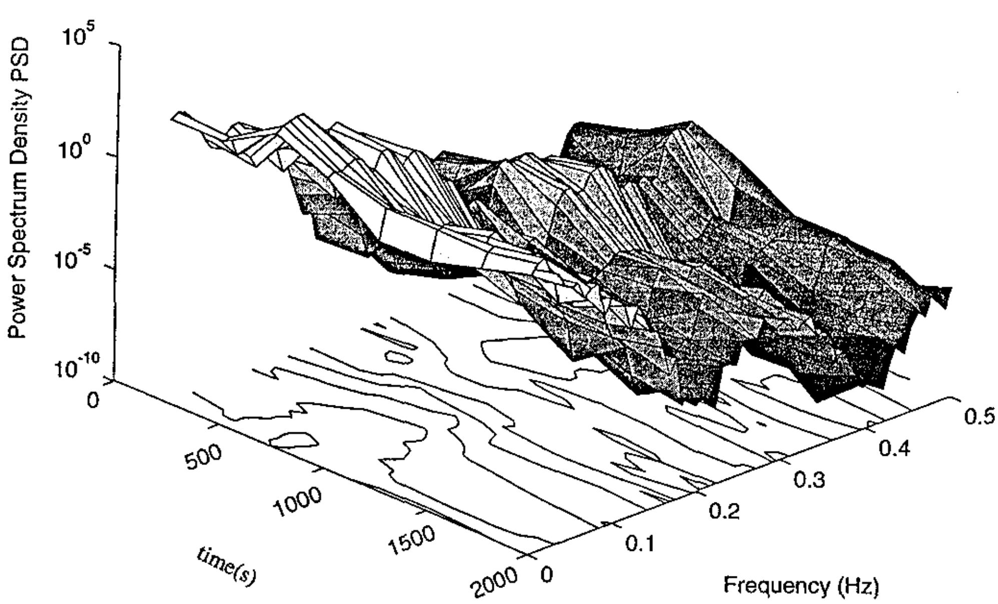

(a) FFT method

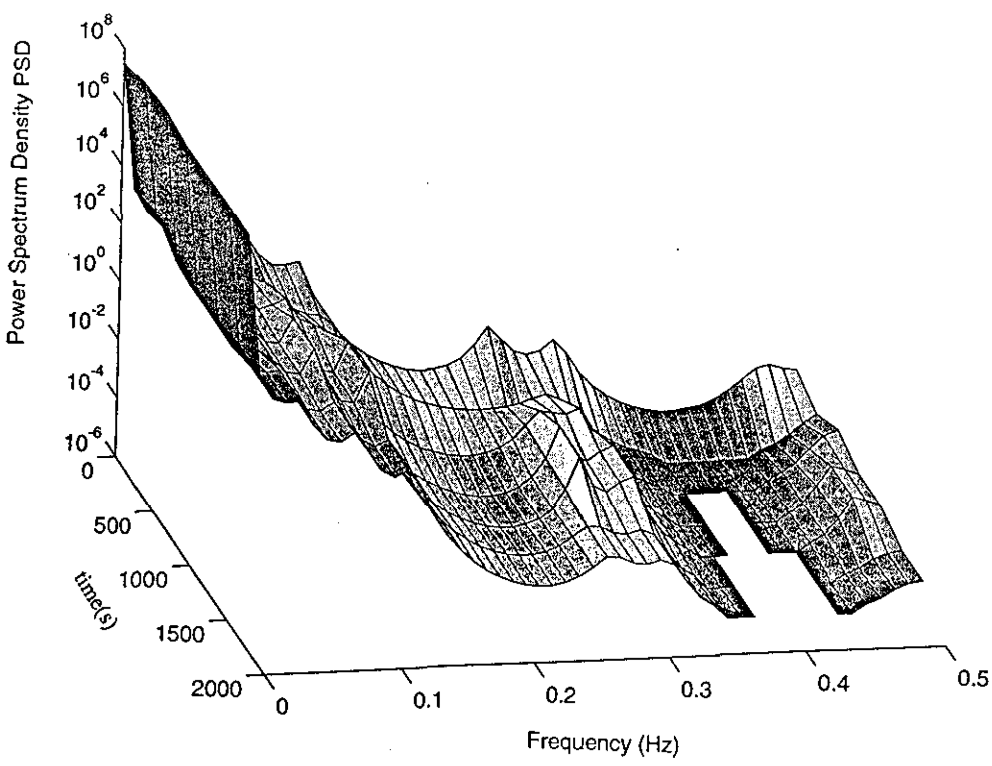

(b) AR method

Fig.6.4 Three-D plot of the power spectral density corresponding to the whole open water dive computed via (a) FFT method and (b) the AR method

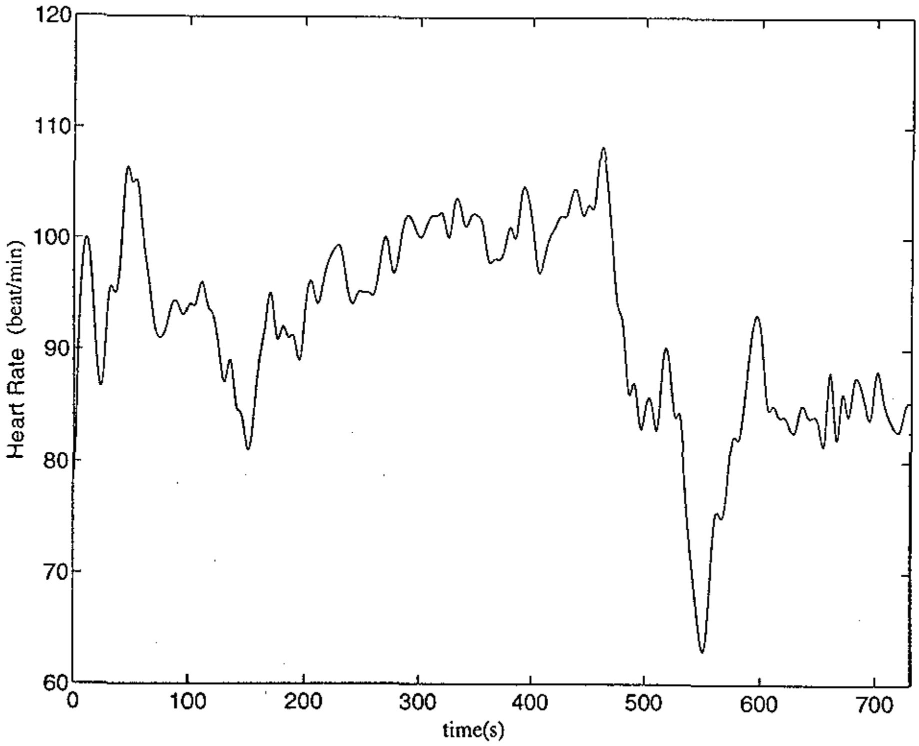

Fig.6.5 Instantaneous heart rate variability tachogram during a tank dive

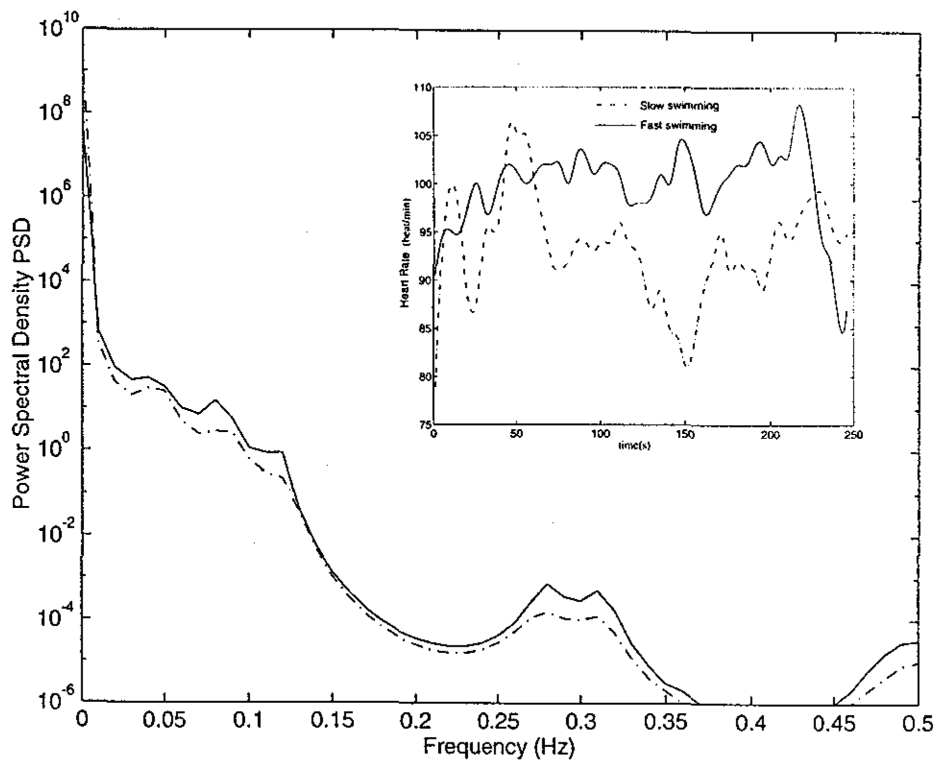

Fig.6.6 The AR power spectrum density in a tank exercise during (a) slow swimming (b) fast swimming

known to have dominant parasympathetic autonomic tone. However,it can also be seen from Fig. 6.1 and Fig. 6.4, that the tachycardia observed when the diver is surfacing may result from the sudden cessation of vagal stimulation and could be facilitated by arterial hypotension (i.e low blood pressure). Further physiological interpretations of these results are beyond the scope of this work and can be referred to physiological and human anatomy texts.

In order to test the findings of the open water dive with a much more restricted and shallower test environment, the same analysis was carried out on phases a and b of the tank dive. Fig.6.5 shows the heart rate variability tachogram.

Fig. 6.6 shows the power spectra calculated using the AR estimation of the two phases and the corresponding heart rate variability in the time domain. We have consistently observed identical distributions of the LF and HF oscillations for the underwater finning exercises and similar to the open water patterns. This validates the hypothesis for underwater finning during the open water dives, and suggests the relative role of the two components of the neuroregulatory control system of the heart rate during such exercise and under different underwater conditions.

6.2.5 Concluding Remarks

This methodologic study has utilized power spectrum analysis of the heart rate variability associated with SCUBA diving, using a comparative analysis of two spectral (FFT and AR estimation) methods. The latter method proved far superior in extracting spectral peaks with smoother and clearer spectral distribution, especially for short time segments of data. The studies were carried out on the heart rate variability signals obtained during controlled diving exercises, and the hypothesis was tested by examining the effect of the exercise under different underwater environments. The preliminary results suggest the role the neuroregulatory control system in adaptive responses to different underwater exercises. The results suggest some consistency with the quantitative explanation of the sympatho-vagal dynamic balance during exercise intensity. However, some of the findings and results remained unexplained such as the effect of deeper depths, effect of the stress and increased plasma level secretion for trainee divers, and the LF/HF distribution ratio that could also indicate the effect of the sympathetic and parasympathetic systems. Further physiological studies are required to better understand and determine the role of the autonomic cardiovascular regulatory system under such conditions.

It may be concluded that this work demonstrates the relevance and validity of the HRV power spectrum as a noninvasive method of determining the cardiovascular control in response to diving exercise. It also seems it could be incorporated into future biotelemetry systems with an on-line analysis facilities to constitute a useful clinical means of measuring the degree of compromise of the dynamic sympatho-vagal balance under diving conditions.

6.3 LIKELIHOOD DETECTION AND CLASSIFICATION OF MEDICAL PROBLEMS ASSOCIATED WITH SCUBA DIVING USING ARTIFICIAL NEURAL NETWORKS

6.3.1 Introduction

There has been a rapid growth in the popularity of SCUBA diving over the past twenty years. In the United States alone there are more than five million people certified as recreational SCUBA divers, with more than 200,000 people trained each year in the use of SCUBA [147]. Reported statistics suggest that there is an increased number of diving accidents with fatalities and non-fatal disabilities [147,148].

Most of these 'accidents' are the result of careless diving practice while breathing compressed air; the problems, which are not commonly encountered in medical practice, are given the general term of Decompression Sickness (DCS). This presents a pathophysiological challenge to physicians to be aware of the specific hazards and medical conditions encountered by divers. Decompression sickness, gas embolism and barotrauma accidents are the most common medical problems associated with SCUBA diving , despite many years of research [149,150], especially on the likelihood of decompression sickness.

Specific statistical analysis of selected air chamber dives has evaluated the probability of the DCS as a function of the dive profile and the decompression models tested, i.e.[150]:

$$P_{DCS}=f(time,depth,model) \tag{6.3}$$

However, such predictive models were limited only to the variability of the DCS and based on the measure of risk knowledge of air dives in hyperbaric chambers. Owing to the limitations of decompression, empirical testing has been necessary to validate a mathematical models of decompression. Many questions remain about the probability of occurrence of such syndromes, given the complexity of the physiological status and the variability of occurrence of a particular disorder, even if dive tables were strictly followed and especially in non-chamber environments. The likelihood of occurrence of other medical disorders as reported in the literature makes the mathematical analysis and model prediction of such disorders difficult, if not impossible, for any given dive profile. The medical aid and assessment of the risk for a particular dive is very important. It is also vital to arrange the proper treatment and to avoid confusing clinical manifestations and late pathological diagnosis that could lead to permanent injury, especially in an emergency and in remote areas. If such aids were available, combined with features such as user-friendliness and low cost, they could significantly enhance knowledge of any diver's physiological status, giving priori-knowledge if any medical disorder should be encountered following a certain dive profile.

In recent years, Artificial Neural Networks (ANN) have been successfully applied to a wide variety of medical problems such as ECG monitoring, medical imaging and pattern recognition problems [152,153]. The motivation behind this study is to demonstrate the feasibility and potential of applying ANN in the classification and prior-detection of related medical problems, especially in this case where mathematical validations have been hindered by their inability to measure a certain model to predict an empirical outcome.

In this section an ANN-based simple classification model is developed to predict and classify the risk of a medical disorder during small test diving profiles. The effectiveness of the model as a diagnostic tool is validated against cited DCS, barotrauma and other medical cases.

We begin by giving a general classification of the main medical problems associated with diving. The next section describes the principles of feedforward neural networks and their basic architecture. Then the mechanics of the back propagation and a description of the learning algorithm is presented for completeness. Next the structure of a neural network as a function of certain dive profiles and decompression data is presented. Finally the simulated model is trained using a combination of the normal decompression data and some medical disorder data corresponding to the same depth ranges. The learning performance of the network, its capability of discriminating medical disorders and its cluster classification from a given random set of data is discussed. This pilot work also illustrates the feasibility of incorporating such networks in the next generation of intelligent biotelemetry systems. These would monitor directly the parameters fed to the system and classify the probability of associated disorders after the dive.

6.3.2. Medical Problems Associated with Scuba Diving

Most of the accidents and morbidity involving diving are related to the behaviour of gases under changing pressures, due to the physiological ramifications of two relevant gas laws, namely Boyle's law and Henry's law [154]. The most frequently occurring and life threatening medical problems are discussed in this work. Several medical references detail the pathophysiology and the medical aspects associated with diving [154,155,156,157]. However, a brief mention of the three most relevant problems is described here.

6.3.2.1 Barotrauma

Barotrauma refers to the tissue injury resulting from the failure of a gas-filled body space (e.g. the lungs, the middle ear and the sinuses) to equalize its internal pressure to correspond to changes in ambient pressure. During a dive, failure to equalize pressure leads to a change in the volume of these body spaces in accordance with Boyle's law. Since cavities located within the bone cannot collapse, the space they take up is filled by engorgement of the mucous membranes, often followed by haemorrhage. The risk of barotrauma is more pronounced near the surface, where a small change in depth may lead to a large change in relative gas volume.

Pulmonary barotrauma occurring during ascent is the most severe and life-threatening form of barotrauma [157]. During ascent, as the ambient pressure decreases, gas within the lungs expands. If a diver does not permit expanding gas to escape from the lungs by exhalation, distention and rupture of the lungs may occur.

The most serious sequel of pulmonary barotrauma is arterial air embolism as a result of the passage of gas into the pulmonary veins and from there into the systemic circulation. The occurrence of unconsciousness or any other necrologic manifestation in a diver surfacing from a deep dive should also suggest the possibility of another diving complication that will be discussed later, namely decompression sickness. This complication can occur alone or in combination with air embolism. The treatment of this form of diving disease is to carry out recompression treatment in dedicated hyperbaric chambers which can be used to administer oxygen at high ambient pressures.

Barotrauma of the middle ear during descent is the other most common disorder in divers. The condition is caused by an inability to equalize the pressure in the middle ear because of blockage of the eustachian tube, upper respiratory infection, or anatomical variations in the nasal skeleton [157,158].

Other less common pressure-related forms of barotrauma such as paranasal-sinus barotrauma, (which is frequently related to chronic dysfunction of the nasal or paranasal sinus, with blockage of the sinus ostia), inner ear barotrauma, and dental barotrauma are not discussed here, but details can be found in the references [155-157].

6.3.2.2 Decompression Sickness

Decompression sickness (DCS) is a function of Henry's law, which states that at equilibrium the amount of gas dissolved in a liquid is proportional to the partial pressure of that gas in contact with the liquid. When a diver breathes air under increased pressure, the tissues are loaded with increased quantities of oxygen and nitrogen. As the diver descends and the ambient pressure increases, proportionately greater quantities of nitrogen and oxygen are dissolved in the blood and carried to the body tissues. Oxygen is used in tissue metabolism, whereas nitrogen, which is physiologically inert, is not. Thus, the nitrogen content of a tissue increases in proportion to the ambient pressure and also in relation to the tissue's fat content, since nitrogen is about five times more soluble in fat than in water [159].

When the ambient pressure decreases as the diver returns to the surface, the sum of the gas tensions in the tissues may exceed the absolute ambient pressure. At this point, a state of supersaturation is created that may lead to the liberation of free gas from the tissues and to the onset of decompression sickness. The liberated gas can disturb organ function by blocking arteries, veins and lymphatic vessels; in addition, its expansion can rupture or compress tissues. It is customary to classify cases of decompression sickness into two types on the basis of clinical manifestations. Type 1 includes a mild form of DCS, and type 2 includes the more severe varieties, which may lead to permanent necrologic injury and death [160,161]. The most common manifestation of the first type is localized joint pain, which generally develops within an hour of surfacing and ranges from mild discomfort to very severe pain, which may gradually increase during the following 24 to 36 hours. Symptoms of the second type of decompression sickness most commonly appear 10 to 30 minutes after the diver surfaces [157], and often start with a feeling of malaise and fatigue. However, the symptoms may develop insidiously over several days. The appearance of clinical symptoms during decompression can be largely avoided if the rates of ascent are controlled with the use of decompression stops during ascent, as specified in decompression tables such as those of the U.S. Navy [162,163], the Royal Navy [164] and many others. However, the treatment of severe decompression sickness is similar to that described earlier to treat air embolism, namely, by the use of hyperbaric oxygen therapeutic regimes as given according to the U.S. Navy treatment tables [162,163].

6.3.2.3 Nitrogen Narcosis

This pressure related syndrome results from breathing air at depths greater than about 100 feet of seawater fsw (30m) [156,157]. The clinical symptoms are similar to that of alcohol intoxication and are characterized by temporary impairment of mental and neuromuscular performance, and by changes in personality and behaviour. Symptoms become increasingly evident as depth increases below 100 feet. At extreme depths of 200-300 feet it may lead to hallucinations, unconsciousness, or death [156]. In sport diving, depths of 200-250 feet are attainable but not recommended. The usual depth limit using SCUBA gear is 130 feet in the U.S or 50 metres in the U.K.. Treatment requires removing the diver from the increased pressure environment. Symptoms disappear immediately upon surfacing and divers recover rapidly from nitrogen narcosis when they ascend to a shallower depth, where the narcotic effects of the gas are reduced [156,157].

6.3.3 Neural-Networks:Basic concepts

The basic concepts of the neural networks are well understood and can be found in several relevant texts [165-168]. However, in this thesis it is necessary to outline briefly the basic concepts for completeness and ease the understanding of the analysis techniques described.

The basic building block in a neural network is a processing element which tries to mimic the operation of a biological neuron in the brain. Thus, these processing elements are also referred to as neurons.The theory of Artificial Neural Networks (ANN) and the Multilayer Perceptron structures (MLP) with different network types, connection topologies, and training rules have been covered in depth in several references [152,153]. ANN's can be placed into one of several classes based on their feedback link connections. The most popular and widely used networks are the 'multi-layer feedforward networks' trained by backpropagation. Such network architectures and learning algorithms, have been very successful in categorization problems in a broad range of areas, and are the archetype of supervised learning algorithms [165-167]. This is dealt with in some depth here as most of the neural network based models and hardware applications developed recently use such networks.

In general, a neural network is a teachable, non-algorithmic layered structure processing system that consists of densely connected simple computing elements called perceptrons (neurons). Each pereceptron consists of a summing junction as shown in Fig.6.7a, which adds together the weighted sum from the other perceptrons in previous layer, and a nonlinear activation function, operating on the weighted sum generates the neuron output from the summing junction output. The output fans out to serve as an input to perceptrons in the next layer. Perceptrons transmit signals to each other via weighted links, which attenuate or amplify the transmitted signal depending on the weight value. The perceptron (*neuron*) of Fig.

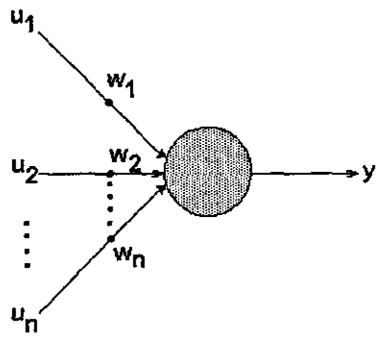

(a) perceptron representation

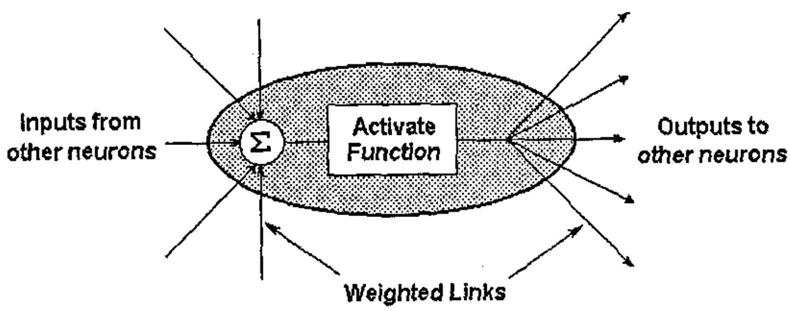

(b) single perceptron model

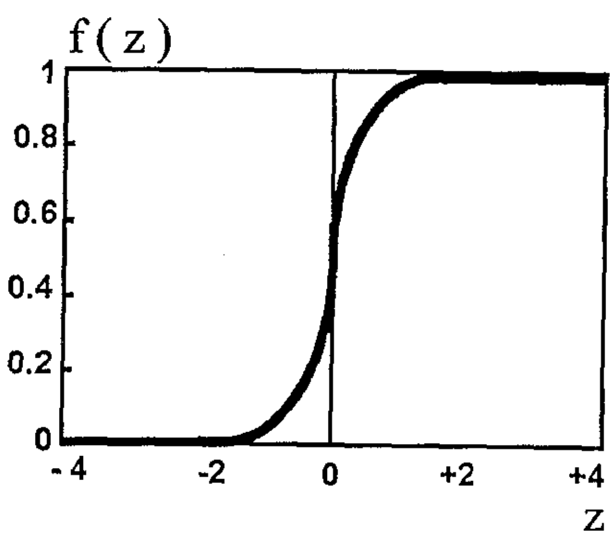

(c) sigmoid activation function

Fig.6.7 Perceptron unit and sigmoid function

6.7a is often depicted as shown in Fig. 6.7b where the input weights, bias, summation and activation function are implicit. A feedforward neural network is constructed by interconnecting a number of neurons so as to form a network in which all connections are made in the forward direction (from input to output without feedback loops). Neural networks of this form usually comprised an input layer, a number of hidden layers and an output layer [168].

The input layer consist of neurons which accept external inputs to the network. Inputs and outputs of the hidden layers are internal to the network, and hence the term "hidden". Outputs of neurons in the output layer are the external outputs of the network. Once the structure of a feedforward network has been decided, i.e. the number of hidden layers and the number of nodes in each hidden layer has been set, a mapping is "learned" by varying the connection weights and the biases so as to obtain the desired input-output response for the network.

For such a network to be trained using a "*supervised*" class learning system a "*training*" data set of example inputs and their corresponding desired output is required. Associated with each connection is an adjustable value called a weight. Basically, a node calculates the weighted sum of the inputs then passes the sum through a function to produce a result which is passed to the next layer. The transfer function is typically a steadily increasing S-shaped curve called the sigmoid or activation function. Fig.6.7c shows a graph representation of the characteristic of the sigmoidal activation function. The output of the neuron in Fig. 6.7 can be expressed in terms of the inputs and weights as follows [166,167]:

$$f(z)=[1+\exp(-z)]^{-1} \tag{6.4}$$

where f represent the non-linear sigmoidal function. The network weights, which will eventually store the learnt patterns, are initially set to small random values. During the learning phase the example inputs are presented to the network and allowed to propagate forward to produce the results which is then compared with the known desired result. The resultant and desired outputs are then compared and an error term is then calculated which is used to adapt the network weights so as to obtain the desired input-output response of the network. The training algorithm used in this study is the back-propagation learning algorithm.

6.3.3.1 The Back-propagation learning algorithm

The governing equations for a back-propagation neural network (BPN) have been derived, and are explained in detail in references [165-167]. A summary description of the network operation is given here for completeness. Fig.6.8 shows the topology of a three layer back-propagation network. The network learns a predefined set of input-output example pairs by using a two-phase *propagate-adapt* cycle. The training in back-propagation networks is accomplished by feeding the network through its input units with a set of examples (exemplars) which are *a priori* classified by a human expert.

After an input pattern has been applied as a stimulus to the first layer of the network units, it is propagated through each layer until an output is generated. This output pattern is then compared to the desired output and an error signal is compared for each output unit. The error signals are then transmitted backward from the output layer to each node in the intermediate layer that contributes directly to the output.

However, each unit in the intermediate layer receives only a portion of the total error signal, based roughly on the relative contribution the unit made to the original output. This process repeats, layer by layer, until each node in the network has received an error signal that describes its relative contribution to the error. Based on the error signal received, connection weights are then updated by each unit to cause the network to converge toward a state that allows all the training patterns to be encoded with minimum error.

Referring to Fig.6.8, the neurons in the input layer simply store the input values. The hidden layer and output layer neurons each carry out two functions. First, they multiply all inputs by corresponding weights to produce the input to the non-linear transfer function of the neuron given as:

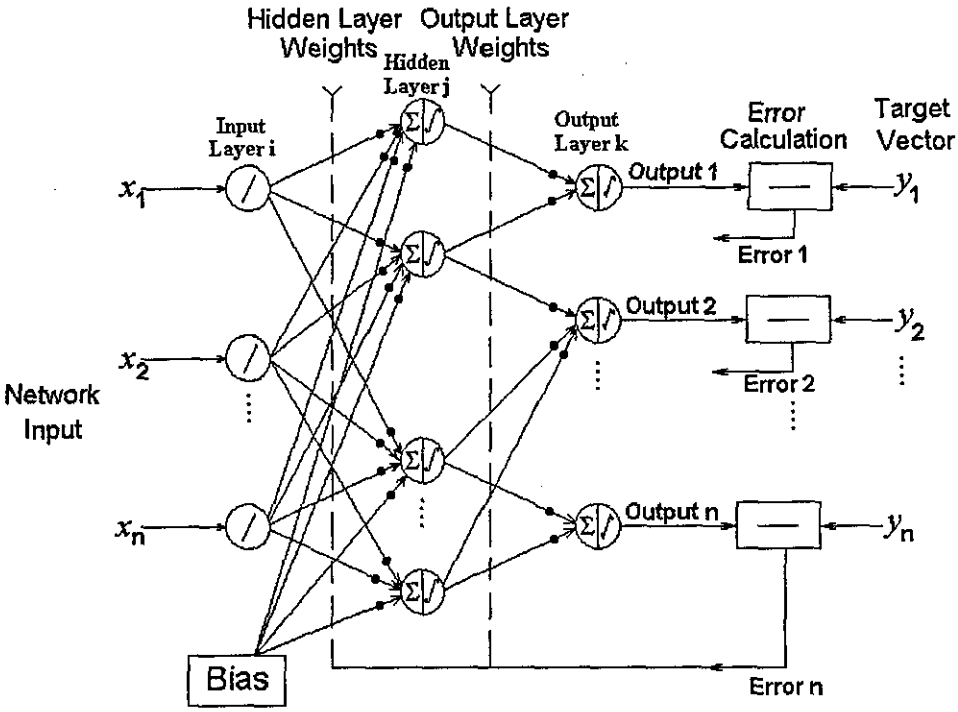

Fig.6.8 Three layer back-propagation algorithm

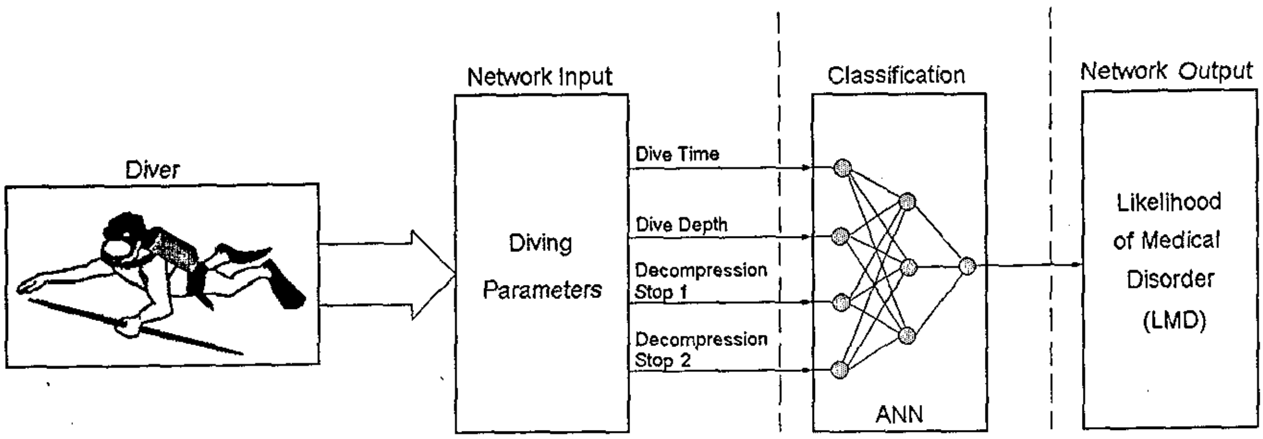

Fig.6.9 The topology of the neural network used in this study

$$S_j=\sum_{i=1}^{n} W_{ij}X_i+\theta_j \tag{6.5}$$

where

X_i is the output of the i-th neuron from previous layer;

W_{ij} the corresponding weight;

S_j is the input to the j-th neuron's transfer function, and θ_j is the bias of neuron j
The inclusion of the bias can be fulfilled by setting $W_{(n+1)j}$ and X_{n+1} =1.

Although non-general conclusions can be drawn regarding the effects of the bias term, since this depends on each specific neural network application, for a fixed structure of neural networks the use of the bias may improve the convergence and speed of training as, equivalently, more weights have been introduced [166].

Second, the output of the J-th neuron , O_j, is calculated as the sigmoidal function of S_j:

$$O_j=f(S_j) \tag{6.6}$$

where f is the sigma function Eq.6.4.

A BPN learns by making changes in its weights in a direction to minimize the sum of squared errors between its actual outputs and target values of the training data set. The system uses the input vector to the network to produce its own output vector and then compare this with the target vector. If there is no difference, no learning takes place, otherwise the weights are changed to reduce the difference. Assuming that there are n input/output vector pairs available for training the network, the weights for the $(n+1)$th iteration is related to those of the (n)th iteration by:

$$W_{ij}(n+1)=W_{ij}(n)+\Delta W_{ij}(n+1) \tag{6.7}$$

where $\Delta W_{ij}(n+1)$ is expressed as:

$$\Delta W_{ij}(n+1)=\eta[(1-\alpha)(\delta_{pj}O_{pj})+\alpha\Delta W_{ij}(n)] \tag{6.8}$$

with δ_{pj} given by :

$$\delta_{pj}=(y_{pj}-O_{pj})O_{pj}(1-O_{pj}) \tag{6.9}$$

for the output layer, and:

$$\delta_{pj}=O_{pj}(1-O_{pj})\sum_{k}\delta_{pk}w_{jk} \tag{6.10}$$

for an arbitrary hidden layer.

The subscripts p and j refer respectively to the p-th training pattern and the j-th neuron to which the weight is connected and k represents the number of neurons in the next layer. If the neuron j is not in the output layer, the δ's are known as the local error signals and are propagated backwards during training, hence the name of the algorithm. Further details of the equations used to calculate the error minimisation using the steepest descent algorithm in the back-propagation are detailed in references [166,167], and are beyond the scope of this work. Basically, the object is to minimise the mean error square between the actual and desired outputs of the network.

The training consists of running patterns through the network forwards, then propagating the errors backwards, and updating the weights according to Eq.6.8. In the weight-adjustment Eq.6.8, the constant η is the learning rate. Its value commonly less than 0.9, is chosen by the neural network user and usually serves to adjust the size of the average weight change.

The constant α is the momentum term and is a smoothing factor which determines the effect of past weight changes on the current direction of movement in the weight space; it improves the convergence and is commonly set around 0.9.

6.3.4 Data set presentation and training architecture

In this study the training data sets represent the module for the random occurrence of medical disorders associated with certain diving profiles and are classified into two general categories: (i) cases with reported medical disorders following a dive, (ii) cases with no medical disorder. In the first category, groups of data were based on reported cases of medical disorders (e.g. decompression sickness, gas embolism, barotrauma) associated with certain diving profiles and the details are published in the literature [147,157,169-176].

The network selection criteria were classified on the basis of (1) dive or bottom time (2) dive depth (3) a decompression stop at 10ft (3m) and (4) a decompression stop at 20ft(6m).

The second category was based on simulated diving profiles extracted from the U.S. Navy Standard Air Decompression Table for air dives [162,163], selected for a maximum allowable depth of 100ft. These were classified on the same basis as the first category.

The training data was selected from a combination of both categories and the output of the network (output layer) was coded into two possibilities:

(a) The first output indicating the likelihood of a medical disorder (LMD) following a certain dive profile.

(b) The second output not indicating such a likelihood (NLMD).

The total training data set represented by the two categories was 35. This was used for training the basic network architecture shown in Fig. 6.9. A Further 35 combined data sets were used for testing the trained network. The units used are in feet to correlate with the US Navy table units and most of the reported cases.

Table 6.1 illustrates the basis of the logical structure and classification of the training set of data (exemplars) based on the analysis described above.

NETWORK INPUTS					NETWORK OUTPUT			
Dive Data	Depth (ft)	Time (min)	Stop 10ft	Stop 20ft	Likelihood of Medical Problem			No Likelihood
					DCS	BAR	EM	
1	65	25	0	0	0	1	0	0
2	70	39	0	0	1	0	0	0
:								
:								
34	60	70	1	0	0	0	0	1
35	80	80	1	1	0	0	0	1

Table 6.1 The training structure of the network

Training was started by presenting one of the patterns from the training set to the input layer and specifying the desired output pattern. The LMD presentation data followed the cited medical cases, while the NLMD followed randomly selected simulated dive profiles extracted from the US Navy dive tables, schedule 1.7, at different air diving decompression stops [162,163]. The first unit in the output layer was arbitrarily identified with "No-Response" i.e. NLMD group. Thus, an output profile of 0 represented the "No-Response" group and 1 represented the "Response", i.e. LMD group. The training was continued until all the exemplars of the training set had been learned according to a preset tolerance 0.1. Hence, a pattern was considered correctly learned when the corresponding output unit had a value of 0.9 or higher and the other unit had a value of 0.1 or lower.

Each experiment for a given input pattern or network parameter was repeated seven times with different random initial weights. A simulation was stopped as being not converging after 2000 iterations, and a new one was initiated until 7 converging simulations were obtained.

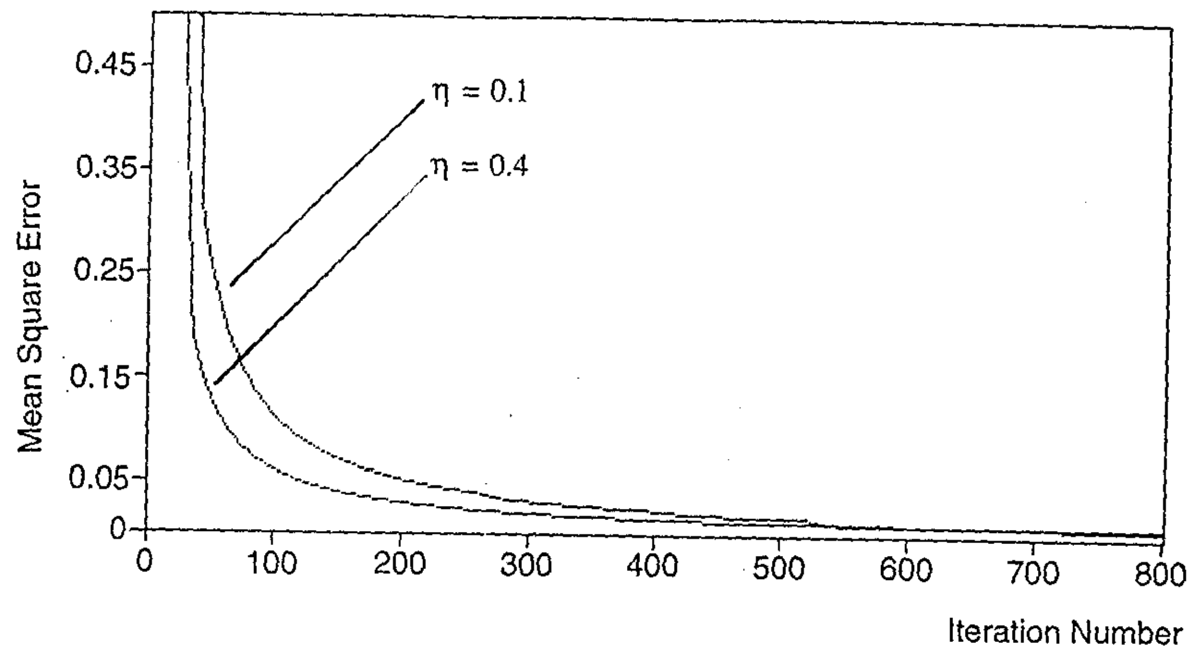

Fig.6.10 Comparison of the training convergence of the network at different learning rates

In order to study the effect of the number of hidden layer units on the correct classification, a two layer fully connected network with different hidden layer units (2-14 unit size) was trained and tested. A typical 8 hidden layer units network with a single output unit was chosen for the analysis and testing as it provided the best classifying results in this case. After the network was successfully trained, when the squared error averaged over the whole training set was less than 0.001, learning was stopped. Fig.6.10 shows the effect of the training convergence sweep for a typical network training experiment with 8 hidden layer units (>6) at two different learning rates (0.1 and 0.4) with a momentum term set at 0.9. It can be seen that the network in both cases converged into solution with an average of 800 iterations. However, the relationship of convergence with hidden layer size was complex, and networks with smaller units (<8 hidden units) required larger numbers of training sweep for convergence. These figures,however, do not include the number of trials that failed to converge within the 2000 training sweeps. While larger networks (>8 hidden units) always converged to a solution, smaller networks (<6 hidden units) did not in some trials. For example, the network with 4 hidden units failed in to converge in 3 trials. This was mainly is because of the limited data set and the trained network.

6.3.5 Performance evaluation and network classification

The discriminant analysis of the network described above was tested and its performance assessed. Fig. 6.11 shows the prediction performance of the network with the effect of the hidden layer size on the recognition accuracy. The experiments performed with a 35 training data sets selected from the combination of the medical and the decompression table classifications have shown that the recognition accuracy of the network was not appreciably affected by increasing the number of hidden layer size (units) from 8 to 14. However, a network of smaller hidden units (<6) resulted in lower recognition accuracy. The average correct classification over all networks with different hidden layer size was 68.1% .

Fig. 6.12 shows the effect of training set size on the increased network recognition rate with the typical 8 hidden units network. It can be seen that adding new exemplars to the training set increased the recognition rate. The average network performance improved from 60% for a training set of 5 exemplars to 71.4% for 10 exemplars. This result shows the steadily improvement in the network recognition with increasing exemplars.

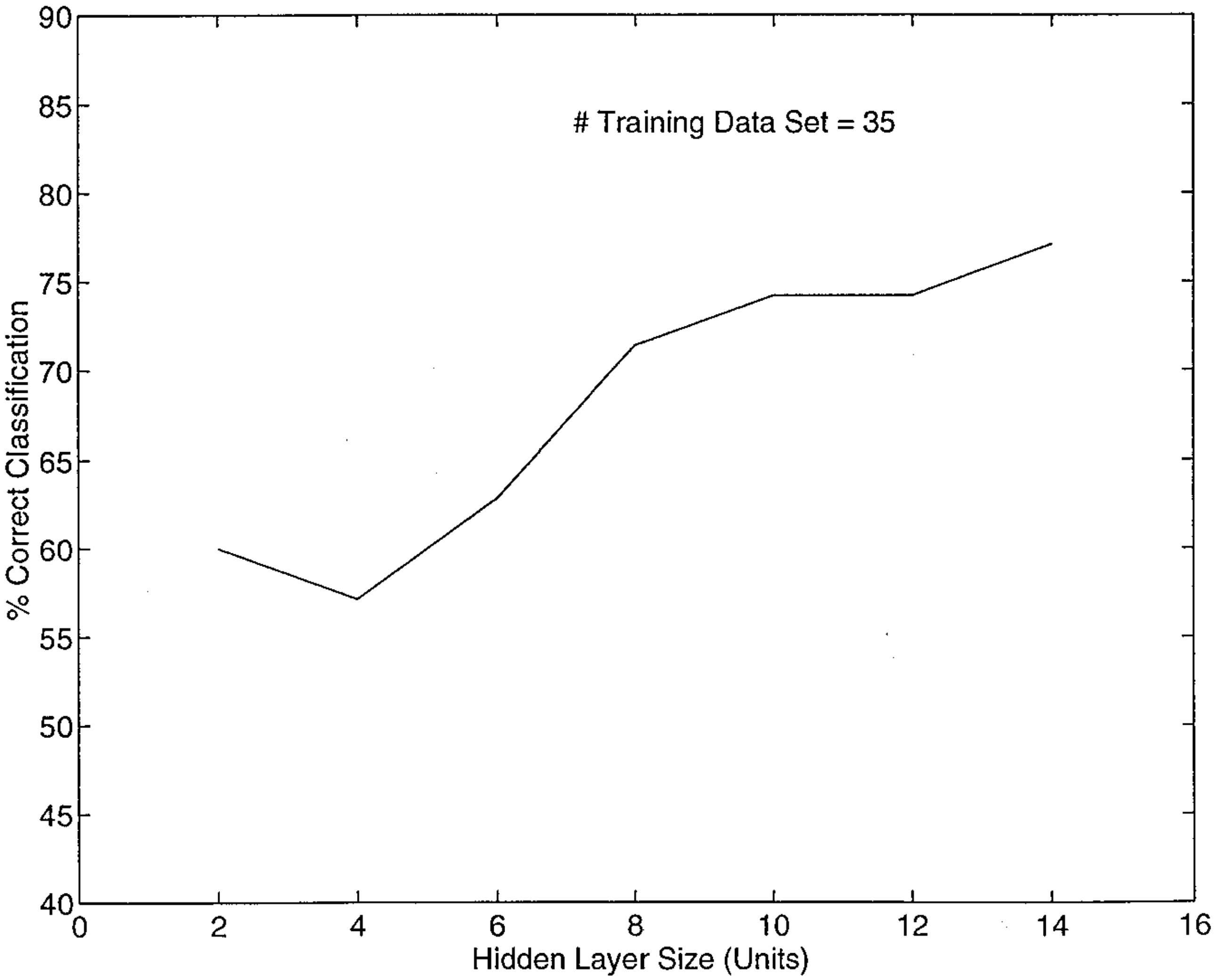

Fig.6.11 The effect of the number of hidden units on the classification accuracy

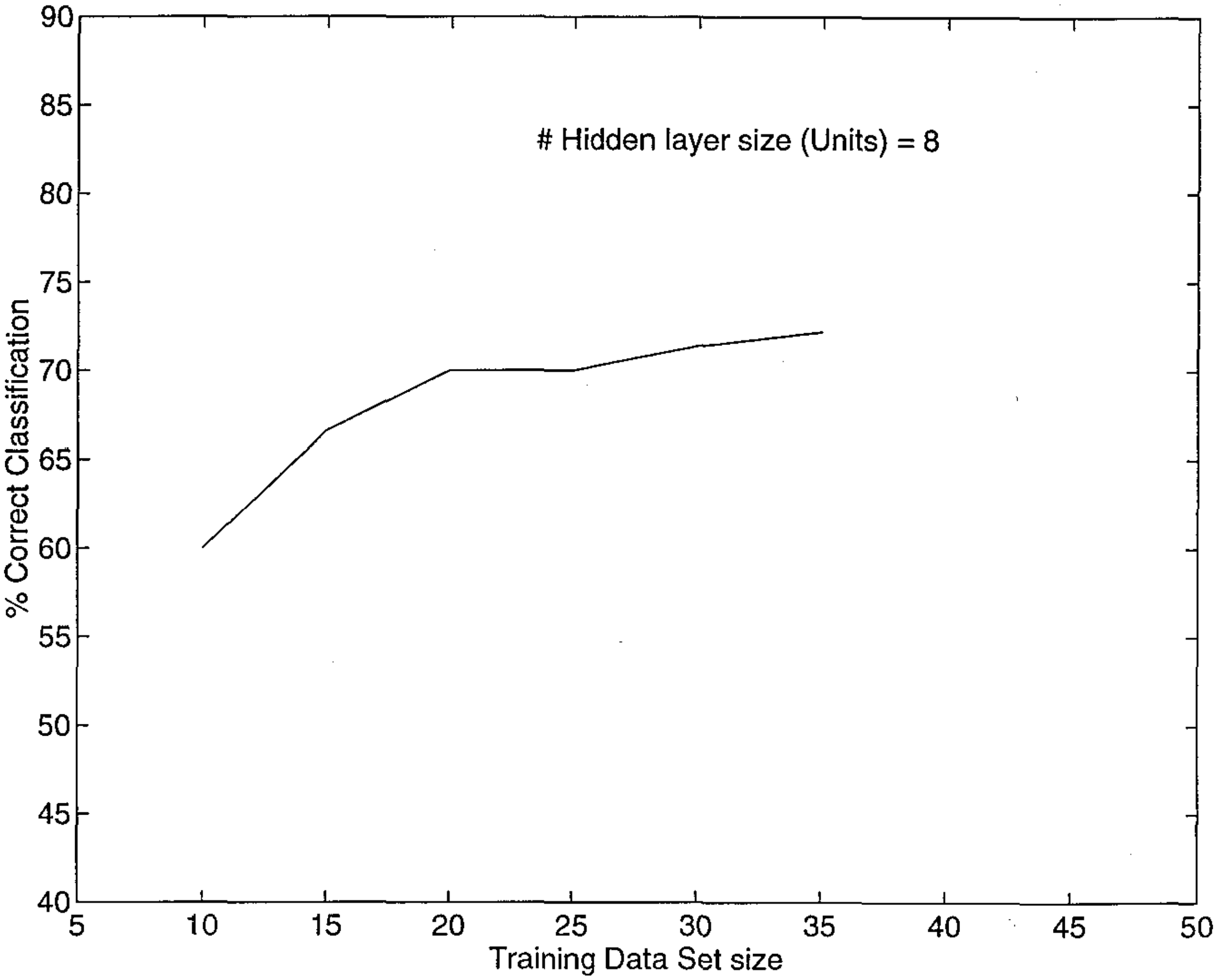

Fig.6.12 The effect of the training data set on the classification accuracy

The network performance was validated by testing the remaining 35 data set which were not included in the training set. The network was considered to have correctly classified a test of LMD patterns if the class corresponding to the output with the larger value coinciding with the pre-specified classification for that pattern. Table 6.2 shows the classification matrix presenting the recognition percentage of the trained network of 8 hidden units for a 35 test data set comprising of combined LMD and NLMD cases. The test performance shows a 20% disagreement between the actual LMD class compared to only 8% of the NLMD class misclassification. However, classification of about 92% among actual NMLD cases coincide with the network classification output.

		Network classification	
Actual (expert) classification		NLMD	LMD
	NLMD	92%	8%
	LMD	20%	80%

Table 6.2 Neural network classification

Judging from the classification results given above, the network successfully classifed and recognizing the risk of a medical disorder from the given number of a random test data set. The fairly difficult recognition problem and the disagreement classification especially in the LMD category can be attributed the small training data set and/or in the number of the network input parameters that has to be increased in order to improve the network performance and classification effectiveness to distinguish more accurately the "Response" and " no Response" cases.

6.3.6 Concluding remarks

The results presented in this preliminary study illustrate the feasibility of using artificial neural networks in automated recognition and classification of the likelihood of predicted medical disorders related to SCUBA diving and the scope to widen the study in the future on a larger and more detailed scale. The small training data set is imposed by the limited open literature data in this topic and the amount of information available at the time of the study. However, the expert model has demonstrated the successful performance of the network to discriminate the risk of medical disorders related to diving cases where classical mathematical and statistical based methods fail to interpret a definite model for such problem due to the complex nature and variability of the parameters involved. The predictive capabilities outlined in this research need to be exploited further to provide a comprehensive and more empirical testing for the model validation. Further studies need to be conducted to generalize the method that depends on the availability of larger well-documented data sets obtained from data banks such as the CANDID (Canadian Dive Data) bank [177] or other British SCUBA clubs. Alternatively, experimental tests can include other physiological parameters such as the ones acquired from the current telemetry system; this should allow the method to be validated on a generalised scale under different dive environments such as in hyperbaric chambers or mixed gas deep dives. Such data are characterized by the intrinsic variability that can occur as a result of different spontaneous mechanisms or as a reaction to occasional stimuli during the diving process and can not be interpreted by classical mathematical analysis methods.

The current availability of real time P.C.-based ANNs capable of continuous, or on-line learning,i.e. after the introduction of a new, non-classifiable example, the network adapts itself quickly to the new class, rather than the off-line learning. This could provide an effective solution to the problems encountered in building on-line diagnostic system that emulates a physician's expertise in such environments by simply incorporating systems in future dive computers or underwater biotelemetry systems.

CHAPTER SEVEN

CONCLUSIONS AND FUTURE WORK

7.1 Conclusions

The main aim of the thesis has been twofold. The first was to study and develop a new practical design for an underwater acoustic digital biotelemetry system suitable for real-time monitoring of a free swimming SCUBA diver or swimmer in a reverberant underwater environment. The second comprised simulation studies carried out to investigate the feasibility of monitoring a diver's physiological well-being from the telemetered data and to investigate how to design future biotelemetry systems. From the foregoing work and the experimental results obtained, the following conclusions may be drawn.

1. A new comprehensive programmable transmitter-receiver for underwater biotelemetry method using single-chip microcontrollers is introduced. The design procedures provide a modular hardware and software organization for the transmitter and the receiver. The microcontroller-based architecture provides the necessary time-base synchronization and trade-off between the acoustic telemetry limitations and the corresponding physiological monitoring.

This versatile modular approach allows the digital telemetry of data such as heart rate, breathing rate and depth and/or analogue signals such as the ECG. It also, allows the desired mode of transmission to be selected and the addition of further monitoring channels without any alteration to the existing hardware and only minor modifications to the software. The detailed transmitter and receiver designs are presented for each channel with the associated I/O microcontroller interface units.

2. A thermal respiratory method has been developed for measuring the breath-to-breath signals and proved successful in telemetering the breathing rate of a free swimming diver.

3. A new interrupt-based multichannel transmission concept has been developed that allows the processor to interrogate each channel by a priority-channel rate multiplexing hierarchy programmed in the transmitter and receiver. This allows accurate telemetry of the different rate signals without the need of synchronization bits and minimum errors in the detection.

4. A novel microcontroller-based algorithm has been developed for the critical task of real-time detection and underwater acoustic transmission of ECG signals. The algorithm allows accurate detection of the QRS complex from the noisy raw signal. The pulsed digital link is provided by a programmed serial-to-parallel and parallel-to-serial conversion format required for the DPCM/OOK communication between the transmitting and receiving processors.

5. The system performance carried out in the departmental tank, simulating a very shallow and reverberant underwater channel, proved reliable. The limitations imposed were relatively short range and corresponding lower ECG transmission bit-rate dictated by the severe multipath interference present in such an environment.

Multichannel transmission proved highly successful, especially with heart rate, as the results were compared with advanced radio telemetry equipment. The ECG signals were reproduced successfully in the receiver and could be used for further data analysis and diagnosis. The received signals had some distortion due to the limited range of diver's movement and the highly reverberant tank. The practical biotelemetry system developed in this work can be used for other real-time monitoring from multiple subjects and other biotelemetry applications.

6. Off-line results of power spectral analysis of the heart rate variability have enabled a new physiological interpretation of the heart rate reflexes during SCUBA diving.
This could eventually explain some of the physiologically unresolved diving or swimming fatalities.

7. A pilot feasibility study of a simple artificial neural network (ANN) for the likelihood detection of medical disorders proved reasonable for detecting the condition of a diver

following a certain dive profile if incorporated in the telemetry link using VLSI neural processing chips.

In summary, the programmable concept presented in this thesis provides a robust practical approach capable of developing an enhanced small size, low power and low weight acoustic telemetry system suitable for a wide range of monitoring application and ameliorates the draw backs and limitations that restricted the use of acoustic biotelemetry in the past.

7.2 FUTURE WORK

Most of the aspects associated with realizing an automated practical underwater biotelemetry system have been addressed in this thesis. However, the work carried out was limited by the resources available in the university, and the way ahead for future development and research of the project remains open.

Although, the use of the PPM coding for the ECG transmission allows an increased bit rate, it introduces an added complexity to the problem of detecting the energy levels of the direct signal in the presence of destructive multipath signals. A comparative performance study in a large lake and in the sea is possible future study. Also, a microcontroller implementation of both PCM and PPM coding methods for monitoring different biomedical signals could be carried out.

Since the transmission bit rate in this study is low (< 50 Hz), no attempt was made to study the effect of the bit error probability of the ASK biotelemetry system. This was expected to be very low ($<10^{-5}$) and has no significant effect on the system performance in the current application. However, if higher bit rates or other coding schemes are used (>1000 Hz) then a future study can investigate the error rates both theoretically and practically.

The addition of battery monitoring and microprocessor watchdog/power failure circuits in the transmitter is another future feature to be added. One possibility for implementing this is the range of LTC692/LTC693 microprocessor supervisory circuits from Linear Technology. In the depth monitoring channel, incorporating an audio alarm circuit that produces periodic pulses by a beep timer to alarm the diver at pre-set depths or for exessive descent/ascent rates is another future topic.

The re-engineering and further miniaturisation of the transmitter and receiver systems for open-water testing is also a future topic for study.

The recent advances in VLSI and application-specific IC's (ASIC) technology make it possible to improve the performance and miniaturize the system further in several ways. For example using surface mounted components and with a redesigned housing could allow further miniaturization of the biotelemetry system. Using alternative single-chip processors such as the 16-bit Intel-80C196 series could improve the performance of the system with modified specifications such as increased speed (0.66 μs), higher vectored interrupt levels (16 levels), and on-chip 10-bit A/D converter with sample/hold.

Another solution is to use a newly developed 8-bit microcontroller based on the 'Smart Power' technology where the single processor IC (H081-SGC-Thompson) incorporates a 60-V DMOS FET H-bridge rated at a continuous current of 1A. This technology makes possible the development of programmable output power transmission features in a single chip.

In the sensor and signal acquisition modules, future options include the use of the newly developed smart sensors using micromechanical system (MEMS) technology. This enables the measurement of different physical and physiological parameters with an in-built processor fabricated with single-chip IC batch processing techniques.

These could lead to the implementation of special purpose underwater biotelemetry processor architectures where the signal identifiers, coding and modulating are prototyped on a single field-programmable gate array (FPGA) chip.

The problem encountered with water leakage through the dry suit to the ECG electrodes during the underwater trials suggest the development of alternative methods for measuring the heart rate. One such method is the use of piezopolymer acoustic pressure sensors to measure the heart rate or the heart sound; these are manufactured with shielded electrodes and silicon rubber insulation similar to those of the heart rate monitor. Another solution is to measure the heart rate from alternative locations in the body surface such as the finger tips or ear lobes where it is possible to detect the heart rate fluctuations by miniaturised optical sensors.

Measurement of other physiological parameters such as EEG, oxygen uptake estimation from heart rate, heart sound (phonocardiogram), and blood pressure are possible for other critical monitoring channels.

Further studies in the topics introduced in chapter six can provide important links between medical monitoring and biotelemetry system designs. Incorporating the recent VLSI neural-chips in the system or on future dive computers provides biotelemetry research with a unique trend in future implementation of application-specific smart biotelemetry and monitoring processors.

APPENDIX (A)

CHARACTERISTIC PARAMETERS OF THE ACOUSTIC TRANSDUCERS

The acoustic transducers used were D/170 ball type electrostrictive spheres (Universal Sonar.Ltd., UK), approximately 30mm in diameter and made of lead zirconate titanate (PZT). The identical projector and hydrophone characteristics were measured in the water at different frequencies and the resultant admittance loci and calibration responses are shown in Fig.A.1 and Fig. A.2.

The other measured resonance parameters characterizing the equivalent circuit for the transducers are:

- Resonant frequency (f_0) = 69.8 kHz,
- Q Factor = 4.105
- Susceptance in water (B_0) = 3.117 x 10-3 mS
- Conductance in water (G_0) = 3.615 x 10-3 mS
- Equivalent resistance(R_s) = 1/G_0 = 276.6 Ω
- Static resistance (C_0) = 710.72 pF

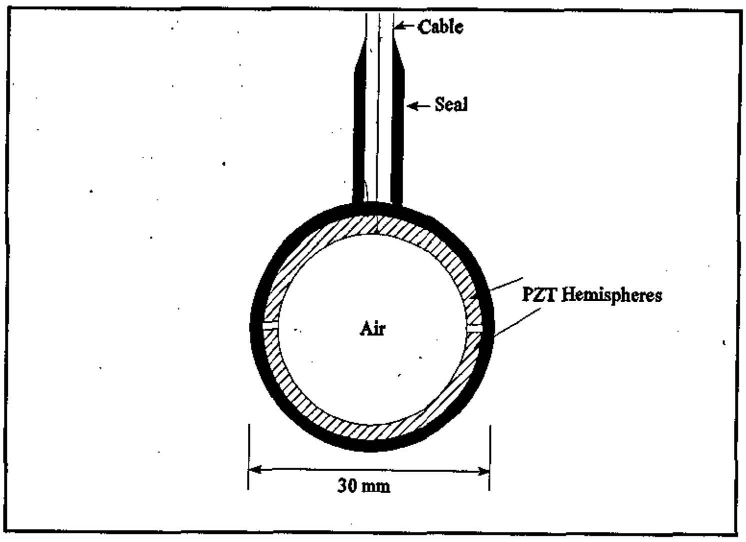

Hydrophone Schematic

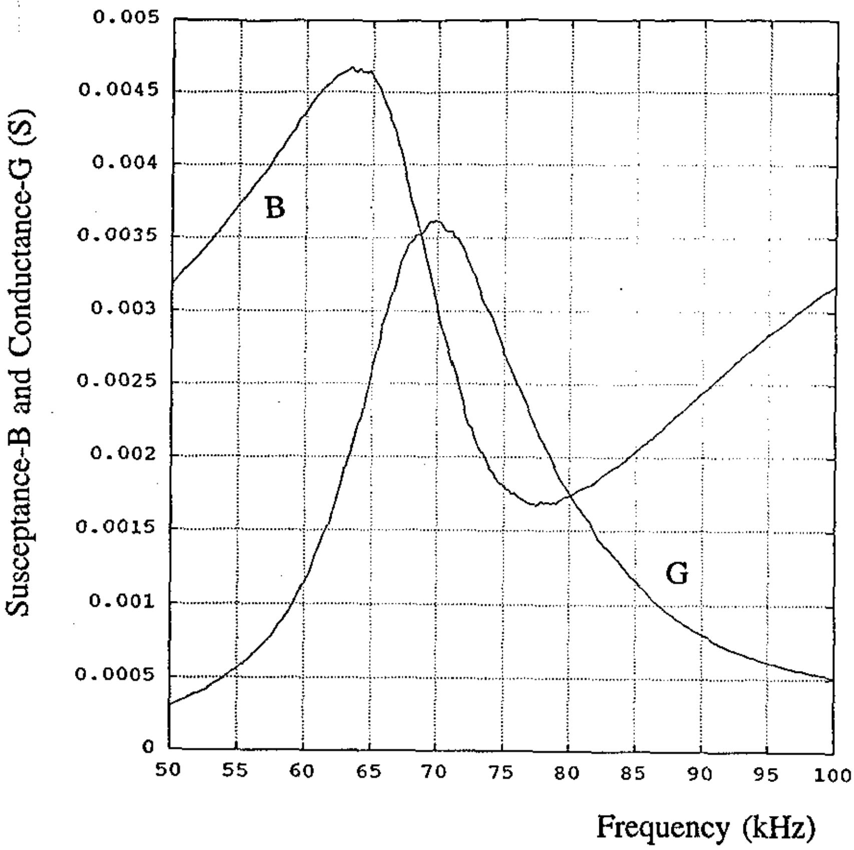

Fig.A.1 Admittance plots of Ball hydrophone (D/170)

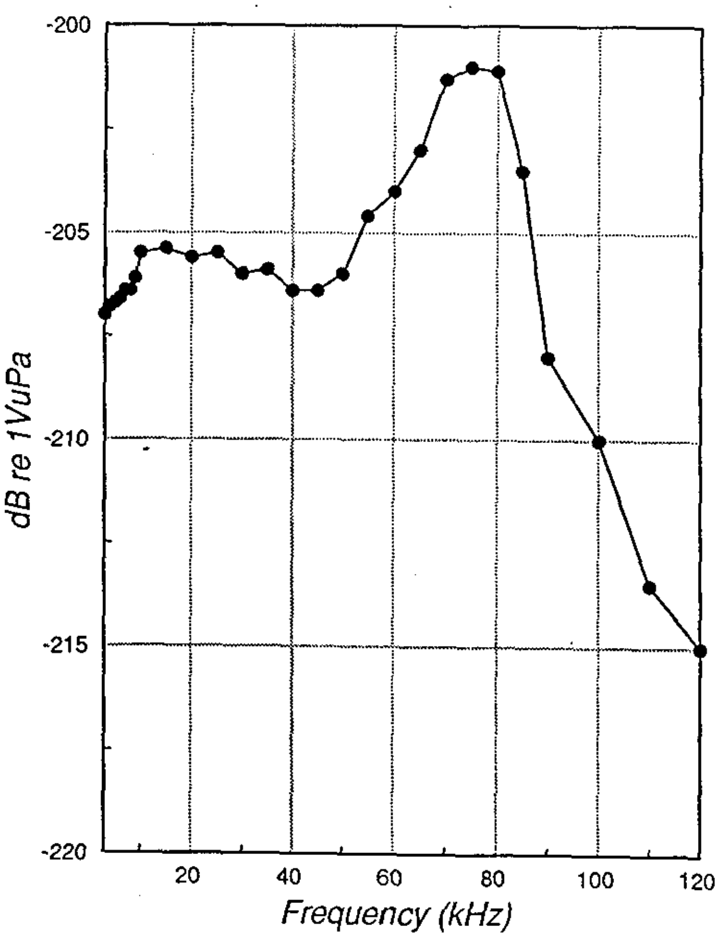

Fig.A.2 Calibration plot of Ball hydrophone (D/170)

APPENDIX B

POWER AMPLIFIER AND MATCHING TRANSFORMER CALCULATIONS

The output stage of the transmitter is effectively the power amplifier allowing CMOS logic signals to drive the piezoelectric projector.

This appendix outlines the design procedure to calculate the transmitting transformer's turns ratio for the class E driver described in section (4.2.2.2).The parameters were calculated from the measured parameters of the acoustic projector given in Appendix (A).

The equivalent circuit of the projector at resonance comprises the static capacitance C_0 of the piezoelectric material in parallel with the load resistance. The projector's static capacitance C_0 is given by:

$$C_0 = B_0 / 2\pi f_0 \qquad \text{(B1)}$$

The projector has a series resonant frequency of 69.8 kHz and a susceptance B_0 in water of 3.117×10^{-3} mS.

Hence, from Eq.(B1), $C_0 = 7.10$ pF. If the power amplifier is to drive a purely resistive load, the projector's C_0 must be tuned out. This may be done with the parallel inductance of the transformer secondary where the turns ratio is chosen to perform L-C impedance matching for maximum power transfer.

Hence for the secondary turns;

$$L_0 = 1 / 4\pi^2 f_0^2 C_0 \qquad \text{(B2)}$$

Substituting the values calculated above, Eq.(B2) yields, $L_0 = 731$ μH.

The Mullard transformer core RM6/160 used here has an inductance factor of A_L = 160 nH/turn. Thus the number of the secondary turns (N_s) needed for the inductance L_0 is :

$$N_s = \sqrt{(L_0/A_L)} = \sqrt{(731 \text{ x } 10\text{-}6 \ / \ 160 \text{ x } 10\text{-}9)} \qquad \text{(B3)}$$
$$\approx 67 \text{ turns}$$

For maximum power transfer at resonance, the projector's load when referred to the primary turns N_p should equal to the source resistance. The source resistance is effectively the ON resistance R_{DS} of the switching FET used (VN66AF), specified at 3Ω.

Hence, the primary turns N_p can be calculated from the relation of resistance ratio and the square of the turns, given as:

$$R_p/R_s = (N_p/N_s)^2 \qquad \text{(B4)}$$

The value of R_s is calculated from the measured conductance given in Appendix A:

$$R_s = 1/G_0 = 1/3.615 \text{ X } 10^{-3} = 276.6\Omega$$

Hence, from Eq. B4, $N_p \approx 7$ turns

In the final design the number of turns in the primary can be adjusted slightly to give the best response from the amplifier output.

APPENDIX C

(AR) TIME SERIES PARAMETER AND MODEL ORDER ESTIMATION

The theory of the autoregressive spectral estimation is explained in details in references [129,130], an abbreviated description of the main aspects are discussed here for completeness.

The autoregressive (AR) model assumes that the current value of the process x_n, can be described by a finite linear aggregate of the previous values of the process and the current value of a white noise driving process n_n. An autoregressive process of order p is defined as

$$x_n = n_n - a_1 x_{n-1} - a_2 x_{n-2} - a_3 x_{n-3} - \ldots\ldots\ldots - a_p x_{n-p} \tag{C1}$$

The autoregressive model contains $P+2$ parameters which have to be estimated from the data: the coefficients, the mean of the samples, and the variance of the white noise. The estimation of the parameters for the AR model result in linear equations, which are computationally easy to implement.

Given the AR Yule-Walker equations [129,130]:

$$\begin{bmatrix} r_{xx}(0) & r_{xx}(-1) & \cdots & r_{xx}(-p+1) \\ r_{xx}(1) & r_{xx}(0) & \cdots & r_{xx}(-p+2) \\ \vdots & \vdots & \vdots & \vdots \\ r_{xx}(p-1) & r_{xx}(p-2) & \cdots & r_{xx}(0) \end{bmatrix} \begin{bmatrix} a_1 & r_{xx}(1) \\ a_2 & r_{xx}(2) \\ \vdots \; = -\!\!\! & \vdots \\ a_p & r_{xx}(p) \end{bmatrix} \tag{C2}$$

$$\sigma^2 = r_{xx}(0) + \sum_{k=1}^{p} a_k r_{xx}(k) \tag{C3}$$

where the autocorrelation lags $r_{xx}(k)$ matrix is Hermitian Topelitz matrix ($r_{ij}= r_{i+1,j+1}$ and $r_{ij}=r_{ji}$), i.e. all elements along each diagonal are equal.

To use Eqs.(C2) and (C3),the autocorrelation values $r_{xx}(k)$ must be estimated. Exploiting the special Toeplitz structure of the $r_{xx}(k)$ matrix, leads to the computationally simple Levinson-Durbin recursion algorithm [129,132] that can be used rapidly to solve for the AR coefficients.

This method uses the important property that the coefficients of an AR(k) process can be computed from the parameters of the AR$(k-1)$ model and K values of the autocorrelation function. The coefficients for the first-order process are first obtained and from these the algorithm proceeds recursively up to the desired order p .

In the following equations two indices are used for the coefficients $a(k,i)$. The first is the order for the AR model and the second, the number of the coefficient.
The first-order AR process is described by:

$$a(1,1) = -r_{xx}(1)/r_{xx}(0) \tag{C4}$$

and

$$\sigma(1)^2 = [1-a(1,1)^2]\, r_{xx}(0) \tag{C5}$$

and then, the following recursion is used to compute consecutive superior orders from $k=2$ to p:

$$a(k,k) = -[r_{xx}(k) + \sum_{i=1}^{K-1} a(k-1,i)\, r_{xx}(k-i)] / \sigma(k-1)^2 \tag{C6}$$

$$a(k,i) = a(k-1,i) + a(k,k)\, a(k-1,k-i) \tag{C7}$$

$$\sigma^2(k) = [1-a(k,k)^2]\, \sigma(k-1)^2 \tag{C8}$$

Once the desired order, p is achieved, the power spectral density estimate of the data is given by:

$$P(f) = \frac{\sigma(p)^2 \delta}{|\sum_{n=0}^{p} a(p,n) \exp(-j2\pi * f * n * \delta|^2} \tag{C8}$$

In Burg algorithm (Maximum Entropy Method) [131,132,133], the spectral estimation is based on upon an extrapolation of the known values of the autocorrelation function using the autoregressive model as the basis for the extrapolation. Hence, in solving Eqns.C2 and C3, rather than estimating the autocorrelation lag values directly, the Burg algorithm estimates a set of reflection coefficients k_p, which are a function of the $r_{xx}(k)$ values from the samples before using the recursive Levinson algorithm to solve for the AR parameters. This algorithm minimizes $\sigma(p)^2$, the power of the model driving noise or the prediction error, as the mean of forward and backward linear prediction errors. The K_p are recursively estimated from the prediction errors and constrained by the Levinson recursion solution to the Yule-Walker equations, which relates the AR parameters of order p to the order p-1 parameters by:

$$a_p[n] = a_{p-1}[n] + K_p a_{p-1}[p-n]\ , 1 \leq n \leq p-1 \tag{C9}$$

Further details and relevant derivations of the forward and backward errors in Burg algorithm are found in modern spectral estimation references [129,130,132,137].

The selection of the model order is typically based on the computation of statistical error criteria. A test often used in parametric estimation is the Akaike Information Criteria or the Final Prediction Error (FPE) [129,136]:

$$FPE(p) = \sigma(p)^2 \frac{N+p+1}{N-p-1} \tag{C10}$$

where N is the number of data samples, p is the estimated AR model order , and $\sigma(p)^2$ is the estimated variance or power of the driving noise of the model. This criteria attempts to balance the estimated prediction error power $\sigma(p)^2$ that generally decreases with increasing order and need the need to maintain a small number of model parameters to estimate. The appropriate model orders are those that minimize the FPE measure.

REFERENCES

1 MACKAY, R.S., 'Biomedical Telemetry: Sensing and Transmitting Biological Information from Animals and Man', 2nd Ed.,New York: John Wiley, 1970.

2 KIMMICH, H.P., 'Multichannel Biotelemetry-Review', Biotelemetry, Vol.2, pp.207-255, 1975.

3 JEUTTER, D.C., 'Overview of Biomedical Telemetry Techniques', IEEE Eng.In Med. & Biol.,Vol.2, pp.17-24, Mar.1983.

4 KIMMICH,H.P.,'Artifact free measurement of biological parameters, biotelemetry a historical review and layout of modern development, In Handbook Biotelemetry and radiotracking,AMLANER,C.J.andMACDONALD,D.W.(eds.),Pergamon press,N.Y.,pp.3-20,1980.

5 FRYER, T.B. and SANDLER, H. , 'A Review of Implant Telemetry Systems', Biotelemetry, 1(6), pp.351-374, 1974.

6 YSENBRANDT, H.J.B.,SELTEN, A.J., KOCH,T., KIMMICH, H.P., Biotelemetry Literature Survey of The Past Decade', Biotelemetry,Vol.3, pp.145-250, 1976.

7 MEINDEL,J.D., and FORD, A.J., 'Implantable telemetry in biomedical research, IEEE Trans. Biomed. Eng., Vol.31,pp. 817-821,1984.

8 ADRIAN, E.D. and LUDWIG, C., 'Nervous Discharge from the olfactory organs of Fish', J. Physiol., 94, pp.441-460, 1938.

9 SLATER, L.E. (ed.), 'Biotelemetry, the use of telemetry in animal behaviour and physiology in relation to ecological problems',Pergamon press, N.Y., 1965.

10 PRIEDE, I.G.,'An analysis of objectives in telemetry studies of fish in the natural environment', In Handbook on biotelemetry and radiotracking, AMLANER, C.J. and MACDONALD, D.W.(eds.), Pergamon press, N.Y., pp.*105-118*, *1980*.

11 FRANK, H.T., 'Telemetring of Electrocardiogram of Free Swimming Fish (*Salmo Irideus*)', IEEE Trans. Biomed. Eng., Vol.15, 2, PP.111-114,1968.

12 SCIDMORE, A.K., BEYER, J.B., WEISS D., and GUCKEL, H., 'EEG Monitoring of Free Swimming Fish, Biotelemetry, 3, pp.227- 230, 1976.

13 KUDO, Y., UEDA, K., 'The measurement of the electrical activity of the olfactory bulb in free swimming carp by underwater telemetry system', IEEE Trans. Biomed. Eng., Vol.27, pp.694-698,1980.

14 WHEATHERLEY, A. H., ROGERS., S.G., PINCKOCK, D.G., and PATCH, J.R., 'Oxygen consumption of active rainbow trout derived from electromyograms obtained by radiotelemetry', J. Fish Biol., Vol.20, pp.479-498,1982.

15 TREFETHEN, P.S.,'Sonic equipment for tracking individual fish', U.S. fish & Wildlife Serv. Spec. Sci., Rep. No.179,1956.

16 STASKO, A.B.,' Underwater biotelemetry,an annotated Bibolography', Canadian Fish. Mar. Serv. Resour. Dev. Branch Marit. Tech. Rep. Ser. MART-534,Canada,31pp.,1975.

17 HENDERSON, F. G. and HASLER, A. D.,'An Ultrasonic Transmitter for use in the Studies of Movement of Fishes', Trans. Am. Fish.Soc.,Vol.95, pp.350-356, 1966.

18 YOUNG,A.H.,TAYLOR,P., and HOLLIDAY, F.G.,' A small sonic tag for the measurement of locomotor behaviour in fish,' J.Fish Biol., Vol.4., pp.57-65,1972.

19 MONAN, G.E., and THORNE, D.L., 'Sonic tags Attached to ALaska King Crab', Marine Fisheries Review, 37(2), pp.9-15, 1973.

20 CAREY, F.G., and LAWSON, K.D.,' Temperature requaltion in free swimming bluefin tuna, Comp. Biochem. Physiol., Vol.44, pp.375-392,1973.

21 RUBINOFF, I., GRAHAM, J.B., and MOTTA J., 'Diving of the Sea Snake (*Pelamis Planturus*) in the Gulf of Panama: I. Diving Depth and Duration', Mar. Biol., Vol. 91, pp.181-191, 1986.

22 WILSON, R.P., GRANT, W.S., and DUFFY, D.C.,'Recording devices on free-ranging marine animals', Ecology, 67, 1091-1093, 1986.

23 PRIEDE, I.G., and YOUNG, A.H.,' The ultrasonic telemetry of cardiac rhythms of wild brown trout as an indicator of bio-energies and behaviour, J. Fish Biol., Vol.10, pp.229-318,1977.

24 BOTTOMS, A. and MARLOW, J.,' A new Ultrasonic Tag for the Telemetry of Physiological Functions from Aquatic Animals', Mar. Biol., 50, pp.127-130, 1979.

25 WARDLE, C.S., and KANWISHER, J.W., 'The significance of heart rate in free swimming Cod (*Gadus Morhua*): Some observations with ultrasonic tags, Mar. Behav. Physiol., Vol.2, pp.311-324, 1973.

26 ROGERS, S.C., WEATHERLEY, A.H., and PINCKOCK, D.G., 'Telemetry electromyograms and oxygen demands of fish activity, Proc. 3rd. Int.Conf. Wildl. Biotelemetry, Univ. of Wyoming, Laramie, July 1981, pp.141-150, 1981.

27 STASKO, A.B., and HORRALL,R.M.,'Method of counting the tail-beats of swimming fish by ultrasonic telemetry', J. Fish Res. Board. Canada, 33, pp.2596- 2598,1976.

28 FERREL, D.W., NELSON, D., STANDORA, T.C., and CARTER, H.C.,'Multichannel ultrasonic biotelemetry system for monitoring marine animal behaviour', Trans. ISA Vol. 13, pp.120-131,1974.

29 BJORDAL, A., FLOEN, S., TODLAND, B., and HUSE, I., ' Monitoring biological and environmental parameters in aquaculture', Model., Ident. and Control, Vol.7, pp.209-218,1986.

30 KANWISHER, J., LAWSON, K., and SAUNDNES, G.,' Acoustic telemetry from fish', Fish. Bullet., Vol.72, pp.251-255,1974.

31 BRAITHWAITE, H., 'Some measurements of acoustic conditions in rivers', J. Sound & Vib., Vol.37, 557-563, 1974.

32 MEISTER, R., and ST. LAURENT, R., 'Ultrasonic absorbtion and velocity in water containing algae in suspension, 'J. Acous. Soc. Amer., Vol.32, pp.556-559, 1960.

33 BRUMBAUGH,D.,'Effect of thermal stratification on range of ultrasonic tags', Underwater telemetry newsletter, Vol.10, pp.1-4,1980.

34 URICK, R.J.,'Principles of underwater sound for engineers', 2nd. Ed., McGraw-Hill:N.Y., 1975.

35 BURT, E.G., and RIGBY, L.,'Electromagnetic through-water communication' J. Soc. Underwater Tech., Vol.11, pp.14-18, 1985.

36 SLATER, L.E. (ed.), 'Biotelemetry', Oxford: Pergamon Press, 1965.

37 MAGEL, J.R., and MCARDLE, W.D., 'Telemetred heart rate response to selected competitive swimming events', J.Applied Physiol., Vol.26, pp.764-770, 1969.

38 BALDWIN, H.A.,'Marine biotelemetry', Bioscinece, Vol.15,pp.95-97, 1965.

39 OKA, Y., UTSYAMA, N., KODA, K., and KIMURA, M.,'Studies of telemetring on ECG and respiratory movements during running, jumping and swimming', Med. Elec. Biol.Eng., Vol.1, pp.574-579,1963.

40 TUCKER, D.G., and BAZEY, B.K.,' Applied underwater acoustic', pergamon press:London, 1966.

41 ANDERSON, V.C.,'Acoustic communication is better than none', IEEE Spectrum, pp. 63-68, 1970.

42 FRAMPTON, C., RIDDLE, H.C., and ROBERTS, J.R., 'An ECG telemetry system for physiological studies on swimmers', Biom. Eng., 11,pp. 87-90, 1976.

43 FRAMPTON, C., RIDDLE, H.C., ROBERTS, J.R., and WATSON, B.W.,'An inductive loop telemetry for recording ECG of a swimmer', J. Physiol., Vol.241, pp.14-16,1974.

44 GLASER, R.M., and MCARDLE, W.D., 'A Radiotelemetry Transmitter for Monitoring Heart rate of Human Engaged in Physical Activity', The Res. Quarter. of The American Assoc. of Health,Physic. Educ. and Recreation, 40(3), pp.640-642, 1969.

45 JACOB,R., RIDDLE, H.C., and WATSON, B.W.,' Circuits for searching a signal from a three aerial system during inductive loop telemetry', Biomed. Eng., Vol.8, pp.295-297,1973.

46 SCHULTZ, C.W.,'Underwater communication using return current density', Proc. IEEE, pp.1025-1026, 1970.

47 ZWEIZIG, J.R., ADEY, W.R., and HANLEY, J., 'EEG monitoring of a free swimming diver at a working depth of 15m', Aerospace Med., 43, pp.403- 407, 1972.

48 UTSUYAMA, U., YAMAGUSHI, H., OBARA, H., and MIYAMATO, H.,' Telemetry of human electrocardiogram in aerial and aquatic environments', IEEE Trans. Biomed. Eng., BME-35., pp.882-884, 1988.

49 WELTMAN, G., and EGSTROM, G.H., 'Heart rate and respiratory response correlation in surface and underwater work', Aerospace Med., 40, pp.479-483, 1969.

50 THALMAN, E.D., SPONHOLTZ, D.K., and LUNDGREN, C.E., Chamber-based system for physiological monitoring of submerged exercising subjects, Undersea Biom. Res., Vol. 5,pp.293-300, 1976.

51 LOVIK, A., LlOYD, J., and TANGEN, J.M., 'A general system for the physiological diver monitoring', Proc. IEEE Ocean'83 Conf., 1, pp.464-466, 1983.

52 PILMANIS, A.A., GIVEN, R.R., and PILMANIS, V.M., 'Physiological and biological studies from The Hydrolab', Hydrolab J. , 1, pp.30-42, Oct. 1971.

53 JUNG, W. and STOLLE, W., 'Behaviour of Heart Rate and Incident of Arrhythmia in Swimming and Diving', Biotelemetry,Vol.8, pp.228-239, 1981.

54 SLATER, A., and BELLET, S., 'An underwater temperature telemetring system', Med. Biol. Eng., Vol.7, pp.633-639, 1969.

55 SLATER, A., BELLET, S., KILPATRICK, D.G.,'Instrumentation for telemetring the electrocardiogram from Scuba Divers', IEEE Trans. Biom. Eng., Vol.16, pp.148-151, 1969.

56 KANWISHER, J., LAWSON, K., and STRAUSS, R., 'Acoustic telemetry from human divers', Undersea Biom. Res., Vol.1, pp.99-109, 1974.

57 SKUTT, R.H., FELL,R.,and HAGSTROM, E.C.,'A multichannel ultrasonic underwater telemetry system', Biotelemetry, Vol.(1), pp.30-38, 1971

58 CLAY, C.S., and MEDWIN, H., 'Acoustical Oceanography: principles and applications', Wiley;N.Y., 1977.

59 BREKHOVSKISH, L. and LYSANOV, Y., 'Fundamentals of ocean acoustics', Springer-Verlag:N.Y.,1982.

60 FLATTE, S.M. (ed.),' Sound transmission through a fluctuating ocean', Cambridge Univ. Press, Cambridge:U.K., 1979.

61 BURDIC, W.S., 'Underwater signal analysis', Prentice-Hall, 1991.

62 JENSEN, F.B., and KUPERMAN, W.A.,'Optimum frequency of, propagation in shallow water environments', J. Acous. Soc. Amr., Vol.73, pp.813-816, 1983.

63 BAGGEROER, A.B., 'Acoustic telemetry-An overview', IEEE J. Ocean. Eng., Vol.9, pp.229-235, 1984.

64 COATES, R., and WILLIAMS, P.,'Underwater acoustic communications: A review and bibliography', Proc. Inst. Acoust., Dec.1987.

65 RAY, C.C. (ed.),' Medical Engineering', Rev., Year book Medical Publishers, Chicago, 1974.

66 JACOBS, I., 'Practical application of coding', IEEE Trans. Inf. Theory , Vol.20, pp.305-310, 1974.

67 PIEPER, J.F., and PROAKIS, J.A.,' Design of efficient coding and modulation for a Rayleigh fading channels', IEEE Trans. Inf. Theory, Vol.24, pp.457-468, 1978.

68 PROAKIS, J.,' Digital communications', McGraw-Hill:N.Y., 1983.

69 VITERBI, A.J, and OMURA, J.K.,'Principles of digital communication and coding', McGraw-Hill:N.Y., 1979.

70 TOMASI, W., 'Advanced electronic communication systems', 2nd. ed.,Prentice - Hall:N.J., 1992.

71 FRYER, T.B., 'A Multichannel EEG telemetry utilizing a PCM subcarrier', Biotelemetry, Vol.1, pp.202-206,1974.

72 HULL, M.L., and MOTE,C.D.,' PCM telemetry in ski injury research, Biotelemetry, Vol.1, pp.182-184, 1974.

73 FALAHATI, A., WOODWARD, B. and BATEMAN, S.C.,' Underwater channel models for 4800 b/s QPSK signals', IEEE J. Ocean. Eng., Vol.18, pp.12-20, 1991.

74 MOHANTY, N., ' Phase tarcking error in a fading channel', Proc. Int. Fed. Telemetry Conf.(IFT), pp.203-205, 1987.

75 CATIPOVIC, J.A., ' Performance limitation in underwater acoustic telemetry', IEEE J. Ocean. Eng., Vol.15, pp.205-216, 1990.

76 BROCK, D.C., BATEMAN, S.C., and WOODWARD, B., ' Underwater acoustic transmission of low-rate digital data', Ultrasonics, Vol.24, pp.183-188, 1986.

77 ANDREWS, R.S., and TURNER, L.F., ' On the performance of underwater data transmission system using amplitude-shift-keying techniques', IEEE Trans. on Sonic and Ultrasonic, Vol.23, pp.64-71, 1977

78 ANDREWS, R.S., and TURNER, L.F., 'Investigation of amplitude fluctuations of high frequency short-dutation pulses propagated under short-range shallow water environment', J. Acoust. Soc. Amer., Vol.58, pp. 331-335, 1976.

79 CARDEN, F.,' Design parameters for FM/FM system', Proc. Int. Telemetering Con. ITC/90, pp.241-247, 1990.

80 CROMWELL, L., and WEIBELI ,F.J.,'Biomedical instrumentation and measurement', Prentice-Hall:N.J., 1980.

81 TOMPKINS, W.J., and WEBESTER, I.G. (eds.),' Design of microcomputer-based medical instrumentation', Prentice- Hall:N.J., 1982.

82 COBBOLD, R.C. ,'Transducers for biomedical measurements; principles and applications', Wiley:N.Y., 1974.

83 GEDDES, L.A., and BAKER, L.E., 'Principles of applied biomedical instrumentation, 3rd ed., Wiley:N.Y., 1989.

84 PLONSEY, R., 'The biophysical basis for electrocardiography', CRC Crit. Rev. Biong.,Vol.1,pp.1-48, 1971.

85 GOLDEN, D.P., WOLTHIUS, R.A. 'A spectral analysis of the normal resting electrocardiogram', IEEE Trans. Biomed. Eng., Vol.20, pp.366-372, 1972.

86 THAKOR, N.V., and WEBSTER, J.G., 'Ground- free ECG recording with two electrodes', IEEE Trans. Biomed. Eng., Vol.27, pp.699-704, 1980.

87 HUHTA, J.C., and WEBSTER, J.G., ' Interference in biopotential recording', In Biomedical electrode technology, in MILLER, H.A. and HARRISON,D.C.(eds.), N.Y., Acadremic Press, 1974.

88 WINTER, B.B., and WEBSTER, J.G., 'Reduction of interference due to common mode voltage in biopotential amplifiers', IEEE Trans. Biomd. Eng., Vol.30, pp.58-62, 1983.

89 THAKOR, N.V., and WEBSTER, J.G., ' Electrode studies for the long-term ambulatory ECG', Med. Biol. Eng. & Comput., Vol.23, pp.116-121, 1985.

90 HAMSTRA, G.H., PEPER, A., and GRIMBERGEN, C.A., 'Low-power, low noise instrumentation amplifier for physiological signals', Med. Biol. Eng. Comput. , Vol.22, pp.272-274, 1984.

91 PIZZUTI, G., CIFALDI, S. and NALFE, G.,'Digital sampling rate and ECG analysis', J. Biomd. Eng., Vol.7, pp.247-251, 1985.

92 MURTHY, V.K.,' Analysis of power spectral density of electrocardiogram', Math. Biosci, Vol.12, pp.41-52, 1971.

93 SCHER, A.M., YOUNG, A.C.,'Frequency analysis of the electrocardiogram', Circ. Res., Vol.8, pp.334-346, 1960.

94 KRUSS, H.L., BOSTIAN, C.W., ' Solid state Radio engineering', N.Y.: Wiley, 1980.

95 MILLMAN, J., and Taub, H., ' Pulse, digital and switching waveforms', N.Y. McGraw-Hill, 1965.

96 ROCHELLE, J.M., 'Design of a gateable transmitter for acoustic telemetering tags', IEEE Trans. Biomed. Eng., Vol.21, pp.63-66, 1974.

97 SOKAL, N.O., and SOKAL, A.D., 'Class-E a new class of high efficiency tuned single-ended switching power amplifiers', IEEE J. Solid-State Circuits., Vol.10, pp.168-176, 1975.

98 RAAB, F.H., 'Idealized operation of class E tuned power amplifier' , IEEE Trans. Circuits Syst., Vol.24, pp.725-735, 1977.

99 RAAB, F.H., 'Effects of circuit variations on the class-E tuned power amplifier', IEEE J. Solid-State Circuits, Vol.13, pp.239-247, 1978.

100 FRYER, T.B., 'Power sources for implanted telemetry system', Biotelemetry, Vol.1, pp.31-40,1974.

101 KO, W.H., 'Power sources for implant telemetry and stimulation systems', In Handbook on biotelemetry and radio tracking, AMLANER,C.J., and MACDONALD,D.W. (eds.), Pergamon press, N.Y., pp.224-245, 1980.

102 WAFERSCALE INTEGRATION, PSD3XX Programmable Peripherals family data, WaferScale Integration WEI, Fermont, Calif., 1992.

103 INTEL CORP., 8-bit microcontrollers Handbook, Intel Corp., U.S.A., 1983.

104 PAHLM, O., and SORONMO, L., 'Software QRS detection in Ambulatory monitoring- a review, Med. Biol. Eng. Comput., Vol.22, pp.289-297, 1984.

105 LINDECRANTZ, K.G., and LILJA, H., 'New software QRS detector algorithm suitable for real -time applications', J. Biomed. Eng., Vol.10, pp.280-284, 1988.

106 OKADA, M., 'A digital filter for the QRS complex detection', IEEE Transs. Biomed. Eng., Vol.26, pp.700-703, 1979.

107 MCARDLE, W.D., KATCH, F.I., KATCH, V.L., 'Exercise Physiology,energy,nutrition and human performance', 3rd.ed., Lea & Febiger Pub., 1991.

108 POWERS, K., HOWLEY, E.T,' Exercise physiology, theory and application to fitness and performance', W.C. Brown Pub., 1991.

109 SAYERS, B.A.,'Analysis of heart rate variability',Erogomics, Vol. 16,pp.17-32,1973.

110 LOMBARDI, F.,SANDRONE, G.,PRENPRUNER, S., SALSA, S., GARIMOLDI,M., CERUTTI, S., ' Heart rate variability as an index of sympathovagal interaction after acute myocardial infraction', Am. J. Cardiol., Vol.60,pp 1239-1245,1987.

111 PAGANI, M.,MALFATTO, G., PIERINI, S., CASATI, R., PASU,R.,POLI,A.,'Spectral analysis of the heart rate variability in the assessment of autonomic diabetic neuropathy, J. Auton. Nerv. Syst.m, Vol.23, pp143-153, 1988.

112 AKSELORD, S.,GORDEN, D.,UBEL, F.A.,SHANNON, D.C.,BARGER,A.C.,COHEN, R.J., 'Power spectrum analysis of the heart rate fluctutions:Aquantitative probe of beat-to-beat cardiovascular control', Science, Vol.213,pp. 220-222,1981.

113 POMERANZ, B.,MACAULAY, R.J., CAUDILL, M.A., Kutz, and ADAM,D.,'Assessment of autonomic function in humans by spectral analysis', Am. J. Physiol., Vol.248, pp.151-153,1985.

114 PAGANI, M., LOMBARDI, F., GUZZETTI, S.,'Power spectral analysis of the heart rate and arterial blood pressure variabilities as a marker of sympatho-vaga interaction in man and conscious dog,Circ.Res.,Vol.59,pp.178-193,1986.

115 DIXON, R.W., FAULKNER, J.A., 'Cardiac output during maximum effort running and swimming', J. Appl. Physiol., Vol.30, pp.635-656,1971.

116 OLDRIDGE, N.B., and HEIGENHAUSER, J.R., 'Resting and exercise heart rate with apnea and facial immersion in female swimmers', J. Appl. Physiol., Vol.45, pp.875-879,1978.

117 GEMMA, K.E., WELLS, C.L., 'Heart rates of elite synchronized swimmers', Phys. sport. Med., Vol.15,pp.99-107,1987.

118 MAGEL, J.L., MCARDLE, W.D., WEISS, N.L., STONE, S., NEWMAN,N.,'Heart Rate response to apnoea and face immersion', J. Sports Med. Phys. Fitness, Vol.22, pp.135-146, 1982.

119 NATELSON, B.H., NARRY, C.A., CURTIS, G.A., CREIGHTON, D., 'Roles of stress and adaptation in the elicitation of face immersion bradycardia', J. Appl. Physiol., Vol.54, pp.661-665, 1983.

120 OLSEN, C.R., FANESTIL, D.D., 'Some effects of breath holding and apnoeic underwater diving on cardiac rhythm in man', J. Appl. Physiol., Vol. 17, pp.461-466, 1962.

121 IRVING, L., ' Bradycardia in human divers', J. Appl. Physiol., Vol. 18, pp. 489-491, 1963.

122 HARDING, P.E., ROMAN, D., WHELAN, R.F., 'Diving Bradycardia in man ', J. Physiol. (London), Vol. 181, pp. 401-409, 1965.

123 STROMME, S.D., KEREME, D., EISSER, R., 'Diving Bradycardia during rest and exercise in relation to physical fitness', J. Appl. Physiol., Vol.28, pp.614-621, 1970.

124 MAGID, N.M., MARTIN, G.J., KEHONE, R.F., 'Diminished heart rate variability in sudden cardiac death', Circ., Vol.72(Suppl.3),P.241(abstarct),1985.

125 ELDRIDGE, L.,'Sudden unexplained death syndrome in cold water SCUBA diving', Undersea Biomed. Res. (Supplement),Vol.6,p.41,1979.

126 KAILATH, T. (ed.),' Modern signal processing', Hemisphere Publ., Washington, 1985.

127 STANLEY, W.D., DOUGHERTY, G.R., DOUGHERTY, R. (eds.), 'Digital signal Processing', Reston Publ.,1984.

128 KAVEL, M., COOPER, G.R., 'An empirical investigation of the properties of the autoregressive spectral estimator',IEEE Trans. on Inform. theory, Vol.22,pp.313-323, 1976.

129 KAY, S.M., MARPLE, S.L., 'spectrum analysis : a modern perspective', Proc. IEEE Vol. 69, pp.1380-1419, 1981.

130 MARPLE, L. 'A new autoregressive spectrum analysis algorithm', IEEE Trans. Acoust.,Speech, and Signal Proc., Vol.28,pp.441-454,1980.

131 BURG,J.P., 'Maximum entropy spectral analysis', Proc. of the 37th Meeting of the Society of Exploration Geophysicists, Oklahoma City, pp.34-41, 1967.

132 CHILDERS, D.G.(ed.),' Modern Spectrum analysis', New York:IEEE, 1978.

133 FABER, L.J.,' Commentary on the denominator recursion for Burg's block algorithm', Proc. IEEE , Vol.74,pp.1046-1047, 1986.

134 IBRAHIM, M.K. ,' On line splitting in the optimum tapered Burg algorithm ', IEEE Trans. Acoustics, Speech, Signal Proc., Vol ASSP-35, pp. 1476-1479, 1987.

135 MAKHOUL, J., 'Spectral linear properties and applications", IEEE Trans. Acoustics, Speech, Signal Proc., Vol. ASSP-29, pp. 282-296,1981.

136 AKAIKE, H.,'A new look at the statistical model identification', IEEE Trans. Aut. Control., Vol.19,pp.716-723, 1974.

137 HAYKIN,S.(ed.),'Nonlinear methods of spectral analysis', Springer-Verlag,1983.

138 KARVONEN, J., CHWALBINSKA, J., SAYNAJAKAGAS, S., 'Comparision of heart rates measured by ECG and microcomputer',The Phys. and Sport Med., Vol.12,6, pp.65-69, 1984.

139 MACFARLANE, D., FOGARTY, B., HOPKINS, W., The accuracy and variability of commercially available heart rate monitors",New Zealand J. Sports Med., Vol.17, pp.51-53, 1989.

140 PAULEV, P.E., HANSEN, H.G., 'Cardiac response to apnoea and water immersion and ambient pressure on human apnoeic bradycardia', J. Appl. Physiol., Vol. 33,pp.193-198,1972.

141 SPECK, D.F., BRUCE D.S.,'Effects of varying thermal and apneic conditions on the human diving reflex', Undersea Biomed. Res, Vol.4, pp.9-14, 1978.

142 HEMPLEMAN, H.V., LOCKWOOD, A.P.,'The physiology of diving in man and other animals', Edward Arnold Publ.,1978.

143 HONG, S.K.,'Physiology of diving-thermal considerations', In:The Physicians guide to diving medicine, C.W. SHILLING,L.B. CARLSTON, and MATHIAS R.A. (Eds.) NY:Plenum Press,pp.153-178, 1984.

144 ROBINSON, O.A., EPESTAIN S.E., BEISER G.D., BRAYN W., 'Control of heart rate by the autonomic nervous system, Studies in man on the interrelation between baroreceptor mechanisms and exercise', Circ. Res., Vol.19, pp.400-411, 1966.

145 PAULEV, P.E.,'Cardiac rhythm during breath-holding and water immersion in man', Acta Physiol. Scand., Vol.73, pp.139-150,1968.

146 ROWELL, L.B., 'Human circulation requaltion during physical stress', NY: Oxford University press, 1986.

147 ZWINGELBERG, K.M., GREEN, J.W., and POWERS, K.,'Primary Causes of Drowning and Near Drowning in Scuba Divers',Physi.and Sport Med., Vol. 14(9),pp.145-151,1986.

148 MCANIFF J.J., 'US Underwater Diving Fatality Statistics 1983-1984', US Department of Commerece, NOAA Undersea Research Program, Washington DC, 1986.

149 VANN, R.D., ' Likelihood analysis of decompression data using haldane and bubble growth modules', Proc. 9th Int. conf. on underwater and hyberbaric physiology, Undersea and hyberbaric medical society, Bethesda, M.D., pp.165-181, 1987.

150 TIKUISIS,T., NISHI,R.Y., and WEATHERSBY, P.K.,'Use of the maximum likelihood method in the analysis of chamber air dives', Undersea Biom. Res., Vol.15, 4, pp.301-313, 1988.

151 SCHILLING,C.W., CARLSTON, C.B., and MATHIAS, R.A.,' The Physician's Guide to Diving Medicine', Plenum Press, N.Y.,1984.

152 MILLER, A.S., BLOTT,B.H., and Hames, T.K., 'Review of neural network applications in medical imaging and signal processing', Med. Biol. Eng. and Comp., Vol.30, pp.449-464, 1992

153 CLARK, J.W., 'Neural network modelling', Phys. in Med. and Biol., Vol.36, pp.1259-1317, 1991.

154 CRAIG, A. B., *Principles and Problems of Underwater Diving', Physi. and Sport* Med., Vol.8(3),pp.72-83,1980.

155 BOVE,A.A., and LOWENTHAL, D.T., 'Exercise Medicine, Physiological Principles and Clinical Applications',Academic Press, 1983.

156 BENNET, P.B., and ELLIOT, D.H., 'The Physiology and Medicine of Diving and Compressed Air Work', 3rd.ed., San Pedro ,CA, Best Publications, 1982.

157 EDMONDS, C., LOWRY C., and PENNEAFTHER, J. (eds.),' Diving and subaquatic medicine', 2nd ed. Mosman, N.S.W., Australia:Diving Medical Centre, 1983.

158 NEBLETT, L.M., 'Otolaryngology and sport scuba diving:update and guidelines', Ann Otol. Rhinol. Laryngol. Suppl.,Vol.115, pp.1-12, 1985.

159 HILLS, B.A., 'Decompression sickness. Vol.1. The biophysical basis of prevention and treatment', Chichester, England:John Wiley, 1977.

160 STRAUSS, R.H., and PROCKPOP, L.D., 'Decompression sickness among scuba divers', J. Amer. Med. Assoc., Vol.223, pp.637-640,1973.

161 GOLDING F.C., GRIFFITHS, P., HEMPLEMAN, H.V.,"Decompression sickness during construction of the construction of the Dartford Tunnel", Br. J. Ind. Med., Vol.17, pp167-180, 1960.

162 Department of the Navy.,'U.S. Navy diving manual', Washington, D.C., Department of the Navy, NAVSEA(0994-LP-001-9010), 1985.

163 SCHILLING, C.W.; and SCHANDELMEISER, N.R. (eds.),'The underawter Handbook, A guide to physiology and performance for the engineer', John Wiley,1976.

164 Ministry of Defence, 'Royal Navy diving manual', London:Ministry of defence, BR 2806, 1987.

165 ALEKSANDER,I. and MORTON, H., 'An Introduction to Neural Computing', Chapman & Hall, New York, 1990.

166 PAO, Y., 'Adaptive Pattern Recognition and Neural Networks', Addison-Wesley, 1989.

167 LIPPMAN, R.P., 'An introduction to computing with neural nets', IEEE ASSP Mag.,4(2),pp.4-21, 1987.

168 RUMELHART, D.E. and McCLELLANMD, J.L. (eds.),'Parallel Distributed Processing', MIT Press, Cambridge, MA, pp.318-362, 1986.

169 REISSMAN, P., SHUPAK, A., NACHIM, Z., and MELAMED,Y.,'Inner ear decompression sickness following a shallow Scuba diving', Avia. Space and Env. Med., pp.563-565, June 1990

170 RICHARD, H. C., HUMPHEREYS,N., PILMANIS, A.A., and HEILIG, R.W.,'Cardiac arrest from gas embolism in Scuba diving',Ann. Emerg. Med., Vol.10, pp.589-592, 1981.

171 LEITCH, D.R., and GREEN, R.D., 'Recurrent Pulmonary Barotruma', Avia. Space and Env. Med., pp.1039-1043, 1986.

172 CRAIG, A. B., Summary of 58 cases of loss of consciousness during underwater swimming and diving', Med. Scien.in Sport, Vol.8, pp.171-175, 1976.

173 JEFFERSON, D.C.,'Decompression sickness in sport Scuba diving', Physi. and Sport Med., Vol.16, pp.109-116, 1986.

174 HALPERN, P. and GREENSTEIN, A., ' Cardiac decompression sickness:report and discussion of case, Avia. Space and Envi. Med., pp.350-353, 1981.

175 GREENHOUSE, A.H. and PAGE, K., ' Scuba diver's thigh', West. J. Med., Vol.145, pp.698-699,1986.

176 MONEY,K.E., BUCKINGHMAM, I.P., CALDER, W.H., JOHNSON, W.H., and LUDMAN,H., ' Damage to the middle ear and the inner ear in underwater divers', Undersea Biom. Res., Vol.12, 1, pp.71-84 ,1985.

177 KUEHN, L.A., SWEENY D.M.,' Canadian diving data: a computerized decompression data bank', Comput. Biomed. Res.,Vol.6, pp266-280, 1973.

AUTHOR'S PUBLICATIONS

1. Habib R Sh and Al-Nouman Q A H, " *Microcomputer based liquid flowrate control system*, Int. J. Electronics, Vol 65, No.1, pp 117-125,1988.

2. Al-Shara K H and Habib R Sh, *An approach to the formulation of high frequency ferrite hysteresis loss*, Modelling,Simulation & Control A, Vol 18, No 1, pp1-8, 1988.

3. Habib R Sh and Sungoor A M H, *Implicit design of a predictive PID controller with computational delay effect,* Proc. IEEE IECON'89, Philadelphia, USA ,pp40-45, 1989.

4. Al-Hadithi B M, Meki Z, and Habib R Sh, *Explicit design of a predictive self-tuned PID controller*, Proc. IEEE IECON'89, Philadelphia,USA , pp291-295, 1989.

5. Habib R Sh and Habib H Sh, *Design of Discrete control System for a Solar Heating Model*, Solar and Wind Technology-Int. Journal, Vol.7, No.5, pp607-610, 1990.

6. Habib R Sh and Habib H Sh," *Microcomputer based variable structure control of reduction of torsional vibration*", J. of Sound and Vibration, Vol.155, No.3, pp403-411, 1992.

7. Habib R Sh , Habib H Sh , and Majeed B, "*Experimental Self-Location Vehicle Based on Ultrasonic wave Guided System*", Int. J. of Elect. Eng. Educ., Vol.30, No.3, pp.224-235,1993.

8. Woodward B, and Habib R Sh, *Physiological monitoring by underwater ultrasonic biotelemetry*, J. Soc. Underwater Technology, Vol.18 , No 1, pp34-44, 1992.

9. Woodward B and Habib R Sh, *Physiological monitoring by ultrasonic biotelemetry,* Proc. 1st European conference on Underwater Acoustics, Luxembourg, M. Weydert (Ed.), Elsevier Applied Sciences, pp.110-113, 1992.

10. Woodward, B and Habib Istepanian R Sh , " *Acoustic biotelemetry of data from Divers*", Proc. IEEE 15 Annual Int. Conference Engineering in Medicine and Biology, San Diego, Calif., pp.1000-1002, 1993.

11. Woodward, B and Habib Istepanian R Sh , "*Progress in underwater biotelemetry*", Proc. Scandinavian Symp. on physical acoustics, Ustaoest Hoyfjellshotel, Norway, 1994.